

https://dspace.org/

Tunable biomimetic hybrid scaffold for wound healing and skin regeneration

Mndlovu, Hillary

2021

https://hdl.handle.net/10539/32050

Downloaded from a DSpace repository. https://dspace.org/

Tunable Biomimetic Hybrid Scaffold for Wound Healing and Skin Regeneration

Hillary Mndlovu

A thesis submitted to the Faculty of Health Sciences, University of the Witwatersrand, in fulfilment of the requirements for the degree of

Doctor of Philosophy



Supervisor: Professor Viness Pillay

Co-supervisors: Pradeep Kumar, Thashree Marimuthu, Pierre P.D. Kondiah, Lisa C. du Toit and Yahya E. Choonara

Wits Advance Drug Delivery Platform, Department of Pharmacy and Pharmacology, School of Therapeutic Sciences, Faculty of Health Science, University of the Witwatersrand, Johannesburg, Gauteng, South Africa

2020

DECLARATION

I, Hillary Mndlovu (674238), a student registered for the Doctor of Philosophy in the Faculty of Health Sciences at the University of the Witwatersrand, Johannesburg, South Africa in the academic year 2020.

Hereby declare the following:

 I am aware that plagiarism (the use of someone else's work without their permission and/or without acknowledging the original source) is wrong.

 I confirm that the work submitted for assessment for the above degree is my own unaided work except where I have explicitly indicated otherwise.

 I have followed the required conventions in referencing the thoughts and ideas of others.

 Prior to this, this thesis has not been submitted for the attainment of any degree or examination at this or any other university.

 I understand that the University of the Witwatersrand may take disciplinary action against me if there is credence that this is not my own unaided work or that I have failed to acknowledge the source of the ideas or words in my writing.

Signature:  Date: 12 November 2020

RESEARCH OUTPUTS

PUBLICATIONS

Mndlovu, H., du Toit, L. C., Kumar, P., Marimuthu, T., Kondiah, P. P., Choonara, Y. E., & Pillay, V. (2019). Development of a Fluid-absorptive Alginate-Chitosan Bioplatform for Potential Application as a Wound Dressing. *Carbohydrate Polymers*, 114988.

Mndlovu, H., du Toit, L. C., Kumar, P., Marimuthu, T., Kondiah, P. P., Choonara, Y. E., & Pillay, V. (2019). Bioplatform Fabrication Approaches Affecting Chitosan Based Interpolymer Complex Properties and Performances in Wound Dressing Application. *Molecules*. DOI

Mndlovu, H., du Toit, L. C., Kumar, P., Marimuthu, T., Kondiah, P. P., Choonara, Y. E., & Pillay, V. (2020). In Situ Forming Partially-Crosslinked Chitosan-Alginate Interpolymer Complex Hydrogel for Wound Dressing Skin Tissue Regeneration. (To be submitted to Advanced Healthcare Materials or nature nanotechnology)

Mndlovu, H., du Toit, L. C., Kumar, P., Marimuthu, T., Kondiah, P. P., Choonara, Y. E., & Pillay, V. (2020). Tunable Biomimetic self-assembling Alg-RGD-CS-sulfacetamide sodium Hybrid Scaffold for Wound Healing and Skin Regeneration. (To be submitted to Acta Biomaterialia)

RESEARCH PRESENTATIONS

Mndlovu, H., du Toit, L. C., Kumar, P., Marimuthu, T., Kondiah, P. P., Choonara, Y. E., & Pillay, V. (2018). Partially-crosslinked Co-complexed Biomaterial Platforms for Potential Wound Healing Applications. **(Oral presentation).** 4th International Conference on Biomedical Polymers & Polymeric Biomaterials | 15-18 July 2018, Kraków, POLAND.

Mndlovu, H., du Toit, L. C., Kumar, P., Marimuthu, T., Kondiah, P. P., Choonara, Y. E., & Pillay, V. (2020). Partially-crosslinked, co-complexed biomaterial platforms for wound dressing applications. **(Oral presentation).** Towards 100 years of excellence, Faculty of Health Science Research Day and Postgraduate Expo, 6 September 2018. University of the Witwatersrand, Johannesburg, South Africa.

Mndlovu, H., du Toit, L. C., Kumar, P., Marimuthu, T., Kondiah, P. P., Choonara, Y. E., & Pillay, V. (2020). **(Flash talk and poster presentation).** Partially-crosslinked, co-complexed biomaterial platforms for wound dressing applications. 9th Cross Faculty Postgraduate Symposium, Showcasing Graduate Research at Wits, 2018. University of the Witwatersrand, Johannesburg, South Africa.

Mndlovu, H., du Toit, L. C., Kumar, P., Marimuthu, T., Kondiah, P. P., Choonara, Y. E., & Pillay, V. (2020). Development of a Fluid-absorptive Alginate-Chitosan Bioplatform for Potential Application as a Wound Dressing. . **(Oral presentation).** 10th Cross Faculty Postgraduate Symposium - 3 and 4 September 2019. 1st place price on the Faculty of Health Science. University of the Witwatersrand, Johannesburg, South Africa.

Mndlovu, H., du Toit, L. C., Kumar, P., Marimuthu, T., Kondiah, P. P., Choonara, Y. E., & Pillay, V. (2020). Development of Tunable Property-Performance Features of Bioplatforms for Tissue Regeneration and Wound Healing. **(Oral presentation).** 11th Cross Faculty Postgraduate Symposium - 13th and 14th October 2020.

ACKNOWLEDGEMENT

The journey towards finishing this challenging task in hand has been memorable and I could not have achieved my goal without the individuals who made the journey bearable. I would very much like to extend my sincerest gratitude to all of them.

I would like to thank the great almighty for entrusting me with life, providing guidance and countless blessings even when I question him and his existence time after time. His presence and love is absolute. To my parents; Mario Ndlovu. Maria Masiye and Belinda Joaquim ubisse whom I'm in great owe of with all their unconditional love, sacrifices and care. To my late sister Busi Khatazile Ndlovu who saw me for who I was, loved, cared, guided and believed in me. To my siblings LucY, Paul, Sagudu, lucky, Aron, Solly, Lazarus and Hellen for their constant understanding, support and trusting my decisions. These are the people who showed and shared life with me; they shaped me to the person I am today. To my high school teachers and the principal from Lambalti high school more in particular T.L Lubisi for her difficult task of guiding and shaping me to be the person I am today. Their contributions in my life are highly appreciated and I hope I make them proud.

I would like to thank my close friends; Tshepo Molefe, Khanyile Ngwejane, Sunday Herry Bila, Rebaone Maribe and Gillian Mahumane. These individuals have always been available in my high and low moments in life

I would like to express my gratitude to Prof. Viness Pillay, Prof. Yahya E. Choonara, P. Kumar, Lisa C. Du toit, Dr T. Marimuthu and Dr P.P.D Kondiah for their guidance, encouragement and useful critique to this research work.

To my colleagues and WADDP staff; thank you for your guidance and companionship. Thank you for the memorable experiences you gave me.

I would like to thank the staff at the Central Animal Service (CAS) of the University of the Witwatersrand for their assistance, lessons, and guidance in carrying out the *in vivo* aspect of this research.

Last but not least, I would like to extend my gratitude to the National Research Foundation (NRF) of South Africa for their financial assistance.

DEDICATION

This thesis is dedicate to my family more specifically my mother, Belinda Joaquim Ubisse. I would not be where I am today If it was not for my family's contribution towards shaping me to the person I am.

ABSTRACT

Skin has the ability to regenerate after traumatic injury. The injury triggers several regenerative process during the overlapping hemostasis, inflammatory, proliferative, and maturation wound healing phases. Cases such as bleeding, infection, and in other cases loss of major skin tissue delays and/or limit the action of the phases above to restore the damaged tissues. Treatment of some injury cases have traditionally focused on allograft and autograft. However, these approaches may take longer to incorporate into the patient's body, and could also be rejected by some patients and lastly the use of autograft results in the loss of tissue from one place to heal another. This gave rise to the tissue engineering field which includes the development of bioplatforms/devices/biomaterials suitable for the treatment of the cases mentioned above. These tissue engineering bioplatforms includes but not limited to hydrogels, gels, foams, nano/microparticles, scaffolds, sponges, fibres, and beads. The design of these bioplatforms ranges from natural/synthetic polymers, antibiotics, bioactives and peptides/proteins.

There has been great advancement in the tissue engineering field. However, there is still no bioplatform that meet the requirements for an ideal wound dressing. The current study outlines the properties of bioplatforms that can be controlled to improve the bioplatforms' translational performance as a wound dressing. To aid the biocompatibility and degradation of the wound dressings, natural polymers such as chitosan (CS) and alginate (Alg) were used along with natural phenolic agents such as transferulic acid (TFA) and tannic acid (TA). The properties of the bioplatforms were tunable by employing the partial crosslinking, freeze-drying, and lyophilization approach to fabricate particulate bioplatforms capable of forming an *in situ* interpolymer complex (IPC) hydrogel in the presence of fluids. The partial crosslinking approach enabled the incorporation of transferulic acid and also the in situ formation of interpolymer complex.

Properties such as fluid absorption [(PC CS-Alg (4343.4%) and PC TFA-CS-Alg (3102%) in 24 hours)], degradation [(PC CS-Alg (78.2%) and PC TFA-CS-Alg (53.5%) in 14 days)], mechanical properties [(rigidity of 2090 Pa, and 640 Pa for PC CS-Alg and PC TFA-CS-Alg, respectively)] were observed in this study. The Bioplatforms' performance such as the TFA encapsulation efficiency of 65.6% with a burst release of 57.5% in 8 hours to a total release of 67.3% in 3 days was also observed in the current study. These properties lead to translation performances such as non-toxic (cell viability > 90%) behaviour when the NIH 3T3 embryonic fibroblast cells were exposed to the bioplatforms for 3 days. Furthermore, the bioplatforms exhibited superior accelerated tissue remodelling and wound healing capabilities at the early stages of wound healing compared to the equivalent commercial product (Pharma-Algi®) and the control group. To elucidate the suitability of tuning bioplatform properties to translational performances, a self-assembling scaffold was developed from the natural polymers mentioned above, RGD peptide and TA.

Properties of the bioplatforms included the optimal swelling behaviour (absorbs fluid instantly), porosity (3-D architecture with an average pore size distribution of 168.4 μm^2), mechanical properties such as tensile strength of 0.0038 and 0.001725 MPa, compressive ultimate strength of 0.0571 and 0.07225 MPa, and storage modulus of 80.9 and 88.6 Pa for Alg-RGD-CS and Alg-RGD-CS-TA, respectively. These properties allowed for TA encapsulating efficiency 86% with a burst release of 57.12% in 24 hours, followed by gradual steady release of 8.45% per day up to 90% in 5 days. The Alg-RGD-CS scaffolds displayed high fluid uptake of 5240% in 24 hours

compared to the 3716% absorbed by the Alg-RGD-CS-TA in 24 hours. These fluid uptake properties where superior to those observed on the particulate bioplatform and the comparative product.

Contrary to the particulate bioplatform degradation properties, the scaffolds exhibited low degradation extent (Alg-RGD-CS (33.68%) and Alg-RGD-CS-TA (16.53%) in 14 days). However, the decrease in the degradation extent from non-crosslinked to crosslinked bioplatforms was still observed. Similarly, for the partial crosslinked bioplatforms the translational performances of the scaffolds were remarkable with a cytocompatible behaviour (cell viability > 80%) and accelerated wound closure at the early stages of wound healing. The scaffold and the particulate bioplatforms displayed desirable wound healing performances highlighted by the regeneration of scar-less skin tissues after 14 days of wound healing. The desirable features of the regenerated skin tissues attest to the effective tunable properties of bioplatforms translation to optimal performances as wound dressings and drug delivery systems.

TABLE OF CONTENTS

CHAPTER ONE
Introduction and Rationale of the Study

1.1. Background of the study xix
1.2. Rationale and motivation 3
1.3. Hypothesis, aim and objectives 5
1.4. Novelty of the study and potential applications of the bioplatforms 6
1.5. Overview of the thesis 6

CHAPTER TWO
Bioplatform Fabrication Approaches Affecting Chitosan-Based Interpolymer Complex Properties and Performance as Wound Dressings

2.1. Introduction 10

2.2. Polymer structural interactions affecting BMP property-performance factors 12

2.3. Effect of polymer processing on physical and mechanical properties of BMPs 16

2.4. Fabrication approaches affecting physical and mechanical properties of chitosan-based interpolymer complexes 19

2.4.1. Scaffold fabrication approaches and their physical and physicochemical properties impacting BMP performance 23

2.4.1.1. Three-dimensional printing of chitosan-based IPC BMPs 23

2.4.1.2. Ionic gelation technique employed for fabrication of chitosan-based IPC BMPs 23

2.4.2. Fibre physical and physicochemical properties impacting BMP performance 25

2.4.2.1. Electrospun chitosan-based IPC BMPs 25

2.4.3. Gels, hydrogels and membranes physical and physicochemical properties impacting BMP performance 32

2.4.3.1. Ionic gelation technique employed in fabrication of chitosan-based IPC BMPs 32

2.4.3.2. Polymer coating, grafting, solvent evaporation, and solvent casting approaches in fabricating chitosan-based IPC BMPs 35

2.4.4. Sponges physical and physicochemical properties impacting BMP performance 36

2.4.4.1. Ionic gelation technique employed in fabrication of chitosan-based IPC BMPs 36

2.4.4.2. Phase separation and grafting approach for the fabrication of chitosan-based IPC BMPs 37

2.5. Standard BMP properties for wound dressing applications 37

2.6. Concluding remarks 37

CHAPTER THREE
Development of a Fluid-absorptive Alginate-Chitosan Bioplatform for Potential Application as a Wound Dressing

3.1. Introduction **57**

3.2. Materials and Methods **59**

3.2.1. Materials 59

3.2.2. Polymer solution preparation and partial-crosslinking 59

3.2.3. Powder flow properties of the bioplatforms 60

3.2.4. Interpolymer complexation of PC-Alg and PC-CS platforms 60

3.2.5. Zeta potential of PC-CS and PC-Alg bioplatforms 61

3.2.6. Determination of molecular vibrational transitions on fabricated bioplatforms 61

3.2.7. X-ray powder diffraction analysis of the bioplatforms 61

3.2.8. Determination of thermophysical properties of the bioplatforms 61

3.2.9. Determination of the degree of crosslinking of the bioplatforms 61

3.2.10. Porositometric and surface topography characterization of bioplatforms employing the Brunauer–Emmett–Teller (BET) theory 62

3.2.11. Evaluation of surface morphology of the fabricated bioplatforms 62

3.2.12. Fluid uptake and degradation of the bioplatforms and comparator wound dressing 62

3.2.13. Rheological evaluation of the viscoelastic properties of the hydrogel 63

3.2.14. Cytotoxicity assessment of the bioplatforms 63

3.3. Results and Discussion **64**

3.3.1. Synthesis of the bioplatforms 64

***3.3.2. In situ* forming IPC hydrogel concept assessment in a physiological environment** 65

3.3.3. Powder flow properties of the bioplatforms 65

3.3.4. Degree of crosslinking of alginate and chitosan 65

3.3.5. Zeta potential analysis of the pristine polymers and bioplatforms 66

3.3.6. Chemical interaction and molecular vibrational transition analysis of the bioplatforms 66

3.3.7. X-ray powder diffraction analysis of the bioplatforms 69

3.3.8. Thermo-physical property analysis of the bioplatforms 70

3.3.9. Porosity analysis of the bioplatforms 72

3.3.10. Scanning electron microscopy analysis of the bioplatforms 73

3.3.11. Rheological properties of the bioplatforms 74

3.3.12. Gelling kinetics and interpolymer complexation of PC-Alg and PC-CS microparticles under SWF/whole blood exposure..... 77
3.3.13. Water uptake and degradation of the bioplatforms and comparator wound dressing..... 79
3.3.14. Cytotoxicity assessment of the bioplatforms 81
3.4. Concluding remarks 82

CHAPTER FOUR

***In Situ* Forming Chitosan-Alginate Interpolymer Complex Hydrogel for Wound Dressing Skin Tissue Regeneration**

4.1. Introduction 89

4.2. Experimental 91

4.2.1. Material 91

4.2.2. Preparation of partial-crosslinked alginate and TFA loaded chitosan micromatrices 91

4.2.3. Zeta Potential of the bioplatforms 91

4.2.4. Molecular vibrational transitions, X-ray powder diffraction pattern, and thermostability properties of the bioplatforms 92

4.2.5. Surface morphology evaluation, fluid uptake and degradation of the bioplatforms 92

4.2.6. Hydrogel formation kinetics of PC TFA-CS-Alg IPC 93

4.2.7. Encapsulation efficiency (EE), drug loading (DL) and in vitro release studies 93

4.2.8. *In vitro* cytocompatibility evaluation of the bioplatforms 94

***4.2.9. In vivo* skin tissue regeneration and wound closure performance of the bioplatforms** 94

4.3. Results and discussion 95

4.3.1. Synthesis of bioplatforms 95

4.3.2. Zeta Potential of bioplatforms 97

4.3.3. Physical and chemical characterisation of bioplatforms 97

4.3.4. Surface morphology, fluid uptake and degradation of bioplatforms 101

4.3.5. Gelling kinetics of PC TFA-CS-Alg interpolymer complex 103

4.3.6. *In vitro* drug incorporation, release and cytocompatibility evaluation of the bioplatforms 105

4.3.7. Evaluation of *In vivo* wound healing performance of bioplatforms 108

4.4. Concluding remarks 118

CHAPTER FIVE
Self-assembling Alg-RGD-CS-TA Hybrid Scaffold for Wound Healing and Skin Regeneration

5.1 Introduction 123

5.2. Methods and materials 125

5.2.1. Materials 125

5.2.2. Fabrication of the self-assembling hybrid scaffold 125

5.2.3. Assessing molecular vibrational transitions and diffraction pattern of the scaffolds 125

5.2.4. Evaluation of the thermophysical properties of the scaffolds 126

5.2.5. Evaluation of surface morphology of the scaffolds 126

5.2.6. Textural mechanical properties of the scaffolds 126

5.2.7. Fluid uptake and degradation kinetics of the scaffolds 126

5.2.8. Encapsulation efficiency (EE), drug loading (DL) and *in vitro* release studies 127

5.2.9. *In vitro* cytotoxicity assessment of the scaffolds 127

5.2.10. *In vivo* Skin tissue regeneration and wound closure assessment of the scaffolds 128

5.3. Results and discussion 129

5.3.1 Development of the self-assembling scaffolds 129

5.3.2. Morphological features of the self-assembled scaffolds. 131

5.3.3. Chemical and physical properties of the scaffolds 134

5.3.4. Mechanical properties of the scaffolds 139

5.3.5. Fluid absorption and degradation of the scaffolds 140

5.3.6. UV-Vis absorption, Drug release and *In vitro* cytocompatibility of scaffolds 142

5.3.7. *In vivo* wound closure and tissue remodelling property of the self-assembled scaffolds 144

5.4. Concluding remarks 155

CHAPTER SIX
Conclusions and Recommendations

6.1. Conclusions 160
6.2. Recommendation 161

APPENDICES

Appendix A: Animal Ethics Clearance Certificate 163
Appendix B: Review Paper.....164
Appendix C: Research Paper 1.....165
Appendix D: Research Paper 2.....166
Appendix E: Research Paper 3.....167
Appendix F: Conference Presentation Certificates.....168

LIST OF FIGURES

Figure 1.1. Schematic Representation of Layers of the Skin and their Thickness……..…….…….2

Figure 1.2. Idealistic Contribution of the Polymers, Peptide and Bioactives for Improving Property Performances of the Bioplatforms Translating to Optimal Performance…….....4

Figure 2.1. Schematic Representation of Steps Required to Design a Suitable Biomedical Platform that Meets Ideal Requirements for an Effective Wound Dressing…….....12

Figure 2. 2. Polyelectrolyte Complexations…….....…15

Figure 2.3. Schematic Representation of the Processing Approaches of Ionic Polymers……18

Figure 2.4. Physical and Mechanical Properties of Chitosan-Based Composites…….....21

Figure 2.5. *In Vivo* Performance of Chitosan-Based Composites…….....22

Figure 3.1. Schematic Representation of the Three-Step Method of Partial-Crosslinking And Interpolymer Complexation of the Polymers…….....60

Figure 3.2. Schematic Representation of the (A) Sodium Alginate Crosslinking, (B) Chitosan Crosslinking and (C) Interpolymer Complexation Reaction…….....…67

Figure 3.3. (A) FTIR Spectra of the Bioplatforms - 'K' Highlights the Positions Most Affected by the Partial-Crosslinking And Interpolymer Complexation. (B) XRD Diffractograms Of The Bioplatforms…..70

Figure 3.4. (A) Differential Scanning Calorimetric Analyses and (B) Thermogravimetric Analyses of the Platforms…..……..……72

Figure 3.5. Scanning Electron Microscopy (SEM) Analyses of the Platforms……..…..74

Figure 3.6. Rheological Analysis Of The Polymers and the Polyelectrolyte Complex……76

Figure 3.7. Kinetic Gelation Of The IPC In (A) SWF (Ph 7.4) And (B) Blood at 37°C……79

Figure 3.8. (A) Biodegradation and (B) Water Uptake Behaviour of the Pristine Polymers, Bioplatforms and the Comparative Prodfuct In PBS (Ph 7.4) Solution At 37 °C at 50rpm…..……..81

Figure 3.9. Cell Viability Evaluation of the NIH 3T3 Cell Line Treated with the Bioplatforms……..…..82

Figure 4.1. (A) FTIR Spectra, (B) X-Ray Diffractograms, (C) DSC And (D) TGA Thermogrames of the Bioplatforms……..……..100

Figure 4. 2. (A) Morphological Evaluation via SEM And (B) Fluid Uptake Capacity and Degradation Of PC FA-CS-Alg IPC. Fluid Uptake and Degradation Evaluation were Performed In PBS (Ph 7.4) Solution at 37 °C at 50 Rpm Orbital Shaker……..……..102

Figure 4.3. The Hydrogel Formation Kinetics of PC FA-CS-Alg in Simulated Wound Fluid (Ph 7.4) at 25 °C……104

Figure 4.4. (A) UV-Vis Absorption Spectra Of Bioplatforms, (B) Trans-Ferulic Acid Release From The PC TFA-CS-Alg Interpolymer Complex in SWF (37 °C, Ph 7.4) and (C) Cell Viability Assessment of Bioplatforms Employing MTT Assay.....107

Figure 4.5. *In Vivo* Representation of the Wound Healing Capabilities of the Bioplatforms and Commercial Product.....110

Figure 4.6. Early Wound Healing Stage of Tissues Treated With Different Groups of Bioplatforms..112

Figure 4.7. Mid Wound Healing Stage of Tissues Treated With Different Groups of Bioplatforms....114

Figure 4.8. Mid-To-Late Wound Healing Stage of Tissues Treated With Different Groups of Bioplatforms.....116

Figure 4.9. Late Wound Healing Stage of Tissues Treated With Different Groups of Bioplatforms...117

Figure 5.1. Schematic representation of the self-assembled hybrid scaffold (a) reaction schematic of the peptide activation and interactions between RGD peptide, chitosan, alginate and TA. (b) dry and hydrated scaffold.....130

Figure 5.2. Morphological features of the self-assembled and co-assembled scaffolds (ai-iii) Alg , (bi-iii) Alg-RGD, (ci-iii) CS, (di-iii) CS-RGD, (ai-iii) Alg-RGD (ai-iii) Alg-RGD-CS-TA scaffolds at 100, 500, and 2000 X magnification respectively.....133

Figure 5.3. The scaffolds' functional groups, chemical composition, and phase changes induced by self-assembly via interactions described above were evaluated via the four analytical techniques (a) FTIR spectra, (b) X-Ray diffractograms, (c) DSC and (d) TGA thermogrames of the scaffolds.....138

Figure 5.4. Fluid absorption and physical degradation of the scaffolds. Both assessments were done in PBS pH 7.4 at 37 °C in an orbital shaker shaking at 25 rpm.....141

Figure 5.5. a) UV-Vis absorption of polymers, peptide and TA, b) *in vitro* cumulative TA release, and c) *in vitro* cytotoxicity evaluation of the peptide, TA and the scaffolds.....144

Figure 5.6. *In vivo* performance of the bioplatforms and commercial product.....146

Figure 5.7. Early wound healing stage of tissues treated with different groups of bioplatforms.....148

Figure 5.8. Mid wound healing stage of tissues treated with different groups of bioplatforms.....150

Figure 5.9. Mid-to-late wound healing stage of tissues treated with different groups of bioplatforms.....152

Figure 5.10. Late wound healing stage of tissues treated with different groups of bioplatforms.....154

LIST OF TABLES

Table 2.1. BMP fabrication approach and properties affecting translational performance in wound dressing applications……..……27

Table 2.2. Chitosan interactive compounds: polymers; bioactives and crosslinkers……..……30

Table 3.1. Porosity analysis of the IPC and polymer complexes after partial-crosslinking……73

Table 4.1. Bioplatform ratios and zeta potential……...……..97

Table 5.1. Scaffold compression properties……...…….…..140

LIST OF EQUATIONS

Equation 3.1 Cross-linking index (%)…..……..…..62

Equation 3.2. Fluid absorption (%)…..…..……..…..62

Equation 3.3. Degradation (%)……..…..63

Equation 4.1. Fluid uptake (%)……..……..92

Equation 4.2. Degradation (%)……..……..92

Equation 4.3. Encapsulation efficiency (%)……..…93

Equation 4.4. Drug loading (%)…..……..93

Equation 4.5. Cummulative release (%)……..……..…..94

Equation 4.6. Wound closure (%)…….…….…….....95

Equation 5.1. Fluid uptake (%)…….…..126

Equation 5.2. Degradation (%)…….…..126

Equation 5.3. Encapsulation efficiency (%)…….…..127

Equation 5.4. Drug loading (%)…….…..127

Equation 5.5. Cummulative release (%)…….…..127

Equation 5.6. Wound closure (%)…….…..128

CHAPTER 1

Introduction and Rationale of the Study

1.1 Background of the study

Skin is considered the largest organ relative to other medium sized organs such as the brain and liver. As a multifunctional organ, skin acts as a primary physical barrier protecting the body against external environmental elements while keeping homeostatic environment by allowing gaseous exchange and nutrients absorption. This multifunctional property of the skin is bestowed by the collective contribution of the layers of the skin. These layers have different architecture and thickness such as the stratum corneum (0.01-0.02 mm), epidermis (0.03-0.13 mm), dermis (1.1 mm), and subcutaneous fat (1.2 mm) (Figure 1.1)(Hendriks et al., 2000). Damage to these layers triggers several cascades necessitating the regeneration of the skin.

The skin regeneration process consist of the four well-defined overlapping phases namely haemostasis, inflammation, proliferation, and wound remodelling (Enoch and Leaper, 2008, Teller and White, 2011, Li et al., 2007). Immediately after skin damage (tissue trauma), the disturbed native acidic milieu (pH 5-6) exposes the underlying tissue and releases fluids which changes the pH to pH 7.4 (Boateng et al., 2015, YE, 1957, Schneider et al., 2007). The first phase of skin regeneration occur after skin tissue injury which works to establish homeostasis. In this phase, several regeneration mediators such as platelets, macrophages, leukocytes, and neutrophils are secreted to adhere to the extracellular matrix (ECM) of the skin to promote tissue regeneration and restoration (Singer and Clark, 1999).

In order to promote accelerated skin regeneration, biomaterials can be leveraged to facilitate and enhance the performance of the mentioned four phases. This means the selection of proteins, polymers and supplements in the design of skin regenerative biomaterial should be directed towards the enhancement of the three skin regeneration phases. The inflammatory phase can be supplemented with anti-oxidant and anti-inflammatory properties, whilst the proliferative phase could be supplemented with adhesive and proliferation enhancing molecules such as natural polymers, bioactives and peptides/proteins. These supplementary materials can be formulated into a gel, hydrogel, particles, foam, scaffolds, fibres, and sponges to contribute to the tissue remodelling process necessitating tissue regeneration and wound healing.

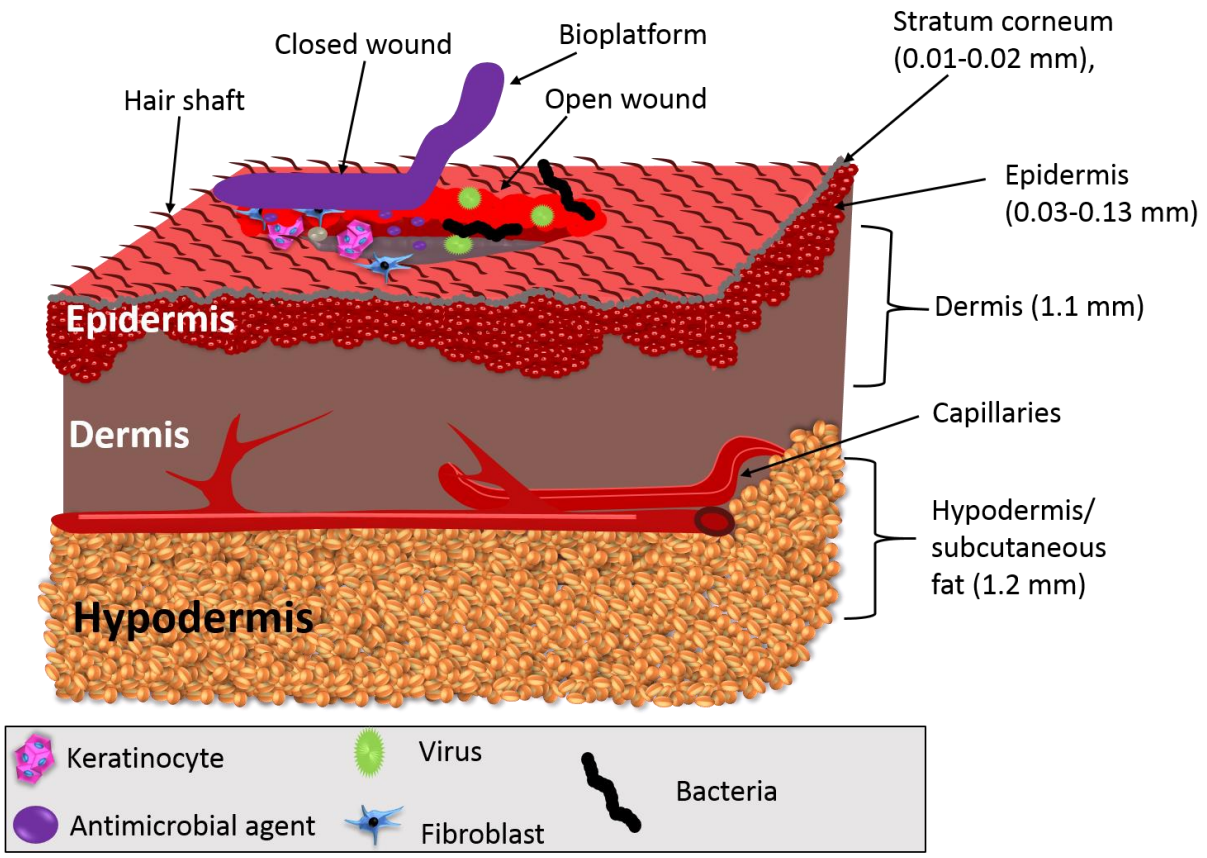


Figure 1.1. Schematic representation of layers of the skin and their thickness.

Hydrogels have drawn much attention in the tissue engineering field due to their versatile formulation strategies available to be designed into a particular form in order to achieve the purpose of the hydrogels. These strategies include but not limited to beads, nano/microparticles and scaffolds that can be used as skin regenerative hydrogels. For a hydrogel to exhibit accelerated skin regeneration properties, it should meet certain requirements such as maintaining a moist wound environment, having minimal frequency of dressing change, absorbing excess exudate from wound site, preventing secondary infection, maintaining adequate gaseous exchange, controlling the release of incorporated bioactives and lastly must assimilate ECM physicomechanical attributes in terms of elasticity and biocompatibility (Mayet et al., 2014, zohourian and Kabiri, 2008). To meet these requirements, extensive research has been conducted on various natural/synthetic polymer blends which include polysaccharides (alginates, chitin, chitosan, heparin, and chondroitin sulphate), proteoglycans and proteins (collagen, gelatin, fibrin, keratin, silk fibroin, eggshell membrane)(zohourian and Kabiri, 2008). The use of natural polymers in wound dressing applications has grabbed the attention of most researchers due to their biocompatible physicochemical and physicomechanical properties and the potential to be tailored to various systems.

Chitosan and alginate are among the most used natural polymers due to their desirable properties in the wound healing and tissue engineering field. Chitosan can be crosslinked by several molecules such as genipin, glutaraldehyde and NaTPP (Frohbergh et al., 2012, Jin et al., 2004, Liu et al., 2019, Biranje et al., 2019). The ionic character of chitosan allows for drug/supplement

incorporation via ionic interaction. The polymeric hydrophobic chain of chitosan also provide structural interactions with hydrophobic moieties of other polymers and additives. The ionic character of chitosan also allows it to interact with other polymers to form interpolymer complexes (Du et al., 2015, Alsharabasy et al., 2016). One of those polymers is sodium alginate. The anionic character of alginate enables crosslinking by calcium cations and epichlorohydrin (Costa et al., 2018, Francis et al., 2017). The ionic character of both chitosan and alginate has seen them being used in different proportions, combinations, crosslinked and allowed for immobilisation of peptides and bioactives such transferulic acid, curcumin, and tannic acid to these interpolymer complex (IPC) formulations (Wang et al., 2019b, Akbar et al., 2018, Ahmadi et al., 2017, Li et al., 2018, Gan et al., 2018).

The properties of these polymers (chitosan and alginate), crosslinkers (Calcium chloride, sodium tripolyphosphate), RGD peptide, and bioactives (transferulic acid and tannic acid) were explored in the current study to accelerate wound healing. The role of natural polymers is for enhancing the interaction between the bioplatforms and regenerating tissues. The properties of these polymers such as biocompatibility, biodegradation, adhesion and bioresorption makes them great tissue engineering candidates. The crosslinkers provide structural stabilization and the degree of crosslinking controls the release of bioactives. The role of bioactives such as tannic acid is to facilitate the mediation of the tissue remodelling in the early stages of wound healing. Trans-ferulic acid and tannic acid are phenolic agents which possess properties such as antioxidant, anti-aging, anti-inflammatory, anti-diabetic, antimicrobial and anticancer activity (Lo and Chung, 1999b, Tsou et al., 2000b, Borges et al., 2013). These properties are achieved by inhibition of cyclooxygenase and nitric oxide synthase function/expression along with the activation of nuclear factor-kappa-light-chain-enhancer B cells in both chronic and acute inflammation (Hosoda et al., 2002, Nagasaka et al., 2007, Khan et al., 2000a). The self-assembly of RGD peptide has been widely researched and it has been reported to play a crucial role in cell adhesion, and facilitating deposition of collagen in the early stages of wound healing (Agrez et al., 1991).

To this end, the biomolecules discussed above will be explored to formulate wound dressing biomaterials. The current study hypothesises that the processing of polymeric biomaterials during bioplatform fabrication has a significant effect on the resulted bioplatforms properties and performances. The significant effects includes the imroprovement of the bioplatform's properties and their performances such as acting as drug delivery systems and wound healing capabilities. To elucidate the hypothesis above, the current study proposes to develop two wound dressing bioplatforms (microparticles and scaffolds) via different fabrication approaches (partial crosslinking and ionic gelation self-assembly) and evaluate the physical, chemical, mechanical properties of these bioplatforms along with their performances such as drug release, cytocompatibility and tissue regenerating capabilities.

1.2 Rationale and motivation

There are various biomaterials that have been developed over the years for skin regeneration applications. However, they still present few limitations as skin regenerative agents. These limitations includes limited cellular and tissue attachment, cell migration, biodegradability and bioresorbability. An ideal skin tissue regenerative biomaterial/wound dressing should exhibit the following properties, (a) providing and maintaining balanced hydration levels through the absorption and control of the wound exudates, (b) facilitate gaseous exchange across the wound site, (c) prevent secondary infections, (d) control and localize the release of incorporated bioactives, and (e) demonstrate extracellular matrix (ECM) equivalent physico-mechanical

characteristics in terms of elasticity, biocompatibility, and biodegradability. Furthermore, there are properties that need to be enhanced or maintained in polymers and bioplatforms such as controlled porosity, controlled biodegradation, high fluid uptake, excellent water vapour transition rate (WVTR), thermostable, optimal hardness, controlled solubility, and optimal viscoelastic properties. To date, only a few bioplatforms can meet most of these properties and performances. This opens a gap in knowledge on the design of bioplatforms that have both ideal properties and performances. This gap can be closed by designing and developing biocompatible, biodegradable and bioresorbable bioplatforms with translation wound healing and skin tissue regenerative performances. These bioplatforms' property-performance features contributing to optimal skin regeneration can be enhanced and achieved by the use of smart environmentally friendly materials (Hoffman et al., 2000), or intelligent polymers (Kikuchi and Okano, 2002). The selection of natural based molecules could contribute greatly to the overall property-performance factors that could attain most properties of an ideal wound dressing bioplatform. The strategic selection of molecules with potential biological properties and tunable fabricated properties along with potential bioplatform performances are given in Figure 1.1 below.

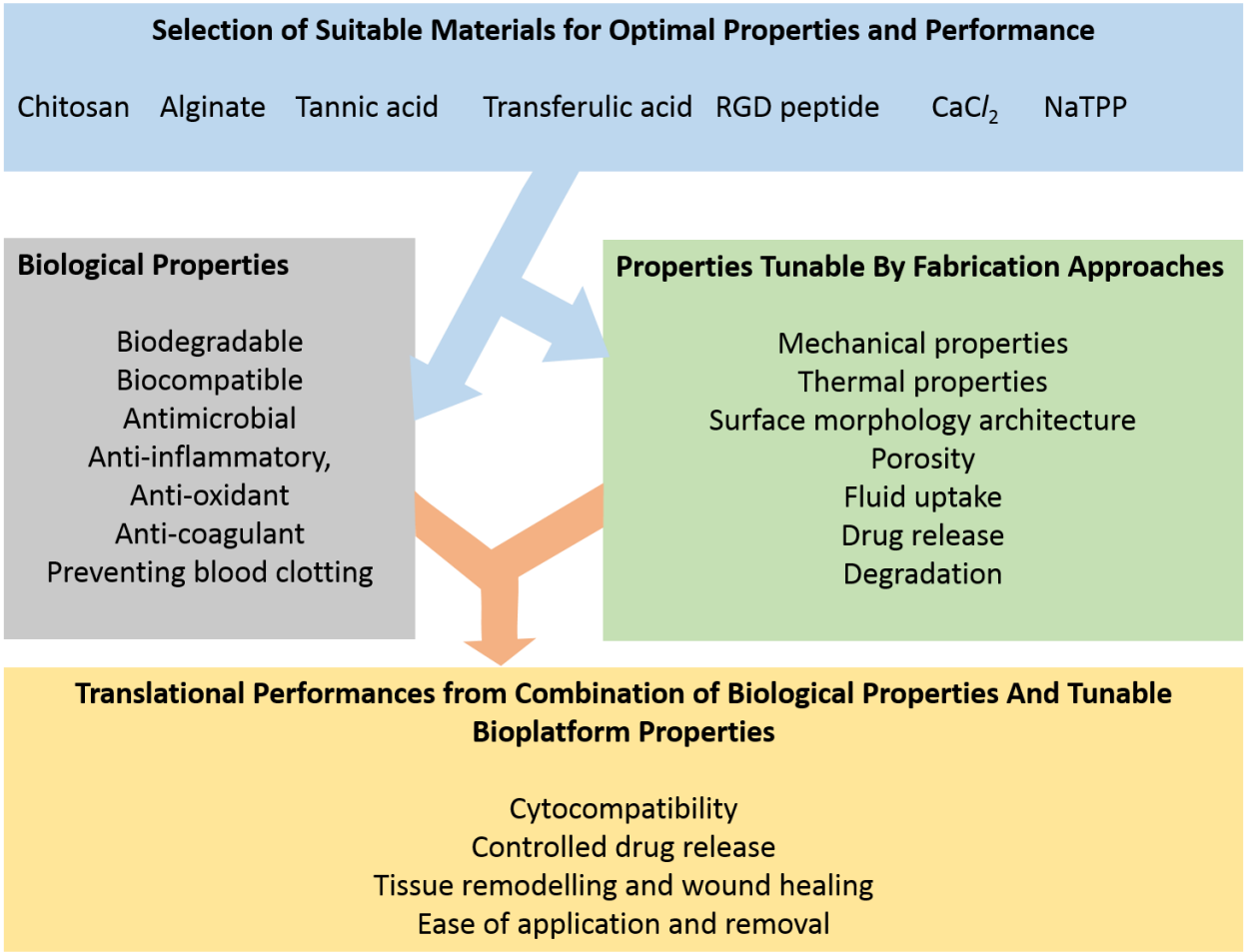


Figure 1.2. Idealistic contribution of the polymers, peptide and bioactives for improving property performances of the bioplatforms translating to optimal performance.

Tuning of the above properties requires an understanding of the polymeric properties and crosslinkers that can be blended in different ratios, sequence and other additives to attain

desirable properties and performances. Optimizing bioplatform fabrication steps could lead to controlled porosity which in turn affects the fluid absorption and cell attachment and mobility. Furthermore, these fabrication steps also influences the mechanical properties, degradation and bioresorption. These fabrication steps includes but not limited to working concentrations (Wu et al., 2010), crosslinking (Ma et al., 2003, Kumar et al., 2017), and complexation reactions (Shen et al., 2000, Florczyk et al., 2011).The current study focuses on the properties mentioned above which translate to optimal bioplatform performances. Of particular interest in this study, is the enhancement of the physical, chemical, and mechanical properties along with biological performances of the bioplatforms. Novel biocompatible bioplatforms with enhanced cytocompatibility, controlled degradation, controlled drug release, and accelerated wound healing and skin tissue regeneration will be developed and assessed. The particulate bioplatform will be developed by introducing the partially-crosslinking of natural polymers (chitosan and alginate) to fine tune the drug (transferulic acid) incorporation and improve physical properties such as high fluid uptake, particles surface area, porosity, texture of bioplatform and degradation.

The idea behind the partial crosslinking of the polymers is to allow for *in situ* formation of the hydrogel under fluid exposure. The *in situ* formation of the hydrogel infers that it can be applied to different wound types such as open wounds and deep cuts. The scaffold bioplatforms will make use of the self-assembly approach to develop a drug delivery (tannic acid), cytocompatible and biomimetic scaffold by employing RGD peptide known for its self-assembly properties and the natural polymers to co-assembly with the peptide. Similarly to the wound filling property of the *in situ* forming hydrogel, the fluid absorption property of the scaffold would allow it to assume the shape of the wound. The ultimate goal of the study is to fabricate bioplatforms with improved properties and performance as a skin regenerative material. The collective contribution of the natural polymers, peptide, and the anti-oxidant, anti-inflammatory, and anti-microbial phenolic agents will improve cell viability and facilitate tissue remodelling for optimal wound healing. A success in this study would be a development of wound dressing bioplatforms that are capable of absorbing fluid, cytocompatible, demonstrating accelerated skin repairing abilities, and painless application to the wound area. The use of inexpensive polymers and additives will assist in decreasing the cost for hydrogel production for wound dressing applications.

1.3 Hypothesis, aim and objectives

The stdudy hypothesizes that the processing of polymeric biomaterials during bioplatform fabrication has a significant effect on the resulted bioplatforms properties and performances.

The aim of the study is to develop superfast gelling and fluid absorbing wound dressing bioplatforms following targeted property-performance fabrication approaches. In order to achieve the above aim, the following objectives were undertaken:

1. To fabricate high fluid uptake, superfast gelling and cytocompatible bioplatforms by employing the partial crosslinking approach for particulate bioplatforms and solution gelation approach for self-assembled scaffold.
2. To determine the physical and chemical characteristics of the bioplatforms
3. To determine fluid uptake and degradation of the bioplatforms under simulated *in vitro* exudative conditions.
4. To evaluate the mechanical characteristics bioplatforms by exploring the matrix resilience, polymer interactions/crosslinking, elasticity and hardness of the hydrogels.

5. To evaluate the *in vitro* bioactive release of transferulic acid in particulate bioplatform and tannic acid in the self-assembled scaffold.
6. To evaluate the cytotoxicity of the bioplatforms in mouse embryonic fibroblast cell line (NIH-3T3) using the cell viability assay
7. To evaluate clinical potential of the bioplatforms by comparatively assessing their wound healing and skin tissue regenerative performances using Sprague–Dawley rat model.

1.4 Novelty of the study and potential applications of the bioplatforms

The novelty of the study lies within the use of the partial crosslinking approach to tailor bioplatform's for desirable properties translating to effective drug delivery, skin tissue regeneration and wound healing. The partial crosslinking allows for drug incorporation via ionic interaction and also allows for further interpolymer complexation due to the controlled degree of crosslinking. The crosslinking of the bioplatform prior interpolymer complexation is strategically designed to exist in powder form and only transition into an interpolymer complex hydrogel *in situ* under fluid exposure. The powder form of the bioplatforms would allow for long term storage and ease of application to wounds of different shapes via sprinkling. The scaffolds will be designed from peptide, natural polymers and polyphenol for optimal wound healing performances. The simplicity of the self-assembling scaffold fabrication approach allows for efficient production of the scaffold with malleable properties. The concept for the design of both novel bioplatforms (microparticles and scaffold) was to produce a bioplatform that can act as a wound filler with optimal properties such fluid uptake and mechanical properties required for wound healing. The incorporation of phenolic agents was to allow for fast wound remodelling at the early stages of wound healing due to the anti-oxidation and anti-inflammatory properties of the phenolic groups. Natural polymers, peptide, salt crosslinkers and polyphenols were used to improve the biocompatibility of the bioplatform and to allow the bioplatforms do degrade as the wound heals. The controlled degradation means that the bioplatform will degrade and fall off while other parts are resorbed by the skin as the wound heals. This means that the patient will not have to change the dressing frequently, and minimal scaring as the bioplatform biodegrade as the wound heals to form a scar-less skin tissue. The property-performance features evaluated and fine-tuned on the bioplatforms will contribute greatly to the wound healing and skin tissue regeneration process.

1.5. Overview of the thesis

Chapter 1: This chapter introduces the background of current research in the field of advanced tissue engineering, highlights the limitations of bioplatforms and outlines the gap in the field which is the premises for the rationale and aim for undertaking the study. Chitosan and alginate were selected as polymers of interest given their documented desirable biological properties.

Chapter 2: The use of different fabrication approaches along with polymeric properties could also enhance bioplatform properties translating to optimal performances. To this end, this chapter provides a comprehensive review of the approaches employed in bioplatform fabrication that affect property-performance factors. It provides literature correlation between fabrication approaches affecting bioplatform properties which in turn influences their performances as wound dressings. Fabrication approaches, processing parameters, supplementary agents, polymer properties, and interactions are appraised in terms of how properties and performances that are reflective of effective bioplatform are tailored for wound healing and skin tissue regeneration.

Chapter 3: This chapter follows the noted gap in designing suitable wound dressings that can be tuned for enhanced properties translating to optimal performances. Herein, a fabrication approach which produces fluid absorptive, biodegradable, cytocompatible and potentially high patient compliable bioplatform was introduced. The three-step approach namely; partial-crosslinking, lyophilisation, and pulverisation of bioplatforms was employed. The synthesis of partially-crosslinked particulate bioplatforms capable of forming an *in situ* interpolymer complex hydrogel under fluid exposure was produced. The particulate form of the bioplatform was strategically designed to be applied by sprinkling the bioplatform in the wound area to prevent pain during application. The targeted properties to be evaluated included fluid uptake, degradation, mechanical properties and cytotoxicity of the bioplatforms. The high fluid uptake, controlled degradation and the cytocompatible nature of the bioplatforms infer that the bioplatform would absorb the wound fluid/blood, degrade as the wound heals and provide optimal mechanical properties for the skin to regenerate.

Chapter 4: This chapter is a continuation from the previous chapter. Herein, the three stepped fabrication approach was undertaken to incorporate an anti-oxidant and anti-inflammatory agent (transferulic acid). This chapter focused on the performance part of the bioplatform such as acting as drug delivery system and also the ability to accelerate wound healing and skin tissue regeneration. In vitro transferulic acid release and in vivo wound healing capabilities of the particulate bioplatforms were evaluated against the control and commercially available comparative product(Pharma-Algi®).

Chapter 5: Having successfully designed a fabrication approach that improves bioplatform property-performance factors, an alternative approach was explored on the polymeric formulations to evaluate other options to produce malleable, fluid absorption, and wound healing bioplatforms. The polymeric formulations were functionalized with RGD peptide and crosslinking with tannic acid to tune them into malleable scaffolds. Herein, the self-assembly technique was employed in developing 3-D architectural scaffolds with high porosity and malleability properties. Cytocompatibility, *in vivo* tissue remodelling and wound healing performances were evaluated against a commercial product (Pharma-Algi®).

Chapter 6: This chapter outlines the properties and performance of the bioplatforms. The outcome of the research along with perspective recommendation in the field of wound dressing and skin tissue regeneration is provided in this chapter.

1.6. References

Agrez, M. V., Bates, R., Boyd, A. W. & Burns, G. 1991. Arg-Gly-Asp-containing peptides expose novel collagen receptors on fibroblasts: implications for wound healing. *Cell regulation,* 2**,** 1035-1044.

Ahmadi, F., Ghasemi-Kasman, M., Ghasemi, S., Tabari, M. G., Pourbagher, R., Kazemi, S. & Alinejad-Mir, A. 2017. Induction of apoptosis in hela cancer cells by an ultrasonic-mediated synthesis of curcumin-loaded chitosan–alginate–sTPP nanoparticles. *International journal of nanomedicine,* 12**,** 8545.

Akbar, M. U., Zia, K. M., Akash, M. S. H., Nazir, A., Zuber, M. & Ibrahim, M. 2018. In-vivo anti-diabetic and wound healing potential of chitosan/alginate/maltodextrin/pluronic-based mixed polymeric micelles: Curcumin therapeutic potential. *International journal of biological macromolecules,* 120**,** 2418-2430.

Alsharabasy, A. M., Moghannem, S. A. & El-Mazny, W. N. 2016. Physical preparation of alginate/chitosan polyelectrolyte complexes for biomedical applications. *Journal of Biomaterials Applications,* 30**,** 1071-1079.

Biranje, S. S., Madiwale, P. V., Patankar, K. C., Chhabra, R., Dandekar-Jain, P. & Adivarekar, R. V. 2019. Hemostasis and anti-necrotic activity of wound-healing dressing containing chitosan nanoparticles. *International journal of biological macromolecules,* 121**,** 936-946.

Boateng, J., Pawar, H. & Tetteh, J. 2015. Evaluation of in vitro wound adhesion characteristics of composite film and wafer based dressings using texture analysis and FTIR spectroscopy: A chemometrics factor analysis approach. *RSC Advances,* 5**,** 107064-107075.

Borges, A., Ferreira, C., Saavedra, M. J. & Simoes, M. 2013. Antibacterial activity and mode of action of ferulic and gallic acids against pathogenic bacteria. *Microbial drug resistance,* 19**,** 256-265.

Costa, M. J., Marques, A. M., Pastrana, L. M., Teixeira, J. A., Sillankorva, S. M. & Cerqueira, M. A. 2018. Physicochemical properties of alginate-based films: Effect of ionic crosslinking and mannuronic and guluronic acid ratio. *Food hydrocolloids,* 81**,** 442-448.

Du, H., Liu, M., Yang, X. & Zhai, G. 2015. The design of pH-sensitive chitosan-based formulations for gastrointestinal delivery. *Drug discovery today,* 20**,** 1004-1011.

Florczyk, S. J., Kim, D. J., Wood, D. L. & Zhang, M. 2011. Influence of processing parameters on pore structure of 3D porous chitosan–alginate polyelectrolyte complex scaffolds. *Journal of Biomedical Materials Research Part A,* 98**,** 614-620.

Francis, N. L., Hunger, P. M., Donius, A. E., Wegst, U. G. & Wheatley, M. A. 2017. Strategies for neurotrophin-3 and chondroitinase ABC release from freeze-cast chitosan–alginate nerve-guidance scaffolds. *Journal of tissue engineering and regenerative medicine,* 11**,** 285-294.

Frohbergh, M. E., Katsman, A., Botta, G. P., Lazarovici, P., Schauer, C. L., Wegst, U. G. & Lelkes, P. I. 2012. Electrospun hydroxyapatite-containing chitosan nanofibers crosslinked with genipin for bone tissue engineering. *Biomaterials,* 33**,** 9167-9178.

Gan, D., Liu, M., Xu, T., Wang, K., Tan, H. & Lu, X. 2018. Chitosan/biphasic calcium phosphate scaffolds functionalized with BMP-2-encapsulated nanoparticles and RGD for bone regeneration. *Journal of Biomedical Materials Research Part A,* 106**,** 2613-2624.

Hendriks, F., Brokken, D., Oomens, C., Baaijens, F. & Horsten, J. 2000. Mechanical properties of different layers of human skin. *Philips Research Laboratories, Eindhoven*.

Hosoda, A., Ozaki, Y., Kashiwada, A., Mutoh, M., Wakabayashi, K., Mizuno, K., Nomura, E. & Taniguchi, H. 2002. Syntheses of ferulic acid derivatives and their suppressive effects on cyclooxygenase-2 promoter activity. *Bioorganic & medicinal chemistry,* 10**,** 1189-1196.

Jin, J., Song, M. & Hourston, D. 2004. Novel chitosan-based films cross-linked by genipin with improved physical properties. *Biomacromolecules,* 5**,** 162-168.

Khan, N. S., Ahmad, A. & Hadi, S. 2000. Anti-oxidant, pro-oxidant properties of tannic acid and its binding to DNA. *Chemico-Biological Interactions,* 125**,** 177-189.

Kikuchi, A. & Okano, T. 2002. Intelligent thermoresponsive polymeric stationary phases for aqueous chromatography of biological compounds. *Progress in Polymer Science,* 27**,** 1165-1193.

Kumar, A., Lee, Y., Kim, D., Rao, K. M., Kim, J., Park, S., Haider, A. & Han, S. S. 2017. Effect of crosslinking functionality on microstructure, mechanical properties, and in vitro cytocompatibility of cellulose nanocrystals reinforced poly (vinyl alcohol)/sodium alginate hybrid scaffolds. *International journal of biological macromolecules,* 95**,** 962-973.

Li, J., Chen, J. & Kirsner, R. 2007. Pathophysiology of acute wound healing. *Clinics in dermatology,* 25**,** 9-18.

Li, N., Yang, X., Liu, W., Xi, G., Wang, M., Liang, B., Ma, Z., Feng, Y., Chen, H. & Shi, C. 2018. Tannic acid cross-linked polysaccharide-based multifunctional hemostatic microparticles for the regulation of rapid wound healing. *Macromolecular Bioscience,* 18**,** 1800209.

Liu, Y., Cai, Z., Sheng, L., Ma, M., Xu, Q. & Jin, Y. 2019. Structure-property of crosslinked chitosan/silica composite films modified by genipin and glutaraldehyde under alkaline conditions. *Carbohydrate polymers,* 215**,** 348-357.

Lo, H. H. & Chung, J.-G. 1999. The effects of plant phenolics, caffeic acid, chlorogenic acid and ferulic acid on arylamine N-acetyltransferase activities in human gastrointestinal microflora. *Anticancer research,* 19**,** 133-139.

Ma, L., Gao, C., Mao, Z., Zhou, J., Shen, J., Hu, X. & Han, C. 2003. Collagen/chitosan porous scaffolds with improved biostability for skin tissue engineering. *Biomaterials,* 24**,** 4833-4841.

Mayet, N., Choonara, Y. E., Kumar, P., Tomar, L. K., Tyagi, C., Du Toit, L. C. & Pillay, V. 2014. A comprehensive review of advanced biopolymeric wound healing systems. *Journal of pharmaceutical sciences,* 103**,** 2211-2230.

Nagasaka, R., Chotimarkorn, C., Shafiqul, I. M., Hori, M., Ozaki, H. & Ushio, H. 2007. Anti-inflammatory effects of hydroxycinnamic acid derivatives. *Biochemical and Biophysical Research Communications,* 358**,** 615-619.

Schneider, L. A., Korber, A., Grabbe, S. & Dissemond, J. 2007. Influence of pH on wound-healing: a new perspective for wound-therapy? *Archives of dermatological research,* 298**,** 413-420.

Shen, F., Cui, Y. L., Yang, L. F., Yao, K. D., Dong, X. H., Jia, W. Y. & Shi, H. D. 2000. A study on the fabrication of porous chitosan/gelatin network scaffold for tissue engineering. *Polymer international,* 49**,** 1596-1599.

Singer, A. J. & Clark, R. A. 1999. Cutaneous wound healing. *New England journal of medicine,* 341**,** 738-746.

Tsou, M. F., Hung, C. F., Lu, H. F., Wu, L. T., Chang, S. H., Chang, H. L., Chen, G. W. & Chung, J.-G. 2000. Effects of caffeic acid, chlorogenic acid and ferulic acid on growth and arylamine N-acetyltransferase activity in Shigella sonnei (group D). *Microbios,* 101**,** 37-46.

Wang, Q., Ju, J., Tan, Y., Hao, L., Ma, Y., Wu, Y., Zhang, H., Xia, Y. & Sui, K. 2019. Controlled synthesis of sodium alginate electrospun nanofiber membranes for multi-occasion adsorption and separation of methylene blue. *Carbohydrate polymers,* 205**,** 125-134.

Wu, X., Liu, Y., Li, X., Wen, P., Zhang, Y., Long, Y., Wang, X., Guo, Y., Xing, F. & Gao, J. 2010. Preparation of aligned porous gelatin scaffolds by unidirectional freeze-drying method. *Acta biomaterialia,* 6**,** 1167-1177.

Ye, R. C. 1957. The relationship of pH of the granulation tissue and the take of the skin graft. *Plastic and reconstructive surgery,* 19**,** 213-217.

Zohourian, M. M. & Kabiri, K. 2008. Superabsorbent polymer materials: a review.

CHAPTER 2

Bioplatform Fabrication Approaches Affecting Chitosan-Based Interpolymer Complex Properties and Performance as Wound Dressings

Published in Molecules

Mndlovu, H., du Toit, L.C., Kumar, P., Choonara, Y.E., Marimuthu, T., Kondiah, P.P. and Pillay, V., 2020. Bioplatform Fabrication Approaches Affecting Chitosan-Based Interpolymer Complex Properties and Performance as Wound Dressings. Molecules, 25(1), p.222.

2.1. Introduction

Wound healing is an intricate physical systematic series of skin restoration reactions necessitating translational therapeutic approaches capable of aiding the overlapping of inflammatory, migratory, proliferative, and remodeling phases for accelerating tissue filling and restoration. The wound dressing biomedical platforms (BMPs) fabricated from the wound-based translational therapeutic approaches should present an ideal tissue restoration environment such as (a) providing and maintaining balanced hydration levels through the absorption and control of the wound exudates, (b) facilitating gaseous exchange across the wound site, (c) preventing secondary infections, (d) controlling and localizing the release of incorporated bioactives, and (e) demonstrating extracellular matrix (ECM)-equivalent physico-mechanical characteristics in terms of elasticity and biocompatibility. The ideal tissue restoration environment facilitated by the dressing's property-performance relationship could easily be detected and followed via observation of the wound healing phases in acute wounds rather than in chronic wounds. This is due to prolonged or excessive inflammatory phase (Eming et al., 2007), persistent, continuous infections, drug-resistant microbial biofilms (Harding and Edwards, 2004, Wolcott et al., 2008), and the ineffective dermal and/or epidermal cells response to reparative stimuli in chronic wounds (Demidova-Rice et al., 2012).

Several property-performance factors should be considered during BMP fabrication to create an optimal tissue restoration environment. These property-performance factors include optimum viscoelasticity, bioadhesiveness, fluid absorption, controlled porosity and biodegradability (Figure 2.1). Even if these factors have been taken into account during BMP fabrication, there are still various *in vitro* and *in vivo* drawbacks such as BMP side effects, toxicity, low patient compliance and limited biodegradability as indicated in bold in Figure 2.1. These drawbacks are a growing concern in BMP fabrication and product costs. Accelerated degradation rates result in loss of tissue integrity and functions, whereas slow degradation rates can result in mechanical mismatches such as stress shielding, which can impede BMP performance (Liu et al., 2007). Therefore, the degradation rate of polymeric matrices must be coordinated with the rate of tissue formation. The performance of chitosan and chitin-based BMPs from *in vitro* cell studies and *in vivo* animal studies have displayed effective cell adhesion, biocompatibility, blood clotting control, and wound healing capabilities (Jayakumar et al., 2011). To ensure the required performance of the BMP, physicochemical and physicomechanical properties achieved via various approaches of BMP fabrication should be evaluated.

The use of polymers in fabricating BMPs has drawn enormous attention over half a century owing to their biocompatibility and ability to be tuned into various BMPs (Wichterle and Lim, 1960). Although synthetic polymers can easily be modified to facilitate certain reactions and properties, natural polymers present great advantages over synthetic polymers due to their biocompatibility, cytocompatibility, and biodegradability. The biocompatibility character of the BMPs assembled from such polymers allows them to be utilized in the construction of artificial organs and also as drug carriers (Hoffman, 2012). The investigation of BMP processing approaches has received much attention in various applications such as fibers (Sweeney et al., 2014), beads (Sankalia et al., 2007), sponges/scaffolds (Li et al., 2005), nanolayered PET films (Carneiro-da-Cunha et al., 2010), drug-loaded membranes (Ke et al., 2010), membranes for soft tissue engineering (Costa et al., 2015), and multilayers (Guzmán et al., 2011, Guzman et al., 2011). However, there is yet to be a BMP engineered that encompasses the ideal biological, physicochemical, and physico-mechanical characteristics of the wound environment (Figure 2.1). The major limitation on recent BMPs is the lack of suitable properties translating to their performance such as effective interaction with biological tissues or cells. Possible considerations that can be taken in fabricating BMPs with tunable properties translating to various performances is shown in Figure 2.1 below.

In some BMP applications, the BMP side effects may not be detected *in vitro* in toxicity studies, instead the BMPs are normally non-toxic and demonstrate effective antimicrobial activity while accelerating wound healing. Skin irritation and rash are amongst the few side effects experienced for most wound dressings. Limited biodegradability results in frequent dressing changes and in some cases the wound dressing needs to be peeled from the healing wound area resulting in bleeding. These limitations encountered in wound dressings may have originated from the approaches employed in fabricating wound dressing BMPs. Therefore, the current review aims to evaluate the properties affected by the approaches employed in fabricating chitosan-based wound dressing interpolymer complex (IPC) BMPs. In this review, the BMP fabrication approaches were evaluated for the effect on the physical properties (morphology/texture, porosity, water vapour transition rate (WVTR), swelling ratio, solubility, thermal stability, particle size, thermal degradation, and biodegradation), mechanical properties (gelling, interpolymer complexation rate, rigidity, visco-elasticity, tensile strength and elongation to break point), and performances (cytocompatibility, bioadhesiveness, antibacterial properties, bioactive release and wound closure). These assessments were proposed to provide insight into crucial considerations when designing BMPs as potential candidates for translation into clinical wound healing applications.

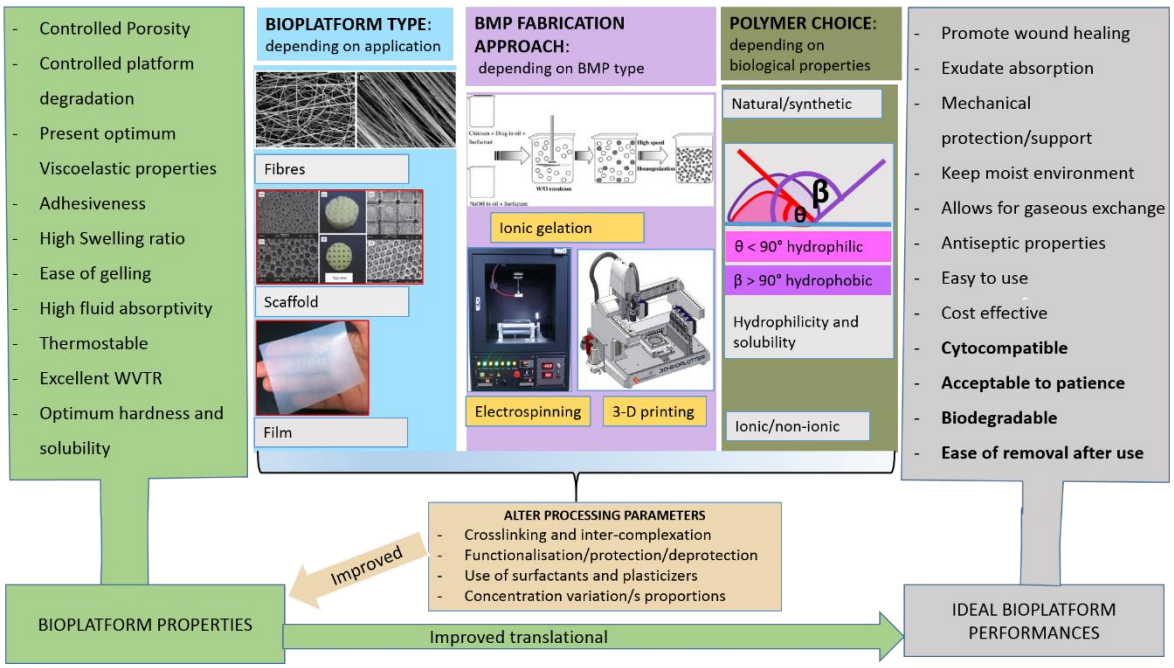


Figure 2.1. Schematic representation of steps required to design a suitable biomedical platform that meets ideal requirements for an effective wound dressing. The ideal performances highlighted in bold print are amongst the in vitro and in vivo drawbacks of fabricated BMPs. Images were taken and adapted from (Nagam Hanumantharao and Rao, 2019, Reis et al., 2006, An et al., 2015) with permission and also under the terms of the creative commons attribution 4.0 international license (https://creativecommons.org/licenses/by/4.0/).

2.2. Polymer structural interactions affecting BMP property-performance factors

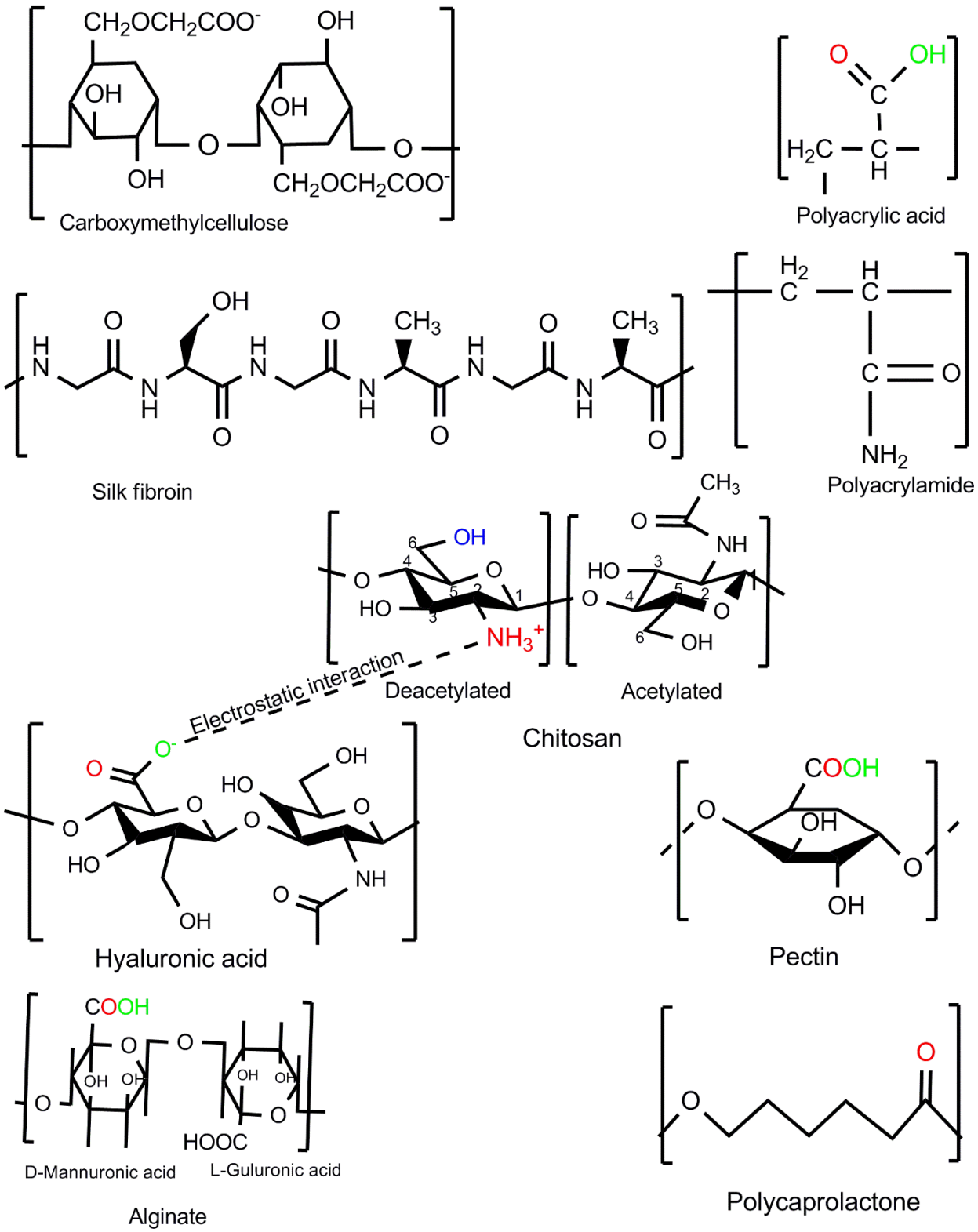
The two main classes of polymer/BMP processing approaches that affect structure and properties of BMPs are physical and chemical crosslinking (Hoffman, 2012, Khan et al., 2015). Chemical crosslinking can be divided into subclasses which includes acryloyl group polymerisation, photo-polymerization, condensation reaction, and co-molecular crosslinking; whilst physical crosslinking includes ionic interactions, hydrogen bonds and hydrophobic interactions. These types of crosslinking can produce various polymer interaction such as linear homopolymers, linear copolymers, block, random or graft copolymers, polyion–multivalent ions, hydrogen-bonded complexes, and hydrophilic networks (Hoffman, 2012). The polymer interactions can be stabilised by hydrophobic domains, physical blends, molecular recognition, self-assembling of polymers, and polypeptides (Hoffman, 2012). These interactions can be employed in fabricating several BMPs such as gauze, nano/micro particles, hydrogels, films, fibers, sponges and printed scaffolds.

Chemical crosslinking provides a permanent junction of networks during BMPs fabrication while physical crosslinking forms transient junction of networks (Matějka et al., 2014). Detailed information on the biophysical and biochemical synthesis of BMP gels with controlled properties is provided in the literature (Nuttelman et al., 2008). Chitosan chemical crosslinkers includes genipin, glutaraldehyde, vanillin, formaldehyde, Trimethylpropanetriglycidyl ether, Ethylene glycoldiglycidyl ether and epichlorohydrin, whilst physical crosslinking would include sodium tri-polyphosphate, citric acid, trisodium citrate, Oxalic acid, Sulfosuccinic acid and sulfuric acid, to name a few (Figure 2.2b). Chitosan also forms interpolymer complexes with anionic polymers such as alginate, pectin, hyaluronic acid, polyacrylamide, and carboxymethylcellulose (Figure 2.2a). The following four factors: a) crosslinking type, b) synthesis approach, c) type of BMP, and

d) polymer choice may allow for the tailoring of the BMP property-performance characteristics to meet the ideal requirements (Figure 2.1). To synthesize BMPs that meet the ideal BMP application requirements, the BMP properties can be targeted and altered until optimum performance is acquired. Selection of polymers with known optimal properties for the specified BMP application is crucial in the sense that only a few additional properties may be introduced to the BMP during synthesis. To this end, chitosan-based IPC BMPs and their fabrication approaches were evaluated owing to the fact that the properties of chitosan are well established.

The chemical composition of chitosan allows for further processing during crosslinking or interpolymer complexation. Chitosan's cationic character allows for IPC via ionic interactions with anionic polymers, enables crosslinking with sodium tripolyphosphate or glutaraldehyde, and can easily dissolve in low acetic acid concentrations (Figure 2.2, Table 2.2). The protonation of NH_2 group on the C-2 position allow for solubilisation of chitosan under acidic media (Figure 2.2) (Rinaudo, 2006). Chitosan becomes insoluble at neutral pH and the pH of chitosan controls its reactivity/complexation with metals and/or other polymers. The chelating property of chitosan depends on the physical state of chitosan, however this property depends highly on the NH_2 content and distribution on each of those physical states (Rinaudo, 2006, Rhazi et al., 2002, Kurita et al., 1979). The chelating property allows for incorporation of silver and ZnO nanoparticles for improved antibacterial properties with minimal cytotoxicity (Rhazi et al., 2002, Rabea et al., 2003). The interaction of chitosan NH_2 group with anionic groups of other polymers allow for the formation of the electrostatic complexes (—COO^{-} $^{+}NH_3$—) (Figure 2). The electrostatic interaction is crucial for drug encapsulation, controlled release, and immobilisation of cells. The biomedical properties of chitosan include tissue repair, antimicrobial, immune-enhancing, antioxidant, metal chelating, hypocholesterolemic, lipid binding, anti-inflammatory, anticancer, antitumor effects, and cellular adhesive abilities (Rabea et al., 2003, Xia et al., 2011). These biological properties may be affected negatively or positively depending on the type of crosslinkers used (ionic or chemical crosslinking), fabricating approach, and the inclusion of other compounds in the final BMP. Chitosan-based platforms are capable of healing different acute wound types (Boateng et al., 2008). These polymer properties along with BMP modifications allow for optimum performance on the BMPs.

a


Carboxymethylcellulose
Polyacrylic acid
Silk fibroin
Polyacrylamide
Deacetylated
Acetylated
Chitosan
Electrostatic interaction
Hyaluronic acid
Pectin
D-Mannuronic acid
L-Guluronic acid
Alginate
Polycaprolactone

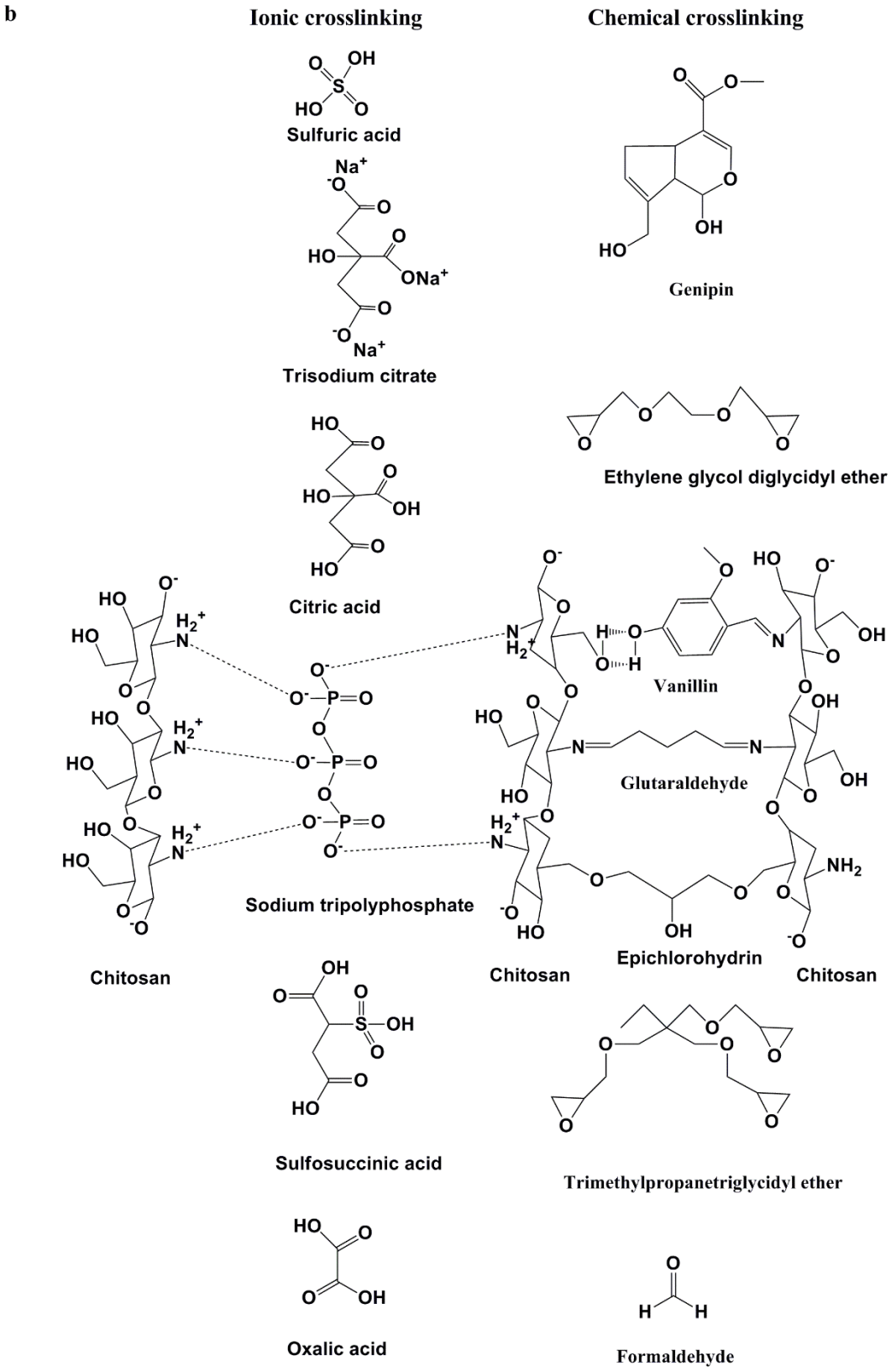


Figure 2.2. Polyelectrolyte complexations: (a) Chitosan-based interpolymer complexes formed with anionic polymers via electrostatic interactions; (b) ionic and chemical crosslinkers of chitosan.

2.3. Effect of polymer processing on physical and mechanical properties of BMPs

The order of mixing polymers and bioactives during BMP fabrication plays a crucial role in directing the extent of interpolymer complexation, texture, and the strength of the BMP. Chitosan (1% $^{w}/_{v}$) and alginate (1% $^{w}/_{v}$) were prepared separately and mixed at different proportions followed by paracetamol addition to evaluate the effect of polymer ratios on the BMP mechanical strength. The order of mixing that was followed is depicted in Figure 2.3bii. Chitosan sponge displayed more resistant to compression than the alginate or mixed BMP (Lai et al., 2003). It was concluded that the order of mixing followed in the study did not produce the columbic interaction between the two materials that has a more robust BMP structure (Lai et al., 2003). Chitosan and alginate exhibited greater breaking strengths when they were prepared separately than when they were combined in the BMP (Lai et al., 2003). The study indicated that there was no correlation between the hardness and tensile force of the BMPs as chitosan showed high rigidity (hardness) and resistance to breakage (tensile force) while alginate displayed softer texture even though it had relatively high strength (Lai et al., 2003). Furthermore, the BMPs from pristine polymers displayed regular network while the BMP from the mixture of the two polymers displayed irregular morphology (Lai et al., 2003). Changing the processing approach of the BMP as displayed in Figure 2.3ai and bi could be evaluated on the morphology and mechanical strength of the biomedical platforms.

In another study chitosan (0.4%$^{w}/_{v}$) and alginate (0.4%$^{w}/_{v}$) were prepared separately. Chitosan solution was added drop-wise to alginate solution at high stirring speed as depicted in Figure 2.3ai followed by dispersion of silver sulfadiazine while stirring. CS/Alg IPC membranes displayed optimal viscosity and accelerated silver sulfadiazine release at 1:1 CS:Alg ratio (Meng et al., 2010). One of the functions of a dressing is to control evaporative water loss from damaged skin tissue (Wu et al., 1996). The evaporative water loss is obtained by calculating the WVTR of the BMPs. The CS/Alg IPC exhibited pH and ionic strength-dependent water uptake properties with the WVTR ranging from 442 to 618 g/m^2/day (Meng et al., 2010), this WVTR range falls within the standard range for suitable wound dressings as indicated in section 2.5 below. The breaking strength of the dry membrane was 52.16MPa with the wet membrane elongation to break of 46.28% (Meng et al., 2010). The elongation to break percentage demonstrate the increase in length at breaking point of BMPs with respect to their original length (Khan et al., 2000b). These properties (elongation to break and breaking strength) gives insights on the elasticity of the BMPs. There was still no correlation between breaking strength and elongation to break of the CS-Alg BMPs as chitosan showed high breaking strength and resistance to breakage while alginate displayed no elongation to break even though it had relatively high dry breaking strength. The lack of elongation to break in alginate BMP is due to the point that alginate dissolves in water. Incorporation of silver sulfadiazine did not change the texture of the BMPs and the BMPs displayed regular morphology compared to the irregular IPC formed from different polymeric ratios (Meng et al., 2010).

Pre- and post-crosslinking of polymers dictates the mechanical strength, matrix hydration and swelling of the BMP. Chitosan/dextran films were processed followed by addition of plasticizer (polypropylene glycol) at increasing concentrations and crosslinked (glutaraldehyde) as indicated in Figure 2.3cii with slight agitation instead of stirring before air drying. Addition of plasticizer did not improve the water vapour penetration on the film however the water equilibrium content and swelling was increased (Wittaya-areekul and Prahsarn, 2006). Furthermore, the breaking strength and the elongation to break were increased (Wittaya-areekul and Prahsarn, 2006). Chitosan-based BMP was crosslinked with genipin as depicted in Figure 2.3cii. The porosity, swelling capacity, mechanical strength, biodegradation, and antimicrobial properties of the BMP were

enhanced by increasing genipin concentration while maintaining moderate WVTR (Gorczyca et al., 2014). It is apparent that pre-crosslinking is mostly employed in fabricating BMPs compared to post-crosslinking. This may be due to the fact that the post-crosslinking may be ineffective in altering BMP properties due to the already formed IPC structures, thereby rendering the crosslinkers unable to interact with the polyelectrolytes. Polymer and bioactive mixing/incorporation via the processing approach observed in figure 3biii is more common than post crosslinking owing to the different function of each added biomolecule. Polymer surface coating provides functions such as cell attachment, antimicrobial properties, tissue attachment and BMP protection from hydrolytic degradation while bioactive coating on BMPs allows for burst drug release and enhanced antimicrobial properties. Post-crosslinking can also offer properties such as enhanced water uptake and delayed surface degradation of BMP.

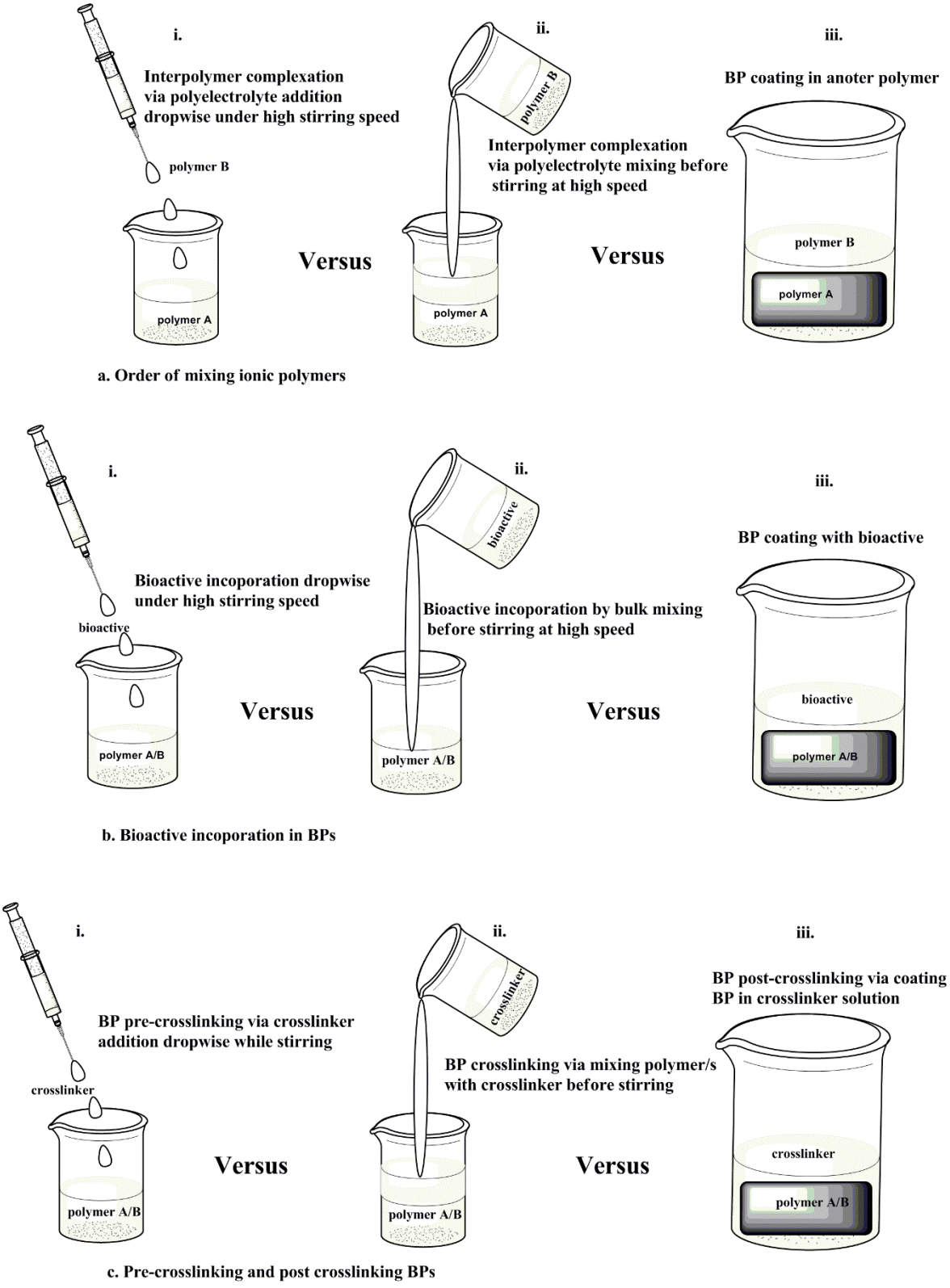


Figure 2.3. Schematic representation of the processing approaches of ionic polymers. (a) Order of mixing polymers; (b) bioactive incorporation into the IPC and (c) crosslinking of the BMP.

2.4. Fabrication approaches affecting physical and mechanical properties of chitosan-based interpolymer complexes

BMP properties are interconnected in the sense that when one property is affected by fabrication approach parameter variations, one or more additional properties will also be simultaneously or sequentially affected by such variations. This has been clearly demonstrated in literature i.e. crosslinking of chitosan BMP renders chitosan more insoluble thereby decreasing porosity, fluid uptake, swelling, degradation and drug release (Pierog et al., 2009, Gonçalves et al., 2005, Mndlovu et al., 2019). Furthermore, hydrophilicity and crosslinking density of the crosslinking agents dictate the stability and swelling behaviour of BMPs (Pierog et al., 2009). Texture and morphology gives information about hardness, adhesiveness, spreadability, and extrudability of BMPs. To demonstrate the manner in which texture is affected by these physical and physicochemical properties a study was conducted on sericin/chitosan-capped silver nanoparticles incorporated hydrogel (Verma et al., 2017). The hydrogel properties such as spreadability (work done: 4.3 ± 0.90mJ), extrudability (239.6 ± 3.93mJ), hardness (45 to 84g), and adhesiveness(19 to 39g) were directly proportional to the concentration (0.5 to 1%) of Carbopol® used in fabricating the hydrogel (Verma et al., 2017). The study demonstrated the control of polymer concentration in fabricating aesthetic pharmaceutical products with optimized texture properties.

Porosity, WVTR, fluid absorption, and swelling ratio are some of the physical properties affected by BMP fabrication and processing parameters. BMPs should have the ability to absorb fluid while maintaining a moist environment on the wound area. Fluid absorption allows the BMP to swell and degrade. When polymeric microspheres with limited fluid absorption capabilities occupy a large space in a hydrogel network, it reduces the amount of fluid uptake by the BMP (Chen et al., 2017). A recent study indicated that high concentrations of gelatin microparticles (GMs) results in a decrease on BMP swelling ratio compared to BMPs without GMs (Figure 2.4I&II) (Chen et al., 2017). This relates in a larger space occupied by GMs in the BMP network structure thereby limiting the BMP from absorbing large fluid quantities. The swelling and degradation kinetics of chitosan-based BMPs displayed that chitosan can swell and degrade more when it is combined with alginate alone than when it is with both alginate and gelatin polymers (Figure 2.4I&II). This infers that BMP degradation and swelling kinetics can be highly affected by the polymers, drugs, surfactants, and crosslinkers involved in BMP fabrication. Drug incorporation into a BMP may increase/decrease its porosity thus its fluid uptake and swelling ratio depending on the fabrication approach and processing parameters such polymer proportion and the use of crosslinkers. This has been documented in several studies such as the incorporation of Ag-ZnO into chitosan BMPs which decreased porosity from 93% to 81-88% and swelling from 26 times to 21-24 times (Lu et al., 2017b), incorporation of ibuprofen into PVA/chitosan membranes decreased porosity, however the membranes were able to maintain high WVTR (Morgado et al., 2017). Incorporation of ZnO nanoparticles into heparinised polyvinylalcohol/chitosan hydrogels increased porosity along with the swelling ratio and WVTR (Khorasani et al., 2018). Incorporation of bioactives is crucial for BMP performance therefore major decisions need to be made in deciding on which property should be prioritised over the other.

Chitosan is insoluble in water, however, processing chitosan with crosslinkers (Mndlovu et al., 2019), functionalisation to produce *O*-carboxymethyl-*N,N,N*-trimethyl chitosan (CMTMC) (Patrulea et al., 2015), and complexation with other biomolecules such as proteins (Kweon et al., 2003) and anionic polymers can enhance its water solubility. Chitosan solubility is crucial for activation of the amine groups which participate in the interpolymer complexation reaction with anionic polymers and peptides. The low aqueous solubility of chitosan allows it to be an effective

material for absorbing large volumes of water/exudate. Matrix hydration rate, fluid absorption and swelling ratio are directly proportional to the BMP physical degradation. These three factors are dependent on the BMP type i.e. sponges and fibers of larger sizes may have low hydration rate, thereby prolonging hydration of the BMP core depending on the processing of the BMP. Partially-crosslinking chitosan beads increased physical degradation by 58% in 14 days with a swelling ratio of 1891.78% in 8 hours (Mndlovu et al., 2019).

Gelling kinetics, rigidity, visco-elasticity, tensile strength and elongation to break are crucial mechanical properties of BMPs that should tuned towards that of the skin. The mechanical and physical characteristics of wound dressings should facilitate the gaseous exchange by possessing a porous structure while maintaining visco-elastic properties (Figure 2.4III&IV). The storage modulus allows for the determination of the hydrogel formation kinetics and also for distinctive analyses of stiff or soft hydrogels. A study by Lv *et al.* [42] employed the ionic gelation approach by stirring varying stock carboxymethyl chitosan (CMCS) and alginate weight ratios (4:1, 2:1, 1.5:1,1:1, 0.67:1, 0.5:1, 0.25:1) and adding D-glucono-δ-lactone (GDL) at different time points (Lv et al., 2018). CMCS-alginate-COS hydrogels were produced by addition of varying chitosan oligosaccharide (COS) concentrations following the above ionic gelation approach (Lv et al., 2018). The addition of COS resulted in two-step hydrogel formation kinetics with a more porous morphology (Figure 4III&IV) (Lv et al., 2018). The graphs in Figure 4III demonstrated that the combination of chitosan and alginate present a single step hydrogel formation kinetics, whereas a combination of chitosan, alginate and chitosan oligosaccharides presented two-step hydrogel formation kinetics. Additionally, the hydrogel was stiffer as the chitosan oligosaccharides concentration was increased (Figure 2.4 III&IV). This infers that the chitosan oligosaccharides produce a more rigid hydrogel while maintaining a porous structure. The study provided insights on how chitosan oligosaccharides can be employed in BMP fabrication to control both viscoelastic properties and morphology of BMPs.

BMP should present high rigidity (G') so as to not be easily agitated out of the wound cavity; on the other hand it should also display elasticity so as to stretch like normal skin. The tensile strength and elongation to break assessments aid in obtaining the toughness of the material in terms of the force required to stretch the BMP to break point or how much force can be applied to the BMP while still maintaining its elasticity. Investigations on alginate-chitosan hydrogels containing tetracycline-loaded gelatin microspheres indicated an accelerated gelation time with increasing gelation microspheres concentration (Chen et al., 2017). The hydrogels displayed a storage modulus (rigidity) of 9.21kPa with the BMP being more elastic than viscous (Chen et al., 2017). High elasticity to viscosity ratios in BMPs were also observed in other studies (Mndlovu et al., 2019), storage modulus at kilopascal range (Tangsadthakun et al., 2017), tensile strength at MPa range (Fan et al., 2016a) and elongation to break between 150% and 300% (Fan et al., 2016a).

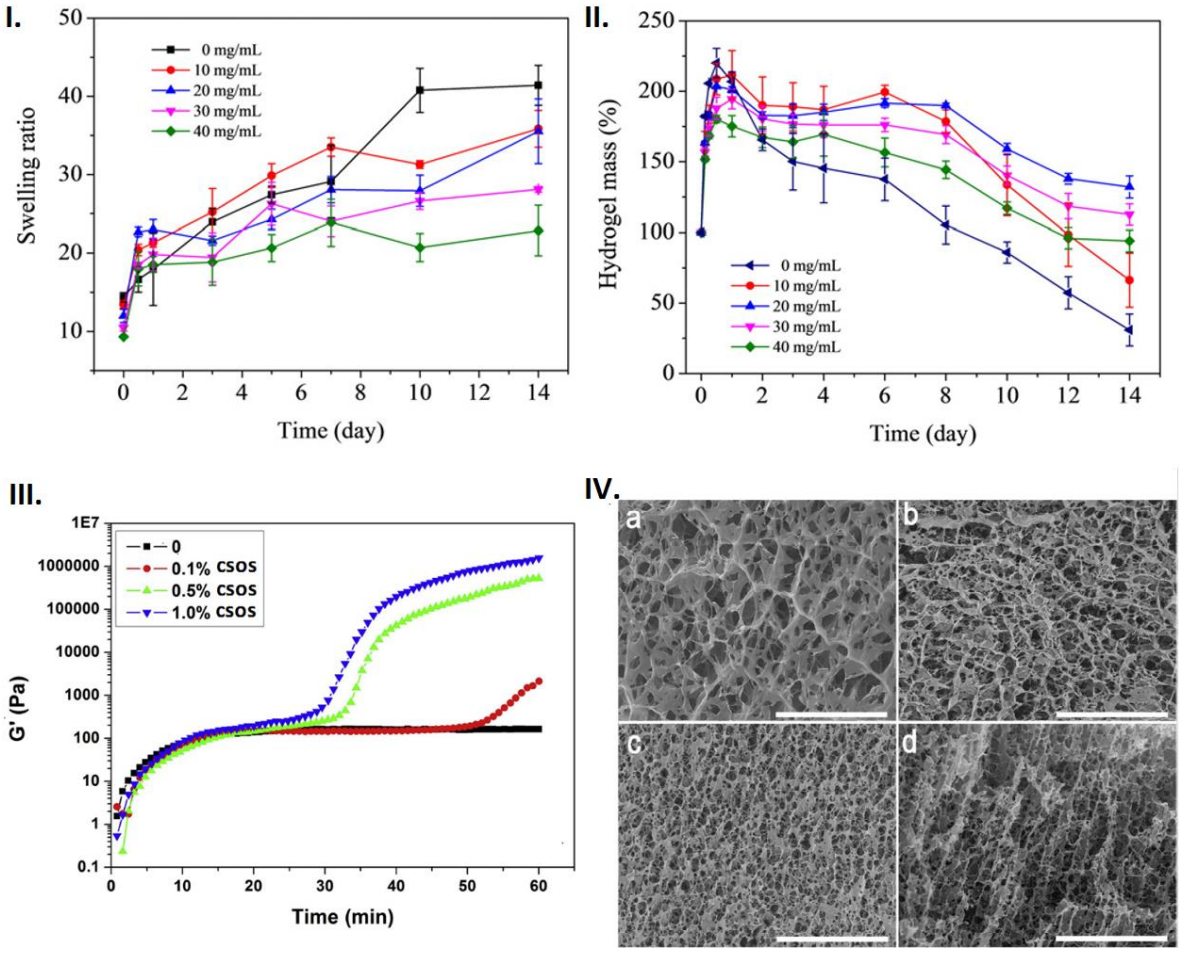


Figure 2.4. Physical and mechanical properties of chitosan-based composites: (I) Swelling and (II) degradation kinetics of tetracycline hydrochloride (TH)/oxidized alginate (OAlg)/carboxymethyl chitosan (CMCS)/gelatin microspheres (GMs) Gel with different concentration of GMs as a function of time in PBS at 37 °C. Image reproduced with permission from Chen et al. (Chen et al., 2017). (III) Gelling kinetics (of carboxymethy chitosan (CMCS)/alginate/Chitosan oligosaccharides (CSOS) hydrogels at different CSOS concentration; (IV) Porosity observed in SEM images of CMCS/alginate (1:1) hydrogels with different concentration of CSOS: (a) no COS 0.1%, (b) CSOS, (c) 0.5% CSOS and (d) 1.0% CSOS; (scale bar=40 μm). Image reproduced with permission from Lv et al. (Lv et al., 2018).

BMP performance such as cytocompatibility, bioadhesiveness, antibacterial properties, bioactive release and wound closure are collectively the target in fabricating biocompatible BMPs. These performances are highly affected by the BMP processing approaches and parameters which consequently affect the BMP properties mentioned above. Increasing bioactive concentration loading in chitosan-based IPCs may reduce cytocompatibility of BMP while enhancing antibacterial, antioxidant and anti-inflammatory properties (Khorasani et al., 2018, Shalumon et al., 2011, Lu et al., 2017b, Poornima and Korrapati, 2017, Lin et al., 2017). A balance between bioactive loading and polymer compositions may be considered in fabricating BMPs with optimal wound healing capabilities. The studies mentioned above have demonstrated that the property-performance factors are highly affected by the crosslinkers (type and concentrations), polymer combination, drug loading, and processing parameters. The polymeric physicochemical properties and processing parameters such as polymer ratios, order of mixing, solubility, temperature, and pH, and molecular weight affected the property-performance factors more than the type of formulation itself. Chitosan-based BMPs are known to facilitate wound healing and

processing of chitosan with other polymers or drugs enhances the wound healing state compared to chitosan-only BMPs (Figure 2.5) (Xie et al., 2018). Chitosan/collagen/alginate complexes have displayed enhanced wound healing performance than normal gauze, and chitosan alone (Figure 5).

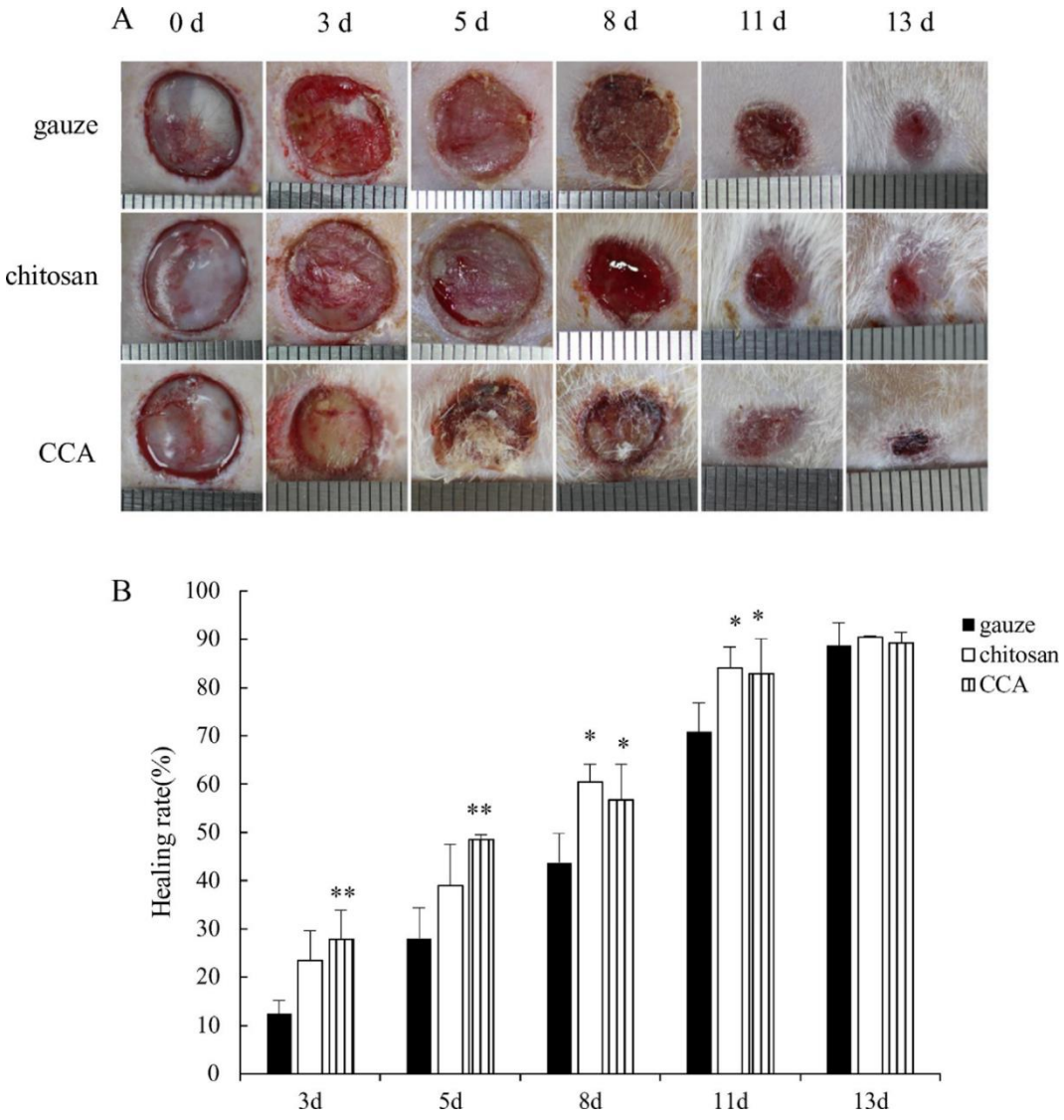


Figure 2.5. *In vivo* performance of chitosan-based composites. (a) Application of wound dressing platforms with improved properties and performance. The bilayered film/scaffold can be loaded with more than one drug owing to the presence of two ionic polymers. The nano/microparticles could also be loaded with more than one drug, and the use of particles would enable the filling of the wound area. (b) The wound healing effect of chitosan-collagen-alginate complex. Wound images were adjusted to the same scale thereby allowing for calculation of the wound area. The wound healing rate was calculated employing the following equation;:Wound healing rate = $(S_0 - St)/S_0 \times 100\%$, where S_0 represents the area of original wound and S_t represents the area of the wound at the testing time (days). Image reproduced with permission from Xie et al., (Xie et al., 2018).

2.4.1. Scaffold fabrication approaches and their physical and physicochemical properties impacting BMP performance

Polymeric scaffolds can be considered to be a biological substitute that restore, maintain and/or improve tissue function (Bonassar and Vacanti, 1998, Atala, 2004) by delivering cells, drugs, and genes (Garg et al., 2012). These biological substitutes can fabricated into many forms such as a typical 3D porous matrix, nanofibrous matrix, a thermosensitive sol-gel transition hydrogel, and porous microspheres (Garg et al., 2012). Scaffolds may be produced via several approaches such as 3-D printing and ionic gelation, further discussed in the ensuing sections.

2.4.1.1. Three-dimensional printing of chitosan-based IPC BMPs

Three-dimensional printing or bioprinting is one of the recent technologies which offers controlled consistent BMP fabrication via computerized models with high layer-by-layer scaffold design flexibility (Guvendiren et al., 2016, Berman, 2012). The advantage of this technique is the fabrication of patient-specific scaffolds with reproducible properties such as orientation and porosity (Guvendiren et al., 2016). The drawbacks of 3-D printing is the lack of variation in biomaterial inks that can be processed into self-sustaining BMPs with tunable physical, mechanical and degradation properties (Guvendiren et al., 2016). Other 3-d printing limitations such as bioink printability can be resolved by taking into account the polymeric composition and selecting a specified printing technique such as filaments for fused deposition modeling (FDM), beads (powders) for selective laser sintering (SLS), solutions and gels for direct ink writing (DIW) and solutions for stereolithography (SLA) (Guvendiren et al., 2016). The methods for printing polymers is described in depth in literature(Guvendiren et al., 2016), the current study reviews the property-performance effect of various chitosan-based IPCs.

The low mechanical resistance property of chitosan confers a limitation on its printability as an individual material. Mixing chitosan with printable polymers such as pectin or gelatin allows for optimal scaffold printability. To assess the effect of gelatin composition on the mechanical properties and biocompatibility of chitosan/gelatin scaffolds, a gelatin-chitosan polyelectrolyte complex was prepared. It was observed that high concentrations of gelatin (5% and 7.5%) displayed high yield stress and viscosity of the polyelectrolyte complex in a gel-like state ($\tan\alpha>1$) (Ng et al., 2016). It was also observed that low gelatin concentration (2.5%) resulted in poor bioprinting and sol-gel state ($\tan \alpha=G'/G''$) was below 1 which indicated that the interpolymer complex was at the sol state (Ng et al., 2016). The biocompatibility study on the HFF-1 cells indicated that the interpolymer complex with 5% gelatin was more biocompatible than chitosan alone (Ng et al., 2016).

2.4.1.2. Ionic gelation technique employed for fabrication of chitosan-based IPC BMPs

Techniques such as electrospinning and 3-D bioprinting offer more consistency in polymer processing and retaining dressing properties. However, these techniques are limited to producing certain dressing types such as nano/micro fibbers and/or scaffolds. Alternative approaches do not produce fibers with consistent properties due to variation in working parameters and elevated degree of errors. That being said, these alternative approaches such as grafting, solvent casting, solution/ionic gelation and dissolution offer a variety of dressing platforms such as films, nano/microparticles, sponges, scaffolds, foams, and sprays. Ionic gelation technique is one of the most widely employed techniques in the biomedical field owing to its non-toxic, organic solvent free, convenient and controllable BMP fabricating process (Agnihotri et al., 2004, Fan et al., 2012). This technique is in the center of polyelectrolyte (Polymer-to-crosslinker/polymer/bioactive) and interpolymer polymer complexes (polymer-to-polymer) where the positively charged primary

amino groups of chitosan ionically interact with negatively charged polyions such as sodium tripolyphosphate (TPP), alginate and hyaluronic acid (Fan et al., 2012). This technique includes a number of sub-techniques such as irradiation and functionalization of polymers or drugs which will be blended with another aqueous solution. The blending may form particles, sponges, layered hydrogels, or pastes.

Physicomechanical properties of scaffolds may differ depending on the technique employed during BMP Fabrication. However, these physicomechanical properties of BMPs should correlate with their application as wound dressings. Composition of various compounds in a blend may affect theses physicomechanical properties. To assess the effect of adding organic compounds on the mechanical properties an oxidized konjacglucomannan (OKGM)-carboxymethyl chitosan (CMCS)-graphene oxide (GO) hydrogel was produced via the Schiff-base reaction between the aldehyde of n (OKGM) and the amino of (CMCS) (Fan et al., 2016b). The increase in GO content in the hydrogel increased the tensile strength and modulus of the hydrogel. A fast gelling, high swelling ratio, minimal water evaporation rate, highly porous structure, stable hydrogel scaffold was produced (Fan et al., 2016b). The study concluded that the hydrogel scaffold was biocompatible but lacked data on rate of degradation, bioadhesiveness, and flexibility of the scaffold. In an independent study, an ice segregation induced self-assembly (ISISA) approach and freeze drying were employed for the fabrication of a glutaraldehyde 3-D Chitosan-gelatin scaffold for wound dressing applications. The scaffolds displayed pore sizes of 59 and 75µm, respectively, which decreased with increasing gelatin proportions (Nieto-Suárez et al., 2016). Equilibrium swelling state was reached in 2 hours with a maximum swelling ratio of 2450% (Nieto-Suárez et al., 2016). The scaffold displayed up to 60% biodegradation in PBS in 21 days which also increased with increasing gelatin concentration (Nieto-Suárez et al., 2016). Physical properties such as swelling, water uptake and degradation of the scaffolds could be varied for optimal performance. Dry scaffolds could be produced via different drying techniques such as lyophilization, hot air and supercritical CO_2 drying. Buffer solutions could be used in evaluating the swelling properties of the scaffolds. Scaffolds exposed to PBS (pH 7.4) buffer displayed a decrease in the swelling ratio in hot air and super critical CO_2 drying and while not affecting the lyophilized sample (Conzatti et al., 2017). The lyophilization approach also enabled high drug loading and low drug release compared to other drying techniques (Conzatti et al., 2017). This is in line with the high surface area observed in lyophilized samples which showed high water uptake thereby exhibiting high drug affinity. The low drug release may be an advantage for prolonged release to maintain the antimicrobial environment. In another study, a solvent gelation coupled with freeze-drying process was undertaken in preparing a TiO_2 loaded Collagen-Chitosan (Coll-CS) porous hydrogel scaffolds. The increase in nano-TiO_2 percentage resulted in a small pores on the scaffold thereby causing a rapid increase in swelling ratio to 925% compared to dry state (Fan et al., 2016d). The approach produced a stable scaffold having only 31% degradation in 4 weeks. The addition of nano-TiO_2 might have greatly impacted the degradation rate of the scaffold. The poor biodegradability of the scaffold may be useful in chronic wounds and normal deep cuts, burns, and or surface cut wounds. This is due to the requirement that BMPs prepared for normal wounds should possess optimum biodegradability in less than 4 weeks. Inhibition of *Staphylococcus aureus* and clustered aggregation of red blood cells to stop bleeding was observed on the scaffold which signified the improved antibacterial properties of the scaffold by adding TiO_2. The studies above revealed the manner in which different scaffold fabrication approaches can affect properties and performance of a scaffold. Furthermore, it is also evident that the use of different polymers, metals and compounds in chitosan blends may have a significant effect on the scaffold degradation and toxicity.

2.4.2. Fibre physical and physicochemical properties impacting BMP performance

2.4.2.1. Electrospun chitosan-based IPC BMPs

Electrospinning is a robust, cost effective and consistent nano- to micro-size electrostatic fibre-producing technique that employs electrical force on natural and/or synthetic polymer solutions during fibre synthesis (Reneker et al., 2000, Ahn et al., 2006). The formed layer of fibres exhibits porous structure which allow for the gaseous exchange, drainage of the wound exudates while prevention microbial organisms to enter the wound site. The controlled evaporative water loss, promoted fluid drainage in blended mats is also controlled by the electrospinning parameters such as polymer concentrations, electric field and spinning distance (Gu et al., 2009).This technique also allows for the incorporation of nano scale drugs which are controllably released in different wound healing stages (Chou et al., 2015). Porosity is one of the properties aimed to be controlled by preparing fibers via electrospinning. Although micro scaled fibres may allow microorganisms to pass through the layer, the antibacterial properties of the fibres are proposed to eradicate incoming microorganisms. An alternative approach in dealing with microbial organisms infecting the wound site, is to develop a multilayered/bilayered nanofibrous system with the upper layer protecting against external threats and acting as a mechanical structure while the lower layer can be loaded with the drug to act against inflammation and bacterial growth (Figure 2.3). To demonstrate the properties of these multi-layered BMPs a polycaprolactone- hyaluronic acid/chitosan-zein bilayered nanofibrous membrane was developed. This bilayered BMP displayed 90% porosity, 30% degradation in 7 days, Young's Modulus of 4.29 ± 1.46 MPa, WVTR of 1762.91 ± 187.50mL/m^2/day, with slow drug release (Figueira et al., 2016). This system displayed optimum translational performance such as cytocompatibility and cell growth. However, the degradation was low which infer that the dressing may require changes as the wound heals which damages the regenerating tissue thereby limiting patient compliance.

Electrospinning of chitosan (CS) with gelatin (GE) or silk fibroin (SF) draws a lot of attention in wound dressing due to its structural stability, biodegradability and biocompatibility. CS-SF polymer combination can produce fibres with high surface to volume ratio, high porosity and good inter-pore connectivity (Cai et al., 2010). Furthermore, the increase in silk fibroin content has previously displayed increased tensile strength and elongation at breakpoint of the nanofiber membranes (Park et al., 2004). Apart from blending chitosan with other polymers, nanoparticle incorporation into fibres may also affect the fibres mechanical properties. To demonstrate the effect of nanoparticles incorporated in fibres a chitosan (CS)-gelatin (GE) composite nanofiber membrane was electrospunned with magnetic Fe_3O_4 nanoparticles (NPs) to improve physicochemical and mechanical properties. The homogeneous Fe_3O_4-CS-GE nanofibers displayed well-dispersed Fe_3O_4 nanoparticles with hydrogen bonding interaction with the matrix composite, improved thermal stability, membrane's optimal mechanical properties of 155% augment of Young's modulus, 128% increase in tensile strength, and 100% boost of toughness from CS-GE (Cai et al., 2016). The increase in concentration of Fe_3O_4 nanoparticles from 1% to 4% resulted in falling down of toughness and a decrease in Young's modulus and the membrane's tensile strength (Cai et al., 2016). The addition of Fe_3O_4 nanoparticles to the CS-GE expanded the trend in the zone of inhibition with chitosan also contributing to the antimicrobial properties of the membrane (Cai et al., 2016, Xue et al., 2015, Lemire et al., 2013). Further gelatin-blended-chitosan (CS-GE) nanofiber mats produced via electrospinning and ultra-sonication displayed increased elastic modulus and elongation to break by using chitosan in the complex (Gu et al., 2016). The ultra-sonication produced enlarged porous CS/GE nanofiber mats with improved blood clotting efficiency, cell viability and cell infiltration compared with non-sonicated CS-GE nanofiber

mats (Gu et al., 2016). This provides insights into employing the ultra-sonication step to improve both physical properties and performance of the electrospunned nanofiber mats. Chitosan can decrease the average diameter of the fibre to a constant uniform size, however the glutaraldehyde crosslinking introduced non-uniformity, and decreased porosity, while increasing the roughness of the nanofiber mats (Alavarse et al., 2017, Lin et al., 2006). These studies infer that blending of chitosan with other polymers may improve certain properties of the fibres but addition of drugs and crosslinking may also negatively affect those properties. Sodium alginate (SAlg) cannot be electrospun due to its low viscosity. High sodium Alg concentrations (2%) were blended with PVA (16%) to aid the electrospinnability of sodium Alg (Bhattarai et al., 2005, Shalumon et al., 2011). Silver nanoparticles (AgNPs) were synthesised via the usage of chitosan as reducing and stabilizing agent followed by coating the chitosan-AgNP on the electrospun alginate membrane (Mokhena and Luyt, 2017). A smooth surface layer with nanoparticles on the surface which were due to crosslinking of alginate with calcium chloride was observed with high swelling ratio upto 276% and WVTR of 1586-1373g/m^2/day with increasing immersion time (Mokhena and Luyt, 2017). However, the coating of alginate nanofibers decreased the WVTR properties. A burst release was observed due to the silver particles situated on the surface of the membrane thereby exhibiting antimicrobial properties against both gram negative and gram positive bacteria however, there was no prolonged drug release (Mokhena and Luyt, 2017). The study above demonstrated that coating may improve drug release while hampering physical properties such as swelling and WVTR. This indicates that bioplatform properties may be tuned towards the application of the BMP. The application of the BMP allows for some properties to be prioritized over others.4.2.2. Ionic gelation technique employed in fabrication of chitosan-based IPC BMPs

The nanofiber formation and morphology are strongly dependent on the polymer molecular weight, blend ratios, polymer concentration, solvent choice, and the degree of deacetylation of chitosan (Ohkawa et al., 2004, Desai et al., 2008). Chitosan is known to be soluble in acetic acid solution. This highlights that the concentration of acetic used in BMP fabrication is capable of affecting property and performance of BMPs. The effect of acetic acid in CS BMP was evaluated by producing chitin-chitosan-glucan (Ch-CS-GC) nonwoven microfiber mats complexed via a wet-dry-spinning technique, which was aided by the dispersion of the polymers under vigorous stirring (Abdel-Mohsen et al., 2016). The tensile strength and elongation to break was highly affected by the amount of acetic acid used. The microfiber mats exhibited strong antibacterial properties against gram negative bacteria *Escherichia coli*, *Klebsiella pneumonia*, and Gram-positive bacteria Staphylococcus aureus with Basillus subtilis. However enhanced antibacterial activity was observed against the Gram-positive bacteria when the degree of acetylation was increased. The microfiber mats were cytocompatible as there was no cytotoxicity against the mouse fibroblast (NIH-3T3) cell line. Due to the lack of toxicity of the Ch-CS-GC mats, it was suggested that urea/sodium hydroxide aqueous solution can be utilized as green solvent for dissolution of the Ch-CS-GC complex (Abdel-Mohsen et al., 2016). There was high cell adhesion to the microfiber mats. Nondiabetic wounds in a rat model treated with nonwoven Ch-CS-GC mats exhibited 95% wound closure in 15 days which was 23% higher than the cotton gauze employed as a control. The Ch-CS-GC mat-treated diabetic rats displayed enhanced wound closure compared to untreated diabetic rats.

A simple alteration of the physical treatment of the biomaterial can transform one platform type to another. The effect of the drying approach was evaluated in a $CaCl_2$ crosslinked chitosan/alginate PEC to observe the change in porosity structures of the hydrogel. The gels were prepared by stirring the solution overnight followed by crosslinking and thereafter expose them to different

drying techniques such as Hot air drying at 50^0C, Lyophilization for 48 hours, and super critical CO_2 drying (Conzatti et al., 2017). Hot air drying resulted in compact structures with no macroporosity which led to collapsing of the PEC network structures. The collapsing of the gel structures led to no adsorption due to no or poor porosity (Conzatti et al., 2017). Freezing samples with liquid nitrogen allows for the frozen water crystals to grow and impede any polymer reorganization thereby preventing the collapsing of the PEC network structure (Conzatti et al., 2017). This produces networked sheets with interconnected pores as described in literature for each chitosan and alginate polymers (Annabi et al., 2010, Cuadros et al., 2015, Kassem et al., 2015). Super critical CO_2 drying produced a 3D nanofibrillated structure without collapsing the PEC network. However, this drying technique required replacement of water with ethanol which in turn affects the morphology of the gel such as shrinking and swelling (Robitzer et al., 2011). The swelling ratio increasing with increasing the surface area or introducing porosity. Super critical CO_2 drying with low surface area displayed the lowest swelling ratio (Conzatti et al., 2017). Collagen/chitosan/alginate (CS-Coll-Alg) fibres were prepared by coating Collagen/chitosan on alginate fibres. Optimum water absorption, increased swelling to 10 times of its dry weight, a tensile strength of 0.3638N/mm ± 0.012 N/mm and elongation to break of 4.96% ± 0.002 (Xie et al., 2018). An optimum cytocompatibility with the cell viability of 100.97% ± 0.071 and higher wound healing ratio was observed in CS-Coll-Alg composite dressing treated rats than in gauze or chitosan treated ones (Xie et al., 2018). In an unrelated study a similar concept in fibre preparation was employed; arginine surface-modified chitosan nanofibers were prepared by attachment of arginine molecules on the surface of chitosan nanofibers using sodium alginate through electrostatic interaction (Hoseinpour Najar et al., 2018). The nanofibers had an average diameter ranging from 100 to 150nm, and also showed high viscosity of 1000cps (Hoseinpour Najar et al., 2018). The high viscosity property allows for the fibres to stay on the wound cavity instead of moving way in heavily exudated wounds. The fibres did not show any burst release, however, about 85% of arginine was release in 24 hours and a wound closure of 93.8% ± 3.1 was observed after nine days (Hoseinpour Najar et al., 2018). The two studies above demonstrated the use of biocompatible polymers to fabricate biocompatible and cytocompatible BMPs with optimal properties. In these two case, biocompatibility of the BMPs were prioritised over overall BMP properties.

Table 2.1. BMP fabrication approach and properties affecting translational performance in wound dressing applications**.**

Polymer composite and approach	BMP system	Platform properties	Platform performance	Ref.
Dissolution of CS-Alg crosslinked with TTP and $CaCl_2$	Gels	Constant pore size, thermal stability, rheology, chemical stability	Biodegradation, cell proliferation, antibacterial activity	(Kurczewska et al., 2017)
mixing glycerol and molecularly imprinted polymer solutions	Gel	Drug release controlled by diffusion and swelling	Antibacterial activity but no significant data for improved wound healing	(Kurczewska et al., 2017)

Table 2.1. BMP fabrication approach and properties affecting translational performance in wound dressing applications.

Polymer composite and approach	BMP system	Platform properties	Platform performance	Ref.
Ionic gelation and irradiation	gel	Decreased crosslinking increased water uptake and platform elasticity	Inhibits Gram-positive bacteria and does not inhibits gram-negative bacteria	(Mozalewska et al., 2017)
Polymer coating and irradiation	Hydrogel	Increased elasticity, maintained 3-D porosity	Burst and sustained release, Accelerated wound healing	(Yang et al., 2017)
Polymer coating	Membrane	Increased tensile strength and reduced porosity	Antibacterial Accelerated wound healing with minimum scar formation	(Anjum et al., 2016)
Polymer coating	Scaffold	Increased solubility and water uptake	Antimicrobial and wound healing	(Xia et al., 2016)
Polymer casting	Film	transparent, soft, flexible	increased cell proliferation	(Dutra et al., 2017)
Electrospinning and ultra-sonication	Scaffold	Porous, decreased tensile strength	blood clotting efficiency, cell viability and cell infiltration	(Du et al., 2016)
Ionic gelation	Sponge	Porous, decreased tensile strength	Antibacterial properties, improved healing	(Lu et al., 2016)
solvent evaporation	Film	pH dependent swelling ration	No platform performance data presented	(Bajpai et al., 2016)
Ionic gelation and freeze-drying	Scaffold	Porous, high swelling ratio, Slow degradation	Antibacterial activity	(Fan et al., 2016c)
electrospinning	Scaffold	Micro-size porous structure	Aid cell attachment and proliferation	(Oh et al., 2016)
electrospinning	Bilayer membrane	3-D porous structure	Antibacterial properties with maintained cell viability	(Figueira et al., 2016)
grafting	-	-	Improved water uptake	(Fan et al., 2016d)
Solvent casting	Film	Enhanced tensile strength, decreased flexibility	High water uptake, aid wound healing	(Rezvanian et al., 2017)
Solvent casting	Membrane	Porous, enhanced mechanical properties	Aid cell proliferation and maintains cell viability	(Behera et al., 2017)
Ionic gelation	Hydrogel	Small pore size porous structure, elastic and biodegradable	Cytocompatible, antibacterial properties, aid wound healing, decreased blood loss	(Zhao et al., 2017)

Table 2.1. BMP fabrication approach and properties affecting translational performance in wound dressing applications.

Polymer composite and approach	BMP system	Platform properties	Platform performance	Ref.
Solvent casting	Film	Flexible, moderate drug release	Low cytotoxicity	(Rezvanian et al., 2016)
Free radical polymerisation	Sponge	Porous and flexible	90% burst release in 4 hours	(Siafaka et al., 2016)
Solvent droplet	Beads	-	Prolonged antibacterial activity	(Ozseker and Akkaya, 2016)
Ionic gelation	Sponge	Porous, high swelling ratio	Antibacterial, aid wound healing	(Lu et al., 2017b)
Ionic gelation	Hydrogel	Porous and high swelling ratio	Aid cell growth	(Huber et al., 2017)
Padding and ionotropic gelation	Gauze and nanoparticles	Moderate water uptake	Poor antimicrobial properties	(El-Feky et al., 2017)
electros pining	Scaffold	Nano size	Antibacterial, antioxidant and accelerated wound healing	(Poornima and Korrapati, 2017)
Dissolution	Sponges	Porous thereby facilitating high fluid absorption	Cytocompatible and antibacterial activity	(Shao et al., 2017)
Solution casting	Membranes	Porous, high swelling ratio	Cytocompatible	(Morgado et al., 2017)
electrospinning	Nanofiber	Porous and High swelling ratio	Antimicrobial properties	(Mokhena and Luyt, 2017)
Ionic gelation	Sponge	Porous, low tensile strength and high swelling ratio	Antibacterial properties with inflammation induction in cells	(Lu et al., 2017a)
Ionic gelation	Gel	Porous structures, high drug loading, and swelling	-	(Conzatti et al., 2017)
needle punching process	Gauze	Porous thereby facilitating high fluid absorption	Aid blood clotting, and blood absorption	(Chan et al., 2016)
Polymer coating	Membrane microfiber	Porous structure	Enhanced wound healing	(Anjum et al., 2016)
Dissolution with wet-dry-spinning	Mats	Maintained thermal stability with improved tensile strength	Enhanced wound closure and cell attachment	(Abdel-Mohsen et al., 2016)
Ionic gelation and droplet extrusion	hydrogel	Lowered swelling ratios, stable mechanical properties(G′ and G″)	Effective antibacterial properties	(Chen et al., 2017)
Ionic gelation	membranes	Higher tensile strength, acceptable fluid uptake, improved polymer dispersion and porosity	no antibacterial properties	(Zorzi Bueno and Maria Moraes, 2011)

Table 2.1. BMP fabrication approach and properties affecting translational performance in wound dressing applications**.**

Polymer composite and approach	BMP system	Platform properties	Platform performance	Ref.
Ionic gelation	Hydrogel sheets	High fluid uptake	Stimulated wound healing	(Murakami et al., 2010)
Ionic gelation approach	Hydrogel	Optimum mechanical properties, porous, and high fluid uptake	Fast re-epithelialization and formation of granulation tissues rate	(Hu et al., 2018)
Ionic gelation	Hydrogel	Optimum mechanical properties	Enhanced wound healing rate	(Lv et al., 2018)
Ionic gelation	Fibers	Optimum fluid uptake and mechanical properties	Cytocompatible, Improved wound healing and EGF expression	(Xie et al., 2018)
Ionic gelation	Nanofibers	Nano size and high viscosity	Enhanced wound healing rate	(Hoseinpour Najar et al., 2018)

The BMP fabrication approach and properties affecting translational performance in wound dressing applications is summarised in Table 2.1. The BMP biological performances such as cytocompatibility, antibacterial properties, and wound healing can be controlled by choosing specific biomolecules which can be conjugated with chitosan. The physicomechanical and physicochemical properties of different BMPs depends highly on the fabrication approach and processing parameters such crosslinking, pH, solvents, and compounds compositions. The use of different compounds (polymers, lipids, and proteins), crosslinkers and Incorporation of bioactives can also affect the property-performance factors of BMPs shown in Table 2.1. The various compounds interacting ionically with chitosan are provided in Table 2.2.

Table 2.2. Chitosan interactive compounds: polymers; bioactives and crosslinkers.

Chitosan interactive compounds (Polymers, lipids, and proteins)	Interactive bioactives	Crosslinkers	Ref.
Silk fibroin	-	-	(Park et al., 2004)
Gelatin	Fe_3O_4	-	(Cai et al., 2016)
Gelatin	-	Glutaraldehyde	(Gu et al., 2016)
Alginate	AgNPs	$CaCl_2$	(Mokhena and Luyt, 2017)
Methoxy poly(ethylene glycol)	VEGF-PDGF-BB	Visible light irradiation and glycidyl methacrylate	(Yang et al., 2017)
Partially oxidized Bletilla striatapolysaccharide	AgNPs	Genipin	(Ding et al., 2017)
Collagen	-	Alginate	(Du et al., 2016)
Collagen	-	Tannin acid	(Lu et al., 2016)
-	Ag-ZnO	-	(Lu et al., 2017b)
Glutamic acid and Hyaluronic acid	Ag	-	(Lu et al., 2017a)

Table 2.2. Chitosan interactive compounds: polymers; bioactives and crosslinkers.

Chitosan interactive compounds (Polymers, lipids, and proteins)	Interactive bioactives	Crosslinkers	Ref.
Alginate	-	$CaCl_2$	(Conzatti et al., 2017)
Collagen	TiO_2	-	(Fan et al., 2016d)
Polyethylene glycol	-	-	(Anjum et al., 2016)
Collagen	-	Transglutaminase biocatalyst	(Fan et al., 2016c)
-	TiO_2	-	(Amin, 2012, Cano et al., 2017, Behera et al., 2017)
PVA and cyclodextrins	Ibuprofen	-	(Temtem et al., 2008, Morgado et al., 2017)
Polyacrylamide	-	Itaconic acid	(Bajpai et al., 2016)
-	-	Succinic anhydride	(Xia et al., 2016)
-	Silver sulfadiazine	-	(Shao et al., 2017)
Glucan	-	-	(Abdel-Mohsen et al., 2016)
Gelatin	-	Glutaraldehyde	(Nieto-Suárez et al., 2016)
Gelatin	-	-	(Fan et al., 2016a)
Gelatin	tetracycline hydrochloride	Glutaraldehyde and oxidized alginate	(Chen et al., 2017)
Alginate	-	$CaCl_2$ as crosslinker, Pluronic F68 and Tween 80 as surfactants	(Zorzi Bueno and Maria Moraes, 2011)
Alginate	fucoidan	$CaCl_2$ and ethylene glycol diglycidyl ether	(Murakami et al., 2010)
Alginate	epidermal growth factor	$CaCl_2$ and epidermal growth factor	(Hu et al., 2018)
Alginate	D-glucono-δ-lactone	-	(Lv et al., 2018)
Alginate and collagen	-	-	(Xie et al., 2018)
Alginate	Arginine	-	(Hoseinpour Najar et al., 2018)

2.4.3. Gels, hydrogels and membranes physical and physicochemical properties impacting BMP performance

2.4.3.1. Ionic gelation technique employed in fabrication of chitosan-based IPC BMPs

The polymer crosslinking along with solution viscosity has a major effect on the properties of hydrogels such as tensile strength, bioactive release, and biocompatibility. To demonstrate how crosslinking affects hydrogel viscosity which consequently affects its property-performance (tensile strength, drug release, cell adhesion and wound healing), a growth factor-loaded chitosan-based hydrogel was prepared. Vascular endothelial growth factor (VEGF) and platelet-derived growth factor-BB (PDGF-BB) loaded visible irradiated light-cured glycol chitosan (GCS) hydrogel systems were prepared. The MPEG/GM-*g*-GC system was prepared by chemically grafting methoxy poly(ethylene glycol) acetic acid (MPEG-COOH) onto (GCS) via a condensation reaction and crosslinking with glycidyl methacrylate (GCM), followed by visible light irradiation for GCS-*g*-GCM amine chain conjugation (Yang et al., 2017). The growth factors were incorporated only on the crosslinking reagent at the photo-curing stage thereby determining the optimum GFs concentration for accelerated wound healing. The low viscosity MPEG/GCM-*g*-GCS gel system was observed with the tensile strength ranging between 56-58Pa which is around the range of desired wound healing hydrogels (Song et al., 2012). The low viscosity property of the hydrogel allowed for an *in vitro* rapid GFs release (60%) within 24 hours, followed by sustained release for 30 days. This release behaviour facilitated improved *in vivo* cell adhesion, spreading, migration and proliferation associated with accelerated wound healing (Yang et al., 2017). The hydrogel samples were compared to the commercially available product Duoderm® and the VEGF-PDGF-MPEG-*g*-GCS hydrogel displayed a faster reduction of wound size. The overall approach used in the study increased the plasticity of the hydrogel and its 3-D porous structures with adequate pore sizes being the key factors contributing to inflammatory and regenerative cells migration and growth. However, the use of radiation light either as a crosslinker or improving polymer properties may have its drawbacks in cytotoxicity. Therefore, the polymers and complexes should be radiated for a very small amount of time. The advantage of increasing the crosslinking concentration is that the pore sizes on the hydrogel decreased greatly. This is crucial for controlled water vapour transmission rate (WVTR). The hydrogels presented optimum cytocompatibility, blood compatibility and the presence of the crosslinker aided the antibacterial activity of the hydrogel. The hydrogels also exhibited adhesive properties which were 5 kPa below the commercially available fibrin glue adhesive (Greenplast®). This property allowed the hydrogel *in vivo* hemostatic properties to be enhanced by reducing the blood loss from 2025.9 ± 507.9mg in the control sample to 214.7 ± 65.1mg in the hydrogel (Zhao et al., 2017). The hydrogel displayed a comparatively fast rate of wound healing owing to the addition of polyaniline.

Gel properties are also improved via a combination of few processing parameters together with several coupled techniques. Partially oxidized *Bletilla striatapolysaccharide* (PO-BSP) blended with silver-loaded chitosan particles was achieved via employing ionic gelation in conjugation with lyophilization approach to obtain a genipin-crosslinked bilayered film for wound dressing application (Ding et al., 2017). Addition of PO-BSP increased water retention, however at 0.5% concentration it decreased the water retention ability of the bilayer films thereby indicating closing of pores in the film. Water retention also increased at acidic pH and alkaline conditions compared to basic pH conditions which is due to high porosity and protonation of the free amino group of chitosan which in turn increases the solubility of the polymer chains (Ding et al., 2017, Silva et al., 2008). Genipin crosslinking resulted in low porosity and low water retention ability of the bilayer films. The tensile strength increased in PO-BSP blended with silver loaded chitosan and the elongation to break was between 14-19%, however the increase in PO-BSP concentration

decreased mechanical properties of the film. The bilayered films displayed optimum L929 cell growth while exerting significant antibacterial activities against *S. aureus* (Gram-positive bacteria), *E. coli* and *P. aeruginosa* (Gram-negative bacteria) (Ding et al., 2017). Optimum wound healing was observed on the bilayered film owing to excellent wound exudate absorption thereby facilitating 88% wound healing by the 14th day after application (Ding et al., 2017). Although tissue re-epithelisation and cell proliferation was observed on the bilayered dressed wound, there were still several inflammatory cells present, therefore anti-inflammatory agents should be incorporated in the platform in future. There are several alginate-chitosan complexes fabricated for wound dressing application in literature (Mndlovu et al., 2019, Xie et al., 2018, Hoseinpour Najar et al., 2018). These two polymers deserve a special review owing to their several properties separately and together. Here in, a short special case for these two polymers will be reviewed. Sodium alginate readily dissolves in water and its anionic character allows it to interact with cationic polymers and ionic crosslinkers such as $CaCl_2$, $AlCl_3$ and $BaCl_2$ (Bajpai and Sharma, 2004). Alginate's anionic character allows for formation of polyelectrolyte complexes with other polymers and facilitate the chelating property with divalent metal ions (Haug and Smidsrod, 1970). The biocompatibility, hydrophilicity, and biodegradability of alginate under normal physiological conditions and its instant gelling character allows it to be employed in various wound dressing applications (Becker et al., 2001b, Li et al., 2005). The use of crosslinkers in alginate BMPs improves the properties of alginate such as maintaining moist environment, decrease bacterial infection, facilitate cell attachment and wound healing (Lee and Mooney, 2012).

Chemical crosslinking has the ability to improve BMP properties while affecting the BMP cytocompatibility. A droplet extrusion approach was undertaken in preparing tetracycline hydrochloride (TH) loaded gelatin/oxidized alginate (OAlg)-carboxymethyl chitosan (CM-CS) hydrogel (Chen et al., 2017). In order to demonstrate the effect of chemical crosslinking the tetracycline hydrochloride (TH) loaded gelatin microspheres were crosslinked with glutaraldehyde while the final hydrogel was crosslinked with oxidized alginate. The use of glutaraldehyde on the TH-loaded gelatin microspheres of 10 to 40mg/ml concentrations improved the hydrogel's properties and performance in terms of decreased gelation time and lowered swelling ratios. The storage modulus (G′) and loss modulus (G″) increased along with the microspheres concentration, reaching more than 10kPa (Chen et al., 2017). The cumulative release of tetracycline hydrochloride was lowest for the TH-Gel-OAlg-CMCS hydrogel when compared to the gelatin microspheres (Chen et al., 2017). This was indicative of the controlled release by incorporation of the gelatin microspheres into the hydrogel, thereby decreasing the hydrogel's inhibition zone diameter against *E. coli* and *S.aureus*. However, the sustained release of tetracycline hydrochloride presented effective antibacterial activity against the *E. coli* and *S.aureus*.

Calcium chloride ionically crosslinks alginate thereby forming insoluble alginate. Sodium alginate, chitin, chitosan, and fucoidan were mechanically blended at a ratio of 60:20:2:4 w/w with a pestle and mortar and allowed to form a paste when exposed to water (Murakami et al., 2010). The paste was crosslinked with $CaCl_2$ and ethylene glycol diglycidyl ether which formed hydrogel sheets. The alginate/chitin/chitosan/fucoidan fibers displayed high fluid absorption (8mL in 18 hours) compared to a commercial product based on calcium alginate fibers (Kaltostat®) (Murakami et al., 2010). Human dermal fibroblast cells (DFCs) and dermal micro-vascular endothelial cells (DMVECs) did not attach and grow on the alginate/chitin/chitosan/fucoidan sheets; however, the cells grew well adjacent to the fibers. The fibers were elastic and did not deform during wound healing (Murakami et al., 2010). Furthermore, wound contraction, re-epithelialization, stimulatory effects on granulation and capillary formation on day 7 were significant ($P<0.05$ and $P<0.01$ for granulation and capillary formation, respectively) on the

alginate-chitin-chitosan-fucoidan fibres compared to calcium alginate fibers (Kaltostat®)(Murakami et al., 2010). The study demonstrated the use of calcium chloride as an ionic crosslinker and fluid absorption was enhanced owing to the insoluble nature of crosslinked alginate.

Crosslinking can improve mechanical properties of hydrogels. To demonstrate this effect, N-carboxymethyl chitosan (CMCS) and alginate-based hydrogels were prepared via both electrostatic interaction and divalent chelation with epidermal growth factor (EGF) (Hu et al., 2018). CMCS/Alg crosslinked with $CaCl_2$ exhibited a G′ value below 30Pa, indicating a fluid (not a gel) state due to low crosslinking density (Hu et al., 2018). The hydrogels displayed steady increase on the storage modules (G′), loss modulus (G″), and complex viscosity (η*) at initial strain when the crosslinking moieties (either electrostatic or divalent crosslinking) were increased (Hu et al., 2018). This is indicative of the higher crosslinking degree with a dual crosslinking approach which increases the viscosity and elasticity of the hydrogel. Furthermore, the increase in Ca^{2+} moieties decreased the strain of the hydrogel from 60% to 5% (Hu et al., 2018). An optimum storage modulus (G') of about 400Pa was observed on the on CMCS-Alg-EGF hydrogel which also displayed 3-D structure with irregular pore sizes (pore diameter of 50-100µm) (Hu et al., 2018). A cell proliferation rate of about 110% on mouse fibroblast (L-929) cells was observed on the hydrogel, and the addition of EGF facilitated the sustained proliferation rate with less than 1% hemolysis ratio (Hu et al., 2018). Blood absorption, fastest re-epithelialization and formation of granulation tissues rate was observed on the hydrogel. The study indicated the dual crosslinking with growth factors and organic compounds which could be a new trend to be adopted in the wound dressing field.

Interpolymer complexation allows for the formation of a hydrogel without the aid of crosslinkers or surfactants. CMCS and alginate formed an interpolymer complex hydrogel when exposed in D-glucono-δ-lactone (GDL) (Lv et al., 2018). The addition of chitosan oligosaccharides to the hydrogel increased the storage modulus to an equilibrium of 170Pa, increased proliferation of human umbilical cord mesenchymal stem cells (HUMSCs), increased thickness and integrity of epidermal tissue, increased formation of collagen fibres, and enhanced expression of vascular endothelial growth factor (Lv et al., 2018). The addition of GDL resulted in a major increase in storage modulus to 6100Pa (Lv et al., 2018), which is too high for wound dressing applications. The high concentrations of chitosan oligosaccharides resulted in cytotoxicity. Moreover, gels do not possess high fluid uptake which may limit the hydrogel in wounds that have high exudate volume. A chitosan/alginate membrane was prepared via the ionic gelation approach. The dispersion of alginate was enhanced by the use of surfactants such as Pluronic F68 and Tween 80 followed by crosslinking with $CaCl_2$. The effect of the surfactants on the properties of the membrane were reported. The membrane treated with Tween 80 had a the highest tensile strength of about 1.5 MPa, elongation at break of 2.1%, fluid uptake from 590 to 1370%, and the membrane increased in thickness up to 3.9 times when immersed in water (Zorzi Bueno and Maria Moraes, 2011). The membranes treated with Pluronic F68 had a tensile strength of 1MPa, elongation at break of 2%, fluid uptake from 774 to 1380% and displayed increased thickness of about 3.2 times after exposure to water (Zorzi Bueno and Maria Moraes, 2011). The tensile strength of both membranes were too high for wound dressing applications, however, the fluid uptake were still at the acceptable range. Although the porosity was not calculated, both membranes were porous, the membrane treated with Pluronic F68 displayed higher porosity than the one treated with Tween 80. The membranes treated either Pluronic F68 or Tween 80 displayed no zone of inhibition against *Pseudomonas aeruginosa* and *Staphylococcus aureus*

(Zorzi Bueno and Maria Moraes, 2011). This implies that the membranes did not possess any antibacterial properties, therefore an antibacterial drug may be introduced to the membranes.

2.4.3.2. Polymer coating, grafting, solvent evaporation, and solvent casting approaches in fabricating chitosan-based IPC BMPs

Polymer processing techniques can be used sequentially or as substitute for one another. Polymers can be coated with nanoparticles or other polymers. Preparation of biomaterials from such polymers may require both solvent casting and solvent evaporation for improved physicochemical properties. To demonstrate how these physicochemical properties are affected by these techniques a membrane was prepared via the grafting technique. A microbial transglutaminase (MTGase) biocatalyst was used in grafting Collagen peptide (CollP) to hydroxypropyl chitosan (HPCS) for wound dressing application. The degree of substitution on the HPCS-CollP complex affected the moisture-absorption and retention ability, a mass ratio of 0.34 MTGase:HPCS displayed optimum moisture-retention ability and cell viability (Fan et al., 2016c). These two processing approaches displayed improved physical and mechanical properties along with fluctuating BMP performance. In a different study, Ibuprofen loaded PVA/CS membranes were prepared via the solution casting method as described in literature (Temtem et al., 2008, Morgado et al., 2017). The membranes displayed large average pore diameter, high porosity, and high swelling ratio (up to 350%) at acidic pH conditions with a far offset WVTR (Morgado et al., 2017). A remarkable 60% degradation was observed in 7 days and no further degradation was observed from day 7 to day 14. Optimum elongation to break of 600% was observed and a low Young's modulus representing the high elasticity of the membrane at acidic pH conditions which remained stable for 21 days. The membrane displayed poor mechanical properties at pH 7.4 and basic pH conditions (Morgado et al., 2017). The drug release studies displayed that the release followed the Fickian diffusion mechanism whereby the solvent transport rate or diffusion is much greater than the process of polymeric chain relaxation (Morgado et al., 2017). Normal human dermal fibroblasts (NHDF) cells adhered and grew in the presence of the membranes and cell viability was not affected by loading ibuprofen into the membranes. Decrease in wound size with no signs of inflammation or the presence of reactive granulomas was observed in wounds treated with ibuprofen-loaded β-cyclodextrins-PVA-CS membranes (Morgado et al., 2017). This study showed that the addition of drugs on BMPs may improve its property and performance. However, specific concentrations and pH conditions should be considered.

The use of crosslinkers may also contribute to the soluble/insoluble character of BMPs at certain pH conditions and this can lead to high fluid absorption. A solvent evaporation method was employed in preparation of [poly(acrylamide(AAm)-co-itaconicacid(IA)] Inter-polymer complex (IPC) films to assess the effect of crosslinking and pH on the BMP swelling and fluid uptake.. The method allowed for preparation of uncrosslinked poly(AAm-co-IA) copolymer which can be complexed with CS solution and having cationic acid as a crosslinking agent. The presence of these acids increased the solubility of the complex and cause better dissolution thereby decreasing water absorption. Moreover, pH conditions allows for optimum swelling at low and higher pH conditions with water vapour transmission rates (WVTR) ranging between 6000–6645g/m^2/day (Bajpai et al., 2016). Although the WVTR were high for the IPC film, the water absorption should be shifted to alkaline conditions by varying polymer proportions and the amount of crosslinking agent. The pH dependent swelling ratio allows for the film to be optimized to best suit the wound environment type. These approaches demonstrated the use other polymers and crosslinkers as potential chitosan complexes for improved biomaterial properties.

2.4.4. Sponges physical and physicochemical properties impacting BMP performance

2.4.4.1. Ionic gelation technique employed in fabrication of chitosan-based IPC BMPs

Chitosan can form an IPC with collagen which can be further crosslinked with glutaraldehyde, epichlorohydrin and tannin acid. Coll-CS blend sponges were crosslinked with tannin acid and freeze-dried. A uniform texture with abundant pores sizes ranging between 145–240 μm was observed on the sponges with 60 times swelling ratio than the dry ones (Lu et al., 2016). However, the hydrophilicity of the sponges resulted in them forming a gel when immersed in water. The sponges were not thermally stable, and showed low tensile strength and elongation to break (Lu et al., 2016). The Coll-CS sponges displayed improved antibacterial properties due to the rough surface property of the sponge which prevented bacterial replication, and the presence of tannic acid and chitosan aided this antibacterial property. The histological analyses of the Coll-CTS sponges displayed improved wound healing in 12 days with minimal cytotoxicity. The antimicrobial property of chitosan-based sponges is also improved by adding silver. AgNP-loaded chitosan-l-glutamic acid (CSG)-hyaluronic acid (HA) IPC sponges were prepared to evaluate silver's effect on the properties of the sponges. Addition of silver on the sponges change the porous structures smooth surface and increased the pore sizes on the sponge to 150–250μm and folded structures. A tensile strength of 0.04MPa and elongation to break of 300% was observed, which suggested resistance to deformation properties (Lu et al., 2017a). The sponges displayed a high swelling ratio of 2900% owing to their high porous structure, however addition of silver nanoparticles decreased the swelling ratio (Lu et al., 2017a). CSG without AgNPs displayed no antibacterial properties while the addition of AgNPs at increasing concentrations increased the inhibition zones against *E. coli* and *S. aureus* (Lu et al., 2017a). The sponges were also cytocompatible as they displayed 80% L929 cell viability in 24 hours indicating low toxicity (Lu et al., 2017a). However, the cell viability may have decreased as more silver was released by the sponge. The *in vivo* studies displayed ulceration and edema with 5% contraction in wounds treated with the gauze (control) in 3 days whereas the wounds treated with the sponges exhibited wound healing with calluses, slight inflammation and up to 69% wound contraction at day 3, with crusting observed in 11 days (Lu et al., 2017a).

In a different study, chitosan/silver sulfadiazine (CS-AgSD) composite sponges were prepared by the dissolution technique and freeze drying. An 80% porous three-dimensional network structures were observed on the sponges with 2% porosity decrease due to AgSD loading (Shao et al., 2017). The swelling of 3980% was observed on the sponges after 4 hours and also decreased with incorporation of AgSD (Shao et al., 2017). Addition of silver to the sponges exhibited antibacterial activity against *E. coli ATCC 25922, C. albicans CMCC(F) 98001, S. aureus ATCC 6538 and B. subtilis ATCC 9372* while maintaining more than 84% of HEK293 cell viability (Shao et al., 2017). In another study, gamma irradiation crosslinking was employed in fabricating chitosan (CS)-gelatin (Gel)-polyvinyl alcohol (PVA) hydrogels to assess its effect on the BMP properties. The tensile strength, elongation to break, and gel content decreased with increasing the CS/Gel ratio and a maximum of 85% gel content was reached at irradiation dose of 40 KGy (Fan et al., 2016a). A 3-D microporous structure of the hydrogel allowed for small water evaporation rate with saturated swelling reached in 24 hours (Fan et al., 2016a). A low blood clotting index was observed which enabled for optimum coagulation. This hydrogel is useful in bleeding wounds, however it can be challenged by wounds with larger volume of exudates which may disturb the porous network of the sponge

Chitosan and alginate are natural polymers that are widely used for interpolymer complexation to produce optimum BMP performance such as cell adhesion, spreading and wound healing (Cao et al., 2011). To demonstrate performance of such biomaterials, collagen (Coll) was sequentially

complexed with both natural crosslinkers chitosan (CS) and alginate dialdehyde (ADA) for thermostability and antibacterial properties. A ten-fold water uptake was observed on the sponges which was crucial for blood clotting and wound healing. A higher denaturation temperature (Td) and 70% antibacterial activity associated with the higher degree of crosslinking was observed on the complex due to addition of ADA as a crosslinking agent (Du et al., 2016).

2.4.4.2. Phase separation and grafting approach for the fabrication of chitosan-based IPC BMPs

A modified thermally-induced phase separation approach was undertaken in fabrication of absorbable/non-absorbable levofloxacin-loaded chitosan/ 2-hydroxyethylacrylate (CS-g-PHEA) sponges as a topical wound delivery dressing. The sponges displayed an average pore size diameter ranging between 152 µm and 225µm which greatly decreased with levofloxacin loading. Sixty percent of the PHEA was grafted into chitosan rendering the sponge partially soluble in alkaline conditions with a saturated swelling ratio of 750% in 4 hours, which demonstrated a major weight loss after 4 hours (Siafaka et al., 2016). The sponge exhibited 80% degradation in the first day which was due to the degradation of chitosan by lysozyme. The low tensile strength indicated the poor stability of the sponge, which was improved by addition of PHEA, thereby rendering the sponge more flexible. A complete levofloxacin loading was achieved in 6 hours whilst it was rapidly released in the first hours with 90% burst release thereby inhibiting bacterial (*P. aeruginosa and S. aureus*) growth with unquantified L929-fibroblast cells viability after 24 hours (Siafaka et al., 2016). Although the sponge demonstrated antibacterial activity, it may be toxic in a long run and the study only presented antibacterial activity and cytotoxicity for only 24 hours which is not long enough to make a conclusive decision about the sponge performance as a potential wound dressing.

2.5. Standard BMP properties for wound dressing applications

The properties of the BMP should be close to those of human skin. Most BMPs possess high strengths compared to the skin, which impairs cellular interactions with the BMP. The tensile strength of BMPs should be at Pascal range, rather than a kilo or mega Pascal range. When the BMP presents extended elongation to break, it implies that the BMP is elastic which is crucial for skin regeneration. The mentioned studies above demonstrated that the tensile strength should be around 56-58Pa. The swelling ratio could be varied to best fit certain wound types. However, a swelling rate of 100-900% is acceptable. The BMP hardness, porosity and solubility can be varied to suit specific dressings and interactions. The WVTR for normal skin is 204 g/m^2/day and for wounded skin from 279 to 5138g/m^2/day depending on the type and nature of the wound. Therefore, the BMP WVTR should proposedly be 250–2500g/m^2/day. All the BMP types such as scaffold/sponge/fiber/membranes, gels, nanoparticles, microparticles, beads/macromatrices, and gauze should adhere to these properties in order to facilitate optimum interaction with the wound environment.

2.6. Concluding remarks

BMP design considerations for improving property-performance factors should be taken into consideration during BMP fabrication. The studies reviewed demonstrate that BMP properties and their translational performance are highly affected by the BMP type, polymer and additives conjugation choices, fabrication approach and processing parameters. All these factors are interconnected in producing biomaterials with optimum properties and performances. Different biomedical conditions require different biomedical platforms for treatment. A drug delivery platform may require a steady release for chronic treatments and a burst release for pain relieving applications. This implies that the platform type dictates the release profile which also depends on the fabrication approach. The fabrication approach may yield BMPs with drugs situated on the

surface or in case of particles, the drug would be incorporated inside the particles. The type of interaction between drugs, crosslinkers, and polymers may also affect the application of the BMPs. In cases where there is strong interaction (covalent interaction) between drug molecules and polymers, the drug may release slowly or require other molecules which the drug presents a high affinity for. The processing parameters such as concentration, temperature, pH, conductivity, type of crosslinkers and quantities highly affect the properties of biomaterials. As described in the above studies, the use of different crosslinkers and concentrations may increase or decrease the porosity, polymer interactions, BMP strength, and subsequently BMP performance such as degradation, drug release, and wound healing. It is advantageous to conjugate polymers with different properties which further improves the BMP properties and performance. However, the interaction of the polymers should not emanate in the release of toxic derivatives after degradation. The selection of additives such as growth factors, antibiotics, plasticizers, metal ions and crosslinkers should solely be for improving the properties and performance of the BMPs with minimum *in vitro* or *in vivo* toxicity. Various platforms can be optimally produced by a selected the number of polymers; therefore, it is crucial to select the best polymers for a specific platform. However, modification of polymers via crosslinking, ionization and/or functionalization can render many polymers fit to the production of many BMPs. The studies reviewed demonstrated that modifications of the polymer or complex may decrease other properties and performances such as porosity, swelling, gelation, adhesiveness, and degradation. Therefore, a degree of polymer/complex modification may be applied to improve those properties.

2.7. References

Abdel-Mohsen, A., Jancar, J., Massoud, D., Fohlerova, Z., Elhadidy, H., Spotz, Z. & Hebeish, A. 2016. Novel chitin/chitosan-glucan wound dressing: Isolation, characterization, antibacterial activity and wound healing properties. *International journal of pharmaceutics,* 510**,** 86-99.

Abdillahi, S. M., Balvanović, S., Baumgarten, M. & Mörgelin, M. 2012. Collagen VI encodes antimicrobial activity: novel innate host defense properties of the extracellular matrix. *Journal of innate immunity,* 4**,** 371-376.

Aderibigbe, B. & Buyana, B. 2018. Alginate in Wound Dressings. *Pharmaceutics,* 10**,** 42.

Agarwal, V., Siddiqui, A., Ali, H. & Nazzal, S. 2009. Dissolution and powder flow characterization of solid self-emulsified drug delivery system (SEDDS). *International journal of pharmaceutics,* 366**,** 44-52.

Agnihotri, S. A., Mallikarjuna, N. N. & Aminabhavi, T. M. 2004. Recent advances on chitosan-based micro-and nanoparticles in drug delivery. *Journal of controlled release,* 100**,** 5-28.

Agrez, M. V., Bates, R., Boyd, A. W. & Burns, G. 1991. Arg-Gly-Asp-containing peptides expose novel collagen receptors on fibroblasts: implications for wound healing. *Cell regulation,* 2**,** 1035-1044.

Ahmadi, F., Ghasemi-Kasman, M., Ghasemi, S., Tabari, M. G., Pourbagher, R., Kazemi, S. & Alinejad-Mir, A. 2017. Induction of apoptosis in hela cancer cells by an ultrasonic-mediated synthesis of curcumin-loaded chitosan–alginate–sTPP nanoparticles. *International journal of nanomedicine,* 12**,** 8545.

Ahmed, S. & Ikram, S. 2016. Chitosan based scaffolds and their applications in wound healing. *Achievements in the life sciences,* 10**,** 27-37.

Ahn, Y., Park, S., Kim, G., Hwang, Y., Lee, C., Shin, H. & Lee, J. 2006. Development of high efficiency nanofilters made of nanofibers. *Current Applied Physics,* 6**,** 1030-1035.

Akbar, M. U., Zia, K. M., Akash, M. S. H., Nazir, A., Zuber, M. & Ibrahim, M. 2018. In-vivo anti-diabetic and wound healing potential of chitosan/alginate/maltodextrin/pluronic-based mixed polymeric micelles: Curcumin therapeutic potential. *International journal of biological macromolecules,* 120**,** 2418-2430.

Akiyode, O. & Boateng, J. 2018. Composite biopolymer-based wafer dressings loaded with microbial biosurfactants for potential application in chronic Wounds. *Polymers,* 10**,** 918.

Alavarse, A. C., De Oliveira Silva, F. W., Colque, J. T., Da Silva, V. M., Prieto, T., Venancio, E. C. & Bonvent, J.-J. 2017. Tetracycline hydrochloride-loaded electrospun nanofibers mats based on PVA and chitosan for wound dressing. *Materials Science and Engineering: C,* 77**,** 271-281.

Alsharabasy, A. M., Moghannem, S. A. & El-Mazny, W. N. 2016. Physical preparation of alginate/chitosan polyelectrolyte complexes for biomedical applications. *Journal of Biomaterials Applications,* 30**,** 1071-1079.

Amidon, G. E. 1995. Physical and mechanical property characterization of powders. *DRUGS AND THE PHARMACEUTICAL SCIENCES,* 70**,** 281-281.

Amin, K. A. M. 2012. Reinforced materials based on chitosan, TiO2 and Ag composites. *Polymers,* 4**,** 590-599.

An, J., Teoh, J. E. M., Suntornnond, R. & Chua, C. K. 2015. Design and 3D printing of scaffolds and tissues. *Engineering,* 1**,** 261-268.

Anjum, S., Arora, A., Alam, M. & Gupta, B. 2016. Development of antimicrobial and scar preventive chitosan hydrogel wound dressings. *International journal of pharmaceutics,* 508**,** 92-101.

Annabi, N., Nichol, J. W., Zhong, X., Ji, C., Koshy, S., Khademhosseini, A. & Dehghani, F. 2010. Controlling the porosity and microarchitecture of hydrogels for tissue engineering. *Tissue Engineering Part B: Reviews,* 16**,** 371-383.

Anseth, K. S., Bowman, C. N. & Brannon-Peppas, L. 1996. Mechanical properties of hydrogels and their experimental determination. *Biomaterials,* 17**,** 1647-1657.

Atala, A. 2004. Tissue engineering and regenerative medicine: concepts for clinical application. *Rejuvenation research,* 7**,** 15-31.

Augst, A. D., Kong, H. J. & Mooney, D. J. 2006. Alginate hydrogels as biomaterials. *Macromolecular bioscience,* 6**,** 623-633.

Baek, K. Y., Kamigaito, M. & Sawamoto, M. 2002. Synthesis of star-shaped copolymers with methyl methacrylate and n-butyl methacrylate by metal-catalyzed living radical polymerization: Block and random copolymer arms and microgel cores. *Journal of Polymer Science Part A: Polymer Chemistry,* 40**,** 633-641.

Bairagi, U., Mittal, P., Singh, J. & Mishra, B. 2018. Preparation, characterization, and in vivo evaluation of nano formulations of ferulic acid in diabetic wound healing. *Drug development and industrial pharmacy,* 44**,** 1783-1796.

Bajpai, M., Bajpai, S. & Jyotishi, P. 2016. Water absorption and moisture permeation properties of chitosan/poly (acrylamide-co-itaconic acid) IPC films. *International journal of biological macromolecules,* 84**,** 1-9.

Bajpai, S. & Sharma, S. 2004. Investigation of swelling/degradation behaviour of alginate beads crosslinked with Ca2+ and Ba2+ ions. *Reactive and Functional Polymers,* 59**,** 129-140.

Balagangadharan, K., Dhivya, S. & Selvamurugan, N. 2017. Chitosan based nanofibers in bone tissue engineering. *International journal of biological macromolecules,* 104**,** 1372-1382.

Barnes, H. A. 2000. A handbook of elementary rheology.

Batista, R. 2014. Uses and potential applications of ferulic acid. *Ferulic acid: antioxidant properties, uses and potential health benefits. 1st ed. New York, NY.: Nova Science Publishers, Inc. p***,** 39-70.

Beck, C. S. & Powers, J. H. 1926. Burns treated by tannic acid. *Annals of surgery,* 84**,** 19.

Becker, T. A., Kipke, D. R. & Brandon, T. 2001a. Calcium alginate gel: a biocompatible and mechanically stable polymer for endovascular embolization. *Journal of Biomedical Materials Research Part A,* 54**,** 76-86.

Becker, T. A., Kipke, D. R. & Brandon, T. 2001b. Calcium alginate gel: a biocompatible and mechanically stable polymer for endovascular embolization. *Journal of Biomedical Materials Research: An Official Journal of The Society for Biomaterials and The Japanese Society for Biomaterials,* 54**,** 76-86.

Behera, S. S., Das, U., Kumar, A., Bissoyi, A. & Singh, A. K. 2017. Chitosan/TiO2 composite membrane improves proliferation and survival of L929 fibroblast cells: Application in wound dressing and skin regeneration. *International journal of biological macromolecules,* 98**,** 329-340.

Berger, J., Reist, M., Mayer, J. M., Felt, O., Peppas, N. & Gurny, R. 2004. Structure and interactions in covalently and ionically crosslinked chitosan hydrogels for biomedical applications. *European Journal of Pharmaceutics and Biopharmaceutics,* 57**,** 19-34.

Berman, B. 2012. 3-D printing: The new industrial revolution. *Business horizons,* 55**,** 155-162.

Bhattarai, N., Edmondson, D., Veiseh, O., Matsen, F. A. & Zhang, M. 2005. Electrospun chitosan-based nanofibers and their cellular compatibility. *Biomaterials,* 26**,** 6176-6184.

Bini, E., Foo, C. W. P., Huang, J., Karageorgiou, V., Kitchel, B. & Kaplan, D. L. 2006. RGD-functionalized bioengineered spider dragline silk biomaterial. *Biomacromolecules,* 7**,** 3139-3145.

Biranje, S. S., Madiwale, P. V., Patankar, K. C., Chhabra, R., Dandekar-Jain, P. & Adivarekar, R. V. 2019. Hemostasis and anti-necrotic activity of wound-healing dressing containing chitosan nanoparticles. *International journal of biological macromolecules,* 121**,** 936-946.

Boateng, J., Pawar, H. & Tetteh, J. 2015. Evaluation of in vitro wound adhesion characteristics of composite film and wafer based dressings using texture analysis and FTIR spectroscopy: A chemometrics factor analysis approach. *RSC Advances,* 5**,** 107064-107075.

Boateng, J. S., Matthews, K. H., Stevens, H. N. & Eccleston, G. M. 2008. Wound healing dressings and drug delivery systems: a review. *Journal of pharmaceutical sciences,* 97**,** 2892-2923.

Bonassar, L. J. & Vacanti, C. A. 1998. Tissue engineering: the first decade and beyond. *Journal of cellular biochemistry,* 72**,** 297-303.

Boonsongrit, Y., Mitrevej, A. & Mueller, B. W. 2006. Chitosan drug binding by ionic interaction. *European journal of pharmaceutics and biopharmaceutics,* 62**,** 267-274.

Borges, A., Ferreira, C., Saavedra, M. J. & Simoes, M. 2013. Antibacterial activity and mode of action of ferulic and gallic acids against pathogenic bacteria. *Microbial drug resistance,* 19**,** 256-265.

Bradford, M. M. 1976. A rapid and sensitive method for the quantitation of microgram quantities of protein utilizing the principle of protein-dye binding. *Analytical biochemistry,* 72**,** 248-254.

Brown, M. A., Daya, M. R. & Worley, J. A. 2009. Experience with chitosan dressings in a civilian EMS system. *The Journal of emergency medicine,* 37**,** 1-7.

Bueno, C. Z., Moraes, Â. M., De Sousa, H. C. & Braga, M. E. M. 2016. Effects of supercritical carbon dioxide processing on the properties of chitosan–alginate membranes. *The Journal of Supercritical Fluids,* 112**,** 128-135.

Caetano, G. F., Frade, M. A. C., Andrade, T. A. M., Leite, M. N., Bueno, C. Z., Moraes, Â. M. & Ribeiro-Paes, J. T. 2015. Chitosan-alginate membranes accelerate wound healing. *Journal of Biomedical Materials Research Part B: Applied Biomaterials,* 103**,** 1013-1022.

Cai, N., Li, C., Han, C., Luo, X., Shen, L., Xue, Y. & Yu, F. 2016. Tailoring mechanical and antibacterial properties of chitosan/gelatin nanofiber membranes with Fe3O4 nanoparticles for potential wound dressing application. *Applied Surface Science,* 369**,** 492-500.

Cai, Z.-X., Mo, X.-M., Zhang, K.-H., Fan, L.-P., Yin, A.-L., He, C.-L. & Wang, H.-S. 2010. Fabrication of chitosan/silk fibroin composite nanofibers for wound-dressing applications. *International journal of molecular sciences,* 11**,** 3529-3539.

Cano, L., Pollet, E., Avérous, L. & Tercjak, A. 2017. Effect of TiO2 nanoparticles on the properties of thermoplastic chitosan-based nano-biocomposites obtained by mechanical kneading. *Composites Part A: Applied Science and Manufacturing,* 93**,** 33-40.

Cao, D., Wu, Y.-P., Fu, Z.-F., Tian, Y., Li, C.-J., Gao, C.-Y., Chen, Z.-L. & Feng, X.-Z. 2011. Cell adhesive and growth behavior on electrospun nanofibrous scaffolds by designed multifunctional composites. *Colloids and Surfaces B: Biointerfaces,* 84**,** 26-34.

Carneiro-Da-Cunha, M. G., Cerqueira, M. A., Souza, B. W., Carvalho, S., Quintas, M. A., Teixeira, J. A. & Vicente, A. A. 2010. Physical and thermal properties of a chitosan/alginate nanolayered PET film. *Carbohydrate Polymers,* 82**,** 153-159.

Carr, R. L., Carr, R., Carr, R. & Carr, R. 1965. Evaluating flow properties of solids.

Chan, L. W., Kim, C. H., Wang, X., Pun, S. H., White, N. J. & Kim, T. H. 2016. PolySTAT-modified chitosan gauzes for improved hemostasis in external hemorrhage. *Acta biomaterialia,* 31**,** 178-185.

Chandrasekaran, A. R., Jia, C. Y., Theng, C. S., Muniandy, T., Muralidharan, S. & Dhanaraj, S. A. 2011. Invitro studies and evaluation of metformin marketed tablets-Malaysia. *Journal of applied pharmaceutical science,* 1**,** 214.

Chang, A. B., Lin, T.-P., Thompson, N. B., Luo, S.-X., Liberman-Martin, A. L., Chen, H.-Y., Lee, B. & Grubbs, R. H. 2017. Design, synthesis, and self-assembly of polymers with tailored graft distributions. *Journal of the American Chemical Society,* 139**,** 17683-17693.

Chejara, D. R., Mabrouk, M., Kumar, P., Choonara, Y. E., Kondiah, P. P., Badhe, R. V., Toit, L. C. D., Bijukumar, D. & Pillay, V. 2017. Synthesis and Evaluation of a Sodium Alginate-4-Aminosalicylic Acid Based Microporous Hydrogel for Potential Viscosupplementation for Joint Injuries and Arthritis-Induced Conditions. *Marine drugs,* 15**,** 257.

Chen, H., Xing, X., Tan, H., Jia, Y., Zhou, T., Chen, Y., Ling, Z. & Hu, X. 2017. Covalently antibacterial alginate-chitosan hydrogel dressing integrated gelatin microspheres containing tetracycline hydrochloride for wound healing. *Materials Science and Engineering: C,* 70**,** 287-295.

Chen, J.-P., Chang, G.-Y. & Chen, J.-K. 2008. Electrospun collagen/chitosan nanofibrous membrane as wound dressing. *Colloids and surfaces a: physicochemical and engineering aspects,* 313**,** 183-188.

Chen, L.-C., Kung, S.-K., Chen, H.-H. & Lin, S.-B. 2010. Evaluation of zeta potential difference as an indicator for antibacterial strength of low molecular weight chitosan. *Carbohydrate Polymers,* 82**,** 913-919.

Chou, S.-F., Carson, D. & Woodrow, K. A. 2015. Current strategies for sustaining drug release from electrospun nanofibers. *Journal of Controlled Release,* 220**,** 584-591.

Conzatti, G., Faucon, D., Castel, M., Ayadi, F., Cavalie, S. & Tourrette, A. 2017. Alginate/chitosan polyelectrolyte complexes: A comparative study of the influence of the drying step on physicochemical properties. *Carbohydrate polymers,* 172**,** 142-151.

Costa, M. J., Marques, A. M., Pastrana, L. M., Teixeira, J. A., Sillankorva, S. M. & Cerqueira, M. A. 2018. Physicochemical properties of alginate-based films: Effect of ionic crosslinking and mannuronic and guluronic acid ratio. *Food hydrocolloids,* 81**,** 442-448.

Costa, R. R., Costa, A. M., Caridade, S. G. & Mano, J. O. F. 2015. Compact saloplastic membranes of natural polysaccharides for soft tissue engineering. *Chemistry of Materials,* 27**,** 7490-7502.

Cota-Arriola, O., Plascencia-Jatomea, M., Lizardi-Mendoza, J., Robles-Sánchez, R., Ezquerra-Brauer, J., Ruíz-García, J., Vega-Acosta, J. & Cortez-Rocha, M. O. 2017. Preparation of chitosan matrices with ferulic acid: physicochemical characterization and relationship on the growth of Aspergillus parasiticus. *CyTA-Journal of Food,* 15**,** 65-74.

Cowen, S. & Al-Abadleh, H. A. 2009. DRIFTS studies on the photodegradation of tannic acid as a model for HULIS in atmospheric aerosols. *Physical Chemistry Chemical Physics,* 11**,** 7838-7847.

Cuadros, T. R., Erices, A. A. & Aguilera, J. M. 2015. Porous matrix of calcium alginate/gelatin with enhanced properties as scaffold for cell culture. *Journal of the mechanical behavior of biomedical materials,* 46**,** 331-342.

Dahl, J. E., Frangou-Polyzois, M. J. & Polyzois, G. L. 2006. In vitro biocompatibility of denture relining materials. *Gerodontology,* 23**,** 17-22.

Dai, M., Zheng, X., Xu, X., Kong, X., Li, X., Guo, G., Luo, F., Zhao, X., Wei, Y. Q. & Qian, Z. 2009. Chitosan-alginate sponge: preparation and application in curcumin delivery for dermal wound healing in rat. *BioMed Research International,* 2009.

Dart, A., Bhave, M. & Kingshott, P. 2019. Antimicrobial Peptide-Based Electrospun Fibers for Wound Healing Applications. *Macromolecular bioscience,* 19**,** 1800488.

Demidova-Rice, T. N., Hamblin, M. R. & Herman, I. M. 2012. Acute and impaired wound healing: pathophysiology and current methods for drug delivery, part 1: normal and chronic wounds: biology, causes, and approaches to care. *Advances in skin & wound care,* 25**,** 304.

Desai, K., Kit, K., Li, J. & Zivanovic, S. 2008. Morphological and surface properties of electrospun chitosan nanofibers. *Biomacromolecules,* 9**,** 1000-1006.

Di Foggia, M., Taddei, P., Torreggiani, A., Dettin, M. & Tinti, A. 2011. Self-Assembling Peptides for Biomedical Applications: IR and Raman Spectroscopies for the Study of Secondary Structure. *Proteomics Research Journal,* 2**,** 231.

Ding, L., Shan, X., Zhao, X., Zha, H., Chen, X., Wang, J., Cai, C., Wang, X., Li, G. & Hao, J. 2017. Spongy bilayer dressing composed of chitosan–Ag nanoparticles and chitosan–Bletilla striata polysaccharide for wound healing applications. *Carbohydrate polymers,* 157**,** 1538-1547.

Disa, J. J., Alizadeh, K., Smith, J. W., Hu, Q.-Y. & Cordeiro, P. G. 2001. Evaluation of a combined calcium sodium alginate and bio-occlusive membrane dressing in the management of split-thickness skin graft donor sites. *Annals of plastic surgery,* 46**,** 405-408.

Dowling, M. B., Kumar, R., Keibler, M. A., Hess, J. R., Bochicchio, G. V. & Raghavan, S. R. 2011. A self-assembling hydrophobically modified chitosan capable of reversible hemostatic action. *Biomaterials,* 32**,** 3351-3357.

Du, H., Liu, M., Yang, X. & Zhai, G. 2015. The design of pH-sensitive chitosan-based formulations for gastrointestinal delivery. *Drug discovery today,* 20**,** 1004-1011.

Du, T., Chen, Z., Li, H., Tang, X., Li, Z., Guan, J., Liu, C., Du, Z. & Wu, J. 2016. Modification of collagen–chitosan matrix by the natural crosslinker alginate dialdehyde. *International journal of biological macromolecules,* 82**,** 580-588.

Du, W.-L., Niu, S.-S., Xu, Y.-L., Xu, Z.-R. & Fan, C.-L. 2009. Antibacterial activity of chitosan tripolyphosphate nanoparticles loaded with various metal ions. *Carbohydrate polymers,* 75**,** 385-389.

Du, W.-L., Xu, Y.-L., Xu, Z.-R. & Fan, C.-L. 2008. Preparation, characterization and antibacterial properties against E. coli K88 of chitosan nanoparticle loaded copper ions. *Nanotechnology,* 19**,** 085707.

Dumitriu, S. & Chornet, E. 1998. Inclusion and release of proteins from polysaccharide-based polyion complexes. *Advanced drug delivery reviews,* 31**,** 223-246.

Dumville, J. C., Keogh, S. J., Liu, Z., Stubbs, N., Walker, R. M. & Fortnam, M. 2015. Alginate dressings for treating pressure ulcers. *Cochrane Database of Systematic Reviews*.

Dutra, J., Carvalho, S., Zampirolli, A., Daltoé, R., Teixeira, R., Careta, F., Cotrim, M., Oréfice, R. & Villanova, J. 2017. Papain wound dressings obtained from poly (vinyl alcohol)/calcium alginate blends as new pharmaceutical dosage form: Preparation and preliminary evaluation. *European Journal of Pharmaceutics and Biopharmaceutics,* 113**,** 11-23.

El-Feky, G. S., Sharaf, S. S., El Shafei, A. & Hegazy, A. A. 2017. Using chitosan nanoparticles as drug carriers for the development of a silver sulfadiazine wound dressing. *Carbohydrate polymers,* 158**,** 11-19.

Eming, S. A., Krieg, T. & Davidson, J. M. 2007. Inflammation in wound repair: molecular and cellular mechanisms. *Journal of Investigative Dermatology,* 127**,** 514-525.

Eskandari, S., Guerin, T., Toth, I. & Stephenson, R. J. 2017. Recent advances in self-assembled peptides: Implications for targeted drug delivery and vaccine engineering. *Advanced drug delivery reviews,* 110**,** 169-187.

Falcão, L. & Araújo, M. E. M. 2014. Application of ATR–FTIR spectroscopy to the analysis of tannins in historic leathers: the case study of the upholstery from the 19th century Portuguese Royal Train. *Vibrational Spectroscopy,* 74**,** 98-103.

Fan, L., Yang, H., Yang, J., Peng, M. & Hu, J. 2016a. Preparation and characterization of chitosan/gelatin/PVA hydrogel for wound dressings. *Carbohydrate polymers,* 146**,** 427-434.

Fan, L., Yi, J., Tong, J., Zhou, X., Ge, H., Zou, S., Wen, H. & Nie, M. 2016b. Preparation and characterization of Oxidized konjac glucomannan/Carboxymethyl Chitosan/Graphene Oxide hydrogel. *International journal of biological macromolecules,* 91**,** 358-367.

Fan, L., Zou, S., Ge, H., Xiao, Y., Wen, H., Feng, H., Liu, M. & Nie, M. 2016c. Preparation and characterization of hydroxypropyl chitosan modified with collagen peptide. *International journal of biological macromolecules,* 93**,** 636-643.

Fan, W., Yan, W., Xu, Z. & Ni, H. 2012. Formation mechanism of monodisperse, low molecular weight chitosan nanoparticles by ionic gelation technique. *Colloids and Surfaces B: Biointerfaces,* 90**,** 21-27.

Fan, X., Chen, K., He, X., Li, N., Huang, J., Tang, K., Li, Y. & Wang, F. 2016d. Nano-TiO2/collagen-chitosan porous scaffold for wound repairing. *International journal of biological macromolecules,* 91**,** 15-22.

Fathi, P., Sikorski, M., Christodoulides, K., Langan, K., Choi, Y. S., Titcomb, M., Ghodasara, A., Wonodi, O., Thaker, H. & Vural, M. 2018. Zeolite-loaded alginate-chitosan hydrogel beads as a topical hemostat. *Journal of Biomedical Materials Research Part B: Applied Biomaterials,* 106**,** 1662-1671.

Fichman, G. & Gazit, E. 2014. Self-assembly of short peptides to form hydrogels: Design of building blocks, physical properties and technological applications. *Acta biomaterialia,* 10**,** 1671-1682.

Figueira, D. R., Miguel, S. P., De Sá, K. D. & Correia, I. J. 2016. Production and characterization of polycaprolactone-hyaluronic acid/chitosan-zein electrospun bilayer nanofibrous membrane for tissue regeneration. *International journal of biological macromolecules,* 93**,** 1100-1110.

Florczyk, S. J., Kim, D. J., Wood, D. L. & Zhang, M. 2011. Influence of processing parameters on pore structure of 3D porous chitosan–alginate polyelectrolyte complex scaffolds. *Journal of Biomedical Materials Research Part A,* 98**,** 614-620.

Francis, N. L., Hunger, P. M., Donius, A. E., Wegst, U. G. & Wheatley, M. A. 2017. Strategies for neurotrophin-3 and chondroitinase ABC release from freeze-cast chitosan–alginate nerve-guidance scaffolds. *Journal of tissue engineering and regenerative medicine,* 11**,** 285-294.

Freier, T., Koh, H. S., Kazazian, K. & Shoichet, M. S. 2005. Controlling cell adhesion and degradation of chitosan films by N-acetylation. *Biomaterials,* 26**,** 5872-5878.

Frohbergh, M. E., Katsman, A., Botta, G. P., Lazarovici, P., Schauer, C. L., Wegst, U. G. & Lelkes, P. I. 2012. Electrospun hydroxyapatite-containing chitosan nanofibers crosslinked with genipin for bone tissue engineering. *Biomaterials,* 33**,** 9167-9178.

Gan, D., Liu, M., Xu, T., Wang, K., Tan, H. & Lu, X. 2018. Chitosan/biphasic calcium phosphate scaffolds functionalized with BMP-2-encapsulated nanoparticles and RGD for bone regeneration. *Journal of Biomedical Materials Research Part A,* 106**,** 2613-2624.

Garg, T., Singh, O., Arora, S. & Murthy, R. 2012. Scaffold: a novel carrier for cell and drug delivery. *Critical Reviews™ in Therapeutic Drug Carrier Systems,* 29.

Ghazali, M., Nawawi, M. & Huang, R. Y. 1997. Pervaporation dehydration of isopropanol with chitosan membranes. *Journal of Membrane Science,* 124**,** 53-62.

Gonçalves, V. L., Laranjeira, M., Fávere, V. T. & Pedrosa, R. C. 2005. Effect of crosslinking agents on chitosan microspheres in controlled release of diclofenac sodium. *Polímeros,* 15**,** 6-12.

Göpferich, A. 1996. Mechanisms of polymer degradation and erosion. *Biomaterials,* 17**,** 103-114.

Gorczyca, G., Tylingo, R., Szweda, P., Augustin, E., Sadowska, M. & Milewski, S. 2014. Preparation and characterization of genipin cross-linked porous chitosan–collagen–gelatin scaffolds using chitosan–CO2 solution. *Carbohydrate polymers,* 102**,** 901-911.

Groen, J. C., Peffer, L. A. & Pérez-Ramírez, J. 2003. Pore size determination in modified micro- and mesoporous materials. Pitfalls and limitations in gas adsorption data analysis. *Microporous and mesoporous materials,* 60**,** 1-17.

Gu, B. K., Park, S. J., Kim, M. S., Lee, Y. J., Kim, J.-I. & Kim, C.-H. 2016. Gelatin blending and sonication of chitosan nanofiber mats produce synergistic effects on hemostatic functions. *International journal of biological macromolecules,* 82**,** 89-96.

Gu, S.-Y., Wang, Z.-M., Ren, J. & Zhang, C.-Y. 2009. Electrospinning of gelatin and gelatin/poly (l-lactide) blend and its characteristics for wound dressing. *Materials Science and Engineering: C,* 29**,** 1822-1828.

Gupta, S., Singh, I., Sharma, A. K. & Kumar, P. 2020. Ultrashort peptide self-assembly: Front-runners to transport drug and gene cargos. *Frontiers in bioengineering and biotechnology,* 8.

Gutowska, A., Jeong, B. & Jasionowski, M. 2001. Injectable gels for tissue engineering. *The Anatomical Record: An Official Publication of the American Association of Anatomists,* 263**,** 342-349.

Guven, S., Chen, P., Inci, F., Tasoglu, S., Erkmen, B. & Demirci, U. 2015. Multiscale assembly for tissue engineering and regenerative medicine. *Trends in biotechnology,* 33**,** 269-279.

Guvendiren, M., Molde, J., Soares, R. M. & Kohn, J. 2016. Designing biomaterials for 3D printing. *ACS biomaterials science & engineering,* 2**,** 1679-1693.

Guzmán, E., Cavallo, J. A., Chuliá-Jordán, R., Gómez, C., Strumia, M. C., Ortega, F. & Rubio, R. G. 2011. pH-induced changes in the fabrication of multilayers of poly (acrylic acid) and chitosan: fabrication, properties, and tests as a drug storage and delivery system. *Langmuir,* 27**,** 6836-6845.

Guzman, E., Chuliá-Jordán, R., Ortega, F. & Rubio, R. G. 2011. Influence of the percentage of acetylation on the assembly of LbL multilayers of poly (acrylic acid) and chitosan. *Physical Chemistry Chemical Physics,* 13**,** 18200-18207.

Han, F., Dong, Y., Su, Z., Yin, R., Song, A. & Li, S. 2014. Preparation, characteristics and assessment of a novel gelatin–chitosan sponge scaffold as skin tissue engineering material. *International journal of pharmaceutics,* 476**,** 124-133.

Harding, K. & Edwards, R. 2004. Bacteria and wound healing vol. 17. United States: Lippincott Williams & Wilkins.

Haug, A. & Smidsrod, O. 1970. Selectivity of some anionic polymers for divalent metal ions. *Acta chem. scand,* 24**,** 843-854.

He, X., Liu, X., Yang, J., Du, H., Chai, N., Sha, Z., Geng, M., Zhou, X. & He, C. 2020. Tannic acid-reinforced methacrylated chitosan/methacrylated silk fibroin hydrogels with multifunctionality for accelerating wound healing. *Carbohydrate Polymers***,** 116689.

Hendriks, F., Brokken, D., Oomens, C., Baaijens, F. & Horsten, J. 2000. Mechanical properties of different layers of human skin. *Philips Research Laboratories, Eindhoven*.

Hersel, U., Dahmen, C. & Kessler, H. 2003. RGD modified polymers: biomaterials for stimulated cell adhesion and beyond. *Biomaterials,* 24**,** 4385-4415.

Hoffman, A. S. 2012. Hydrogels for biomedical applications. *Advanced drug delivery reviews,* 64**,** 18-23.

Hong, H.-J., Jin, S.-E., Park, J.-S., Ahn, W. S. & Kim, C.-K. 2008. Accelerated wound healing by smad3 antisense oligonucleotides-impregnated chitosan/alginate polyelectrolyte complex. *Biomaterials,* 29**,** 4831-4837.

Hoseinpour Najar, M., Minaiyan, M. & Taheri, A. 2018. Preparation and in vivo evaluation of a novel gel-based wound dressing using arginine–alginate surface-modified chitosan nanofibers. *Journal of biomaterials applications,* 32**,** 689-701.

Hosoda, A., Ozaki, Y., Kashiwada, A., Mutoh, M., Wakabayashi, K., Mizuno, K., Nomura, E. & Taniguchi, H. 2002. Syntheses of ferulic acid derivatives and their suppressive effects on cyclooxygenase-2 promoter activity. *Bioorganic & medicinal chemistry,* 10**,** 1189-1196.

Hosoyama, K., Lazurko, C., Muñoz, M., Mctiernan, C. D. & Alarcon, E. I. 2019. Peptide-based functional biomaterials for soft-tissue repair. *Frontiers in Bioengineering and Biotechnology,* 7**,** 205.

Hu, Y., Zhang, Z., Li, Y., Ding, X., Li, D., Shen, C. & Xu, F. J. 2018. Dual-Crosslinked Amorphous Polysaccharide Hydrogels Based on Chitosan/Alginate for Wound Healing Applications. *Macromolecular rapid communications***,** 1800069.

Huber, D., Tegl, G., Baumann, M., Sommer, E., Gorji, E. G., Borth, N., Schleining, G., Nyanhongo, G. S. & Guebitz, G. M. 2017. Chitosan hydrogel formation using laccase activated phenolics as cross-linkers. *Carbohydrate polymers,* 157**,** 814-822.

Hussain, F., Khurshid, M., Masood, R. & Ibrahim, W. 2017. Developing antimicrobial calcium alginate fibres from neem and papaya leaves extract. *Journal of wound care,* 26**,** 778-783.

Il'ina, A., Varlamov, V., Ermakov, Y. A., Orlov, V. & Skryabin, K. 2008. Chitosan is a natural polymer for constructing nanoparticles. Doklady Chemistry. Springer, 165-167.

Jayakumar, R., Prabaharan, M., Kumar, P. S., Nair, S. & Tamura, H. 2011. Biomaterials based on chitin and chitosan in wound dressing applications. *Biotechnology advances,* 29**,** 322-337.

Jia, Z. & Shen, D. 2002. Effect of reaction temperature and reaction time on the preparation of low-molecular-weight chitosan using phosphoric acid. *Carbohydrate Polymers,* 49**,** 393-396.

Jin, J., Song, M. & Hourston, D. 2004. Novel chitosan-based films cross-linked by genipin with improved physical properties. *Biomacromolecules,* 5**,** 162-168.

Jing, J., Liang, S., Yan, Y., Tian, X. & Li, X. 2019. Fabrication of Hybrid Hydrogels from Silk Fibroin and Tannic Acid with Enhanced Gelation and Antibacterial Activities. *ACS Biomaterials Science & Engineering,* 5**,** 4601-4611.

Kassem, M. A., Elmeshad, A. N. & Fares, A. R. 2015. Lyophilized sustained release mucoadhesive chitosan sponges for buccal buspirone hydrochloride delivery: formulation and in vitro evaluation. *AAPS PharmSciTech,* 16**,** 537-547.

Ke, G., Xu, W. & Yu, W. 2010. Preparation and properties of drug-loaded chitosan-sodium alginate complex membrane. *International Journal of Polymeric Materials,* 59**,** 184-191.

Khan, F., Tanaka, M. & Ahmad, S. R. 2015. Fabrication of polymeric biomaterials: a strategy for tissue engineering and medical devices. *Journal of Materials Chemistry B,* 3**,** 8224-8249.

Khan, N. S., Ahmad, A. & Hadi, S. 2000a. Anti-oxidant, pro-oxidant properties of tannic acid and its binding to DNA. *Chemico-Biological Interactions,* 125**,** 177-189.

Khan, T. A., Peh, K. K. & Ch'ng, H. S. 2000b. Mechanical, bioadhesive strength and biological evaluations of chitosan films for wound dressing. *J Pharm Pharm Sci,* 3**,** 303-311.

Khattak, S. F., Chin, K. S., Bhatia, S. R. & Roberts, S. C. 2007. Enhancing oxygen tension and cellular function in alginate cell encapsulation devices through the use of perfluorocarbons. *Biotechnology and bioengineering,* 96**,** 156-166.

Khorasani, M. T., Joorabloo, A., Moghaddam, A., Shamsi, H. & Mansoorimoghadam, Z. 2018. Incorporation of ZnO nanoparticles into heparinised polyvinyl alcohol/chitosan hydrogels for wound dressing application. *International journal of biological macromolecules,* 114**,** 1203-1215.

Kikuchi, A. & Okano, T. 2002. Intelligent thermoresponsive polymeric stationary phases for aqueous chromatography of biological compounds. *Progress in Polymer Science,* 27**,** 1165-1193.

Kim, J. H. & Lee, Y. M. 1993. Synthesis and properties of diethylaminoethyl chitosan. *Polymer,* 34**,** 1952-1957.

Kim, T., Silva, J., Kim, M. & Jung, Y. 2010. Enhanced antioxidant capacity and antimicrobial activity of tannic acid by thermal processing. *Food Chemistry,* 118**,** 740-746.

Kong, M., Chen, X. G., Xing, K. & Park, H. J. 2010. Antimicrobial properties of chitosan and mode of action: a state of the art review. *International journal of food microbiology,* 144**,** 51-63.

Kozlovskaya, V., Kharlampieva, E., Drachuk, I., Cheng, D. & Tsukruk, V. V. 2010. Responsive microcapsule reactors based on hydrogen-bonded tannic acid layer-by-layer assemblies. *Soft Matter,* 6**,** 3596-3608.

Kozlovskaya, V., Zavgorodnya, O., Chen, Y., Ellis, K., Tse, H. M., Cui, W., Thompson, J. A. & Kharlampieva, E. 2012. Ultrathin polymeric coatings based on hydrogen-bonded polyphenol for protection of pancreatic islet cells. *Advanced functional materials,* 22**,** 3389-3398.

Kulig, D., Zimoch-Korzycka, A., Jarmoluk, A. & Marycz, K. 2016. Study on alginate–chitosan complex formed with different polymers ratio. *Polymers,* 8**,** 167.

Kumar, A., Lee, Y., Kim, D., Rao, K. M., Kim, J., Park, S., Haider, A. & Han, S. S. 2017. Effect of crosslinking functionality on microstructure, mechanical properties, and in vitro cytocompatibility of cellulose nanocrystals reinforced poly (vinyl alcohol)/sodium alginate hybrid scaffolds. *International journal of biological macromolecules,* 95**,** 962-973.

Kumar, P., Choonara, Y. E., Toit, L. C. D., Modi, G., Naidoo, D. & Pillay, V. 2012. Novel high-viscosity polyacrylamidated chitosan for neural tissue engineering: fabrication of anisotropic neurodurable scaffold via molecular disposition of persulfate-mediated polymer slicing and complexation. *International journal of molecular sciences,* 13**,** 13966-13984.

Kurczewska, J., Cegłowski, M., Pecyna, P., Ratajczak, M., Gajęcka, M. & Schroeder, G. 2017. Molecularly imprinted polymer as drug delivery carrier in alginate dressing. *Materials Letters,* 201**,** 46-49.

Kurita, K., Sannan, T. & Iwakura, Y. 1979. Studies on chitin. VI. Binding of metal cations. *Journal of Applied Polymer Science,* 23**,** 511-515.

Kweon, D.-K., Song, S.-B. & Park, Y.-Y. 2003. Preparation of water-soluble chitosan/heparin complex and its application as wound healing accelerator. *Biomaterials,* 24**,** 1595-1601.

Lai, H. L., Abu'khalil, A. & Craig, D. Q. 2003. The preparation and characterisation of drug-loaded alginate and chitosan sponges. *International journal of pharmaceutics,* 251**,** 175-181.

Lee, K. Y. & Mooney, D. J. 2012. Alginate: properties and biomedical applications. *Progress in polymer science,* 37**,** 106-126.

Lemire, J. A., Harrison, J. J. & Turner, R. J. 2013. Antimicrobial activity of metals: mechanisms, molecular targets and applications. *Nature Reviews Microbiology,* 11**,** 371.

Li, B., Chen, J. & Wang, J. H. C. 2006. RGD peptide-conjugated poly (dimethylsiloxane) promotes adhesion, proliferation, and collagen secretion of human fibroblasts. *Journal of Biomedical Materials Research Part A,* 79**,** 989-998.

Li, J., Chen, J. & Kirsner, R. 2007. Pathophysiology of acute wound healing. *Clinics in dermatology,* 25**,** 9-18.

Li, N., Yang, X., Liu, W., Xi, G., Wang, M., Liang, B., Ma, Z., Feng, Y., Chen, H. & Shi, C. 2018. Tannic acid cross-linked polysaccharide-based multifunctional hemostatic microparticles for the regulation of rapid wound healing. *Macromolecular Bioscience,* 18**,** 1800209.

Li, Z., Ramay, H. R., Hauch, K. D., Xiao, D. & Zhang, M. 2005. Chitosan–alginate hybrid scaffolds for bone tissue engineering. *Biomaterials,* 26**,** 3919-3928.

Lin, T., Fang, J., Wang, H., Cheng, T. & Wang, X. 2006. Using chitosan as a thickener for electrospinning dilute PVA solutions to improve fibre uniformity. *Nanotechnology,* 17**,** 3718.

Lin, Y. H., Lin, J. H. & Hong, Y. S. 2017. Development of chitosan/poly-γ-glutamic acid/pluronic/curcumin nanoparticles in chitosan dressings for wound regeneration. *Journal of Biomedical Materials Research Part B: Applied Biomaterials,* 105**,** 81-90.

Liu, C., Xia, Z. & Czernuszka, J. 2007. Design and development of three-dimensional scaffolds for tissue engineering. *Chemical Engineering Research and Design,* 85**,** 1051-1064.

Liu, Y., Cai, Z., Sheng, L., Ma, M., Xu, Q. & Jin, Y. 2019. Structure-property of crosslinked chitosan/silica composite films modified by genipin and glutaraldehyde under alkaline conditions. *Carbohydrate polymers,* 215**,** 348-357.

Lo, H.-H. & Chung, J. 1999a. The effects of plant phenolics, caffeic acid, chlorogenic acid and ferulic acid on arylamine N-acetyltransferase activities in human gastrointestinal microflora. *Anticancer research,* 19**,** 133-139.

Lo, H. H. & Chung, J.-G. 1999b. The effects of plant phenolics, caffeic acid, chlorogenic acid and ferulic acid on arylamine N-acetyltransferase activities in human gastrointestinal microflora. *Anticancer research,* 19**,** 133-139.

López-León, T., Carvalho, E., Seijo, B., Ortega-Vinuesa, J. & Bastos-González, D. 2005. Physicochemical characterization of chitosan nanoparticles: electrokinetic and stability behavior. *Journal of Colloid and Interface Science,* 283**,** 344-351.

Lu, B., Lu, F., Zou, Y., Liu, J., Rong, B., Li, Z., Dai, F., Wu, D. & Lan, G. 2017a. In situ reduction of silver nanoparticles by chitosan-l-glutamic acid/hyaluronic acid: Enhancing antimicrobial and wound-healing activity. *Carbohydrate polymers,* 173**,** 556-565.

Lu, B., Wang, T., Li, Z., Dai, F., Lv, L., Tang, F., Yu, K., Liu, J. & Lan, G. 2016. Healing of skin wounds with a chitosan–gelatin sponge loaded with tannins and platelet-rich plasma. *International journal of biological macromolecules,* 82**,** 884-891.

Lu, Z., Gao, J., He, Q., Wu, J., Liang, D., Yang, H. & Chen, R. 2017b. Enhanced antibacterial and wound healing activities of microporous chitosan-Ag/ZnO composite dressing. *Carbohydrate polymers,* 156**,** 460-469.

Lv, X., Liu, Y., Song, S., Tong, C., Shi, X., Zhao, Y., Zhang, J. & Hou, M. 2018. Influence of chitosan oligosaccharide on the gelling and wound healing properties of injectable hydrogels based on carboxymethyl chitosan/alginate polyelectrolyte complexes. *Carbohydrate Polymers*.

Ma, L., Gao, C., Mao, Z., Zhou, J., Shen, J., Hu, X. & Han, C. 2003. Collagen/chitosan porous scaffolds with improved biostability for skin tissue engineering. *Biomaterials,* 24**,** 4833-4841.

Ma, L., Yu, W. & Ma, X. 2007. Preparation and characterization of novel sodium alginate/chitosan two ply composite membranes. *Journal of Applied Polymer Science,* 106**,** 394-399.

Madgulkar, A., Bhalekar, M. & Swami, M. 2009. In vitro and in vivo studies on chitosan beads of losartan duolite AP143 complex, optimized by using statistical experimental design. *AAPS PharmSciTech,* 10**,** 743.

Mandal, D., Shirazi, A. N. & Parang, K. 2014. Self-assembly of peptides to nanostructures. *Organic & biomolecular chemistry,* 12**,** 3544-3561.

Mason, T. O. & Buell, A. K. 2019. The Kinetics, Thermodynamics and Mechanisms of Short Aromatic Peptide Self-Assembly. *Biological and Bio-inspired Nanomaterials.* Springer.

Matějka, L., Janata, M., Pleštil, J., Zhigunov, A. & Šlouf, M. 2014. Self-assembly of POSS-containing block copolymers: Fixing the hierarchical structure in networks. *Polymer,* 55**,** 126-136.

Mayet, N., Choonara, Y. E., Kumar, P., Tomar, L. K., Tyagi, C., Du Toit, L. C. & Pillay, V. 2014. A comprehensive review of advanced biopolymeric wound healing systems. *Journal of pharmaceutical sciences,* 103**,** 2211-2230.

Mcclure, R. D. & Allen, C. I. 1935. Davidson tannic acid treatment of burns: ten year results. *The American Journal of Surgery,* 28**,** 370-388.

Meng, X., Tian, F., Yang, J., He, C.-N., Xing, N. & Li, F. 2010. Chitosan and alginate polyelectrolyte complex membranes and their properties for wound dressing application. *Journal of Materials Science: Materials in Medicine,* 21**,** 1751-1759.

Miraftab, M., Qiao, Q., Kennedy, J., Anand, S. & Groocock, M. 2003. Fibres for wound dressings based on mixed carbohydrate polymer fibres. *Carbohydrate polymers,* 53**,** 225-231.

Mndlovu, H., Du Toit, L. C., Kumar, P., Choonara, Y. E., Marimuthu, T., Kondiah, P. P. & Pillay, V. 2020. Bioplatform Fabrication Approaches Affecting Chitosan-Based Interpolymer Complex Properties and Performance as Wound Dressings. *Molecules,* 25**,** 222.

Mndlovu, H., Du Toit, L. C., Kumar, P., Marimuthu, T., Kondiah, P. P., Choonara, Y. E. & Pillay, V. 2019. Development of a Fluid-absorptive Alginate-Chitosan Bioplatform for Potential Application as a Wound Dressing. *Carbohydrate Polymers***,** 114988.

Mohamed, M. F., Abdelkhalek, A. & Seleem, M. N. 2016. Evaluation of short synthetic antimicrobial peptides for treatment of drug-resistant and intracellular Staphylococcus aureus. *Scientific reports,* 6**,** 29707.

Mokhena, T. & Luyt, A. 2017. Electrospun alginate nanofibres impregnated with silver nanoparticles: Preparation, morphology and antibacterial properties. *Carbohydrate polymers,* 165**,** 304-312.

Morgado, P. I., Miguel, S. P., Correia, I. J. & Aguiar-Ricardo, A. 2017. Ibuprofen loaded PVA/chitosan membranes: A highly efficient strategy towards an improved skin wound healing. *Carbohydrate polymers,* 159**,** 136-145.

Moura, M. J., Figueiredo, M. M. & Gil, M. H. 2007. Rheological study of genipin cross-linked chitosan hydrogels. *Biomacromolecules,* 8**,** 3823-3829.

Mozalewska, W., Czechowska-Biskup, R., Olejnik, A. K., Wach, R. A., Ulański, P. & Rosiak, J. M. 2017. Chitosan-containing hydrogel wound dressings prepared by radiation technique. *Radiation Physics and Chemistry,* 134**,** 1-7.

Müller, R., Jacobs, C. & Kayser, O. 2001a. Nanosuspensions as particulate drug formulations in therapy: rationale for development and what we can expect for the future. *Advanced drug delivery reviews,* 47**,** 3-19.

Müller, R. H., Jacobs, C. & Kayser, O. 2001b. Nanosuspensions as particulate drug formulations in therapy: rationale for development and what we can expect for the future. *Advanced drug delivery reviews,* 47**,** 3-19.

Murakami, K., Aoki, H., Nakamura, S., Nakamura, S.-I., Takikawa, M., Hanzawa, M., Kishimoto, S., Hattori, H., Tanaka, Y. & Kiyosawa, T. 2010. Hydrogel blends of chitin/chitosan, fucoidan and alginate as healing-impaired wound dressings. *Biomaterials,* 31**,** 83-90.

Nagam Hanumantharao, S. & Rao, S. 2019. Multi-functional electrospun nanofibers from polymer blends for scaffold tissue engineering. *Fibers,* 7**,** 66.

Nagasaka, R., Chotimarkorn, C., Shafiqul, I. M., Hori, M., Ozaki, H. & Ushio, H. 2007. Anti-inflammatory effects of hydroxycinnamic acid derivatives. *Biochemical and Biophysical Research Communications,* 358**,** 615-619.

Nair, R., Reddy, B. H., Kumar, C. A. & Kumar, K. J. 2009. Application of chitosan microspheres as drug carriers: a review. *Journal of pharmaceutical sciences and research,* 1**,** 1.

Nassar, E. J., Ciuffi, K. J., Calefi, P. S., Rocha, L. A., De Faria, E. H., E Silva, M. L., Luz, P. P., Bandeira, L. C., Cestari, A. & Fernandes, C. N. 2011. Biomaterials and Sol–Gel Process: A Methodology for the Preparation of Functional Materials. *Biomaterials science and engineering.* IntechOpen.

Natarajan, V., Krithica, N., Madhan, B. & Sehgal, P. K. 2013. Preparation and properties of tannic acid cross-linked collagen scaffold and its application in wound healing. *Journal of Biomedical Materials Research Part B: Applied Biomaterials,* 101**,** 560-567.

Ng, W. L., Yeong, W. Y. & Naing, M. W. 2016. Polyelectrolyte gelatin-chitosan hydrogel optimized for 3D bioprinting in skin tissue engineering. *International Journal of Bioprinting,* 2**,** 53-62.

Ngwuluka, N. C., Choonara, Y. E., Kumar, P., Modi, G., Toit, L. C. D. & Pillay, V. 2013. A hybrid methacrylate-sodium carboxymethylcellulose interpolyelectrolyte complex: rheometry and in silico disposition for controlled drug release. *Materials,* 6**,** 4284-4308.

Nieto-Suárez, M., López-Quintela, M. A. & Lazzari, M. 2016. Preparation and characterization of crosslinked chitosan/gelatin scaffolds by ice segregation induced self-assembly. *Carbohydrate polymers,* 141**,** 175-183.

Ninan, N., Forget, A., Shastri, V. P., Voelcker, N. H. & Blencowe, A. 2016. Antibacterial and anti-inflammatory pH-responsive tannic acid-carboxylated agarose composite hydrogels for wound healing. *ACS applied materials & interfaces,* 8**,** 28511-28521.

Nuttelman, C. R., Rice, M. A., Rydholm, A. E., Salinas, C. N., Shah, D. N. & Anseth, K. S. 2008. Macromolecular monomers for the synthesis of hydrogel niches and their application in cell encapsulation and tissue engineering. *Progress in polymer science,* 33**,** 167-179.

O'meara, S. & Martyn-St James, M. 2013. Alginate dressings for venous leg ulcers. *Cochrane Database of Systematic Reviews*.

Oh, G.-W., Ko, S.-C., Je, J.-Y., Kim, Y.-M., Oh, J. & Jung, W.-K. 2016. Fabrication, characterization and determination of biological activities of poly (ε-caprolactone)/chitosan-caffeic acid composite fibrous mat for wound dressing application. *International journal of biological macromolecules,* 93**,** 1549-1558.

Ohkawa, K., Cha, D., Kim, H., Nishida, A. & Yamamoto, H. 2004. Electrospinning of chitosan. *Macromolecular Rapid Communications,* 25**,** 1600-1605.

Ong, S.-Y., Wu, J., Moochhala, S. M., Tan, M.-H. & Lu, J. 2008. Development of a chitosan-based wound dressing with improved hemostatic and antimicrobial properties. *Biomaterials,* 29**,** 4323-4332.

Otvos Jr, L. & Ostorhazi, E. 2015. Therapeutic utility of antibacterial peptides in wound healing. *Expert review of anti-infective therapy,* 13**,** 871-881.

Ozseker, E. E. & Akkaya, A. 2016. Development of a new antibacterial biomaterial by tetracycline immobilization on calcium-alginate beads. *Carbohydrate polymers,* 151**,** 441-451.

Pan, G. X., Thomson, C. I. & Leary, G. J. 2002. UV–vis. spectroscopic characteristics of ferulic acid and related compounds. *Journal of wood chemistry and technology,* 22**,** 137-146.

Pandit, G., Roy, K., Agarwal, U. & Chatterjee, S. 2018. Self-Assembly Mechanism of a Peptide-Based Drug Delivery Vehicle. *ACS omega,* 3**,** 3143-3155.

Parikh, D. V., Fink, T., Delucca, A. J. & Parikh, A. D. 2011. Absorption and swelling characteristics of silver (I) antimicrobial wound dressings. *Textile Research Journal,* 81**,** 494-503.

Park, W. H., Jeong, L., Yoo, D. I. & Hudson, S. 2004. Effect of chitosan on morphology and conformation of electrospun silk fibroin nanofibers. *Polymer,* 45**,** 7151-7157.

Patrulea, V., Hirt-Burri, N., Jeannerat, A., Applegate, L., Ostafe, V., Jordan, O. & Borchard, G. 2016. Peptide-decorated chitosan derivatives enhance fibroblast adhesion and proliferation in wound healing. *Carbohydrate polymers,* 142**,** 114-123.

Patrulea, V., Ostafe, V., Borchard, G. & Jordan, O. 2015. Chitosan as a starting material for wound healing applications. *European Journal of Pharmaceutics and Biopharmaceutics,* 97**,** 417-426.

Paul, W. & Sharma, C. P. 2004. Chitosan and alginate wound dressings: a short review. *Trends Biomater Artif Organs,* 18**,** 18-23.

Perlin, L., Macneil, S. & Rimmer, S. 2008. Production and performance of biomaterials containing RGD peptides. *Soft matter,* 4**,** 2331-2349.

Pierog, M., Gierszewska-Drużyńska, M. & Ostrowska-Czubenko, J. 2009. Effect of ionic crosslinking agents on swelling behavior of chitosan hydrogel membranes. *Progress on Chemistry and Application of Chitin and its Derivatives. Polish Chitin Society, Łódź,* 75**,** 82.

Pires, A. L. R. & Moraes, Â. M. 2015. Improvement of the mechanical properties of chitosan-alginate wound dressings containing silver through the addition of a biocompatible silicone rubber. *Journal of Applied Polymer Science,* 132.

Poormand, H., Leili, M. & Khazaei, M. 2017. Adsorption of methylene blue from aqueous solutions using water treatment sludge modified with sodium alginate as a low cost adsorbent. *Water Science and Technology,* 75**,** 281-295.

Poornima, B. & Korrapati, P. S. 2017. Fabrication of chitosan-polycaprolactone composite nanofibrous scaffold for simultaneous delivery of ferulic acid and resveratrol. *Carbohydrate polymers,* 157**,** 1741-1749.

Qandil, A. M., Obaidat, A. A., Ali, M. A. M., Al-Taani, B. M., Tashtoush, B. M., Al-Jbour, N. D., Al Remawi, M. M., Al-Sou'od, K. A. & Badwan, A. A. 2009. Investigation of the interactions in complexes of low molecular weight chitosan with ibuprofen. *Journal of solution chemistry,* 38**,** 695-712.

Qin, Y. 2008. Alginate fibres: an overview of the production processes and applications in wound management. *Polymer international,* 57**,** 171-180.

Qu, J., Zhao, X., Liang, Y., Xu, Y., Ma, P. X. & Guo, B. 2019. Degradable conductive injectable hydrogels as novel antibacterial, anti-oxidant wound dressings for wound healing. *Chemical Engineering Journal,* 362**,** 548-560.

Rabea, E. I., Badawy, M. E.-T., Stevens, C. V., Smagghe, G. & Steurbaut, W. 2003. Chitosan as antimicrobial agent: applications and mode of action. *Biomacromolecules,* 4**,** 1457-1465.

Rai, M., Ingle, A. P., Pandit, R., Paralikar, P., Gupta, I., Chaud, M. V. & Dos Santos, C. A. 2017. Broadening the spectrum of small-molecule antibacterials by metallic nanoparticles to overcome microbial resistance. *International journal of pharmaceutics,* 532**,** 139-148.

Ramburrun, P., Choonara, Y. E., Kumar, P., Du Toit, L. C. & Pillay, V. 2015. Design of chitospheres loaded with pristine polymer particles for extended drug delivery via polyelectrolyte complexation and particulate leaching. *International journal of pharmaceutics,* 479**,** 189-206.

Ranoszek-Soliwoda, K., Tomaszewska, E., Socha, E., Krzyczmonik, P., Ignaczak, A., Orlowski, P., Krzyzowska, M., Celichowski, G. & Grobelny, J. 2017. The role of tannic acid and sodium citrate in the synthesis of silver nanoparticles. *Journal of Nanoparticle Research,* 19**,** 273.

Rao, K. R. & Buri, P. 1989. A novel in situ method to test polymers and coated microparticles for bioadhesion. *International journal of pharmaceutics,* 52**,** 265-270.

Reis, C. P., Neufeld, R. J., Ribeiro, A. J. & Veiga, F. 2006. Nanoencapsulation I. Methods for preparation of drug-loaded polymeric nanoparticles. *Nanomedicine: Nanotechnology, Biology and Medicine,* 2**,** 8-21.

Reneker, D. H., Yarin, A. L., Fong, H. & Koombhongse, S. 2000. Bending instability of electrically charged liquid jets of polymer solutions in electrospinning. *Journal of Applied physics,* 87**,** 4531-4547.

Rezaeiroshan, A., Saeedi, M., Morteza-Semnani, K., Akbari, J., Gahsemi, M. & Nokhodchi, A. 2020. Development of trans-Ferulic acid niosome: an optimization and an in-vivo study. *Journal of Drug Delivery Science and Technology***,** 101854.

Rezvanian, M., Ahmad, N., Amin, M. C. I. M. & Ng, S.-F. 2017. Optimization, characterization, and in vitro assessment of alginate-pectin ionic cross-linked hydrogel film for wound dressing applications. *International journal of biological macromolecules,* 97**,** 131-140.

Rezvanian, M., Amin, M. C. I. M. & Ng, S.-F. 2016. Development and physicochemical characterization of alginate composite film loaded with simvastatin as a potential wound dressing. *Carbohydrate polymers,* 137**,** 295-304.

Rhazi, M., Desbrieres, J., Tolaimate, A., Rinaudo, M., Vottero, P. & Alagui, A. 2002. Contribution to the study of the complexation of copper by chitosan and oligomers. *Polymer,* 43**,** 1267-1276.

RINAUDO, M. 2006. Chitin and chitosan: properties and applications. *Progress in polymer science,* 31**,** 603-632.

Robitzer, M., Tourrette, A., Horga, R., Valentin, R., Boissière, M., Devoisselle, J.-M., Di Renzo, F. & Quignard, F. 2011. Nitrogen sorption as a tool for the characterisation of polysaccharide aerogels. *Carbohydrate polymers,* 85**,** 44-53.

Roe, A. J., O'byrne, C., Mclaggan, D. & Booth, I. R. 2002. Inhibition of Escherichia coli growth by acetic acid: a problem with methionine biosynthesis and homocysteine toxicity. *Microbiology,* 148**,** 2215-2222.

Sæther, H. V., Holme, H. K., Maurstad, G., Smidsrød, O. & Stokke, B. T. 2008. Polyelectrolyte complex formation using alginate and chitosan. *Carbohydrate Polymers,* 74**,** 813-821.

Sakugawa, K., Ikeda, A., Takemura, A. & Ono, H. 2004. Simplified method for estimation of composition of alginates by FTIR. *Journal of Applied Polymer Science,* 93**,** 1372-1377.

Salerno, A., Zeppetelli, S., Di Maio, E., Iannace, S. & Netti, P. A. 2010. Novel 3D porous multi-phase composite scaffolds based on PCL, thermoplastic zein and ha prepared via supercritical CO2 foaming for bone regeneration. *Composites Science and Technology,* 70**,** 1838-1846.

SALMON, S. & HUDSON, S. 1997. Crystal Morphology, biosynthesis, and physical assembly of cellulose, chitin, and chitosan, Rev. *Macromol. Chem. Phys. c37 (2),* 199.

Sankalia, M. G., Mashru, R. C., Sankalia, J. M. & Sutariya, V. B. 2007. Reversed chitosan–alginate polyelectrolyte complex for stability improvement of alpha-amylase: optimization and physicochemical characterization. *European journal of pharmaceutics and biopharmaceutics,* 65**,** 215-232.

Sartori, C., Finch, D. S., Ralph, B. & Gilding, K. 1997. Determination of the cation content of alginate thin films by FTi. r. spectroscopy. *Polymer,* 38**,** 43-51.

Schneider, L. A., Korber, A., Grabbe, S. & Dissemond, J. 2007. Influence of pH on wound-healing: a new perspective for wound-therapy? *Archives of dermatological research,* 298**,** 413-420.

Shalumon, K., Anulekha, K., Nair, S. V., Nair, S., Chennazhi, K. & Jayakumar, R. 2011. Sodium alginate/poly (vinyl alcohol)/nano ZnO composite nanofibers for antibacterial wound dressings. *International journal of biological macromolecules,* 49**,** 247-254.

Shao, W., Wu, J., Wang, S., Huang, M., Liu, X. & Zhang, R. 2017. Construction of silver sulfadiazine loaded chitosan composite sponges as potential wound dressings. *Carbohydrate polymers,* 157**,** 1963-1970.

Shao, X. & Hunter, C. J. 2007. Developing an alginate/chitosan hybrid fiber scaffold for annulus fibrosus cells. *Journal of Biomedical Materials Research Part A: An Official Journal of The Society for Biomaterials, The Japanese Society for Biomaterials, and The Australian Society for Biomaterials and the Korean Society for Biomaterials,* 82**,** 701-710.

She, Z., Zhang, B., Jin, C., Feng, Q. & Xu, Y. 2008. Preparation and in vitro degradation of porous three-dimensional silk fibroin/chitosan scaffold. *Polymer Degradation and Stability,* 93**,** 1316-1322.

Shen, F., Cui, Y. L., Yang, L. F., Yao, K. D., Dong, X. H., Jia, W. Y. & Shi, H. D. 2000. A study on the fabrication of porous chitosan/gelatin network scaffold for tissue engineering. *Polymer international,* 49**,** 1596-1599.

Shoichet, M. S., Li, R. H., White, M. L. & Winn, S. R. 1996. Stability of hydrogels used in cell encapsulation: An in vitro comparison of alginate and agarose. *Biotechnology and bioengineering,* 50**,** 374-381.

Siafaka, P. I., Zisi, A. P., Exindari, M. K., Karantas, I. D. & Bikiaris, D. N. 2016. Porous dressings of modified chitosan with poly (2-hydroxyethyl acrylate) for topical wound delivery of levofloxacin. *Carbohydrate polymers,* 143**,** 90-99.

Silva, J. M., García, J. R., Reis, R. L., García, A. J. & Mano, J. F. 2017. Tuning cell adhesive properties via layer-by-layer assembly of chitosan and alginate. *Acta biomaterialia,* 51**,** 279-293.

Silva, S. S., Motta, A., Rodrigues, M. T., Pinheiro, A. F., Gomes, M. E., Mano, J. F., Reis, R. L. & Migliaresi, C. 2008. Novel genipin-cross-linked chitosan/silk fibroin sponges for cartilage engineering strategies. *Biomacromolecules,* 9**,** 2764-2774.

Sing, K. S. 1985. Reporting physisorption data for gas/solid systems with special reference to the determination of surface area and porosity (Recommendations 1984). *Pure and applied chemistry,* 57**,** 603-619.

Singer, A. J. & Clark, R. A. 1999. Cutaneous wound healing. *New England journal of medicine,* 341**,** 738-746.

Singh, A. V. 2011. Biopolymers in drug delivery: a review. *Pharmacologyonline,* 1**,** 666-674.

Smith, M. M. & Hartley, R. D. 1983. Occurrence and nature of ferulic acid substitution of cell-wall polysaccharides in graminaceous plants. *Carbohydrate Research,* 118**,** 65-80.

Smitha, B., Sridhar, S. & Khan, A. 2005. Chitosan–sodium alginate polyion complexes as fuel cell membranes. *European Polymer Journal,* 41**,** 1859-1866.

Song, A., Rane, A. A. & Christman, K. L. 2012. Antibacterial and cell-adhesive polypeptide and poly (ethylene glycol) hydrogel as a potential scaffold for wound healing. *Acta biomaterialia,* 8**,** 41-50.

Sproul, E., Nandi, S. & Brown, A. 2018. Fibrin biomaterials for tissue regeneration and repair. *Peptides and proteins as biomaterials for tissue regeneration and repair.* Elsevier.

Sudarsan, S., Franklin, D. & Guhanathan, S. 2015. Imbibed salts and pH-responsive behaviours of sodium alginate based eco-friendly biopolymeric hydrogels—a solventless approach. *Macromol Int J,* 11**,** 24-29.

Sudheesh Kumar, P., Lakshmanan, V.-K., Anilkumar, T., Ramya, C., Reshmi, P., Unnikrishnan, A., Nair, S. V. & Jayakumar, R. 2012. Flexible and microporous chitosan hydrogel/nano ZnO composite bandages for wound dressing: in vitro and in vivo evaluation. *ACS applied materials & interfaces,* 4**,** 2618-2629.

Sweeney, I., Miraftab, M. & Collyer, G. 2014. Absorbent alginate fibres modified with hydrolysed chitosan for wound care dressings–II. Pilot scale development. *Carbohydrate polymers,* 102**,** 920-927.

Tangsadthakun, C., Kanokpanont, S., Sanchavanakit, N., Banaprasert, T. & Damrongsakkul, S. 2017. Properties of collagen/chitosan scaffolds for skin tissue engineering. *Journal of Metals, Materials and Minerals,* 16.

Temtem, M., Casimiro, T., Mano, J. F. & Aguiar-Ricardo, A. 2008. Preparation of membranes with polysulfone/polycaprolactone blends using a high pressure cell specially designed for a CO2-assisted phase inversion. *The Journal of Supercritical Fluids,* 43**,** 542-548.

Thalberg, K., Lindholm, D. & Axelsson, A. 2004. Comparison of different flowability tests for powders for inhalation. *Powder technology,* 146**,** 206-213.

Trombino, S., Ferrarelli, T. & Cassano, R. 2014. A New Pro-Prodrug Aminoacid-Based for Trans-Ferulic Acid and Silybin Intestinal Release. *Journal of functional biomaterials,* 5**,** 99-110.

Tsou, M., Hung, C., Lu, H., Wu, L., Chang, S., Chang, H., Chen, G. & Chung, J. 2000a. Effects of caffeic acid, chlorogenic acid and ferulic acid on growth and arylamine N-acetyltransferase activity in Shigella sonnei (group D). *Microbios,* 101**,** 37-46.

Tsou, M. F., Hung, C. F., Lu, H. F., Wu, L. T., Chang, S. H., Chang, H. L., Chen, G. W. & Chung, J.-G. 2000b. Effects of caffeic acid, chlorogenic acid and ferulic acid on growth and arylamine N-acetyltransferase activity in Shigella sonnei (group D). *Microbios,* 101**,** 37-46.

Ueno, H., Mori, T. & Fujinaga, T. 2001. Topical formulations and wound healing applications of chitosan. *Advanced drug delivery reviews,* 52**,** 105-115.

Van Den Kerckhove, E., Stappaerts, K., Boeckx, W., Van Den Hof, B., Monstrey, S., Van Der Kelen, A. & De Cubber, J. 2001. Silicones in the rehabilitation of burns: a review and overview. *Burns,* 27**,** 205-214.

Varshosaz, J., Arabloo, K., Sarrami, N., Ghassami, E., Yazdani Kachouei, E., Kouhi, M. & Jahanian-Najafabadi, A. 2020. RGD peptide grafted polybutylene adipate-co-terephthalate/gelatin electrospun nanofibers loaded with a matrix metalloproteinase inhibitor drug for alleviating of wounds: An in vitro/in vivo study. *Drug Development and Industrial Pharmacy,* 46**,** 484-497.

Venkatesan, J., Lee, J.-Y., Kang, D. S., Anil, S., Kim, S.-K., Shim, M. S. & Kim, D. G. 2017. Antimicrobial and anticancer activities of porous chitosan-alginate biosynthesized silver nanoparticles. *International journal of biological macromolecules,* 98**,** 515-525.

Verma, J., Kanoujia, J., Parashar, P., Tripathi, C. B. & Saraf, S. A. 2017. Wound healing applications of sericin/chitosan-capped silver nanoparticles incorporated hydrogel. *Drug delivery and translational research,* 7**,** 77-88.

Wang, C., Zhou, H., Niu, H., Ma, X., Yuan, Y., Hong, H. & Liu, C. 2018. Tannic acid-loaded mesoporous silica for rapid hemostasis and antibacterial activity. *Biomaterials science,* 6**,** 3318-3331.

Wang, K. & He, Z. 2002. Alginate–konjac glucomannan–chitosan beads as controlled release matrix. *International journal of pharmaceutics,* 244**,** 117-126.

Wang, L., Gong, C., Yuan, X. & Wei, G. 2019a. Controlling the self-assembly of biomolecules into functional nanomaterials through internal interactions and external stimulations: a review. *Nanomaterials,* 9**,** 285.

Wang, L., Khor, E., Wee, A. & Lim, L. Y. 2002. Chitosan-alginate PEC membrane as a wound dressing: Assessment of incisional wound healing. *Journal of Biomedical Materials Research: An Official Journal of The Society for Biomaterials, The Japanese Society for Biomaterials, and The Australian Society for Biomaterials and the Korean Society for Biomaterials,* 63**,** 610-618.

Wang, Q., Ju, J., Tan, Y., Hao, L., Ma, Y., Wu, Y., Zhang, H., Xia, Y. & Sui, K. 2019b. Controlled synthesis of sodium alginate electrospun nanofiber membranes for multi-occasion adsorption and separation of methylene blue. *Carbohydrate polymers,* 205**,** 125-134.

Wichterle, O. & Lim, D. 1960. Hydrophilic gels for biological use. *Nature,* 185**,** 117.

Wittaya-Areekul, S. & Prahsarn, C. 2006. Development and in vitro evaluation of chitosan–polysaccharides composite wound dressings. *International journal of pharmaceutics,* 313**,** 123-128.

Wolcott, R. D., Rhoads, D. D. & Dowd, S. E. 2008. Biofilms and chronic wound inflammation. *Journal of wound care,* 17**,** 333-341.

Wu, P., Nelson, E., Reid, W., Ruckley, C. & Gaylor, J. 1996. Water vapour transmission rates in burns and chronic leg ulcers: influence of wound dressings and comparison with in vitro evaluation. *Biomaterials,* 17**,** 1373-1377.

Wu, X., Liu, Y., Li, X., Wen, P., Zhang, Y., Long, Y., Wang, X., Guo, Y., Xing, F. & Gao, J. 2010. Preparation of aligned porous gelatin scaffolds by unidirectional freeze-drying method. *Acta biomaterialia,* 6**,** 1167-1177.

Xia, G., Lang, X., Kong, M., Cheng, X., Liu, Y., Feng, C. & Chen, X. 2016. Surface fluid-swellable chitosan fiber as the wound dressing material. *Carbohydrate polymers,* 136**,** 860-866.

Xia, W., Liu, P., Zhang, J. & Chen, J. 2011. Biological activities of chitosan and chitooligosaccharides. *Food Hydrocolloids,* 25**,** 170-179.

Xie, H., Chen, X., Shen, X., He, Y., Chen, W., Luo, Q., Ge, W., Yuan, W., Tang, X. & Hou, D. 2018. Preparation of chitosan-collagen-alginate composite dressing and its promoting effects on wound healing. *International journal of biological macromolecules,* 107**,** 93-104.

Xu, D., Hawk, J. L., Loveless, D. M., Jeon, S. L. & Craig, S. L. 2010. Mechanism of shear thickening in reversibly cross-linked supramolecular polymer networks. *Macromolecules,* 43**,** 3556-3565.

Xu, F., Weng, B., Gilkerson, R., Materon, L. A. & Lozano, K. 2015. Development of tannic acid/chitosan/pullulan composite nanofibers from aqueous solution for potential applications as wound dressing. *Carbohydrate polymers,* 115**,** 16-24.

Xue, J., Niu, Y., Gong, M., Shi, R., Chen, D., Zhang, L. & Lvov, Y. 2015. Electrospun microfiber membranes embedded with drug-loaded clay nanotubes for sustained antimicrobial protection. *ACS nano,* 9**,** 1600-1612.

Yadav, P., Yadav, H., Shah, V. G., Shah, G. & Dhaka, G. 2015. Biomedical biopolymers, their origin and evolution in biomedical sciences: A systematic review. *Journal of clinical and diagnostic research: JCDR,* 9**,** ZE21.

Yamada, K. M. 1991. Adhesive recognition sequences. *Journal of Biological Chemistry,* 266**,** 12809-12812.

Yang, D. H., Seo, D. I., Lee, D.-W., Bhang, S. H., Park, K., Jang, G., Kim, C. H. & Chun, H. J. 2017. Preparation and evaluation of visible-light cured glycol chitosan hydrogel dressing containing dual growth factors for accelerated wound healing. *Journal of industrial and engineering chemistry,* 53**,** 360-370.

Yang, G., Zhang, L., Peng, T. & Zhong, W. 2000. Effects of Ca2+ bridge cross-linking on structure and pervaporation of cellulose/alginate blend membranes. *Journal of Membrane Science,* 175**,** 53-60.

Ye, R. C. 1957. The relationship of pH of the granulation tissue and the take of the skin graft. *Plastic and reconstructive surgery,* 19**,** 213-217.

Yuvarani, I., Kumar, S. S., Venkatesan, J., Kim, S.-K. & Sudha, P. 2012. Preparation and characterization of curcumin coated chitosan-alginate blend for wound dressing application. *Journal of Biomaterials and Tissue Engineering,* 2**,** 54-60.

Zakhem, E., Raghavan, S., Gilmont, R. R. & Bitar, K. N. 2012. Chitosan-based scaffolds for the support of smooth muscle constructs in intestinal tissue engineering. *Biomaterials,* 33**,** 4810-4817.

Zhang, S. & Gonsalves, K. 1995. Synthesis of calcium carbonate–chitosan composites via biomimetic processing. *Journal of applied polymer science,* 56**,** 687-695.

Zhang, Y., Li, Z., Zhang, K., Yang, G., Wang, Z., Zhao, J., Hu, R. & Feng, N. 2016. Ethyl oleate-containing nanostructured lipid carriers improve oral bioavailability of trans-ferulic acid ascompared with conventional solid lipid nanoparticles. *International Journal of Pharmaceutics,* 511**,** 57-64.

Zhao, W., Li, J., Jin, K., Liu, W., Qiu, X. & Li, C. 2016. Fabrication of functional PLGA-based electrospun scaffolds and their applications in biomedical engineering. *Materials Science and Engineering: C,* 59**,** 1181-1194.

Zhao, X., Wu, H., Guo, B., Dong, R., Qiu, Y. & Ma, P. X. 2017. Antibacterial anti-oxidant electroactive injectable hydrogel as self-healing wound dressing with hemostasis and adhesiveness for cutaneous wound healing. *Biomaterials,* 122**,** 34-47.

Zhu, J., Tang, C., Kottke-Marchant, K. & Marchant, R. E. 2009. Design and synthesis of biomimetic hydrogel scaffolds with controlled organization of cyclic RGD peptides. *Bioconjugate chemistry,* 20**,** 333-339.

Zohourian, M. M. & Kabiri, K. 2008. Superabsorbent polymer materials: a review.

Zorzi Bueno, C. & Maria MoraeS, Â. 2011. Development of porous lamellar chitosan-alginate membranes: Effect of different surfactants on biomaterial properties. *Journal of Applied Polymer Science,* 122**,** 624-631.

CHAPTER 3

Development of a Fluid-absorptive Alginate-Chitosan Bioplatform for Potential Application as a Wound Dressing

Published in Carbohydrate Polymers

Mndlovu, H., du Toit, L.C., Kumar, P., Marimuthu, T., Kondiah, P.P., Choonara, Y.E. and Pillay, V., 2019. Development of a fluid-absorptive alginate-chitosan bioplatform for potential application as a wound dressing. Carbohydrate polymers, 222, p.114988.

3.1. Introduction

Wound dressings contribute greatly towards acceleration of wound healing and can act as both physical and mechanical barrier to prevent blood loss and against foreign bodies such as bacteria. Natural polymers such as chitosan (CS) and alginate (Alg) have drawn much attention in the wound dressing field due to their ionic character and biological properties. Their ionic character allows them to form interpolymer complexes (IPCs) which can be tuned into various bioplatforms (BPs) such as gauze (Xie et al., 2018), beads (Fathi et al., 2018), nanoparticles (Venkatesan et al., 2017), films/membranes (Bueno et al., 2016, Silva et al., 2017), and hydrogel sponges/scaffolds (Chen et al., 2017). To date, there is still no promising gauze, film, or scaffold capable of treating wounds, such as deep cuts. This leaves foams, injectable hydrogels, nanoparticles and beads/microparticles as potentially desirable bioplatforms to treat deep cut wounds were conventional dressings cannot be applied. Recent studies on CS-Alg IPC beads/microparticles have indicated great advancement in potential properties such as improving bioplatform swelling capacity, erythrocyte adhesion, cytocompatibility, antimicrobial, and drug/growth factor release (Chen et al., 2017, Venkatesan et al., 2017, Fathi et al., 2018). Incorporation of toxic agents such as silver and zeolite, and UV-radiation crosslinking of CS-Alg IPC bioplatforms may improve physical properties such as swelling ratio and pore size while introducing cytotoxicity (Fathi et al., 2018, Venkatesan et al., 2017, Dowling et al., 2011). The use appropriate crosslinkers and selection of suitable fabrication approaches can produce cytocompatible CS-Alg IPCs with optimal physicochemical and physicomechanical properties. The current study was undertaken for the attainment of enhanced physicochemical and physicomechanical properties of the CS-Alg IPC microparticles by the use of $CaCl_2$ and sodium tripolyphosphate for partial crosslinking of chitosan and alginate.

Further, in this investigation, surfactants, drugs, and potentially toxic compounds have been excluded. Thus the fabricated bioplatform performance would depend on the biological properties of the polymers and the improved properties attained via the partial-crosslinking approach. The biological properties of chitosan include tissue repair, antimicrobial, immune-enhancing, antioxidant, metal chelating, hypocholesterolemic, lipid binding, anti-inflammatory, anticancer, and antitumor effects (Rabea et al., 2003, Xia et al., 2011). Additional chitosan properties, such as the ability to be tuned into an amphiphilic biopolymer with the potential to gel blood, renders chitosan a preferable material to design haemostatic dressings for heavily bleeding wound conditions. Hydrophobically-modified chitosan introduces the ability of chitosan to rapidly gel blood, which facilitates blood clotting at the wound site to counteract blood loss (Dowling et al.,

2011). The blood gelation process can be reversed by introducing sugar-based supramolecules such as α-cyclodextrin, as the polymer hydrophobes unbind from blood cells, embedding within cyclodextrins, thereby disrupting the cell network (Dowling et al., 2011). Chitosan is soluble under acidic conditions (pH<6), thereby aiding its biodegradable character (Khan et al., 2000b). Chitosan comprises of D-glucosamine and N-acetyl glucosamine units. These units give chitosan its cationic character as there are three reactive functional groups namely; an amino/acetamide group, and both primary and secondary hydroxyl groups at the C-2, C-3 and C-6 positions of the linear polysaccharide molecule.

Alginate is a naturally occurring copolymer of 1,4-linked β-D-mannuronic acid and α-$_L$-guluronic acid. Sodium alginate is soluble in alkaline conditions and chemically stable at pH conditions between 5 and 10. However, it tends to decarboxylate at highly acidic conditions (Wang and He, 2002). The biocompatibility, hydrophilicity, and biodegradability of alginate under normal physiological conditions and its instant gelling character allows for application in various tissue therapeutic dressings (Becker et al., 2001a, Gutowska et al., 2001, Li et al., 2005). The carboxylic group of alginate confers its anionic character which allows alginate to interact with cationic polymers such as a stable ionic bond formation with the amine group of chitosan (Li et al., 2005, Kulig et al., 2016). The use of calcium chloride as a crosslinker in sodium alginate solutions, aids effective and sufficient binding to chitosan compared to other methods of interpolymer complexation (Sankalia et al., 2007). The presence of salt in these polymers facilitates favourable binding energies between the two polymers.

The interpolymer interaction leads to polymerisation which can emanate in hydrogel formation or precipitation, depending on the interpolymer complex experimental conditions such as concentrations, ionic strength, pH, temperature, order of mixing, flexibility of polymers, and chemical composition of the polymers (Sæther et al., 2008, Berger et al., 2004, Smitha et al., 2005, Kulig et al., 2016). The interpolymer complexation reaction is aided by an electrostatic neutralisation of charges and other structural compensations such as hydrogen bonding, Coulomb forces, Van der Waals forces, and transfer forces that occur during the attraction type of interaction, within fragments of these polyions (Dumitriu and Chornet, 1998). This implies that the polymer with lower charge density will be required to be at higher proportion, to achieve a neutralised charge of the overall interpolymer complex. Recent studies have indicated that Zeolite-loaded alginate-chitosan hydrogel beads are cytocompatible and displayed great erythrocyte adhesion to help control haemorrhage (Fathi et al., 2018). The favourable gel-forming and wound-healing properties and ionic interactions of these two polymers has enabled them to be employed in various FDA approved wound dressings (separately or in combination) on the market such as Tegagen™ (3M), Algisite™ (Smith and Nephew), Algi-Fiber (Core Leader Biotech), Syvek-Patch, Chitopack C, Tegasorb, HemCon Bandage, and KytoCel (Chen et al., 2008, Brown et al., 2009, Han et al., 2014, Sudheesh Kumar et al., 2012, Zakhem et al., 2012, O'Meara and Martyn-St James, 2013, Dumville et al., 2015).

Most of the wound dressing devices require a slight force applied to the wound area during dressing application. This process results in pain at the wound area thereby leading to poor patient compliance with the dressing type. Wound dressings that require frequent changes imply that they are not easily biodegraded and bioresorbed. This increases the patient compliance issues with scaffolds, gauzes, and bandages as wound dressings. Thus, the aim of this study was to explore the partial-crosslinking approach for synthesising pulverised bioplatforms with *in situ* hydrogel forming capabilities in simulated wound fluid (SWF). The polyelectrolyte interaction

between the polymers and their crosslinkers along with the interpolymer complexation between the crosslinked polymers were studied and confirmed as the provenance of hydrogel formation between the polymers. Chitosan was crosslinked with sodium tripolyphosphate and alginate crosslinked with $CaCl_2$. The rationale of the study is to improve sodium alginate and chitosan physicochemical and physicomechanical properties while maintaining their interpolymer complexation capabilities by simply partially-crosslinking the two polymers separately. The properties sought to be improved included their mechanical (viscoelastic properties and rigidity/storage modulus (G')/ or gel strength), chemical (ionic interaction/ interpolymer complexation), and physical properties (porosity, swelling, fluid absorption, thermostability, and controlled platform degradation). The bioplatform was exposed to simulated wound fluid (SWF) and whole blood to simulate the transitory wound environment for detailed analysis on gel strength, complex modulus, and viscosity, to assess the interpolymer complexation in a simulated wound environment. Fluid uptake and degradation properties of the bioplatform was compared to a commercial product, an alginate-based wound dressing, to assess the potential of this platform as a wound dressing for an acute exudative wound.

3.2. Materials and Methods

3.2.1. Materials

Medium molecular weight chitosan (75-85% deacetylation) Sigma-Aldrich (St. Louis, MO, USA). The calculated degree of deacetylation of 84.36% was determined on chitosan by employing NMR analyses at 70°C on the dissolved chitosan in a 1:1 ratio of deuterated acetic acid and deuterated oxide. Sodium alginate Sigma-Aldrich (St. Louis, MO, USA). The calculated mannuronic acid and guluronic acid concentration ratio (A_{1025}/A_{1078}) of 1.51 was obtained via FTIR analyses as described in literature (Sakugawa et al., 2004). Glacial acetic acid, calcium chloride, sodium tripolyphosphate and Coomassie brilliant blue G-250 were purchased from Sigma-Aldrich (St. Louis, MO, USA). Simulated wound fluid (SWF) comprised 2% $^{w}/_{w}$ bovine serum albumin (BSA), 0.02M $CaCl_2$, 0.4M $NaCl_2$, and 0.08 M tris(Hydroxymethyl) aminomethane dissolved in deionised water to pH 5 and 7.4 (Boateng et al., 2015), prepared to simulate the disturbed acidic skin (pH 5-6). Whole blood was collected from healthy donors, approved with ethical clearance (ethics clearance number; M180978). A commercial alginate-based wound dressing (Pharma-Algi®, Pharmaplast) was acquired for comparative studies.

3.2.2. Polymer solution preparation and partial-crosslinking

Pristine (used as received from the manufacturer without further modification) chitosan (P-CS) (2g) powder was dissolved in 2% $^{v}/_{v}$ glacial acetic acid and partially-crosslinked with 2% $^{w}/_{v}$ sodium tripolyphosphate (TPP) solution. The partially-crosslinking of chitosan was achieved by dropwise addition of chitosan solution to the 2% $^{w}/_{v}$ TPP solution with quick removal of the formed soft beads/macromatrices after 60 seconds. The partially-crosslinked beads were rinsed and immediately placed in a -80 °C freezer for 24 hours. The freezing step was followed by the lyophilisation process (Free zone 12 lyophiliser, Labcono, Kansas City, USA) for 24 hours. The lyophilised chitosan beads were pulverised via a pestle and mortar to produce partially-crosslinked chitosan (PC-CS) microparticles. The particles obtained after pulverisation were passed through a 63μm sieve to control the particle size distribution. Microparticles coated with polymers have been previously defined as macromatrices (Rao and Buri, 1989). To highlight the difference in the particle size, beads of a size greater than 1000 μm were considered macromatrices and they were pulverised to a micro size (<1000 μm). Pristine sodium alginate (P-Alg) beads were prepared in the same manner as the chitosan beads. Briefly, a 2% $^{w}/_{v}$ solution of

sodium alginate was crosslinked with 2% $CaCl_2$ $^{w}/_{v}$ and rinsed with deionised water before frozen at -80 °C and lyophilised for 24 hours (Figure 3.1). The lyophilised alginate beads were pulverised via a pestle and mortar to produce partially-crosslinked alginate (PC-Alg) microparticles. The *in situ* forming interpolymer complex (IPC) was achieved by sprinkling 100mg (1 PC-CS:1 PC-Alg) into 3 mL PBS buffer (pH 7.4)/SWF(pH 5/7.4) or whole blood.

3.2.3. Powder flow properties of the bioplatforms

The microparticles where tested for their flow properties by employing Carr's method (Carr et al., 1965). Briefly, microparticles were passed through an 80 mm long glass tube with a 6 mm diameter in each opening. The glass tube was fixed 50 mm from the horizontal surface and allowed the powder to flow until the tip of the conical pile was approximately 20 mm from the glass tube. The diameter and the height of the powder cone was measured to determine the static angle of repose.

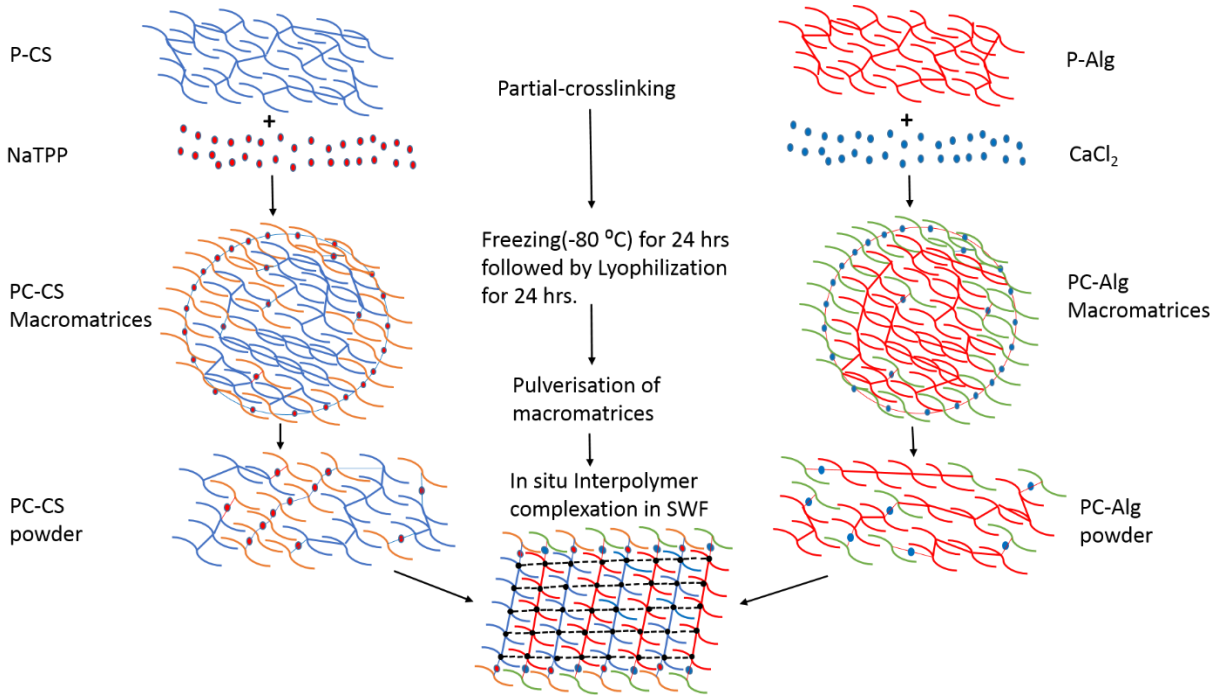


Figure 3.1. Schematic representation of the three-step method of partial-crosslinking and interpolymer complexation of the polymers.

3.2.4. Interpolymer complexation of PC-Alg and PC-CS platforms

The gelling of the polymers was undertaken via interpolymer complexation. The gelling and ionic polymerization process of the complex was achieved via the use of the phosphate buffered saline (pH 7.4), whole blood and simulated wound fluid (SWF) (pH 5, 7.4, and 9.36) separately at 25 °C and at 37 °C. Even though PBS and whole blood have the same pH, the high viscosity of blood could increase the stiffness of the formed IPC. The powdered polymers were mixed in equal proportions (1:1 in weight) to achieve a homogenous powder blend. The mixture (50 mg PC-Alg and 50mg PC-CS) was then added to a 3 mL solution of the PBS at pH 7.4 or SWF, and allowed to gel for 24 hours before lyophilisation. The gelling, water absorption, interpolymer complexation, and swelling behaviour was determined.

3.2.5. Zeta potential of PC-CS and PC-Alg bioplatforms

A Zetasizer NanoZS instrument (Malvern Instruments (Pty) Ltd., Worcestershire, UK) was employed in quantifying the particle surface charge of pristine and partial crosslinked polymers. The technique works by following the electric potential in the double artificial layer. The obtained point where the diffuse and the stern layers are bonded gives insights on the stability of the colloidal dispersions, thereby indicating the repulsion degree among adjacent particles charged in a dispersion. The prepared PC-CS and PC-Alg bioplatforms were sonicated in distilled water and filtered before suspended in the cell for analysis of zeta potential at 25 °C.

3.2.6. Determination of molecular vibrational transitions on fabricated bioplatforms

The FTIR spectra of the bioplatforms were analysed for specific interactions between the pristine polymers (chitosan and alginate) and the partial-crosslinked microparticles. This was undertaken to determine their ability to form an interpolymer complex (IPC). The FTIR spectra of the partially crosslinked beads before pulverisation were also compared to that of the pulverised PC-CS and PC-Alg to establish the effects of pulverisation on the molecular structure. FTIR parameters were set as follows; 64 scans and a wavenumber range of 4000–650 cm^{-1} using a PerkinElmer Spectrum 2000 ATR-FTIR (PerkinElmer 100, Llantrisant, Wales, UK) spectrometer fitted with a single-reflection diamond MIRTGS detector.

3.2.7. X-ray powder diffraction analysis of the bioplatforms

The Alg and CS beads, lyophilised and pulverised polymer blends (PC-Alg and PC-CS) and pristine polymers were further analysed by X-ray diffraction to characterize the types of phases present. X-ray diffraction spectra were recorded on a benchtop MiniFlex 600 (Rigaku, Japan) diffractometer using CuKα radiation at 40 kV and 15 mA. The 2θ scan range was selected between 10-90 degrees at a scan rate of 10 degrees/minute. This diffraction analyses allowed for the observation of the degree of crystallinity of the bioplatforms.

3.2.8. Determination of thermophysical properties of the bioplatforms

The thermophysical properties of the fabricated bioplatforms and pristine polymers were determined using a differential scanning calorimeter (DSC) (Mettler Toledo, DSC, STARe System, Swchwerzenback, ZH, Switzerland). Bioplatforms and pristine polymer samples of 3 to 10 mg were sealed in aluminum crucibles and heated over a temperature range of 20 to 400 °C at a heating rate of 10 °C/min under a N_2 atmosphere. DSC curves were plotted as heat flow against temperature. The temperature range with which the formulations degraded were determined using a thermo-gravimetric analyser (TGA) (PerkinElmer, TGA 4000, Llantrisant, Wales, UK). Samples were heated at a rate of 10 °C/min from 30 to 900 °C under continuous nitrogen purging. Thermograms were generated as percentage weight vs. temperature.

3.2.9. Determination of the degree of crosslinking of the bioplatforms

The degree of crosslinking was calculated by employing the Bradford assay (Bradford, 1976). The Bradford reagent was prepared by dissolving 50 mg of Coomassie brilliant blue G-250 in 25 mL of 95% ethanol. Phosphoric acid (50 mL) was added to this solution followed by dilution to 500mL with deionised water. The test samples were prepared as follows: an aqueous solution of 9mL Bradford reagent was mixed with 1mL of either 2% $^{w}/_{v}$ crosslinked or uncrosslinked chitosan solution dissolved in 2% $^{v}/_{v}$ acetic acid. The absorbance of the resulting solution was measured at 595 nm using a UV Visible spectrophotometer (Specord 40 UV-Vis Spectrophotometer, Analytik Jena AG, Jena, Germany). An aqueous solution containing 1mL of 2% $^{v}/_{v}$ acetic acid and

9 mL of Bradford reagent was used as a reference. The amount of free amino groups in the chitosan material before crosslinking (Ci) and after crosslinking (Cf) is proportional to the optical absorbance of the solution. The percentage crosslinking index was calculated using Equation 3.1:

$$\% \text{ Cross-linking index} = \left(\frac{Ci-Cf}{Ci}\right) x100 \quad \text{Equation 3. 1}$$

The degree of crosslinking in partially-crosslinked alginate was determined by observing the absorption of pristine versus partially-crosslinked alginate on the affected carboxylic groups using FTIR and applying Equation 1. The analyses was also compared to the back titration analyses to obtain the degree of COO^-/mole in both pristine and partially crosslinked alginate, which were then substituted in Equation 1. The average of three titrations were reported.

3.2.10. Porositometric and surface topography characterization of bioplatforms employing the Brunauer–Emmett–Teller (BET) theory

The surface area, pore size and pore volume of samples were evaluated using a Porositometric analyzer (Micromeritics ASAP 2020, Norcross, GA, USA). Each sample (0.3 g) was introduced to the sample tube and degassed. The analysis of the surface area, pore size and pore volume was undertaken in accordance with the BET and BJH models on the platforms. The experimental conditions were as follows, an evacuation rate of 50mm Hg/s with a temperature ramp rate of 10 °C/min, target temperature of 115 °C and held temperature at 30 °C for 900 minutes before completing analyses.

3.2.11. Evaluation of surface morphology of the fabricated bioplatforms

Scanning electron microscopy (SEM) (Phenom™ Scanning Electron Microscope, FEI Company, OR, USA) and energy dispersive spectroscopy (EDS) ((FEI Company, OR, USA) with an accelerating voltage from 10 to 15 kV was employed for the analysis of the surface morphology of the designed formulations. The energy dispersive spectroscopy analyses were performed in an integrated system. Before analysis, all formulations were mounted on aluminum stubs using a carbon adhesive tape and coated with carbon/gold in a 2:1 ratio.

3.2.12. Fluid uptake and degradation of the bioplatforms and comparator wound dressing

Hydration due to water or fluid uptake and degradation (weight loss) of the bioplatforms and comparator wound dressing product were performed under simulated *in vitro* exudative conditions. The orbital shaking incubator (LM-530-2, MRC Laboratory Instruments Ltd. Hahistadrut, Holon, Israel) was used for this study, maintained at 37 °C, and set at a speed of 50 rpm. Five different samples P-CS, P-Alg, PC-CS, PC-Alg, and the IPC were prepared by weighing 50 mg of each sample into vials and added 5 mL PBS (pH 7.4). Swelling of the bioplatforms occurred rapidly over the first 8 hours and stabilised by 24 hours, thus for water uptake studies, measurements were taken over 24 hours. Excess fluid was removed from the wet samples by slightly blotting the samples. The degree of degradation was measured on days 1, 2, 3, 5, 7, 10, and 14 days; and on each of these days, the dried mass was measured for the determination of change in mass. The wet samples were left to air-dry for 72 hours to ensure complete removal of residual moisture before being weighed to determine the eroded mass. The water uptake (swelling) was measured using Equation 3.2 and the mass loss of the bioplatforms after degradation at each time point was calculated via Equation 3.3:

$$FU\ (\%) = \left(\frac{Mh-Md}{Md}\right) x\ 100 \quad \text{Equation 3. 2}$$

Where *FU%* is the percentage fluid uptake, *Mh* and *Md* is the mass of the bioplatforms in hydrated and dry state, respectively.

$$Degradation\ (\%) = \frac{Mo-Md}{Mo}\ x\ 100 \qquad \text{Equation 3. 3}$$

Where *Mo* is the initial mass of the sample before fluid immersion.

3.2.13. Rheological evaluation of the viscoelastic properties of the hydrogel

Rheological analysis of the polymer solutions and the IPC was carried out via the use of a Haake Modular Advanced Rheometer System (II) Modular Advanced Rheometer system (Thermo Fisher Scientific, Johannesburg, South Africa), using a cone plate geometry (Rotor C35/1, D = mm, 1 Titan) with a gap measurement of 0.050mm. The IPC hydrogel (2% $^{w}/_{v}$), chitosan (2% $^{w}/_{v}$), and alginate solution (2% $^{w}/_{v}$) were prepared and stored at 10°C for 24 hours before determining their rheological properties. The following types of rheological experiments were conducted at 37°C: oscillation frequency sweep, creep-recovery, and hysteresis loop area determination. Oscillation stress sweeps were performed by applying increasing shear stress logarithmically from 0.05 Pa to 100 Pa at a fixed frequency of 1Hz. The yield stress assessment for all the samples was performed from 0.01 to 100 Pa. The inherent thixotropic properties of the samples were analysed using the hysteresis loop area technique, where different shear rates were applied in the range of 0.1 to 50 s^{-1} for 500 s. The hydrogel and network formation during interpolymer complexation were evaluated using the ElastoSens™ Bio^2 (Rheolution instruments, Canada). The kinetic gelation of the polyelectrolytes was determined by mixing a total of 100 mg of the partially-crosslinked polymers and initiated the polyelectrolyte complexation by pouring the polymer mixture into 3 mL of PBS/SWF/whole blood into the sample holder at 37 °C. The gelling, ionic interaction, and viscoelastic (G' and G*) properties of semi-stiff IPC hydrogel was determined over time. The ElastoSens™ BIO^2 technique measures in real time, the shear storage (G') and loss (G") moduli of gels as function of time or temperature. The analysis is based on the gentle mechanical vibration of a sample confined in a sample holder and the response is detected via a laser. The pH dependence of the IPC gelation, SWF absorption, and viscosity was determined.

3.2.14. Cytotoxicity assessment of the bioplatforms

Pristine CS-Alg and PC CS-Alg were prepared for cell viability analysis on the mouse embryonic fibroblast NIH-3T3 cell line. The NIH 3T3 cells were grown in DMEM medium supplemented with 10% FBS and 1% of the relevant antibiotics. A total of 1 mg Pristine CS-Alg (1:1 CS:Alg ratio) and 1mg PC CS-Alg were sterilised under UV light and mixed in 100 µL DMEM medium in a 96 well plate overnight to cover the bottom surface of the wells. After overnight IPC formation on the DMEM medium, 100 µL of NIH 3T3 cells (1 x 10^4 cell/ml) were seeded on each well plate and incubated in a humidified chamber overnight at 37°C with an atmosphere containing 5% CO_2 for predetermined time points: 24, 48, and 72 hours. NIH 3T3 cells where maintained with DMEM medium to serve as the live control and cells treated with Dimethyl Sulfoxide (DMSO) for 6 hours served as the dead control. Ten microliters of MTT (3-(4,5-Dimethyl-2-thiazolyl)-2,5-diphenyl tetrazolium Bromide) was added to each well plate after each of the predetermined time points and incubated for 4 hours. Thereafter, the medium and the interpolymer complex on the well plates was discarded followed by addition of 100µL DMSO and incubated overnight on the orbital shaker (at 37 °C) to dissolve the formazan. The well plates were measured at an absorbance of 570 nm to calculate the percentage cell viability for each bioplatform.

3.3. Results and Discussion

This work demonstrated the application of partially-crosslinked polymers to produce an *in situ* forming interpolymer complex as a novel approach for potential treatment of deep cut wounds and ulcerated wounds. The pristine alginate (P-Alg), pristine chitosan (P-CS), partially-crosslinked alginate (PC-Alg), partially-crosslinked chitosan (PC-CS) bioplatforms, and interpolymer complex (IPC), were analysed for structural, physical and mechanical property transitions. The investigation presented herein focused on the effect of the partial-crosslinking approach on the properties of the bioplatforms.

3.3.1. Synthesis of the bioplatforms

Sodium alginate was dissolved in distilled water whereas chitosan was dissolved in glacial acetic acid. At low glacial acetic acid concentrations there was limited chitosan solubility while high acetic acid concentrations were avoided due to their possible inhibition of cell growth and potential skin irritation (Khan et al., 2000b, Roe et al., 2002). An optimum acetic acid concentration of 2% $^{v}/_{v}$ was employed in the study. The bioplatforms were fabricated from low concentrations of the polymer and crosslinking (2% $^{w}/_{v}$ and 2% $^{v}/_{v}$, respectively) to control the degree of crosslinking. The crosslinking of alginate with calcium chloride decreased the solubility of alginate but enhanced its gelation through establishing a partially ionically crosslinked, interconnected system thus allowing alginate to act as a wound filler and a wound surface protective agent (Qin, 2008). Calcium chloride also enhanced the resistance of alginate to weight loss which would improve gel strength during interpolymer complexation (Miraftab et al., 2003). The calcium salts from the partially crosslinked, lower solubility alginate would be released via the ion exchange process with sodium under exudative conditions (Miraftab et al., 2003, Qin, 2008). The released calcium salts could further provide haemostatic properties such as preventing blood clotting (Miraftab et al., 2003). Crosslinking of chitosan with NaTPP reportedly improves the hydration (water uptake) of chitosan. The mechanical strength of the hydrogel is also improved by the sodium tripolyphosphate crosslinking, through formation of an interconnected network. The presence of tripolyphosphate would also contribute to the procoagulant properties of the bioplatform (Ong et al., 2008). The pulverisation of the bioplatforms decreased the size of the particles thereby increasing the surface area-to-volume ratio of the bioplatform thus enhancing fluid diffusion. Fluid penetration to the microparticles was quicker due to the shorter distance from the surface to the centre of the particle. Thus pulverisation would serve to enhance the rate interaction between the PC-Alg and PC-CS in the presence of fluid. The increase in surface area-to-volume ratio also increases the rate of erosion in this water permeable bioplatform.

The partial-crosslinking of polymers instantly formed soft beads/macromatrices (>1000 µm) and the degree of crosslinking was increased by increasing the duration of exposure of the polymers to their respective crosslinking solutions. The partial-crosslinking was achieved by allowing the macromatrices to be formed and soaked for 60 seconds before they were rinsed with deionised water to stop the crosslinking process. The freeze-drying step allowed for removal of excess water and formation of dry, porous macromatrices. The macromatrices were pulverized, resulting in a mixture of both crosslinked and uncrosslinked powdered polymer particles. The formulation of powdered bioplatforms was to enable a wide range of applications in wound dressing and drug delivery. The ionic character of each of these processed polymers allowed for enhanced interpolymer complexation on fluid exposure and interaction with other ionic compounds.

3.3.2. In situ forming IPC hydrogel concept assessment in a physiological environment

The rationale behind the three-step approach (partial-crosslinking, lyophilisation, and pulverisation of bioplatforms) was to improve the strength of the *in situ*-formed interpolymer complex, increase porosity, swelling ratio, degradation and gelling kinetics. The concept of partial crosslinking was also confirmed by analyses of the surface charge on the bioplatforms and their pristine counterpart. The gelling kinetics was followed in both acidic (5-6) and neutral pH (7.4) conditions due to the point that the skin acidic milieu is disturbed in wounds thus exposing the underlying tissue with the body's internal pH milieu of 7.4 (Schneider et al., 2007).

3.3.3. Powder flow properties of the bioplatforms

The powder flow properties of the microparticles were characterised by assessing the angle of repose. The angle of repose measurement relates to the interparticulate friction or resistance to movement between microparticles in the glass tube. Knowledge of the flow properties is important for ascertaining the ease of application of the bioplatform to the wound site. Several studies indicated that the angle of repose did not correlate with other measures of flow properties, thus making it an unreliable measure of flow properties (Amidon, 1995, Thalberg et al., 2004, Agarwal et al., 2009). However, its ease of use allowed it to be employed in various pharmaceutical products (Amidon, 1995). The powder flow properties as described by Carr classified the angle of repose range of 25-30°, 31-35 °, and 36-40 ° as having excellent, good, and fair flow properties, respectively (Carr et al., 1965). The angle of repose of the bioplatform were as follows P-Alg (26 ± 1.5), PC-Alg (36±1.5), P-CS (27±1), and PC-CS (30±1.2). The pristine polymers displayed excellent flow properties which decreased to good and fair flow properties after partially-crosslinking. The flow properties of the bioplatforms are within an acceptable range to be manufactured industrially.

3.3.4. Degree of crosslinking of alginate and chitosan

The degree of deacetylation on chitosan was determined to be 84.36% via NMR analysis as described by Jia, & Shen (Jia and Shen, 2002). All analysis on chitosan such as degree of crosslinking took into account the obtained degree of deacetylation. The obtained mannuronic and guluronic acid (M/G) ratio in sodium alginate was 1.51 via FTIR analysis. Calcium alginate contains the M/G ratio at absorbance combination of A_{1030}/A_{1080} as described by Sagugawa et al. and these absorbance combinations are in agreement with the observations of the current study (Sakugawa et al., 2004). The degree of crosslinking in partially-crosslinked chitosan was 40.14% which implied that the remaining 59.86% of chitosan was available for further interpolymer complexation reactions.

The degree of crosslinking in partial-crosslinked alginate (PC-Alg) was 21.44% which decreased the solubility of alginate in water. Although there is a slight difference in the degree of crosslinking obtained in these two techniques; they indicated the low crosslinking observed in PC-Alg. These observations correlated with those observed for the matrix hydration, swelling and degradation analyses which highlighted a slight decrease in alginate solubility after partial crosslinking. The high solubility of pristine alginate (P-Alg) may result in rapid bioresorption thereby decreasing the swelling ratio and render it difficult to perform degradation analyses. Therefore, a slight decrease in solubility contributed in achieving an optimum swelling ratio, interpolymer complexation, controlled fluid absorption and degradation. High fluid absorption is a crucial property for wound dressing bioplatforms. The partial-crosslinking process improved the hydrophilicity of the polymer thereby allowing it to retain a high volume of PBS/SWF/whole blood.

3.3.5. Zeta potential analysis of the pristine polymers and bioplatforms

The significance of surface charge analyses is that it provides insights to the potential antimicrobial properties of the particles (Kong et al., 2010, Du et al., 2008) and also the stability of particles (Du et al., 2009) in terms of the ionic interactions that may exist between polymers, drugs (Qandil et al., 2009), and bacterial organisms. Microbes carry a negative surface charge which interacts with the positive surface charge of chitosan, affecting microbial membrane integrity, thus inhibiting microbial growth (Chen et al., 2010). The average zeta potentials of the pristine polymers and the bioplatforms were -45.3±6.45, -25.8 ± 3.74, 53.83±3.77, and 29.2 ± 5.83(mV) for P-Alg, PC-Alg, P-CS, and PC-CS, respectively. The pristine polymers displayed the highest surface charge which decreased after partial-crosslinking. The decrease on the surface charge signifies the crosslinking of the polymers. Furthermore the high surface charge of the partially-crosslinked polymers inferred that there was partial-crossliking since the crosslinking did not decrease the surface of charge of the polymers to be below 10mV. The high surface charge on the partially-crosslinked polymers could allow for further ionic interaction which would aid drug incorporation and interpolymer complexation. Müller and co-workers reported that a zeta potential of ±30mV is required as minimum in physically stable nanosuspensions, solely stabilized by electrostatic repulsion (Müller et al., 2001b). However in the case of combined electrostatic and steric stabilization, a zeta potential of ±20mV was sufficient (Müller et al., 2001b). All of the bioplatforms produced had a zeta potential that was above 25mV, which implies that the bioplatforms could be stabilized by the electrostatic and steric interactions.

3.3.6. Chemical interaction and molecular vibrational transition analysis of the bioplatforms

The crosslinking reaction of sodium alginate is demonstrated in Figure 3.2a, chitosan in Figure 3.2b and the interpolymer complexation in Figure 3.2c. Calcium chloride has a higher ionic strength than sodium. This leads to the effective substitution of sodium with excess calcium chloride. The divalent calcium interacts with two carboxylic groups of alginate. Those groups of alginate that have interacted with calcium do not undergo further ionic interaction. The same applies to crosslinked chitosan. The tripolyphosphate groups interact with the primary amine of chitosan. The remaining non-crosslinked amines of chitosan interact with the non-crosslinked carboxylic groups of alginate under fluid exposure to form an interpolymer complex. The resulted IPC consists of both crosslinked and non-crosslinked polymer chains as depicted in Figure 3.1 above.

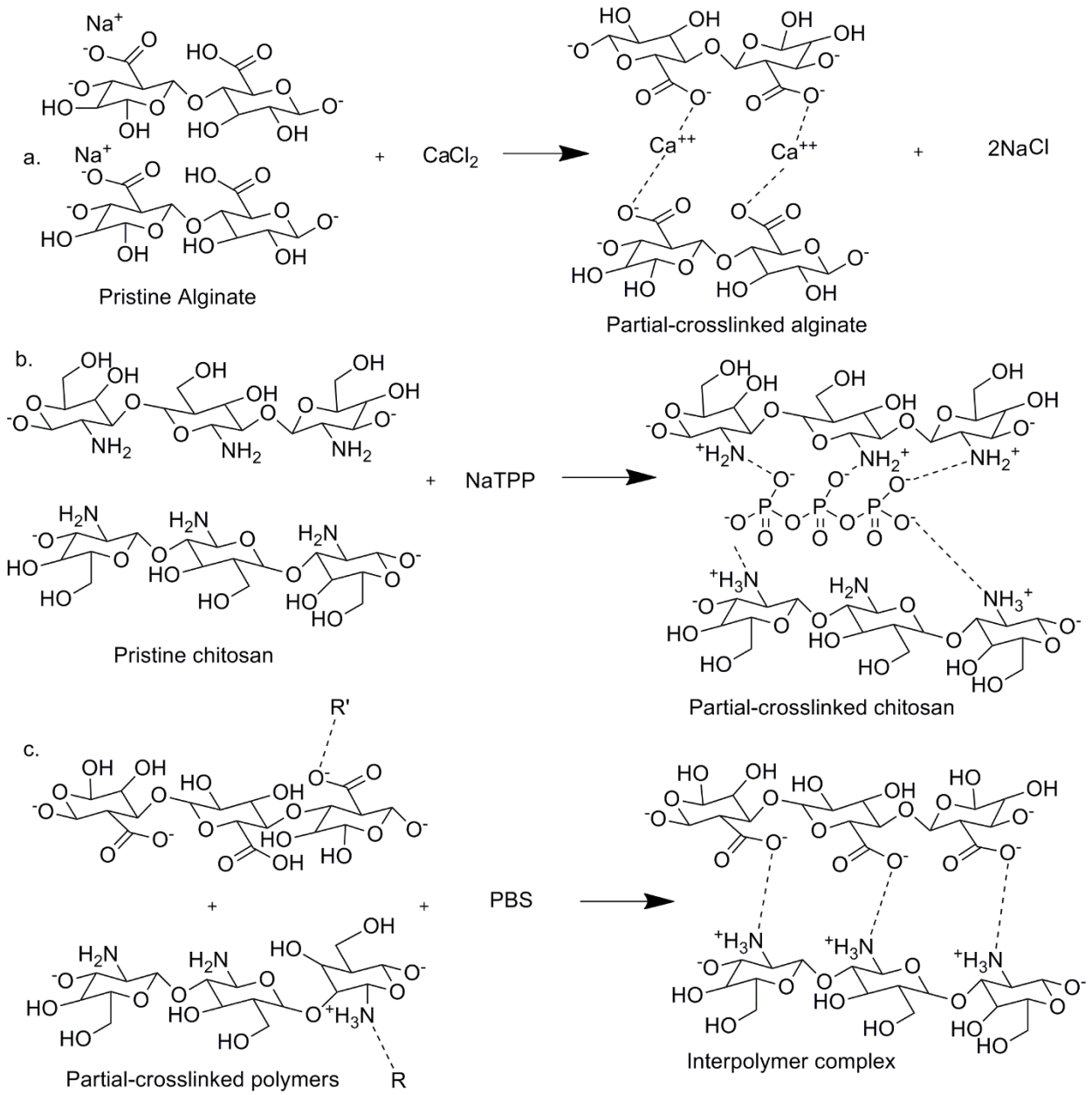


Figure 3.2. Schematic representation of the (a) sodium alginate crosslinking, (b) chitosan crosslinking and (c) interpolymer complexation reaction. R and R' represent the crosslinked portion of the polymers by their respective crosslinkers.

The partial-crosslinking and interpolymer complexation reactions were analysed via FTIR analysis. The pristine chitosan (P-CS) bioplatform displayed the characteristic broad absorption peaks at 3286 cm^{-1} (OH stretch), 2870 cm^{-1} (CH stretch), 1648 cm^{-1} and 1586 cm^{-1} (amide II stretch and C=O stretch), and 1374 cm^{-1} (C-C bending) (Figure 3a). These observations are in agreement with those reported in the literature (Xia et al., 2011, Kumar et al., 2012). The other sharp absorption peaks at 1150 cm^{-1} and 1023 cm^{-1} are representative of the anti-symmetric stretching of the C-O-C bridge and skeletal vibrations around the C–O stretching which are the features of its saccharide chemical structure (Ghazali et al., 1997, Smitha et al., 2005). These peaks were consistent with those observed on the CS-beads and PC-CS bioplatform: 3171 cm^{-1}

(O—H stretch), 2875 cm^{-1} (C—H stretch), 1650 cm^{-1} (C=O stretch), 1542 cm^{-1} (NH_2 bending), 1404 cm^{-1} (asymmetric C—O—C), and 1019 cm^{-1} (secondary C-OH stretch) (Figure 3.3a). However, the slight shift on the amine peak (3286 to 3171cm^{-1}) and the amide (I) (1648 to 1650cm^{-1}) suggest that partial crosslinking of chitosan with sodium tripolyphosphate occurred. The amine group (-NH_2) existed as [–NH_3^+----O^-] which was represented by the merging of the 1648cm^{-1} and 1694cm^{-1} on the P-CS to form the 1542cm^{-1} on the PC-CS. The similarity of the CS-beads and PC-CS microparticles IR spectrum confirms that the pulverisation step does not disturb the chemical structures of partially crosslinked chitosan.

The P-Alg powder contained saccharide structural characteristic peaks at 3243cm^{-1} (O—H stretch), 2921 cm^{-1} (C-H stretch), 1693 cm^{-1} (asymmetric stretching of carboxylate salt group (COO^----Na^+)), 1413 cm^{-1} (symmetric carboxylate stretching (C=O), and 1024 cm^{-1} (C—O—C stretching) (Figure 3.3a). Similar observations were made in previous investigations (Sartori et al., 1997, Smitha et al., 2005, Poormand et al., 2017). These peaks were consistent with those observed on the alginate beads and PC-Alg bioplatform; 3243 cm^{-1} (O—H stretch), 2931 cm^{-1} (C-H stretch), 1592 cm^{-1} (asymmetric stretching of carboxylate salt group (COO^----Ca^{2+})), 1413 cm^{-1} symmetric carboxylate stretching (C=O), 1025 cm^{-1} (C—O—C stretching) (Figure 3.3a). However, the significant shift in the carboxylate salt group peak from 1693 to 1592 cm^{-1} is indicative of the partial crosslinking at that specific position. The resultant surface structure existed as COO^-Ca^{2+} instead of COO^-Na^+. There is also a possibility of bidentate coordination to calcium cations, thereby affecting the molecular organization of the crosslinked polymers. The low degree of crosslinking and subsequent pulverisation of alginate did not drastically disturb the chemical structure. This is crucial for facilitating further interpolymer complexation with cationic polymers.

The IPC formed in SWF exhibited molecular vibrations at 3269, 1604, 1410, and 1030 cm^{-1} were assigned to the O—H stretch, amide deformation, asymmetric –COO stretching, and symmetric –C-O-C stretching, respectively (Figure 3.3a). The ionic interaction of these polymers displayed a chemical shift from interacting groups (Zhang and Gonsalves, 1995). In comparison to pristine chitosan, there was a notable downward shift of C=O (Amide (I) stretching vibrations in the FTIR spectrum of partially-crosslinked chitosan (Figure 3.3a) from 1648 cm^{-1} to 1542 cm^{-1} which was suggestive of the interpolymer complexation. The other shift was observed on the carboxylic groups of the pristine and partial-crosslinked alginate which overlapped with the IPC. This observation was also considered a display of the amide II deformation, which was a further indication of the interpolymer complexation of PC-CS and PC-Alg bioplatforms. The ionic interaction also contributed to the presence of the asymmetric carboxylic stretching at 1410cm^{-1}. The slight shift on the carboxylate group (C=O (Amide (I)) stretching vibrations) also confirmed that the carboxylate groups of the noncrosslinked portion of alginate complexed with the cationic amino groups of noncrosslinked portion of chitosan through electrostatic interaction (Takahashi et al., 1990). In addition to that, as the IPC formation proceeds, the presence of O–H bonding was expected to increase, and this contributed to the broad 3269 cm^{-1} peak. This is characteristic of an increase in inter-molecular interaction such as hydrogen bonding between sodium alginate and chitosan (Zhang and Gonsalves, 1995, Smitha et al., 2005). The IPC formed in whole blood displayed a strong OH stretch, C=O (Amide (I) stretch, and carboxylate stretching at position 3282, 1635, and 1538 cm^{-1}, respectively. Furthermore, there was a weak CH stretch, asymmetric carboxylate stretch, C-C bending, secondary C-OH stretch and C—O—C stretching, at position 2959, 1453, 1394, 1240, 1083 cm^{-1}, respectively. From the molecular vibrations of the IPC formed in SWF and whole blood given above, it is apparent that there is major differences in their spectra.

These differences may be due to the solvent and its interactive molecules with the forming IPC. The major differences included the shift and transition of the C—O—C stretching from 1030 cm^{-1} to 1083 cm^{-1} and change from strong to weak stretch between the IPC (SWF) to IPC (blood), respectively. The other differences included the formation of a narrow strong OH stretch and upward shift of the amide (I) and carboxylate groups on the IPC formed in blood. This was indicative of enhanced hydrogen bonding and electrostatic interactions in whole blood than in SWF (Sankalia et al., 2007).

3.3.7. X-ray powder diffraction analysis of the bioplatforms

The X-ray diffractogram of pristine chitosan depicted in Figure 3.3b exhibited a characteristic saccharide amorphous peak at a 2θ of 11 ° and a semi-crystalline amorphous peak at 20.5 ° (Smitha et al., 2005, Salmon and Hudson, 1997, Siafaka et al., 2016). The CS beads and PC-CS bioplatform showed a smooth semi-crystalline peak at a 2θ of 21 ° (Figure 3.3b). This peak was more amorphous than the one on P-CS therefore indicating a slight phase change during partial-crosslinking. The absence of the 11 ° peak on the partial-crosslinked bioplatform confirms the partial-crosslinking that occurred on the NH_2 group of chitosan thereby removing the hydrated polymorph of chitosan but retaining the characteristic peak at 21 °. The similarity of the diffraction pattern of the chitosan beads and the PC-CS microparticles is indicative of the retained physical phase (degree of crystallinity) of chitosan after pulverisation. This infers that partial crosslinking and pulverisation of did not drastically alter the chemical structure of chitosan. However, the porosity, degradation, water uptake, and hydrogel formation is improved by these two polymer modification strategies. The diffraction pattern of pristine alginate demonstrated typical alginate amorphous peaks at 14, 25 ° respectively and a third one at 40 ° (Figure 3.3b) (Yang et al., 2000). The partially-crosslinked alginate bioplatform and Alg beads diffraction pattern exhibited two amorphous peaks at 22 degrees and 43 degrees, in addition to that there were crystalline peaks at 32, 46, 57, 76 and 84 degrees (Figure 3.3b). The 15 degrees peak observed on the pristine counterpart was not present on the PC-Alg and Alg beads bioplatform due to partial-crosslinking of the carboxylic part of alginate. Alg beads displayed a larger crystalline peak at 22 degrees compared to PC-Alg microparticles (Figure 3.3b). This was due to the pulverisation of the beads into microparticles exposing non-crosslinked amorphous alginate particles as a result of a potentially greater degree of crosslinking at the Alg bead surface. These crystalline peaks corresponded to those of the $CaCl_2$ diffractogram which are representative of calcium and calcium oxide as confirmed by SEM-EDS analyses, and this indicates that the partial-crosslinking occurred (Nassar et al., 2011). The use of $CaCl_2$ as a crosslinker resulted in an increase in crystallinity of the alginate bioplatform due to the Ca^{2+} crosslinking (Yang et al., 2000). The IPC also exhibited the same crystalline pattern and the two amorphous peaks at 22 degrees and a broad minor peak at 46 degrees representative of the alginate and chitosan components of the IPC (Figure 3.3b). The crystalline peaks were observed at 26, 32 and 46 degrees which were indicative of calcium while the other peaks at 67, 76, and 84 degrees were representative of the calcium phosphate salt and calcium oxide (Nassar et al., 2011). The Ca^{2+} diffraction pattern on the IPC bioplatform suggest that the chitosan-alginate ionic interaction displaced the calcium-salts-containing alginate portions to the surface when the polymerization was underway on the non-crosslinked alginate portion. The IPC did not show the 10 or 15 degree peaks as observed on the pristine polymers, this signified the interpolymer complexation of the partial-crosslinked polymers. The formation of the interpolymer complex is a result of ionic interaction between non-crosslinked amino groups of chitosan and the non-crosslinked carboxylic groups of alginate. These interactions are possible due to the hydrogen bond deformation on the chitosan backbone

(Kim and Lee, 1993). The phosphate salt formation was confirmed by preparing the IPC bioplatform with water instead of the phosphate buffer and the results showed no crystalline peaks.

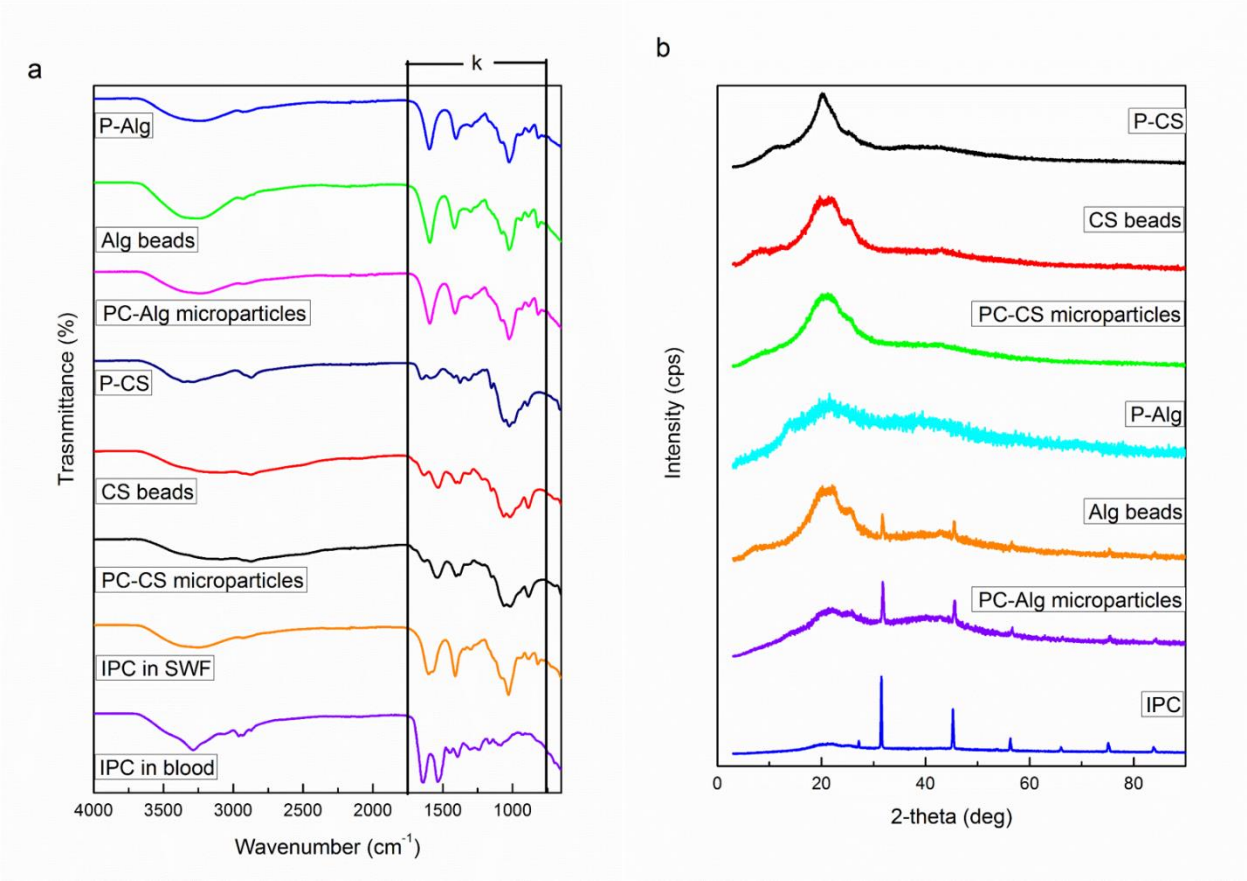


Figure 3.3. (a) FTIR spectra of the bioplatforms - 'k' highlights the positions most affected by the partial-crosslinking and interpolymer complexation. (b) XRD diffractograms of the bioplatforms.

3.3.8. Thermo-physical property analysis of the bioplatforms

The P-CS thermogram depicted in Figure 4a exhibited a conserved dehydration process with the PC-CS platform at 104 °C. However, there was a shift on the exothermic behaviour from 280 °C to 240 °C on the pristine and partially-crosslinked chitosan bioplatforms, respectively (Figure 3.4a). This shift inferred that the partial-crosslinking decreased the degradation temperature of chitosan. The consistent dehydration temperature of the chitosan platform was indicative that its internal structure was maintained. However, the presence of the second endothermic behaviour on the P-CS bioplatform signified that the partial-crosslinking process occurred thereby possessing an additional pre-degradation behaviour at ~190 °C. The second endothermic peak (~190 °C) and the exothermic peak at 240 °C are representative of the degradation process (Figure 3.4a). P-Alg (Figure 3.4a) also displayed a consistent major dehydration process at 105 °C with its partially-crosslinked counterpart at 115 °C. Unlike the chitosan bioplatforms, there was a shift to higher temperatures of in the exothermic peak of the pristine and PC-Alg from 244 °C to 266 °C (Figure 3.4a). This shift is interpreted as a transition of the thermal properties of the polymer due to partial-crosslinking thereby increasing the degradation temperature. The second endothermic peak around 200 °C and the exothermic peak around 244 °C are indicative of the

degradation process of the polymers (Figure 3.4a). The IPC bioplatform showed a glass transition temperature at 130 °C, an endothermic peak at 135 °C and an exothermic behaviour between 240 °C and 260 °C (Figure 3.4a). The endothermic peak at 135 °C and the exothermic peak around 245 °C are indicative of the dehydration and thermal degradation process. The interpolymer complexation was further emphasised by the decrease in degradation temperature range.

P-CS analysis on TGA showed a major weight loss (38.23%) at a temperature range of 321°C and 366°C (Figure 3.4b). This P-CS feature correlated with the DSC analyses as the higher exothermic behaviour from 280 °C was in line with the degradation process displayed on the TGA. The PC-CS bioplatform showed a major weight loss (32.91%) between 223 and 321 °C (Figure 3.4b). This is suggestive that partial-crosslinking resulted in a decreased degradation temperature range and it is in line with the observed decreased exothermic behaviour on the DSC analyses. Pristine alginate showed a major weight loss (35.64%) between 265 and 316 °C while the partially-crosslinked alginate bioplatform exhibited a major weight loss (27.24%) at 248 – 355 °C (Figure 3.4b). This is indicative of a decreased degradation temperature due to the partial-crosslinking. The IPC showed the lowest weight loss (22.26%) between 248 and 354 °C (Figure 3.4b). These results correlates with the DSC findings which showed a shift on the exothermic behaviour towards the low temperatures on the partial-crosslinked platforms compared to the pristine polymers. The exothermic behaviour of all the bioplatforms observed between 240 and 300 °C in DSC analysis is representative of the thermal degradation of the main chains of chitosan and/or alginate which correlates with the major weight loss observed between 225 °C and 355 °C on the TGA. The partially-crosslinked bioplatforms showed a decreased degradation temperature which is due to the partial-crosslinking and the hydrogen bond deformation (Kim and Lee, 1993). The partial-crosslinking decreased the degradation temperature range. However, the percentage weight loss was also decreased in partially-crosslinked polymers than in pristine polymers. This is indicative of controlled thermal degradation by partially-crosslinking polymers.

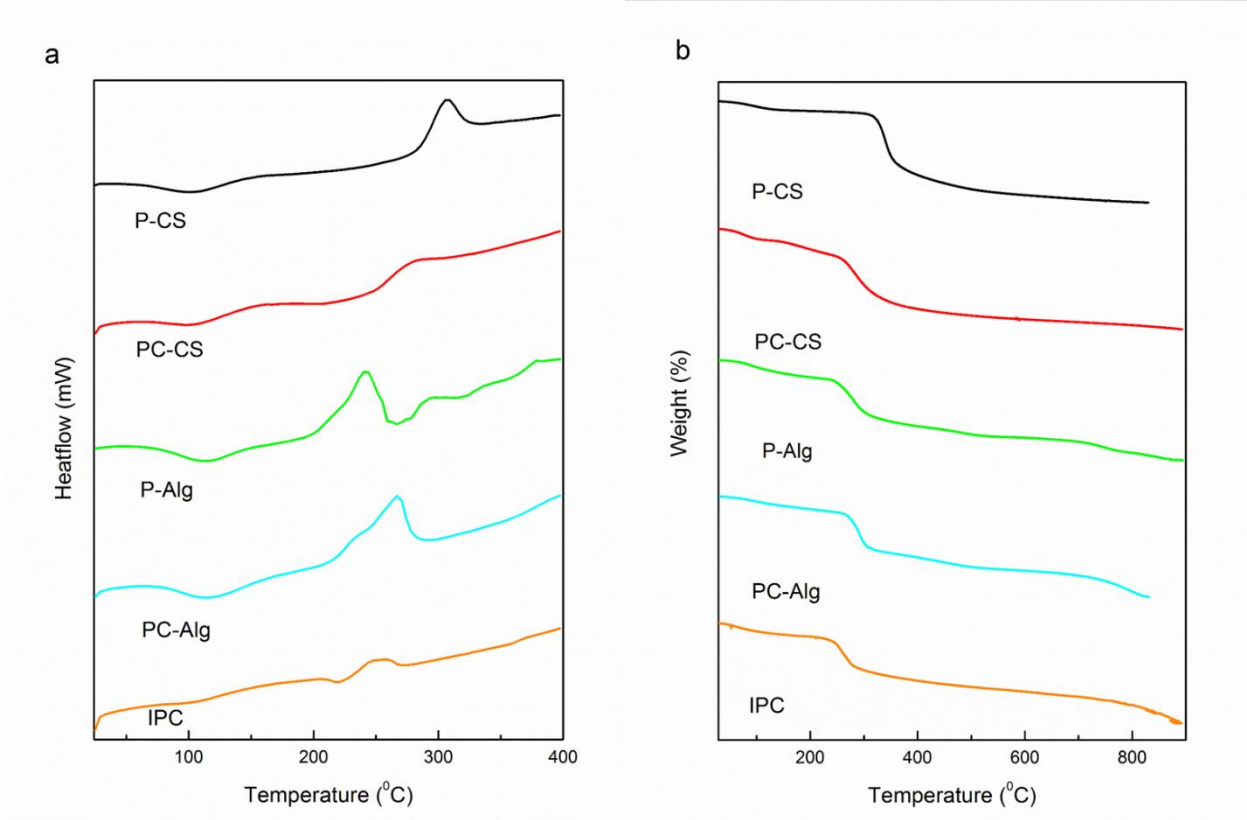


Figure 3.4. (a) Differential scanning calorimetric analyses and (b) Thermogravimetric analyses of the platforms.

3.3.9. Porosity analysis of the bioplatforms

Porositometric analysis on the bioplatforms displayed varying surface area, pore size, and pore volume with interpolymer complexation. Bioplatforms with degree of porosity allows for gaseous exchange which is one of the requirements for an ideal wound dressing biomaterial. Partial-crosslinking of alginate allowed the observation of both absorption and desorption properties thereby allowing for the formation of a type III physisorption isotherm with an H3 hysteresis loop (Table 3.1). The pore size and pore volume contribute to the cumulative surface area on the bioplatform surface pores whereby the increase in pore diameter and depth increases the pore surface area while decreasing the BET total surface area (Ramburrun et al., 2015). The IPC exhibited the highest surface area, lowest pore size and pore volume compared to P-CS, and PC-Alg (Table 3.1). These observations are in line with those made by Ramburrun et al. (Ramburrun et al., 2015). This suggested that the partial-crosslinking along with interpolymer complexation increased the surface area such that the internal matrix could be optimally accessed by PBS/SWF thus facilitating sufficient gaseous exchange while decreasing the pore size and volume. These properties may be useful in preventing microorganisms from passing through the bioplatform during wound healing. The IPC high surface area property correlates with the high degree of water uptake as indicated in section 3.4.13 below.

The nitrogen gas adsorption technique over a range of relative pressures for the determination of pore characteristics produce adsorption isotherms which provide insightful information regarding the pore size distribution in terms of pore width categorised as micro- (<2 nm), meso- (2–50 nm)

and macropore (>50 nm) ranges (Sing, 1985, Groen et al., 2003). According to this classification, the pore size distribution of all the platforms lies within the mesopore (Table 3.1). The IPC displayed a Type II isotherm with a H3 hysteresis loop indicating a monolayer-multilayer adsorption of a macroporous plate-like particles giving rise to slit-shaped pores with complete pore filling including capillary condensation which occurs in the presence of mesopores (Sing, 1985). The PC-CS exhibited a Type III isotherm with an H3 hysteresis loop suggestive of the presence of a multilayer material with complete pore filling, including capillary condensation which occurs in the presence of mesopores (Sing, 1985, Groen et al., 2003). The presence of a H3 hysteresis loop signifies the presence of an interconnected pore system of specialised distribution within the microplatform matrix (Groen et al., 2003). The interpolymer complexation in conjugation with partial-crosslinking brings about a physisorption isotherm shift from a Type III isotherm and H3 hysteresis loop towards a Type II isotherm.

Table 3.1. Porosity analysis of the IPC and polymer complexes after partial-crosslinking

Formulations	Surface area	Pore volume	Pore size		
	Single point surface area at P/Po = 0.300161792: (m^2/g)	Single point adsorption total pore volume of pores less than 865.527 Å diameter at P/Po = 0.995500633: (cm^3/g)	Adsorption average pore width (4V/A by BET): (nm)	BJH Adsorption average pore diameter (4V/A): (nm)	BJH Desorption average pore diameter (4V/A): (nm)
PC-Alg	5.4288	0.068172	47.07659	30.2164	42.0384
PC-CS	0.8972	0.009570	39.46834	22.7050	32.4229
PC CS-Alg IPC	10.1896	0.029213	8.7220	11.4088	9.0702

3.3.10. Scanning electron microscopy analysis of the bioplatforms

Scanning electron microscopy (SEM) images of the bioplatforms displayed different aspects of the bioplatforms such as porosity and the presence of smaller particles on the surface of the bioplatforms. The P-Alg displayed a number of shapes such as bulky smooth surface particles, and block shape. The inconsistently shaped P-Alg particles were not porous, instead they exhibited a dense surface. The morphology of PC-Alg bioplatform was different to that of its pristine counterpart, the particles displayed a layer-like morphology containing smaller nano-crystalline salt particles on the surface as confirmed by SEM-EDS analysis. These alginate microparticles showed pores with smaller cubic particles residing close to the pores. The small cubic particles were calcium, oxygen, sodium and chlorine salts on the surface of the alginate platform. These SEM-EDS observations correlate with those observed on the porosity analyses and XRD results which displayed increased pore area along with the pore width of the particles and crystalline peaks due to the calcium chloride and phosphate salt present in the bioplatform (Table 3.1). Similar to the P-Alg, the P-CS exhibited a smooth, circular and polygonal particle shapes which were completely dense and without pores (Figure 3.5).

The PC-CS bioplatform on the contrary displayed a rough surface with areas concentrated with pores and cubic particles on the surface owing to the crosslinking agent sodium tripolyphosphate (Figure 3.5). Unlike the partial-crosslinked alginate, the particles on the surface of the PC-CS were not crystalline as confirmed by SEM-EDS analysis. This is in agreement with the observations on the XRD and porosity analyses which showed amorphous peaks and increased pore width and area for the PC-CS bioplatforms. The IPC exhibited similar morphology with the partially-crosslinked alginate and chitosan with more pores and salt crystals on the bioplatform surface (Figure 3.5). The SEM-EDS confirmed that the small cubic particles were calcium, oxygen, sodium and chlorine and phosphorus salts which were due to the phosphate buffer and the crosslinking agents. The change on the surface topology of the pristine and partially-crosslinked polymers signified that the crosslinking took place. The observed morphology confirmed the increased adsorption average pore width (4V/A by BET) on the partially-crosslinked polymers particles (Table 3.1). The IPC bioplatform exhibited increased number of pores compared to the individual partially-crosslinked polymers. These findings are in line with the porosity analysis of the IPC which displayed the highest adsorption average pore width (4V/A by BET) compared to the individual polymers.

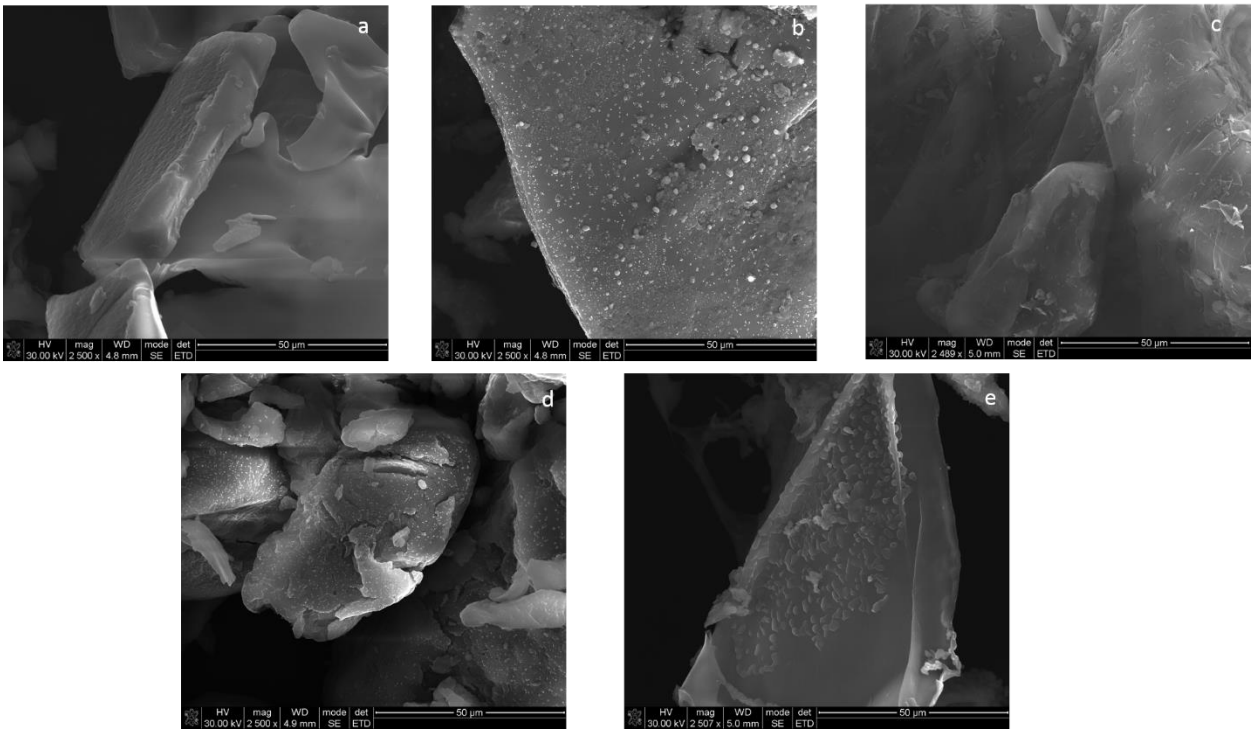


Figure 3. 5. Scanning electron microscopy (SEM) analyses of the platforms, (a) pristine alginate, (b) partially crosslinked alginate, (c) pristine chitosan, (d) partially-crosslinked chitosan, (e) interpolymer complex.

3.3.11. Rheological properties of the bioplatforms

The apparent yield stress values of chitosan, alginate and the IPC were calculated using the software RheoWin PC version 3, and were 0.2825 Pa, 0.1216Pa, and 3.843 Pa respectively. The yield stress increased as the fluid substance became more viscous. This is line with the point that a material may generate apparent yield stress when following the increase in viscosity in a shear stress versus shear rate region (Barnes, 2000, Ngwuluka et al., 2013). The visco-elastic

properties of the polymers and the IPC were assessed by following the elastic modulus G' as a function of shear stress at a frequency of 0.1Hz (Figure 3.6a).

Chitosan and alginate did not exhibit a significant visco-elastic region as was no resistance to deformation when the shear stress increased (Figure 3.6a and b), thus the individual polymers lacked elasticity. However, more resistance to deformation as the shear stress increased was observed for the IPC thus showing an extended visco-elastic region compared to the polymers (Figure 3.6c). This extended resistance to deformation on the IPC was due to the presence of large intermolecular forces which enabled ionic groups to interact among the alginate and chitosan solutions, which in turn caused an increased resistance to deformation and a solid-like behaviour of the IPC. The major increase in elastic modulus at the breaking point is due to the applied shear which initiates intermolecular chain association transformation (Xu et al., 2010). The IPC eventually yielded to deformation as all the associations were transformed/broken thus causing a decrease in elastic modulus. The three-dimensional network gel confirms the improved structural elasticity and stability which a crucial property for any ECM-mimicking complex. Shear viscosity confirmed the unthickening of the solutions as the shear viscosity displayed gradual decrements with increasing shear rate (Figure 3.6b). The IPC rheogram showed rather a major decrease in shear viscosity with increasing shear rate compared to the viscous polymer solutions. It was also noticed that the viscosity of each of the polymers and the IPC was higher at every shear rate at 37 °C compared to those at 20 °C (results not shown). This infer a temperature dependent shear-viscosity and shear-rate properties. In addition to that, the IPC showed the highest viscosity at 37 °C compared to the polymer solutions. However, the viscosity decreased with increasing shear rate. This is indicative of the strong gel network formation due to the hydrogen bond interaction between the complex and surrounding water (Chejara et al., 2017). This was also associated with the hysteresis loop area observed for the IPC at the applied shear rate which indicated the IPC's thixotropic nature (Figure 3.6b). The thixotropic area (%) of the IPC was notably higher than that of the individual polymer solutions. This was indicative of a strong thixotropic property of the IPC.

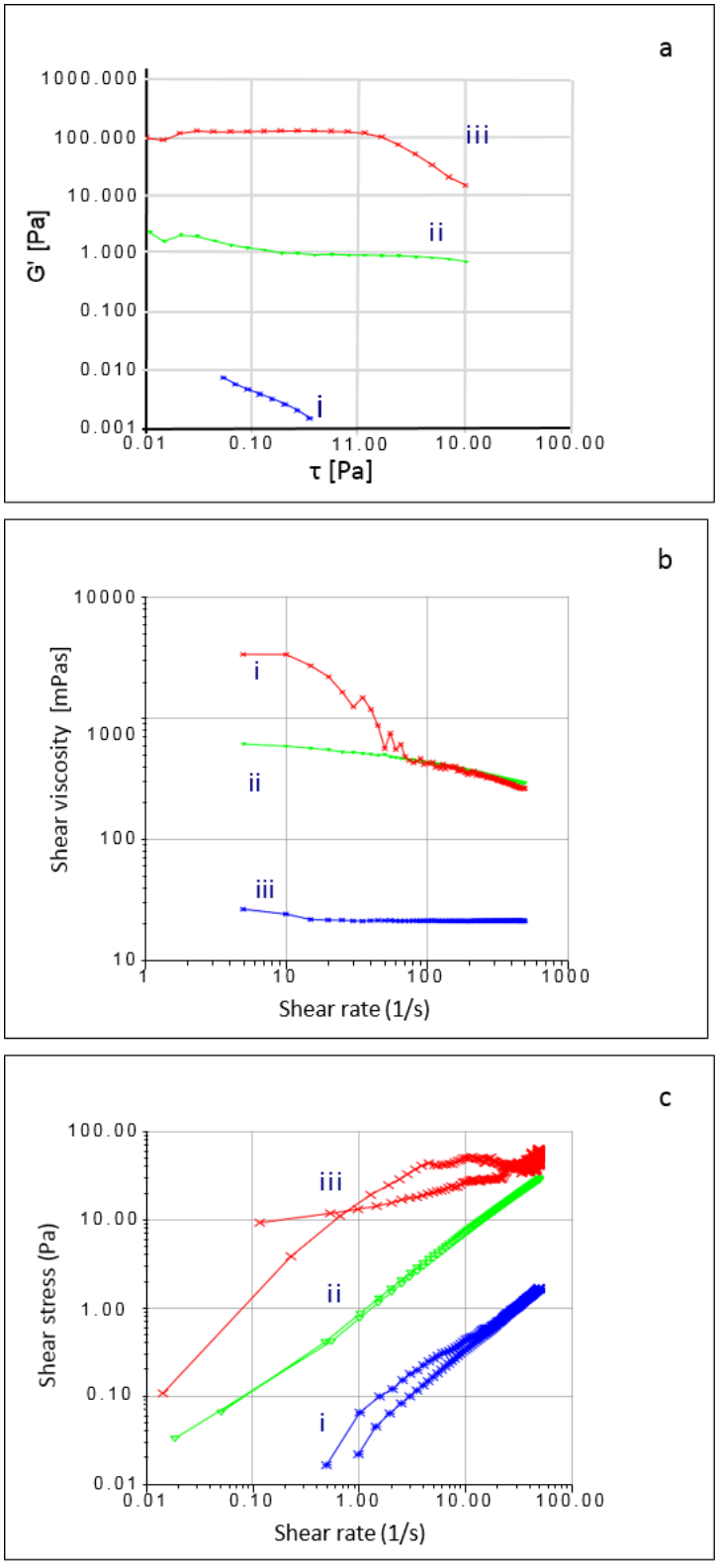


Figure 3.6. Rheological analysis of the polymers and the polyelectrolyte complex. (a) Elastic modulus as a function of shear stress for (i) alginate (2%$^{w}/_{v}$), (ii) chitosan (2% $^{w}/_{v}$), and (iii) PEC (2% $^{w}/_{v}$) performed at a frequency of 0.1 Hz. Shear viscosity (b) and (c) hysteresis loop area of the (i) alginate (2% $^{w}/_{v}$), (ii) chitosan (2% $^{w}/_{v}$) and (iii) IPC (2% $^{w}/_{v}$) platforms performed at 37°C.

3.3.12. Gelling kinetics and interpolymer complexation of PC-Alg and PC-CS microparticles under SWF/whole blood exposure

Hydrogels should present mechanical properties which mimics the skin environment. This includes the gel strength (G') and viscoelastic properties represented by the loss tangent (G'/G"). Hydrogels should be capable of absorbing the wound fluid, maintain the moist environment and present high viscous property to remain in the wound cavity while sustaining their flexibility. Partially-crosslinked Chitosan (50 mg) and alginate (50 mg) were exposed to the SWF/Whole blood (3 mL) and allowed to gel over time. The hydrogel formation process resulted on the *in situ* interpolymer complex hydrogel formation. The interpolymer complexation is via hydrogen bonding and electrostatic interactions between chitosan and alginate (Sankalia et al., 2007).

The gelling kinetics of partially-crosslinked alginate-chitosan was followed by measuring the shear storage modulus (G'), shear loss modulus (G"), loss tangent (tan δ= G"/G'), and swelling as a function of time at different pH conditions (pH 5, 7.4, 9.36) at 37 °C (Figure 3.7). The increase in storage modulus correlates with the high degree of intermolecular interaction between the polyions. This interaction resulted in an increase in viscosity represented by the loss modulus (G") during gelation. Optimum gelling of the *in situ*-forming-IPC was observed in the SWF (pH 7.4) at 37 °C, with the maximum average storage modulus of 2090 ± 100 Pa. Under these experimental conditions, the viscosity (loss modulus) increased at the same rate as the elastic (storage modulus) with a major decrease in sample height.

The visco-elastic properties and rigidity of the IPC indicated the flexibility and sol-gel state of the IPC. The decrease in sample height was indicative of major SWF absorption during the gelling and formation of the IPC. The loss tangent did not change over time, which further confirms the presence of both visco-elastic properties along with the constant sol-gel state of the IPC (Figure 3.7a,cii). The gelling kinetics of the bioplatforms in whole blood displayed continuous increase on the shear storage modulus, shear loss modulus, and the shear complex modulus. Furthermore, the loss tangent was below 1 which indicated that the system existed in a sol phase even with continual blood absorption. The maximum average storage modulus of the IPC at pH 5 was 760 ± 50 Pa and at pH 9.36 it was 1355± 150 Pa. These values were lower than that observed at pH 7.4, this indicated the formation of semi-stiff hydrogel compared to the very soft hydrogel formed at pH 5 and semi-stiff hydrogel at pH 9.36. This infers that the pH of wound environment has an effect on the stiffness of the hydrogel. Hydrogels should present viscous properties to stay on the wound cavity while maintaining a moist environment (Hoseinpour Najar et al., 2018). Furthermore, they should not be too stiff as would impair interactions with the ECM.

The mechanical properties of the gel should mimic or be close to that of the skin environment. From the observations above, the hydrogel obtained in SWF (pH 5) exhibited desirable gel strength (G') in the sense that it is a soft and viscous hydrogel. The gelling kinetics at acidic conditions (pH 5) displayed a decrease in viscosity as the elasticity increased until an equilibrium was reached where both visco-elastic properties were observed as indicated by the loss tangent (Figure 3.7bii). The opposite was observed at pH 9.36 where the viscosity (G") increased up to its maximum and started to gradually decrease until equilibrium was reached after 8 hours. Based on the observations made at different pH conditions, the viscosity fluctuations depend on the pH of the environment of the hydrogel and at acidic conditions the amine group becomes protonated along with the carboxylic group thereby dictating gelling and viscosity. Low interpolymer complexation and formation of a very soft gel was observed at acidic conditions, while under basic conditions a semi-hard gel with minor viscosity fluctuations was observed. The lack of viscosity

changes at acidic and basic conditions infer that the *in situ*-forming IPC assumed a rigid rod type-conformation.

The gelling kinetics of the IPC at acidic and basic conditions displayed low sample height changes which infer that there was low fluid absorption. However, at pH 7.4, the hydrogel displayed visco-elastic properties, major fluid absorption and higher rate of interpolymer complexation and flexible IPC structures. The increase in the storage/rigidity modulus during gelation, increases the mechanical strength of the forming IPC (Anseth et al., 1996, Moura et al., 2007). The polyions displayed accelerated interpolymer interaction when they were exposed to the SWF than when they were in whole blood. This was represented by a steep slope of the shear storage modulus (G') from 1202 to 1802Pa in less than 22 minutes before a steady interpolymer complexation in SWF. The IPC in blood displayed a slow interpolymer complexation in the kPa range. This indicates that the bioplatforms forms a stiffer IPC system in whole blood than in SWF. This is due to the high viscosity of blood as indicated by a loss tangent that is below 1 which further confirms the high viscosity of the system.

A disturbed skin environment drastically changes pH from 5-6 to 7.4, however, at a later stage the pH returns to 5-6 which is the normal pH of the skin (Schneider et al., 2007). Therefore, wound dressing hydrogels should be able to form the complex at pH 7.4 and become less rigid as the wound site normalizes to a pH of 5-6. The hydrogel (SWF) obtained in the current study, demonstrated high gel strength at pH 7.4 and low gel strength at pH 5. The hydrogel in whole blood also displayed a high gel strength with approximately 76% blood absorption in less than 2 hours whilst the hydrogel in SWF displayed 75% SWF absorption in less than 8 hours. The accelerated fluid absorption is an advantageous hydrogel property in the sense that high wound fluid volumes are experienced during the trauma which requires a hydrogel with high gel strength to remain in the wound cavity while absorbing the wound fluid. The stiff gel at the neutral pH conditions corresponds to the early stages of the wound where the hydrogel would be required to act as a mechanical barrier against blood loss and also serve as a protective layer against foreign bodies. The decrease in gel stiffness at acidic conditions follows progressive stages of wound were the skin milieu returns to its normal acid state and the soft IPC gel network can interact effectively with the ECM.

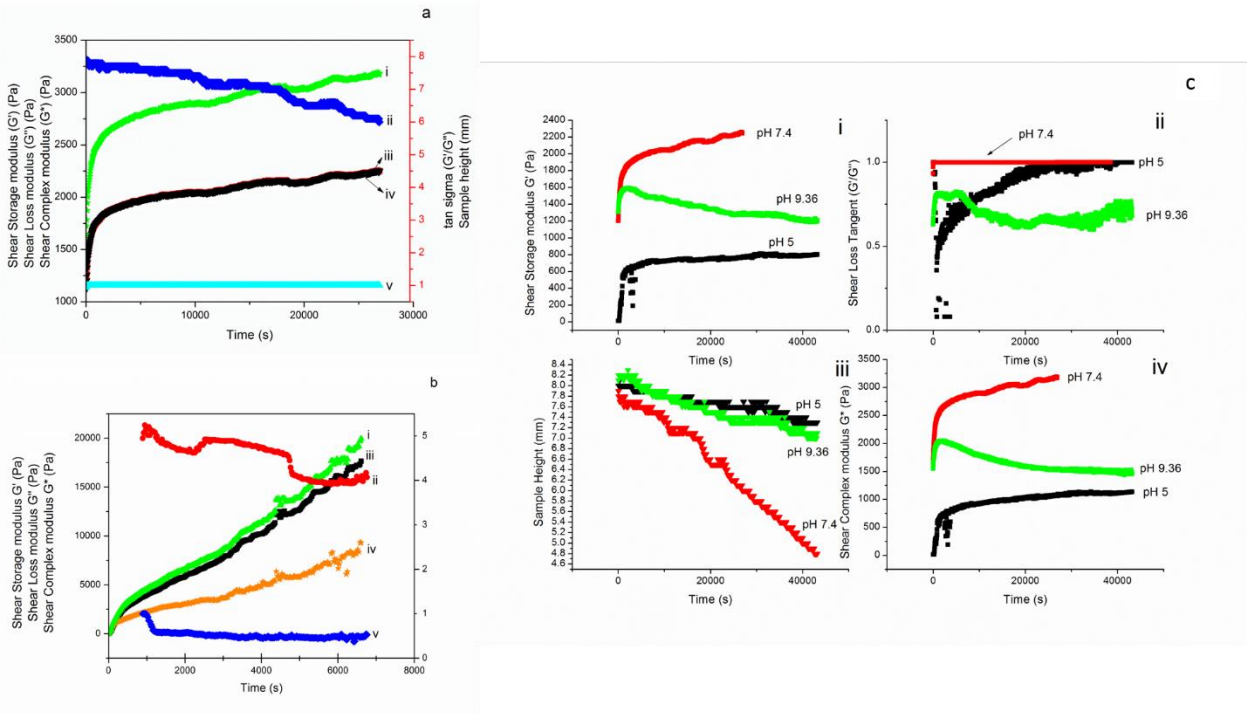


Figure 3.7. Kinetic gelation of the IPC in **(a)** SWF (pH 7.4) and **(b)** blood at 37°C. (i) represent the shear complex modulus (G*)(Pa), (ii) sample height (mm), (iii) shear storage modulus (G')(Pa), (iv) shear loss modulus (G")(Pa), (v) loss tangent (G'/G"). **(c)** The pH-dependent Kinetic gelation of the in situ forming IPC in SWF at 37°C, where **(i)** represent the shear storage modulus (G*)(Pa), **(ii)** loss tangent (G'/G"), **(iii)** sample height (mm), and **(iv)** shear complex modulus (G*)(Pa).

3.3.13. Water uptake and degradation of the bioplatforms and comparator wound dressing

Wound dressing hydrogels with controlled biodegradation are of great importance in wound healing as they wound degrade as the wound heals which will eliminate the need for frequent dressing changes. Chitosan is a hydrophilic biomaterial and thus absorbs water which facilitates its degradation by cleavage of hydrolytically sensitive glycosidic bonds (She et al., 2008). Partial crosslinking enhances chitosan water absorption capabilities while subsequent interaction with alginate would serve to improve the degradation process compared to pristine chitosan, with potentially enhanced cleavage of chitosan glycosidic bonds producing non-toxic oligosaccharides of variable length which can be incorporated in metabolic pathways or excreted (Balagangadharan et al., 2017). Pristine alginate is highly hydrophilic. Partial crosslinking enhances the gelation of alginate (via water absorption). Thus, the crosslinking of alginate with calcium chloride and chitosan with NaTPP increased the degree of fluid uptake as indicated by the comparatively higher water uptake by the partially crosslinked bioplatforms versus the pristine polymers (Figure 3.8b) due to the incorporation of ions.

Degradation of the partially crosslinked alginate was via the outward diffusion out of the divalent ions (Ca^{2+}) due to exchange reactions with monovalent cations such as sodium ions which allows alginate to dissolve in water (Shoichet et al., 1996). Interpolymeric complexation decreases the solubility of the bioplatform compared to pristine and partially crosslinked alginate (Augst et al., 2006). Biodegradation of the IPC is thus anticipated to ensue at a more controlled rate compared to pristine alginate. The current study employed the partial-crosslinking approach to control both degradation and mechanical strength of the bioplatform. The bioplatform's degradation (weight

loss) and fluid uptake behaviour was compared to Pharma-Algi® (Pharmaplast). Pharma-Algi® is a haemostatic absorbent primary wound pad. The pad is composed of nonwoven absorbent fibers, coated with a powdered blend of sodium alginate and calcium alginate.

The IPC bioplatform displayed a higher degree and rate of fluid uptake compared to the Pharma-Algi®, P-Alg, P-CS, PC-Alg, and PC-CS (Figure 8b). Pulverisation of beads/macromatrices into microparticles exposed a larger surface area of the partially-crosslinked sodium alginate and chitosan for enhanced fluid uptake and increased matrix hydration compared to the pristine polymers and promoted formation of the IPC. The IPC rapidly formed a hydrogel when it was in contact with fluid, thus it would purportedly rapidly absorb the fluid exudate and swell to fill the wound cavity. The swelling observed for each system after 8 and 24 hours was as follows: P-CS (785.16%; 1143.1%), PC-CS (1891.78%; 2007.22%), P-Alg (619.69%; 111.14%), PC-Alg (2000.34%; 2043.79%), Pharma-Algi® (2168.21%; 1612.56%), and the IPC (3306.61%; 4343.4%). Thus, the respective slight increase in swelling with partial-crosslinking of each native polymer, and the notable increase in swelling of the IPC is evident. This attests to the positive effect of the partial crosslinking approach.

The degradation of these systems is an important consideration for the wound healing process (Sproul et al., 2018). Partial crosslinking and pulverisation collectively increased fluid uptake and allowed for controlled degradation properties as achieved by the IPC (Figure 3.8a). The high fluid diffusion rate into the polymer bulk owing to the small particle size (63µm) of the IPC is proposed to result in bulk degradation of the bioplatform. If the diffusion of water into the bioplatform exceeds to degradation of polymer bonds, bulk erosion occurs as the degradation is not confined to the surface. Thus, swelling of the bioplatforms notably affected the degradation mechanism. The bulk degradation/erosion mechanism of the pristine polymers and partially crosslinked bioplatforms was due to hydrolytic cleavage of the polymer bonds throughout the IPC. Pharma-Algi® on the contrary is proposed to display a surface erosion degradation mechanism due moderate swelling kinetics. Thus, the fluid took longer to reach the core of the dressing resulting in slower degradation from the surface of the dressing, with limited to no degradation observed over certain time periods, as visualised in Figure 8a. Furthermore, Pharma-Algi® scaffold retained its initial shape but shrunk in size, which correlates to the surface erosion type of degradation mechanism (Göpferich, 1996).

P-CS showed inconsistent and slight degradation. P-Alg on the other hand was highly affected by its solubility in water thereby displaying drastic weight loss after 24 hours and reached ~90% degradation in 3 days. The partial-crosslinked platforms exhibited a step-wise degradation with time. This confirms that controlled degradation was achieved by partial-crosslinking of the polymers. Although PC-Alg displayed a high degradation rate, its solubility was somewhat decreased with crosslinking to improve its degradation rate compared to P-Alg. PC-CS displayed an increased solubility thereby having an improved and controlled degradation compared to its pristine counterpart. The IPC also displayed a more improved step-wise degradation compared to both P-CS and PC-CS over time with 78.2% degradation on the 14th day. Pharma-Algi® displayed a slow degradation with 16.26% degradation in 14 days. When compared with similar systems on the market or under investigation: Algisite^{TM} (Smith and Nephew) has displayed 21.19g/100cm^2 fluid absorption and 34% change in fibre diameter when comparing its diameter after 1 week of water exposure against its dry state (Parikh et al., 2011). A chitosan-alginate IPC scaffold reported by Shao and Hunter displayed a degradation of 15.06% in 14 days (Shao and Hunter, 2007). Thus, the IPC formulated in the current study demonstrated an improved swelling

and degradation profile compared to the alginate dressing on the market evaluated herein (Pharma-Algi®) and alginate/ chitosan-alginate based scaffolds provided in literature.

Therefore, compared to the comparator wound dressing and other alginate-based dressings reported, the water uptake and degradation properties of the IPC is proposed to further facilitate the wound healing process. Firstly, the IPC bioplatform rapidly absorbs the wound exudate, swelling to fill the wound cavity independent of the wound shape, thus facilitating the required haemostasis and providing an environment of controlled moisture for wound healing to proceed. Secondly, the continually controlled, but fairly constant rate of degradation of the IPC is proposed to enable the stages of wound healing to occur (establishment of haemostasis and cellular infiltration) without impeding subsequent stages of tissue remodelling (which extends anywhere from 4 to 24 days) (Sproul et al., 2018). In addition, this rapid swelling and gelation response, followed by controlled degradation could eliminate the need for changing a dressing, as well as removing the dressing, which could emanate in subsequent damage to healing tissues. This addresses the problem encountered in most wound dressing platforms where by patients complain about the frequency of dressing changes and cost of the dressings. The platform degradation results in a colour change to a yellow-orange colour, and un-degraded platforms such as the P-CS showed no colour change thus its microparticles were white. As demonstrated, the IPC displayed a high water uptake compared to individual polymer particles. This confirms the bioresorbability and biodegradability property of the complex. The error bars were small which indicated that the values taken did not vary amongst themselves, highlighting the precise degradation of the polymers and the bioplatforms.

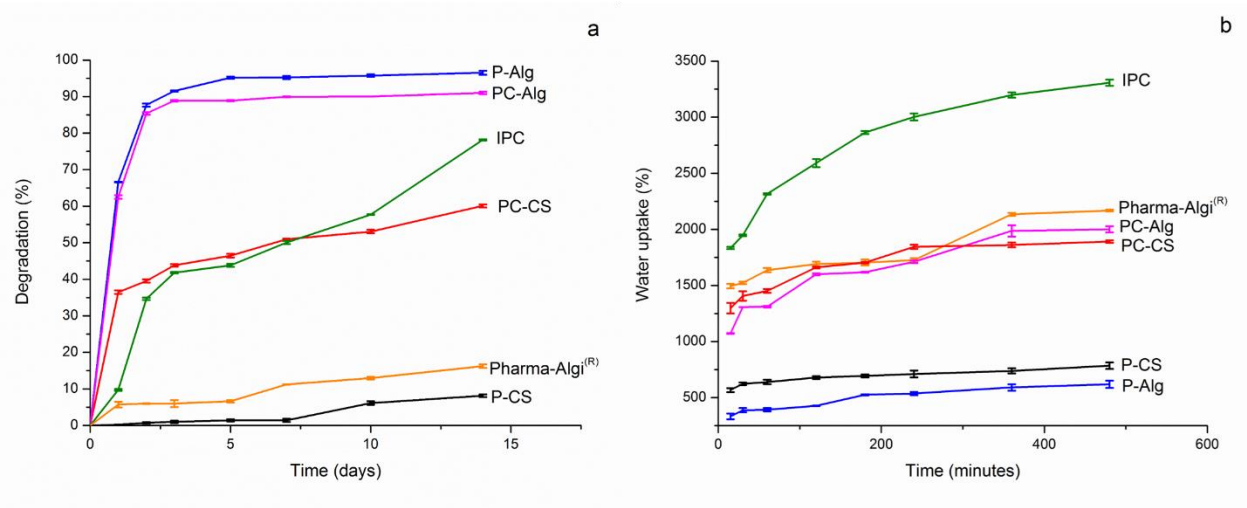


Figure 3.8. (a) Biodegradation (weight loss) and (b) water uptake behaviour of the pristine polymers, bioplatforms and Pharma-Algi® in PBS (pH 7.4) solution at 37°C at 50 rpm.

3.3.14. Cytotoxicity assessment of the bioplatforms

Bioplatforms which are fabricated for wound treatment should not contain or release toxic agents which may hamper the wound healing process. *In vitro* cytocompatibility assessment of bioplatforms allows for a rapid detection of toxic agents. The cytocompatibility is directly related to the cell viability. Chitosan with 80% degree of deacetylation has approximately 50% cell viability as reported by Freier and co-workers (Freier et al., 2005). Alginate was found to have approximately 80% cell viability in a HepG2 cell line (Khattak et al., 2007). The cytocompatibility of the bioplatforms was assessed *in vitro* by measuring the NIH 3T3 cell viability on the Pristine

CS-Alg IPC and PC CS-Alg IPC. The *in vitro* studies revealed that PC CS-Alg displayed higher cell viability than the pristine interpolymer complex. The cell viability increased with time which infers that the bioplatform did not inhibit cell growth. The PC CS-Alg IPC had a cell viability of approximately 99% compared to the 86% for the pristine CS-Alg IPC in 72 hours (Figure 3.9). These results confirm that the partial-crosslinking approach improved the cytocompatibility of the bioplatform. The use of $CaCl_2$ and NaTPP potentially contributed towards the improved cytocompatibility of the bioplatform. Other chitosan-alginate interpolymer complexes reported in literature indicated a cell viability of 60-80% after 4 days when the IPC was crosslinked with both $CaCl_2$ and gamma irradiation (Wang et al., 2002). The current IPC displayed improved cytocompatibility by employing $CaCl_2$ and NaTPP as crosslinkers.

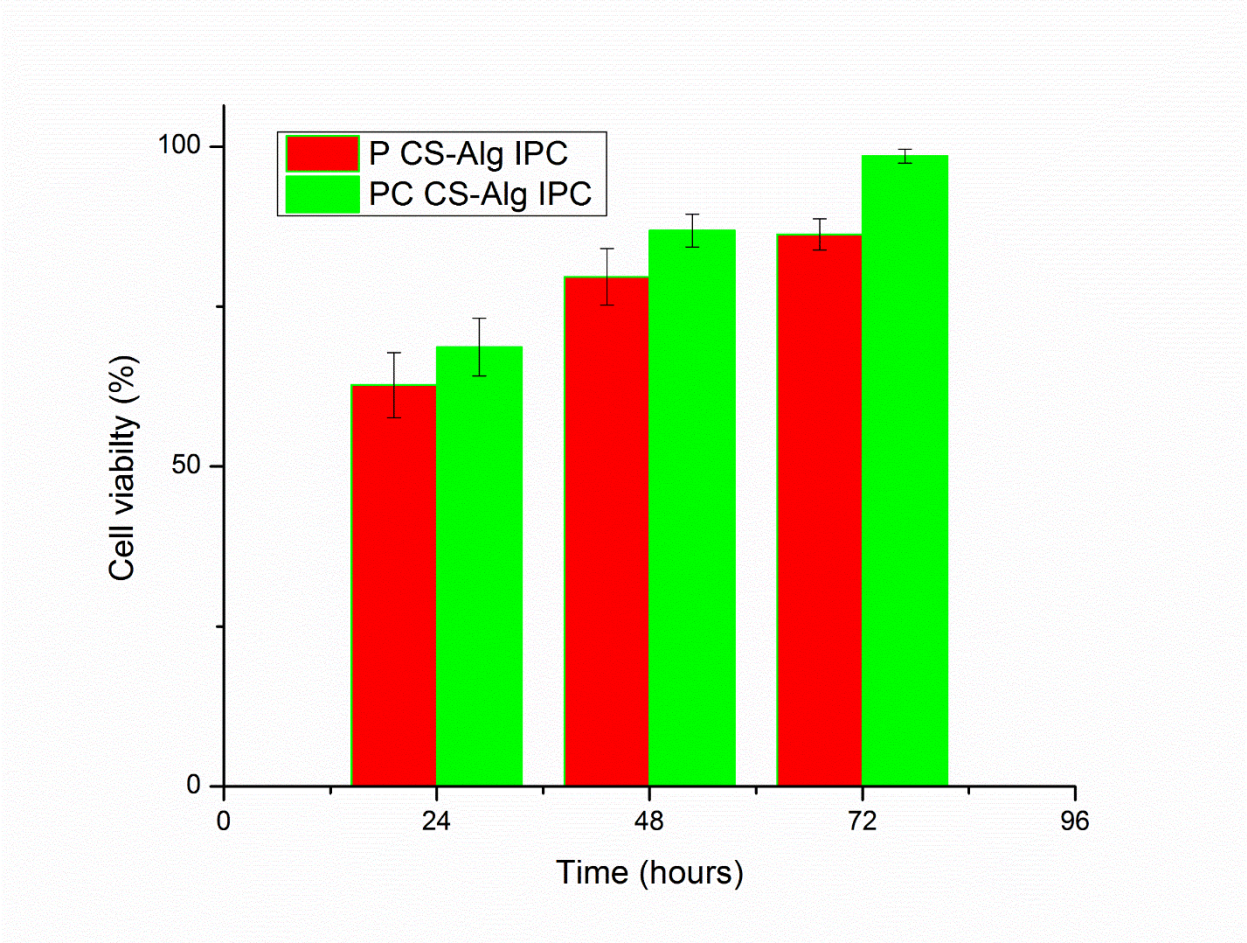


Figure 3.9. Cell viability evaluation of the NIH 3T3 cell line treated with the bioplatforms

3.4. Concluding remarks

This study assessed the potential of partial-crosslinking of alginate and chitosan to form novel bioplatforms as an approach for enhancing the properties of the component polymers, for ultimate employment in wound dressing applications. The thermo-physical properties were improved along with additional bioplatform properties such as increased porosity, fluid uptake, rheological properties (yield stress, thixotropy, and displayed both visco-elastic properties) and biodegradation rate, which positively affected performance of the platform. The similarity of the diffraction patterns and vibrational spectra of the beads and the partial crosslinked microparticles

was indicative of a retained physical phase and chemical structure of the bioplatforms after pulverisation. This infers that partial crosslinking and pulverisation does not drastically alter the chemical structure and diffraction pattern of the bioplatforms. However, the porosity, degradation, water uptake, and hydrogel formation was improved by these two polymer modification strategies.

The formation of soft macromatrices in SWF allowed for a transition in the morphology of these properties to a more porous structure, and also increased the IPC rigidity (G') during *in situ* hydrogel formation. The bioplatform formed in whole blood was stiffer than that formed in SWF and PBS. This indicates that whole blood reacted as a glue that maintains the integrity of the bioplatform. The increased stiffness would allow the bioplatform to be retained in the wound cavity even in wounds with high volumes of exudate. The partial-crosslinking further improved the biodegradation of the polymers. The lyophilisation process aided pore formation within the partially-crosslinked structure, thereby increasing the water uptake of the bioplatforms. This allowed for further ionic interaction on hydration, which enhanced the bioplatform physicomechanical properties. The crosslinking step complemented the lyophilisation process on achieving highly porous and partially-crosslinked polymeric chains, which aided instant gelling following water absorption at physiological conditions. The fabricated bioplatform displayed enhanced water uptake and controlled degradation compared to the commercial product. The PC CS-Alg IPC was cytocompatible and demonstrated improved cytocompatibility compared to the pristine CS-Alg IPC and other chitosan-alginate IPCs reported in literature. The advantage of applying this dressing includes its controlled biodegradability, and platform mechanical strength for wound dressing. Furthermore, the ionic character of the platform signifies its potential application as a drug carrier.

3.5. References

Agarwal, V., Siddiqui, A., Ali, H. & Nazzal, S. 2009. Dissolution and powder flow characterization of solid self-emulsified drug delivery system (SEDDS). *International journal of pharmaceutics,* 366**,** 44-52.

Amidon, G. E. 1995. Physical and mechanical property characterization of powders. *Drugs And The Pharmaceutical Sciences,* 70**,** 281-281.

Anseth, K. S., Bowman, C. N. & Brannon-Peppas, L. 1996. Mechanical properties of hydrogels and their experimental determination. *Biomaterials,* 17**,** 1647-1657.

Augst, A. D., Kong, H. J. & Mooney, D. J. 2006. Alginate hydrogels as biomaterials. *Macromolecular bioscience,* 6**,** 623-633.

Balagangadharan, K., Dhivya, S. & Selvamurugan, N. 2017. Chitosan based nanofibers in bone tissue engineering. *International journal of biological macromolecules,* 104**,** 1372-1382.

Barnes, H. A. 2000. A handbook of elementary rheology.

Becker, T. A., Kipke, D. R. & Brandon, T. 2001. Calcium alginate gel: a biocompatible and mechanically stable polymer for endovascular embolization. *Journal of Biomedical Materials Research: An Official Journal of The Society for Biomaterials and The Japanese Society for Biomaterials,* 54**,** 76-86.

Berger, J., Reist, M., Mayer, J. M., Felt, O., Peppas, N. & Gurny, R. 2004. Structure and interactions in covalently and ionically crosslinked chitosan hydrogels for biomedical applications. *European Journal of Pharmaceutics and Biopharmaceutics,* 57**,** 19-34.

Boateng, J., Pawar, H. & Tetteh, J. 2015. Evaluation of in vitro wound adhesion characteristics of composite film and wafer based dressings using texture analysis and FTIR spectroscopy: A chemometrics factor analysis approach. *RSC Advances,* 5**,** 107064-107075.

Bradford, M. M. 1976. A rapid and sensitive method for the quantitation of microgram quantities of protein utilizing the principle of protein-dye binding. *Analytical biochemistry,* 72**,** 248-254.

Brown, M. A., Daya, M. R. & Worley, J. A. 2009. Experience with chitosan dressings in a civilian EMS system. *The Journal of emergency medicine,* 37**,** 1-7.

Bueno, C. Z., Moraes, Â. M., De Sousa, H. C. & Braga, M. E. M. 2016. Effects of supercritical carbon dioxide processing on the properties of chitosan–alginate membranes. *The Journal of Supercritical Fluids,* 112**,** 128-135.

Carr, R. L., Carr, R., Carr, R. & Carr, R. 1965. Evaluating flow properties of solids.

Chejara, D. R., Mabrouk, M., Kumar, P., Choonara, Y. E., Kondiah, P. P., Badhe, R. V., Toit, L. C. D., Bijukumar, D. & Pillay, V. 2017. Synthesis and Evaluation of a Sodium Alginate-4-Aminosalicylic Acid Based Microporous Hydrogel for Potential Viscosupplementation for Joint Injuries and Arthritis-Induced Conditions. *Marine drugs,* 15**,** 257.

Chen, H., Xing, X., Tan, H., Jia, Y., Zhou, T., Chen, Y., Ling, Z. & Hu, X. 2017. Covalently antibacterial alginate-chitosan hydrogel dressing integrated gelatin microspheres containing tetracycline hydrochloride for wound healing. *Materials Science and Engineering: C,* 70**,** 287-295.

Chen, J.-P., Chang, G.-Y. & Chen, J.-K. 2008. Electrospun collagen/chitosan nanofibrous membrane as wound dressing. *Colloids and surfaces a: physicochemical and engineering aspects,* 313**,** 183-188.

Chen, L.-C., Kung, S.-K., Chen, H.-H. & Lin, S.-B. 2010. Evaluation of zeta potential difference as an indicator for antibacterial strength of low molecular weight chitosan. *Carbohydrate Polymers,* 82**,** 913-919.

Dowling, M. B., Kumar, R., Keibler, M. A., Hess, J. R., Bochicchio, G. V. & Raghavan, S. R. 2011. A self-assembling hydrophobically modified chitosan capable of reversible hemostatic action. *Biomaterials,* 32**,** 3351-3357.

Du, W.-L., Niu, S.-S., Xu, Y.-L., Xu, Z.-R. & Fan, C.-L. 2009. Antibacterial activity of chitosan tripolyphosphate nanoparticles loaded with various metal ions. *Carbohydrate polymers,* 75**,** 385-389.

Du, W.-L., Xu, Y.-L., Xu, Z.-R. & Fan, C.-L. 2008. Preparation, characterization and antibacterial properties against E. coli K88 of chitosan nanoparticle loaded copper ions. *Nanotechnology,* 19**,** 085707.

Dumitriu, S. & Chornet, E. 1998. Inclusion and release of proteins from polysaccharide-based polyion complexes. *Advanced drug delivery reviews,* 31**,** 223-246.

Dumville, J. C., Keogh, S. J., Liu, Z., Stubbs, N., Walker, R. M. & Fortnam, M. 2015. Alginate dressings for treating pressure ulcers. *Cochrane Database of Systematic Reviews*.

Fathi, P., Sikorski, M., Christodoulides, K., Langan, K., Choi, Y. S., Titcomb, M., Ghodasara, A., Wonodi, O., Thaker, H. & Vural, M. 2018. Zeolite-loaded alginate-chitosan hydrogel beads as a topical hemostat. *Journal of Biomedical Materials Research Part B: Applied Biomaterials,* 106**,** 1662-1671.

Freier, T., Koh, H. S., Kazazian, K. & Shoichet, M. S. 2005. Controlling cell adhesion and degradation of chitosan films by N-acetylation. *Biomaterials,* 26**,** 5872-5878.

Ghazali, M., Nawawi, M. & Huang, R. Y. 1997. Pervaporation dehydration of isopropanol with chitosan membranes. *Journal of Membrane Science,* 124**,** 53-62.

Göpferich, A. 1996. Mechanisms of polymer degradation and erosion. *Biomaterials,* 17**,** 103-114.

Groen, J. C., Peffer, L. A. & Pérez-Ramírez, J. 2003. Pore size determination in modified micro- and mesoporous materials. Pitfalls and limitations in gas adsorption data analysis. *Microporous and mesoporous materials,* 60**,** 1-17.

Gutowska, A., Jeong, B. & Jasionowski, M. 2001. Injectable gels for tissue engineering. *The Anatomical Record: An Official Publication of the American Association of Anatomists,* 263**,** 342-349.

Han, F., Dong, Y., Su, Z., Yin, R., Song, A. & Li, S. 2014. Preparation, characteristics and assessment of a novel gelatin–chitosan sponge scaffold as skin tissue engineering material. *International journal of pharmaceutics,* 476**,** 124-133.

Hoseinpour Najar, M., Minaiyan, M. & Taheri, A. 2018. Preparation and in vivo evaluation of a novel gel-based wound dressing using arginine–alginate surface-modified chitosan nanofibers. *Journal of biomaterials applications,* 32**,** 689-701.

Jia, Z. & Shen, D. 2002. Effect of reaction temperature and reaction time on the preparation of low-molecular-weight chitosan using phosphoric acid. *Carbohydrate Polymers,* 49**,** 393-396.

Khan, T. A., Peh, K. K. & Ch'ng, H. S. 2000. Mechanical, bioadhesive strength and biological evaluations of chitosan films for wound dressing. *J Pharm Pharm Sci,* 3**,** 303-311.

Khattak, S. F., Chin, K. S., Bhatia, S. R. & Roberts, S. C. 2007. Enhancing oxygen tension and cellular function in alginate cell encapsulation devices through the use of perfluorocarbons. *Biotechnology and bioengineering,* 96**,** 156-166.

Kim, J. H. & Lee, Y. M. 1993. Synthesis and properties of diethylaminoethyl chitosan. *Polymer,* 34**,** 1952-1957.

Kong, M., Chen, X. G., Xing, K. & Park, H. J. 2010. Antimicrobial properties of chitosan and mode of action: a state of the art review. *International journal of food microbiology,* 144**,** 51-63.

Kulig, D., Zimoch-Korzycka, A., Jarmoluk, A. & Marycz, K. 2016. Study on alginate–chitosan complex formed with different polymers ratio. *Polymers,* 8**,** 167.

Kumar, P., Choonara, Y. E., Toit, L. C. D., Modi, G., Naidoo, D. & Pillay, V. 2012. Novel high-viscosity polyacrylamidated chitosan for neural tissue engineering: fabrication of anisotropic neurodurable scaffold via molecular disposition of persulfate-mediated polymer slicing and complexation. *International journal of molecular sciences,* 13**,** 13966-13984.

Li, Z., Ramay, H. R., Hauch, K. D., Xiao, D. & Zhang, M. 2005. Chitosan–alginate hybrid scaffolds for bone tissue engineering. *biomaterials,* 26**,** 3919-3928.

Miraftab, M., Qiao, Q., Kennedy, J., Anand, S. & Groocock, M. 2003. Fibres for wound dressings based on mixed carbohydrate polymer fibres. *Carbohydrate polymers,* 53**,** 225-231.

Moura, M. J., Figueiredo, M. M. & Gil, M. H. 2007. Rheological study of genipin cross-linked chitosan hydrogels. *Biomacromolecules,* 8**,** 3823-3829.

Müller, R. H., Jacobs, C. & Kayser, O. 2001. Nanosuspensions as particulate drug formulations in therapy: rationale for development and what we can expect for the future. *Advanced drug delivery reviews,* 47**,** 3-19.

Nassar, E. J., Ciuffi, K. J., Calefi, P. S., Rocha, L. A., De Faria, E. H., E Silva, M. L., Luz, P. P., Bandeira, L. C., Cestari, A. & Fernandes, C. N. 2011. Biomaterials and Sol–Gel Process: A Methodology for the Preparation of Functional Materials. *Biomaterials science and engineering.* IntechOpen.

Ngwuluka, N. C., Choonara, Y. E., Kumar, P., Modi, G., Toit, L. C. D. & Pillay, V. 2013. A hybrid methacrylate-sodium carboxymethylcellulose interpolyelectrolyte complex: rheometry and in silico disposition for controlled drug release. *Materials,* 6**,** 4284-4308.

O'meara, S. & Martyn-St James, M. 2013. Alginate dressings for venous leg ulcers. *Cochrane Database of Systematic Reviews*.

Ong, S.-Y., Wu, J., Moochhala, S. M., Tan, M.-H. & Lu, J. 2008. Development of a chitosan-based wound dressing with improved hemostatic and antimicrobial properties. *Biomaterials,* 29**,** 4323-4332.

Parikh, D. V., Fink, T., Delucca, A. J. & Parikh, A. D. 2011. Absorption and swelling characteristics of silver (I) antimicrobial wound dressings. *Textile Research Journal,* 81**,** 494-503.

Poormand, H., Leili, M. & Khazaei, M. 2017. Adsorption of methylene blue from aqueous solutions using water treatment sludge modified with sodium alginate as a low cost adsorbent. *Water Science and Technology,* 75**,** 281-295.

Qandil, A. M., Obaidat, A. A., Ali, M. A. M., Al-Taani, B. M., Tashtoush, B. M., Al-Jbour, N. D., Al Remawi, M. M., Al-Sou'od, K. A. & Badwan, A. A. 2009. Investigation of the interactions in complexes of low molecular weight chitosan with ibuprofen. *Journal of solution chemistry,* 38**,** 695-712.

Qin, Y. 2008. Alginate fibres: an overview of the production processes and applications in wound management. *Polymer international,* 57**,** 171-180.

Rabea, E. I., Badawy, M. E.-T., Stevens, C. V., Smagghe, G. & Steurbaut, W. 2003. Chitosan as antimicrobial agent: applications and mode of action. *Biomacromolecules,* 4**,** 1457-1465.

Ramburrun, P., Choonara, Y. E., Kumar, P., Du Toit, L. C. & Pillay, V. 2015. Design of chitospheres loaded with pristine polymer particles for extended drug delivery via polyelectrolyte complexation and particulate leaching. *International journal of pharmaceutics,* 479**,** 189-206.

Rao, K. R. & Buri, P. 1989. A novel in situ method to test polymers and coated microparticles for bioadhesion. *International journal of pharmaceutics,* 52**,** 265-270.

Roe, A. J., O'byrne, C., Mclaggan, D. & Booth, I. R. 2002. Inhibition of Escherichia coli growth by acetic acid: a problem with methionine biosynthesis and homocysteine toxicity. *Microbiology,* 148**,** 2215-2222.

Sæther, H. V., Holme, H. K., Maurstad, G., Smidsrød, O. & Stokke, B. T. 2008. Polyelectrolyte complex formation using alginate and chitosan. *Carbohydrate Polymers,* 74**,** 813-821.

Sakugawa, K., Ikeda, A., Takemura, A. & Ono, H. 2004. Simplified method for estimation of composition of alginates by FTIR. *Journal of Applied Polymer Science,* 93**,** 1372-1377.

Salmon, S. & Hudson, S. 1997. Crystal Morphology, biosynthesis, and physical assembly of cellulose, chitin, and chitosan, Rev. *Macromol. Chem. Phys. c37 (2),* 199.

Sankalia, M. G., Mashru, R. C., Sankalia, J. M. & Sutariya, V. B. 2007. Reversed chitosan–alginate polyelectrolyte complex for stability improvement of alpha-amylase: optimization and physicochemical characterization. *European journal of pharmaceutics and biopharmaceutics,* 65**,** 215-232.

Sartori, C., Finch, D. S., Ralph, B. & Gilding, K. 1997. Determination of the cation content of alginate thin films by FTi. r. spectroscopy. *Polymer,* 38**,** 43-51.

Schneider, L. A., Korber, A., Grabbe, S. & Dissemond, J. 2007. Influence of pH on wound-healing: a new perspective for wound-therapy? *Archives of dermatological research,* 298**,** 413-420.

Shao, X. & Hunter, C. J. 2007. Developing an alginate/chitosan hybrid fiber scaffold for annulus fibrosus cells. *Journal of Biomedical Materials Research Part A: An Official Journal of The Society for Biomaterials, The Japanese Society for Biomaterials, and The Australian Society for Biomaterials and the Korean Society for Biomaterials,* 82**,** 701-710.

She, Z., Zhang, B., Jin, C., Feng, Q. & Xu, Y. 2008. Preparation and in vitro degradation of porous three-dimensional silk fibroin/chitosan scaffold. *Polymer Degradation and Stability,* 93**,** 1316-1322.

Shoichet, M. S., Li, R. H., White, M. L. & Winn, S. R. 1996. Stability of hydrogels used in cell encapsulation: An in vitro comparison of alginate and agarose. *Biotechnology and bioengineering,* 50**,** 374-381.

Siafaka, P. I., Zisi, A. P., Exindari, M. K., Karantas, I. D. & Bikiaris, D. N. 2016. Porous dressings of modified chitosan with poly (2-hydroxyethyl acrylate) for topical wound delivery of levofloxacin. *Carbohydrate polymers,* 143**,** 90-99.

Silva, J. M., García, J. R., Reis, R. L., García, A. J. & Mano, J. F. 2017. Tuning cell adhesive properties via layer-by-layer assembly of chitosan and alginate. *Acta biomaterialia,* 51**,** 279-293.

Sing, K. S. 1985. Reporting physisorption data for gas/solid systems with special reference to the determination of surface area and porosity (Recommendations 1984). *Pure and applied chemistry,* 57**,** 603-619.

Smitha, B., Sridhar, S. & Khan, A. 2005. Chitosan–sodium alginate polyion complexes as fuel cell membranes. *European Polymer Journal,* 41**,** 1859-1866.

Sproul, E., Nandi, S. & Brown, A. 2018. Fibrin biomaterials for tissue regeneration and repair. *Peptides and proteins as biomaterials for tissue regeneration and repair.* Elsevier.

Sudheesh Kumar, P., Lakshmanan, V.-K., Anilkumar, T., Ramya, C., Reshmi, P., Unnikrishnan, A., Nair, S. V. & Jayakumar, R. 2012. Flexible and microporous chitosan hydrogel/nano ZnO composite bandages for wound dressing: in vitro and in vivo evaluation. *ACS applied materials & interfaces,* 4**,** 2618-2629.

Thalberg, K., Lindholm, D. & Axelsson, A. 2004. Comparison of different flowability tests for powders for inhalation. *Powder technology,* 146**,** 206-213.

Venkatesan, J., Lee, J.-Y., Kang, D. S., Anil, S., Kim, S.-K., Shim, M. S. & Kim, D. G. 2017. Antimicrobial and anticancer activities of porous chitosan-alginate biosynthesized silver nanoparticles. *International journal of biological macromolecules,* 98**,** 515-525.

Wang, K. & He, Z. 2002. Alginate–konjac glucomannan–chitosan beads as controlled release matrix. *International journal of pharmaceutics,* 244**,** 117-126.

Wang, L., Khor, E., Wee, A. & Lim, L. Y. 2002. Chitosan-alginate PEC membrane as a wound dressing: Assessment of incisional wound healing. *Journal of Biomedical Materials Research: An Official Journal of The Society for Biomaterials, The Japanese Society for Biomaterials, and The Australian Society for Biomaterials and the Korean Society for Biomaterials,* 63**,** 610-618.

Xia, W., Liu, P., Zhang, J. & Chen, J. 2011. Biological activities of chitosan and chitooligosaccharides. *Food hydrocolloids,* 25**,** 170-179.

Xie, H., Chen, X., Shen, X., He, Y., Chen, W., Luo, Q., Ge, W., Yuan, W., Tang, X. & Hou, D. 2018. Preparation of chitosan-collagen-alginate composite dressing and its promoting effects on wound healing. *International journal of biological macromolecules,* 107**,** 93-104.

Xu, D., Hawk, J. L., Loveless, D. M., Jeon, S. L. & Craig, S. L. 2010. Mechanism of shear thickening in reversibly cross-linked supramolecular polymer networks. *Macromolecules,* 43**,** 3556-3565.

Yang, G., Zhang, L., Peng, T. & Zhong, W. 2000. Effects of Ca2+ bridge cross-linking on structure and pervaporation of cellulose/alginate blend membranes. *Journal of Membrane Science,* 175**,** 53-60.

Zakhem, E., Raghavan, S., Gilmont, R. R. & Bitar, K. N. 2012. Chitosan-based scaffolds for the support of smooth muscle constructs in intestinal tissue engineering. *Biomaterials,* 33**,** 4810-4817.

Zhang, S. & Gonsalves, K. 1995. Synthesis of calcium carbonate–chitosan composites via biomimetic processing. *Journal of applied polymer science,* 56**,** 687-695.

CHAPTER 4

In Situ Forming Partially-Crosslinked Chitosan-Alginate Interpolymer Complex Hydrogel for Wound Dressing Skin Tissue Regeneration

4.1. Introduction

Natural polymers are highly used and attractive compounds in designing wound dressing bioplatforms. Alginate is one of these versatile and attractive polymers owing to its biological properties which includes water solubility, cytocompatibility, biocompatibility and fluid resorbability (Sudarsan et al., 2015). Natural polymers may present a wide range of exceptional properties for wound healing applications. However, their poor mechanical properties limit their individual use in designing wound dressing bioplatforms. For this reason, natural polymers are often combined with synthetic polymers to fabricate bioplatforms with controlled degradation (Yadav et al., 2015). The use of synthetic polymers in wound dressing has its own drawbacks such as toxicity, non-degradability, poor bioresorbability and they are not as effective in accelerating wound healing or antimicrobial activity (Van den Kerckhove et al., 2001, Aderibigbe and Buyana, 2018). Optimum combination of natural polymers such as chitosan with calcium alginate has demonstrated efficient healing and pain relieving activity in both chronic and acute wounds which includes ulcers and burns (Disa et al., 2001, Paul and Sharma, 2004). Alginate forms interpolymer complex with chitosan via the ionic interaction of alginate's carboxylic group and the amine group of chitosan. This interaction allows for fabrication of various bioplatforms and loading of drugs. The biological properties of both alginate and chitosan allows them to be employed in various dressings.

Chitosan is a cationic polymer capable of forming intermolecular network with other anionic polymers and drug molecules. The protonation of the free amine group $-NH_2$ in an alkaline condition to $–NH_3^+$ in acidic condition allows for controlled drug release (Il'ina et al., 2008, López-León et al., 2005). Other than the ionic interaction between chitosan and anionic polymers, anionic compounds such Trans-4-Hydroxy-3-methoxycinnamic acid (TFA) can also have an ionic interaction with chitosan via the use of the carboxylic group of TFA and the amine groups of chitosan. Furthermore, the hydrophobic property of TFA could also facilitate hydrophobic interaction with the hydrophobic chain of chitosan. Trans-4-Hydroxy-3-methoxycinnamic acid also known as Trans-ferulic acid (TFA) is a ubiquitous phenolic antioxidant, antimicrobial, anti-aging, anti-diabetic, and anticancer compound predominantly found in plant cell wall. TFA antioxidant, antimicrobial, and anti-inflammatory properties allows it to be incorporated in wound dressing bioplatforms. TFA presented a wide range of antimicrobial activities against both Gram-positive and Gram-negative bacteria by facilitating the inhibition of arylamine N-acetyltransferase in the bacteria (Lo and Chung, 1999, Tsou et al., 2000, Borges et al., 2013). Cyclooxygenase and nitric oxide synthase function/expression along with the activation of nuclear factor-kappa-light-chain-enhancer B cells are inhibited by TFA in both chronic and acute inflammation (Hosoda et al., 2002, Nagasaka et al., 2007, Batista, 2014). TFA can easily be used along with natural polysaccharides such as chitin and chitosan. This is due to the occurrence of TFA in polysaccharides, glycoproteins, polyamines, lignin and hydroxylated fatty acids of seeds and leaves (Smith and Hartley, 1983).

The rapid oxidation tendency of TFA in the environment limits its application in the cosmetic, food and biomedical field. However, it has been reported that chitosan based films, nanoparticles and

microparticles with improved matrix characteristics present exceptional incorporation, protection and controlled release of a variety of compounds including antibiotics, anti-inflammatory and anti-cancer drugs (Nair et al., 2009). With use of chitosan and its properties, TFA could be encapsulated, protected and released in a controlled manner. A recent study highlighted the effective immobilization, protection, and release of TFA in microparticles than in nanoparticles bioplatforms (Cota-Arriola et al., 2017). Furthermore, the interaction of TFA and chitosan affected the microparticles and nanoparticles bioplatform's morphology which improved the bioplatform's anti-fungal activity on growth, spore germination, and morphology of *A. parasiticus* (Cota-Arriola et al., 2017). The hydrophobic character of TFA along with limited solubility in aqueous solution limits TFA's encapsulation, loading and bioavailability thereby reducing its clinical efficiency. These limitations can be improved by the use of natural based polymeric bioplatforms as carrier systems and also to increase TFA's solubility, bioavailability and cytocompatibility. Although there is promising performance in TFA loaded chitosan bioplatforms, other bioplatforms such as microcapsules still present poor activity against fungi due to undesirable matrix characteristics (Cota-Arriola et al., 2017, Nair et al., 2009).

The crosslinking of polymers has received much interest in the biomedical field due to improved mechanical properties. Nevertheless, there is scant reports on the exploration of partial-crosslinking of alginate and drug loaded chitosan for wound dressing applications. The ionic character of chitosan allows it to be crosslinked by anionic crosslinkers such as glutaraldehyde and salts such as sodium tripolyphosphate (NaTPP). A number of studies indicated efficient fabrication of nano/micro particles and beads by crosslinking chitosan with tripolyphosphate (Madgulkar et al., 2009, Cota-Arriola et al., 2017). These drug loaded bioplatforms can be formed by employing the droplet extrusion method where the drug loaded chitosan solution is poured drop-wise into sodium TPP aqueous solution (Madgulkar et al., 2009) or with the ionotropic gelation approach where the chitosan solution is sprayed on the drug loaded TPP solution (Cota-Arriola et al., 2017). On the previous study, a novel three–step approach (partial-crosslinking, free-drying, and pulverization of bioplatforms) in fabricating partially crosslinked bioplatforms with improved physical and mechanical properties was introduced (Mndlovu et al., 2019). Properties such as porosity, fluid uptake, degradation, visco-elasticity, and cytocompatibility were improved by employing the three-step approach.

The partial-crosslinking made use of salts such as calcium chloride for crosslinking alginate and NaTPP for crosslinking chitosan into beads (Mndlovu et al., 2019). The beads and nano/microparticle bioplatforms have been reported to allow for optimum incorporation of antioxidants (Nair et al., 2009). However, the incorporation of TFA in bioplatforms has its limitations. Those limitations includes TFA's poor solubility and low bioavailability in the body limited by the first pass metabolism (Zhang et al., 2016). These limitations lead to the exploration of various approaches in an attempt to improve the encapsulation efficiency and release of TFA. These approaches included but not limited to the immobilization of TFA in, (a) nanoparticles (Bairagi et al., 2018), (b) nanostructured lipid carriers & solid lipid nanoparticles (Zhang et al., 2016), and (c) niosomes (Rezaeiroshan et al., 2020). Based on these literature data, the conceptualisation of this study and the aim to fabricate cytocompatible, biodegradable and fluid absorbing drug loaded microparticles which would form a hydrogel *in situ* under fluid environment, thereby presenting optimum TFA release and wound healing properties was crafted. The objective of this study was to employ the three-step approach in (1) partial-crosslinking alginate and TFA loaded chitosan, (2) lyophilization, and (3) pulverisation of the bioplatforms. It was envisaged that the three-step approach would improve the physical and mechanical properties of

the bioplatform while the loading of TFA and the biological properties of the two natural polymers will facilitate accelerated wound healing performances such as faster wound closure and enhanced skin tissue regeneration.

4.2. Experimental

4.2.1. Material

Medium molecular weight chitosan (75-85% deacetylation, 190 – 300 kDa) Sigma-Aldrich (St. Louis, MO, USA). The calculated degree of deacetylation was 84.36% and it was obtained by employing ^{1}H NMR analysis. Chitosan was dissolved in a 1:1 ratio of deuterated acetic acid and deuterated oxide and the analysis was acquired at 70 °C. Sodium alginate was procured from Sigma-Aldrich (St. Louis, MO, USA). The calculated mannuronic acid and guluronic acid concentration ratio (A1025/A1078) of 1.51 was obtained via FTIR analyses as described in literature (Sakugawa et al., 2004). Glacial acetic acid Sigma-Aldrich (St. Louis, MO, USA). Calcium chloride Sigma-Aldrich (St. Louis, MO, USA). Sodium tripolyphosphate Sigma-Aldrich (St. Louis, MO, USA). Trans-4-Hydroxy-3-methoxycinnamic acid (Trans-Ferulic acid 99%) was purchased from Sigma-Aldrich (St. Louis, MO, USA). Simulated wound fluid constituted from 2% (w/w) bovine serum albumin (BSA), 0.02 M $CaCl_2$, 0.4 M $NaCl_2$, and 0.08 M tris(Hydroxymethyl) aminomethane dissolved in distilled water and adjusted to a pH 7.4. A commercial alginate-based wound dressing (Pharma-Algi®, Pharmaplast) was acquired for comparative studies.

4.2.2. Preparation of partial-crosslinked alginate and FA loaded chitosan micromatrices

Partial-crosslinked alginate (PC Alg) and TFA loaded chitosan (PC TFA-CS) micromatrices were prepared as described in our previous work (Mndlovu et al., 2019). Briefly, Chitosan powder (2 g) was dissolved in 2% $^{V}/_{V}$ glacial acetic acid aqueous solution and partially-crosslinked (PC) with 2% $^{W}/_{V}$ Sodium tripolyphosphate (TPP) solution. A 0.67% $^{W}/_{V}$ TFA solution was prepared by dissolving 0.67 g of TFA in DMSO and mixed with chitosan solution to make a final 0.5% $^{W}/_{V}$ DMSO solution. The partial-crosslinking of TFA-CS suspension was achieved by pouring the suspension drop-wise into the 2% $^{W}/_{V}$ TPP solution and the formed TFA loaded beads were immediately rinsed with water to control the degree of crosslinking. The rinsed beads were immediately placed in the -80 °C freezer for 24 hours, followed by the lyophilization process using the Lyophilizer (Free zone 12, Labcono, Kansas City, USA) for 24 hours. Using the pestle and mortar, the lyophilized beads were pulverised into micromatrices. The sodium alginate beads were prepared in the same manner as the chitosan beads. Briefly; a 2% $^{W}/_{V}$ solution of sodium alginate was crosslinked with 2% $^{W}/_{V}$ $CaCl_2$ and rinsed with deionized water before being frozen at -80 °C for 24 hours and lyophilized for 24 hours. The partially-crosslinked alginate beads were also pulverised into micromatrices. The PC-Alg and the PC TFA-CS particles were mixed (1:1 ratio) and sprinkled into simulated wound fluid for the *in situ* formation of the TFA loaded interpolymer complex (IPC). The formed IPC was allowed to gel overnight followed by freeze drying before characterisation.

4.2.3. Zeta Potential of the bioplatforms

The nano zetasizer technique was employed to determine the particle surface charge of the PC TFA-CS bioplatform and to confirm the interaction between the biomolecules by comparing the shift in the zeta potentials of the crosslinked, uncrosslinked and TFA loaded bioplatforms. The zeta potential was evaluated using the Zetasizer Nano ZS instrument (Malvern Instruments (Pty) Ltd.,Worcestershire, UK). The prepared PC TFA-CS and PC Alg bioplatforms were sonicated in

distilled water and filtered before the suspension was transferred to the cell for the analysis of the zeta potential at 25 °C.

4.2.4. Molecular vibrational transitions, X-ray powder diffraction pattern, and thermostability properties of the bioplatforms

The shifts and changes in the bonds of the main functional groups that were involved in interactions in the micromatrices were determined using the FTIR spectra of wavelength between 4000–650 cm^{-1} at 64 scans using a PerkinElmer Spectrum 2000 ATR-FTIR (PerkinElmer 100, Llantrisant, Wales, UK) spectrometer fitted with a single-reflection diamond MIRTGS detector. Furthermore, the changes in the phase present in the micromatrices was assessed comparatively by recoding the X-ray diffraction diffractogram on the benchtop MiniFlex 600 (Rigaku, Japan) diffractometer using CuKα radiation at 40 kV and 15 mA. The 2θ scan range was between 3-90 degrees at a scan rate of 10 degree/minute. The thermophysical properties of the bioplatforms were followed via the use of the differential scanning calorimeter (DSC) (Mettler Toledo, DSC, STARe System, Swchwerzenback, ZH, Switzerland) and thermo-gravimetric analyser (TGA) (PerkinElmer, TGA 4000, Llantrisant, Wales, UK). Sample preparation of bioplatforms for DSC analysis were as follows, 3 to 10 mg samples were sealed in aluminium crucibles and heated over a temperature range of 0 to 400 °C at a heating rate of 10 °C/min under a N_2 atmosphere. DSC curves were plotted as a function of heat flow against temperature. Samples were also prepared for TGA analysis and heated at a rate of 10 °C/min from 30 to 900 °C under continuous nitrogen purging. Thermograms were generated as percentage weight versus temperature.

4.2.5. Surface morphology evaluation, fluid uptake and degradation activity of the bioplatforms

Zeiss sigma scanning electron microscopy (FESEM, 300 VP, ZEISS Research Microscopy Solutions, Jena, Germany) with an accelerating voltage from 10 to 15 kV was employed for the evaluation of the surface morphology of the micromatrices. The micromatrices were mounted on aluminium stubs using carbon adhesive tape and coated with carbon/gold-palladium in a 2:1 ratio.

Fluid uptake and degradation of the bioplatforms were performed under simulated in vitro exudative conditions via the use of the orbital shaking incubator (LM-530-2, MRC Laboratory Instruments Ltd. Hahistadrut, Holon, Israel) maintained at 37 °C, and set at a speed of 50 rpm as previously reported (Mndlovu et al., 2019). PC TFA-CS-Alg IPC bioplatform was weighed (50mg) into vials and PBS 5mL (pH 7.4) was added. Fluid uptake of the bioplatforms were measured at 1, 2, 4, 8, and 24 hours. The fluid uptake was calculated using equation 4.1. The rate of degradation was measured after 1, 3, 7, 10, and 14 days. The degree of degradation was obtained via the use of equation 4.2.

$$FU(\%) = \left(\frac{Mh-Md}{Md}\right) x\ 100 \qquad \text{Equation 4. 1}$$

$$Degradation\ (\%) = \left(\frac{Mo-Md}{Md}\right) x\ 100 \qquad \text{Equation 4. 2}$$

Where FU% is the percentage fluid uptake, Mo, in the initial dry mass of sample before immersed in fluid, Mh and Md is the mass of the bioplatforms in hydrated and dry state, respectively.

4.2.6. Hydrogel formation kinetics of PC TFA-CS-Alg IPC

The hydrogel formation and interpolymer complexation were evaluated using the ElastoSens™ Bio2 (Rheolution instruments, Canada). The real-time *in situ* forming hydrogel kinetics of the interpolymer complex were determined by mixing PC Alg and PC TFA-CS in a 1: 1 ratio to a total of 100 mg bioplatform mixture and initiated the interpolymer complexation by pouring 3 mL of the simulated wound fluid into the sample holder at 37 °C. The gelling, ionic interaction, fluid absorption and viscoelastic (G' and G*) properties of semi-stiff IPC hydrogel was determined over time. The ElastoSens™ BIO2 technique measures in real time and non-destructively the shear storage (G') and loss (G") moduli of hydrogels as function of time or temperature. The analysis is based on the gentle mechanical vibration of a sample confined in a sample holder and the response is detected by a laser.

4.2.7. Encapsulation efficiency (EE), drug loading (DL) and in vitro release studies

PC FA-CS-Alg was stirred in simulated wound fluid pH 7.4 to allow for complete release of TFA. The bioactive loading and encapsulation efficiency was determined via the use of the standard curve obtained from the measurement of 0, 5, 10, 15, 20, 25 µg/mL standard solutions of TFA in SWF at the wavelength of 310 nm using UV-Visible spectrophotometer (IMPLEN, NP80 NPOS 4.2 built 14900 UV-Vis nanophotometer, Jena, Germany). Total drug to polymer ratio were calculated in order to get the expected amount (mass in milligrams) of TFA in any given weighed bioplatform amount (mass). The expected TFA amount per bioplatform mass would give insights on the encapsulation efficiency and drug loading of the bioplatform via the use the equations below;

$$EE\ (\%) = \left(\frac{Mi}{Mf}\right) x\ 100 \qquad \text{Equation 4. 3}$$

$$DL\ (\%) = \left(\frac{Mi}{Mt}\right) x\ 100 \qquad \text{Equation 4. 4}$$

Where Mi is the calculated amount (mass) of TFA in the bioplatform as per in the sample preparation method, Mf is the amount (mass) of drug obtained from the standard curve after complete release, and Mt is the total weighed bioplatform mass used for drug release study. The TFA release study was carried out based on the total mass that the bioplatform can release (Mf) and not the mass from the drug to polymer ratio (Mi).

The release study was carried out in 100 mL simulated wound fluid medium (pH 7.4) using the Snake Skin dialyses tube (3.5K MWCO, 22 mm, Thermo Fisher scientific Inc.) diffusion technique maintained at 37 °C stirring at 30 rpm on the orbital shaking incubator (LM-530-2, MRC Laboratory Instruments Ltd. Hahistadrut, Holon, Israel) for 72 hours. Aliquots (2 mL) were withdrawn at predetermined time points (1, 2, 4, 8, 12, 24, 48, and 72 hours) from the release medium and replaced with an equivalent volume of fresh media to maintain sink condition. The amount of the TFA encapsulated in the micromatrice and released at predetermined time points in the simulated wound fluid medium was determined at 310 nm with UV-Vis spectrophotometer. The average absorbance (done in triplicates) of TFA released at time (t) was used in the standard curve to obtain the concentration of TFA released and multiplied by the dilution factor to get the undiluted concentration of released TFA at pre-determined time points. The concentration was divided by the bath volume to get the mass of TFA released at those predetermined time points. The percentage release was obtained by getting percentage mass fraction of TFA released at time t to the amount of TFA that was completely released from the bioplatform (Mf) which was

represented as pt. The cumulative drug release was determined using the formula bellow as described Chandrasekaran et al. (Chandrasekaran et al., 2011);

$$\text{Cumulative release} = (\text{sample volume with drown/bath volume})\ x\ \text{p(t} - 1) + \text{pt} \qquad \text{Equation 4. 5}$$

Where pt is the percentage released at time t and p(t-1) is the percentage released before time t.

4.2.8. *In vitro* cytocompatibility evaluation of the bioplatforms

A comparative commercial product , TFA and PC TFA-CS-Alg were prepared for cell viability tests on the mouse embryonic fibroblast NIH-3T3 cell line. The NIH 3T3 cells were grown in DMEM medium supplemented with 10% FBS and 1% antibiotics. NIH 3T3 cells (100 µL of 1 x 10^4 cell/mL) were seeded on each 96 well plate and incubated in a humidified chamber overnight at 37 °C with an atmosphere containing and 5% CO_2. This was followed by adding 1 mg of PC TFA-CS-Alg containing 100 µL DMEM medium per well. This was done in replicates (6 times). The same approach was done for the comparative product (5 mm diameter) and TFA. The cells exposed to samples were incubated in a humidified chamber overnight at 37 °C with an atmosphere containing 5% CO_2 for predetermined time points; 24, 48, and 72 hours. For positive control, NIH 3T3 cells where maintained with DMEM medium without any additions and for negative control, the cells were killed and maintained with Dimethyl sulfoxide (DMSO). Ten microliters of MTT (3-(4,5-Dimethyl-2-thiazolyl)-2,5-diphenyl tetrazolium Bromide) was added to each well plate after each of the predetermined time points and incubated for 4 hours. Thereafter, the medium and the bioplatforms on the well plates were discarded followed by addition of 100 µL DMSO and incubated overnight on the orbital shaker (at 37 °C) to dissolve the formazan. The 96-well plates were measured at absorbance of 570 nm and 690 nm to subtract the 690nm absorbance from the 570 nm absorbance to calculate the percentage cell viability on each bioplatforms at the given time points.

4.2.9. In vivo skin tissue regeneration and wound closure performance of the bioplatforms

In vivo assessment of the wound healing performances of the bioplatforms was followed in a rat model. Female Sprague–Dawley rats (6-8 weeks old) were housed individually, in cages at room temperature (± 25 °C), maintained under a 12 hour light:dark cycle. The animals were fed water and *ad libitum* and allowed to acclimatize to the environment for a week prior to surgery. The animals were monitored according to prescribed central animal services (CAS) protocol. All procedures were done in accordance with the Animal Ethics Control Committee of the University of the Witwatersrand animal care regulations following approval by the Animal Ethics Screening Committee of the University of the Witwatersrand (ethics number: 2018/10/49c).

Rats where prepared for punch biopsy surgical procedure by anesthetizing them with an Isofor and Oxygen gas at 1:3 % mixture and intraperitoneal injection of a 2.7 mL/kg mixture containing: midazolam (1.25 mg/mL), and 0.079 mg/mL fentanyl to maintain the rats. The skin over the dorsal area was shaved, application fields were outlined with a marking pen just before skin excisions. A full-thickness (2 mm thick) wound of 6 mm diameter was created at the dorsal area of the rat employing the skin punch biopsy apparatus. Using forceps the skin was lifted in the middle of the wound outline created by the punch biopsy and then the iris scissors (with curved tips) was used to excise the circular piece of tissue. The excised tissue plugs (wound plugs) were fixed in 10% buffered-formalin for later processing. A total of two wound areas were created on the dorsal area of each rat. In each group, the rats contained the following treatments on the wound area; untreated (gauze and bandage), comparative product, PC Alg-CS, PC TFA-CS-Alg. The

bioplatforms were sterilized with UV before sprinkled on rats. The dressings were not changed but the bandage was changed weekly. The animals were allowed to heal for 3, 7, 10 and 14 days whereas the wounds were examined, photographed, and excised to measure the reduction in wound size on day 4, 8, 11, and 15 respectively. Wound healing was followed by determining the degree of wound closure (%) given by the size of the wound calculated from the following equation.

$$Wound\ closure\ (\%) = \frac{(Wound\ area\ day\ 0 - wound\ area\ day\ (t)}{(Wound\ area\ day\ 0)}\ x\ 100 \qquad \text{Equation 4. 6}$$

Histological analysis

The excised wound plugs at each predetermined wound healing time points allowed for the skin tissues to be stored in 10% formalin for collective evaluation via histopathological analysis. After sufficient fixation of the collected specimens in 10% buffered formalin, the samples were cut according to standard operating procedure (IdexxSA-AP-SOP-26) and processed according to routine histological tissue processing in an automated tissue processor with standard operating procedures IdexxSA-AP-SOP-27. Following tissue processing, sections were cut of 5-6µm (IdexxSAAP- SOP-30) and the slides produced stained in an automated Haematoxylin and Eosin tissue stainer (IdexxSA AP-SOP-205) before histological evaluation. Histological analysis of the different healing times was performed using light microscopy. In brief, biopsies were fixed in buffered paraformaldehyde and embedded in paraffin wax (Lin et al., 2017, Yuvarani et al., 2012). Sections (6 µm) was stained with hematoxylin eosin. The stained sections of each sample was subsequently examined under a light microscope for analysis of tissue inflammatory reaction and regeneration (Yuvarani et al., 2012). To measure the length of re-epithelialization, wound edges were determined as the border between the original dermis with the hair follicles and the newly developed fibrotic dermis without hair follicles (Lin et al., 2017). Scoring of the wound morphology was done according to 5 features notably: epitheliazation, fibroblasts, angiogenesis, epidermal-dermal attachment, and mononuclear leukocytes. The mode appearance of each bioplatform was used to describe the morphology of the wound plugs.

4.3. Results and discussion

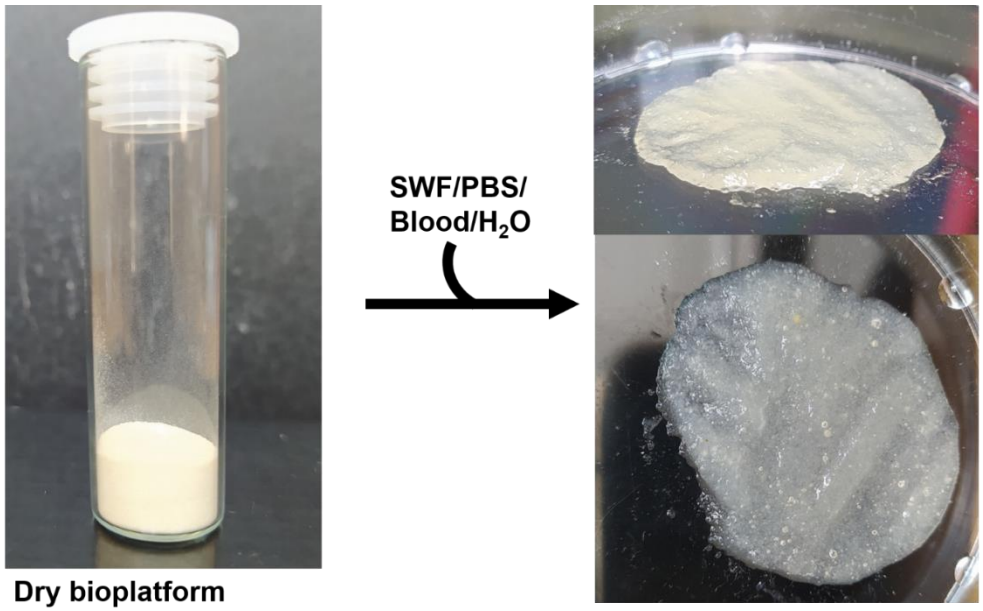
The investigations herein, are building on previous chapter carried out in this study which dealt with the effect of the partial-crosslinking approach on the properties of the bioplatforms. The *in situ* forming hydrogel's structural, physical and mechanical property transitions were investigated (Mndlovu et al., 2019). Herein, the performance of the bioplatform was investigated in terms of acting as a bioactive delivery system, cytocompatibility, and *in vivo* deep-cut wound healing performance. The natural polymers chitosan and alginate have been extensively researched in the wound healing field. The performance of these polymers could be enhanced by incorporating bioactives with various properties such antimicrobial, antioxidant, anti-inflammatory and wound healing capabilities. Transferulic acid was used in the study owing to its reported antioxidative and antimicrobial properties. Furthermore, the point that TFA is naturally derived makes it an attractive bioactive to be used along with natural polymers for developing wound dressings with multi-properties.

4.3.1. Synthesis of bioplatforms

The bioplatforms were synthesized by employing the three-step approach namely partial-crosslinking, freeze-drying and pulverisation of macromatrices as previously reported (Mndlovu et al., 2019). The percentage of the crosslinkers ($CaCl_2$ and NaTPP) and the polymers (chitosan

and alginate) were kept the same at 2%. Bioactives can be incorporated to bioplatforms in various methods such as bulk mixing where the whole bioactive volume/mass is added into polymeric solutions, drop-wise addition of bioactive into a polymeric solution, and coating of a polymeric system in a bioactive solution (Mndlovu et al., 2020). In this study, transferulic acid was added drop-wise into chitosan solution to allow for ionic and hydrophobic interaction to form TFA-CS suspension before the crosslinking step. The carboxylic group of transferulic acid interacted with the primary amine groups of chitosan. The hydrophobic character of TFA could also have interacted with the hydrophobic chain of chitosan. The concept of mixing TFA with CS was to allow for interactions between the two biomolecules which in turn could control the release of TFA by reducing the amount of TFA released at certain time points. This control on TFA release was further strengthened by partial-crosslinking TFA-CS with NaTPP to protect the bound and unbound TFA from oxidation. The control of drug release by ionic interaction and crosslinking has been reported in literature (Boonsongrit et al., 2006). The addition of TFA in CS solution resulted in the spontaneous formation of particles which were further crosslinked into macromatrices with NaTPP. The formed PC TFA-CS was confirmed by observing the zeta potential of the bioplatform against its pristine counterpart (Table 4.1).

The PC TFA-CS particulate bioplatform was mixed with PC Alg in a 1:1 ratio in simulated wound fluid (pH7.4) to allow for ionic interaction between the bioplatforms thus facilitating *in situ* hydrogel formation (see image below). Hydrogel formation happens instantly upon exposure to fluid such as SWF/PBS/water/blood. The hydrogel formation kinetics are discussed in more details in the mechanical properties section below. The transition of bioplatform from powdered form to a hydrogel state upon exposure to fluid is crucial in the sense that it allows the powder to be applied in the form of sprinkles and enables the use of wound fluid to form the hydrogel. The application of the powdered bioplatform via sprinkles would reduce pain introduced by the pressure applied on wound during dressing application whereas the use of wound fluid as a source of hydration would contribute in formation of a hydrogel and also retain most of the nutrients from the wound fluid aid wound healing.



Dry bioplatform
PC TFA-CS: PC Alg (1:1)

Hydrated *in situ* formed hydrogel

4.3.2. Zeta Potential of bioplatforms

Table 4.1. Bioplatform ratios and zeta potential

Bioplatforms	Bioplatform ratios	Zeta Potential (mV)
PC Alg	0 TFA: 0 CS : 1 Alg	-25.8 ± 3.74
PC CS	0 TFA: 1 CS : 0 Alg	+29.2 ± 5.83
PC TFA-CS	0.335 TFA: 1 CS : 0 Alg	+20.1 ± 3.17
PC TFA-CS-Alg	1 TFA-CS : 1 Alg	-3.58 ± 2.74

The significance of surface charge analysis is that it gives insights on the potential antimicrobial properties of the bioplatforms (Du et al., 2008, Kong et al., 2010) and also the stability of the bioplatform (Du et al., 2009) in terms of the ionic interactions that may exist between polymers, drugs (Qandil et al., 2009), and bacterial organisms. Table 1 above indicated that PC Alg, PC CS, and PC TFA-CS had high surface charges as expected for pristine and partially-crosslinked polymers. The high surface charges inferred that the partial-crosslinking of chitosan and alginate did not deplete all the polymeric ions. The slight change in zeta potential from pristine to partially crosslinked polymers also confirms that the polymers were partial-crosslinked. Furthermore, the decrease on the surface charge on the TFA loaded chitosan, suggest that there was ionic interaction between transferulic acid and chitosan. The high surface charge on PC TFA-CS allowed for further ionic interaction between PC TFA-CS and PC Alg. The point that the zeta potential of PC TFA-CS was below ±30 mV (+20.1) implies that the suspension was not physically stabilized by electrostatic repulsion (Müller et al., 2001). Thus it could allow for substitution of TFA with a more ionically stable PC Alg during IPC formation. However, a portion of PC TFA-CS would still exist in the IPC owing to the following points; the interaction of CS with TFA is also based on (1) steric stabilization, (2) hydrophobic interaction and (3) ionic interaction. The zeta potential of PC TFA-CS was above 20 mv which inferred that it was sufficient in stabilizing some parts of TFA-CS on the bioplatform (Müller et al., 2001) and such a position also received stability contribution from partial crosslinking. The hydrophobic interaction between chitosan chain and transferulic acid aided the stability of the PC TFA-CS bioplatform. The high zeta potential of PC TFA-CS, loading of transferulic acid, and the partial-crosslinking of alginate with calcium chloride may contribute to the antibacterial properties of the bioplatform (Hussain et al., 2017, Du et al., 2008, Du et al., 2009, Cota-Arriola et al., 2017). The PC Alg, PC CS and PC TFA-CS had different zeta potentials which confirmed partial-crosslinking, loading of FA and interpolymer complexation. The PC TFA-CS-Alg IPC bioplatform displayed a zeta potential of -3.58 mv which was indicative of a neutral potential as it was close to zero. The change of zeta potential from both negative and positive intermediate product to neutral potential is suggestive of the ionic interaction that took place between partial crosslinked alginate (-25.8 mv) and TFA loaded partial-crosslinked chitosan (+20.1 mv).

4.3.3. Physical and chemical characterisation of bioplatforms

ATR-FTIR spectroscopy was employed to assess the polymer crosslinking, transferulic acid incorporation and interpolymer complexation. The transferulic acid FTIR spectrum displayed its characteristic bands at 3430 cm^{-1}(O-H stretch), 3078 cm^{-1} $(C\text{-}H)_{aromatic\ and\ C=C}$, 3018 cm^{-1} $(C\text{-}H)_{aromatic\ and\ C=C}$, 2970 cm^{-1} $(C\text{-}H)_{aromatic\ and\ C=C}$, 2841 cm^{-1} $(C\text{-}H)_{aromatic\ and\ C=C}$, 1687 cm^{-1} (C=C), 1662 cm^{-1}(C=O stretch), 1618 cm^{-1} $(C=C)_{aromatic}$, 1591 cm^{-1}(C-O stretch), 1511 $cm^{-1}$$(C=C)_{aromatic}$, 1460 cm^{-1}(O-H deformation vibration), 1377 cm^{-1}(COO^{-}), 1324 $cm^{-1}$$(C\text{-}H)_{aromatic\ and\ C=C}$, 1265 cm^{-1} $(C\text{-}H)_{C=C}$, 1202 $cm^{-1}$$(C\text{-}OH\ stretch)_{aromatic}$, 1164 cm^{-1} $(C\text{-}H)_{aromatic}$, 1112 cm^{-1} $(C\text{-}H)_{aromatic}$, and 1034 cm^{-}

^{1} (C-O stretch) (Figure 4.1a). These TFA FTIR bands correlated with those reported in other studies (Mathew and Abraham, 2007, Wang et al., 2011). There was a disappearance of the characteristic transferulic acid bands in TFA loaded chitosan at 3430 cm^{-1}, 1662 cm^{-1}, 1460 cm^{-1}, 1202 cm^{-1} which were assigned to O-H stretch, C=O stretch, O-H deformation vibration, and C-O stretch, respectively. There was also a major chemical shift and overlapping of the primary amine in chitosan by those signals of TFA. These observations infer that there was an interaction between chitosan and TFA which further suggest successful loading of TFA on chitosan. TFA loaded chitosan IR spectrum displayed the following bands; 2942 cm^{-1} (C-H stretch), 1620 cm^{-1} (C=C stretch, 1598 cm^{-1} (C=O amide I), 1544 cm^{-1} $(CC)_{aromatic}$, 1517 cm^{-1} (C=O amide II), 1489 cm^{-1} $(CC)_{aromatic}$, 1429 cm^{-1} (O-H deformation), 1324 cm^{-1} (carboxylate stretching), 1268 cm^{-1} $(C-H)_{C=C}$, 1231 cm^{-1} $(C-OH\ stretch)_{aromatic}$, 1204 cm^{-1} $(C-O)_{aromatic}$, 1165 cm^{-1} $(C-H)_{aromatic}$, 1124 cm^{-1} (C-H stretch), 1063 cm^{-1} $(CH)_{aromatic}$, and 1033 cm^{-1} (C-O-C asymmetric stretch) (Figure 4.1a). The disappearance and shifting of the C-H bands (aromatic) around position 3078 cm^{-1}, 3018 cm^{-1}, 2970 cm^{-1}, 2841 cm^{-1}, infer that there was also hydrophobic interaction between the aromatic ring of TFA and the chitosan's hydrophobic chains.

The presence of additional bands was observed in the FTIR spectrum of PC TFA-CS-Alg complex relative to the pristine compounds. The following molecular vibrations can be ascribed to the bands in PC TFA-CS-Alg; 3283 cm^{-1}(O-H stretch), 2934 cm^{-1} (C-H stretch), 1648 cm^{-1}(amide deformation), 1538 cm^{-1} (asymmetric COO^{-} stretch), 1407 cm^{-1} (C-C bending), 1277 cm^{-1} $(C-O\ stretch)_{aromatic}$, 1030 cm^{-1} (C-O-C asymmetric stretch) (Figure 4.1a). Compared to the FTIR spectrum of transferulic acid, chitosan and alginate, bands shifted while others disappeared in the spectrum of PC TFA-CS-Alg. This observation was due to both ionic interaction and hydrophobic interaction amongst the two polymers, crosslinkers and the incorporated transferulic acid. The pristine chitosan amide I band at 1648 cm^{-1} (Mndlovu et al., 2019) underwent bathochromic shift to 1598 cm^{-1} in PC TFA-CS followed by a hypsochromic shift to 1648 cm^{-1} in the interpolymer complex (PC TFA-CS-Alg). Furthermore, the carboxylic group band at 1538 cm^{-1} in the interpolymer complex can be assigned to C=O bands from both alginate and TFA. The characteristic bands for Transferulic acid bands disappeared due to the high polymer to bioactive weight ratio. The high percentage composition of polymer to drug resulted in most molecular structural moieties transferulic acid being incorporated in the interpolymer network matrix thereby diminishing transferulic acid intensity bands while some parts of TFA were on the surface hence dominating the 1407 cm^{-1} band on PC TFA-CS-Alg IPC. Portion of TFA was also distributed on the surface of the bioplatform which resulted on the splitting of the 1604 cm^{-1} amide deformation band on the PC CS-Alg to 1648 cm^{-1}(amide deformation), 1538 cm^{-1} (asymmetric COO^{-} stretch) on PC TFA-CS-Alg. Incorporation of TFA on the bioplatform was further associated with the deformation of the O-H stretch and the major shift of signals of the polymers interacting functional groups. The O-H stretch in the complex was very similar to the one observed in TFA spectrum, and the appearance of the C-OH band along with intensified C-O-C stretch was consistent with those observed in the FTIR spectrum of pristine TFA.

In the diffractogram of TFA, the X-ray diffraction pattern was found to be characteristic of pristine TFA and those characteristic peaks were also observed in transferulic acid loaded chitosan. TFA gave characteristic crystalline peaks at 8.98, 10.44, 12.78, and 15.6 degrees which were indicative of highly crystalline phases followed by less crystalline phases at 20-23.2°, and finally more crystalline phases at 24.56, 26.46, 29.5, 31.56 degrees (Figure 4.1b). Similar X-ray diffraction pattern of TFA was reported (Wang et al., 2011). Relative to the XRD diffractogram of pristine TFA, most diffraction peaks observed for TFA, except for signal at 27.32° were observed

in the XRD diffractogram of PC TFA-CS-Alg IPC. The remaining diffraction peaks observed on the PC TFA-CS-Alg IPC were due to the crystalline salts deposited to the surface of bioplatform as a result of ionic interaction between polymers with respective crosslinkers and the incorporation of TFA ions. The semi-crystalline diffraction pattern of chitosan was still observed along with the transferulic acid crystalline peaks on PC TFA-CS. The PC TFA-CS-Alg IPC exhibited the conserved crystalline peaks observed in PC CS-Alg as reported previously and also in Figure 4.1b (Mndlovu et al., 2019). The presence of TFA diffraction peaks confirmed that TFA was successfully incopoarated on the bioplatform, and the presence of calcium salts peaks was indicative of the use of crosslinked alginate on the complex. Apart from the crystalline phases, the diffraction pattern indicative of amorphous phases was consistent with the one observed on the pristine polymers and the partially crosslinked bioplatforms in terms of following the 110 lattice packing reflection amorphous peaks at 14, 25, 40 degrees on alginate based bioplatforms with chitosan having its saccharide peak 11 and 20.5 degrees (Mndlovu et al., 2019). These changes on the bioplatforms properties lead to more evaluations of their thermo-stability characteristics.

Detailed thermo-stability property evaluations of the bioplatforms were discussed in the previous chapter. The effect of partial-crosslinking on chitosan bioplatforms displayed a conserved dehydration process while exhibiting a shift on the exothermic behaviour from 280 °C to 240 °C on the pristine and partially-crosslinked bioplatform, respectively (Mndlovu et al., 2019). Herein, transferulic acid with a melting point at 173 °C was incorporated to CS prior crosslinking (Figure 2c). The TFA endothermic peak at 173 °C correlate with the reported 178 °C endothermic peak for TFA (Wang et al., 2011). The incorporation of TFA and partial crosslinking of CS resulted in a bioplatform that had a conserved dehydration endothermic behaviour at 101 °C, an additional endothermic behaviour at 164 °C and an exothermic degradation behaviour at 288 °C (Figure 4.1c). The degradation profile of PC TFA-CS was more similar to pristine CS than to the PC CS. The endothermic peak at 164 °C on PC TFA-CS was a contribution from the melting of TFA incorporated in CS. On the contrary to the PC CS-Alg IPC with a dehydration process at 135 °C, the PC TFA-CS-Alg displayed a conserved dehydration endothermic peak at 112°C and sharp endothermic peak at 146 °C arising from the incorporated TFA, a broad endothermic melting point at 219 °C, and a more pronounced exothermic degradation behaviour at 150 °C (Figure 4.1c). The PC CS-Alg IPC and PC TFA-CS-Alg bioplatform displayed a conserved melting point at approximately 220 and degradation process between 240 and 260 °C (Figure 4.1c). This confirms that the same interpolymer complex had formed and additionally, the sharp endothermic peak at 146 °C confirms the incorporation of TFA into the bioplatform. The incorporation of TFA to the bioplatform decreased the melting point of TFA from 173 °C in its pristine form, to 164 °C when incorporated in CS followed by partially-crosslinking and finally to 146 °C after interpolymer complexation. These findings were correlated with TGA results of the bioplatforms which showed a single step degradation for TFA and PC CS-Alg IPC whist PC TFA-CS and PC TFA-CS-Alg IPC displayed a two-step degradation profile (Figure 4.1d). TFA displayed major (88.24%) degradation from 147 °C to 165 °C whilst PC TFA-CS exhibited two degradation steps with the first one (8.02% weight loss) from 150 to 200 °C and the second one (20%) from 250 to 308 °C. The PC TFA-CS-Alg IPC also displayed a two sequential degradation profile with the first one (15.3% weight loss) from 140 to 178 °C and the second one (20%) from 250 to 320 °C (Figure 4.2d). The first step degradation profile of PC TFA-CS and PC TFA-CS-Alg was representative of the degrading TFA in the bioplatforms. The second step degradation profile of PC TFA-CS was due to the degrading PC CS which correlated with degradation profile range of PC CS previously reported. Similarly to

the degradation profiles observed for PC TFA-CS and PC CS, the second step degradation profile of PC TFA-CS-Alg IPC was at the same degradation range as the one for PC CS-Alg previously reported in chapter 3. Moreover, the degradation profile of PC TFA-CS and PC TFA-CS-Alg were similar.

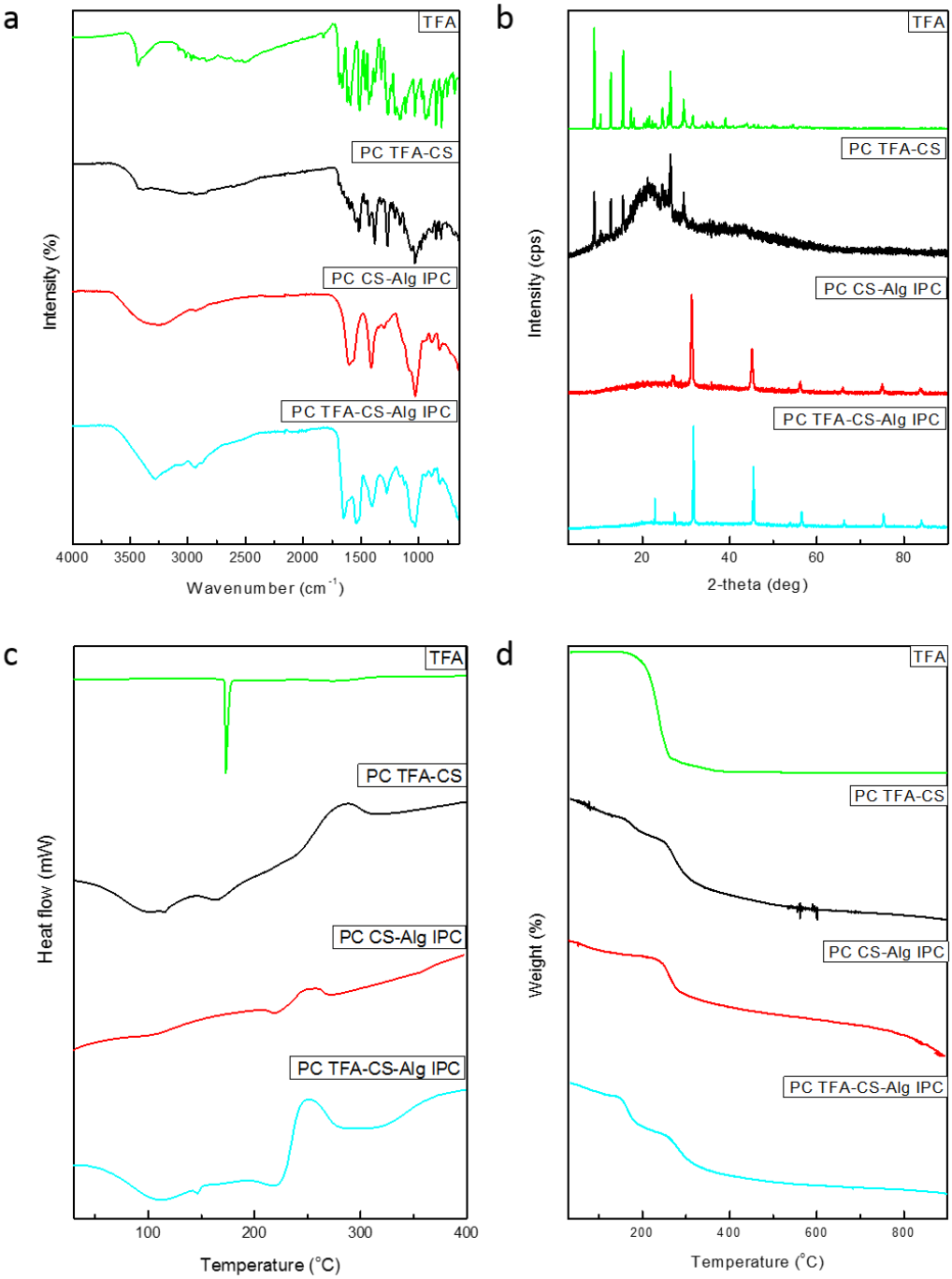


Figure 4.1. The bioplatform's functional groups, chemical composition, and phase changes induced by partial-crosslinking and TFA loading on the polymers were evaluated via the four analytical techniques (a) FTIR spectra, (b) X-Ray diffractograms, (c) DSC and (d) TGA thermograms of the bioplatforms.

4.3.4. Surface morphology, fluid uptake and degradation of bioplatforms

Morphological evaluation of the PC TFA-CS-Alg was undertaken via the use of SEM and it displayed a slightly different morphological appearance to that of PC CS-Alg previously reported (chapter 3) (Mndlovu et al., 2019). The morphological appearance of PC TFA-CS-Alg did not have particles distributed on the surface as observed in PC CS-Alg, instead PC TFA-CS-Alg showed porous curly bundle like structures formed on its surface (Figure 4.2 a). PC TFA-CS-Alg also displayed flat surfaces without particles on the surface whilst other flat surfaces displayed thread like network structures owing to the interaction of chitosan and alginate which was indicative of the network structures. The network structures are indicated by the red arrow (Figure 3a) and they are predominantly visible where there are no curly bundle structures. The occurrence of curly bundles were introduced by loading TFA in CS which suggest that TFA had interacted with CS. In areas where bundle like structures were observed, there was limited to no CS-Alg interactions. In areas where there was no interaction between TFA and CS, there was more favourable CS-Alg interactions hence the network formed in clear surfaces (Figure 4.2a). These interactions may have been due to few factors as mentioned previously, TFA-CS hydrophobic interactions, and also ionic interaction between TFA and CS thus preventing further ionic interaction between CS and Alg in places where CS had already interacted with TFA. The similar morphology between PC TFA-CS-Alg and PC CS-Alg was found to be the presence of a flat surface with curly bundles on some part of the bioplatforms. The difference between two bioplatforms was found to be the interconnected sheet like structures on PC CS-Alg whereas PC TFA-CS-Alg was a bulk single structure with various morphological features. The curly bundles were also observed on the PC CS-Alg with low occurrences compared to PC TFA-CS-Alg. The high occurrences of the curly bundle structures on the surface of PC TFA-CS-Alg were due to the incorporation of TFA which also increased the porosity on those bundle structures. The increased porosity on the bundle structures contributed to the accelerated fluid uptake as seen in Figure 4.2b.

The previous chapter demonstrated the enhanced fluid uptake and physical degradation capabilities of the bioplatforms by employing the partial-crosslinking, freeze-drying and pulverisation approach. In this chapter, the same approach was undertaken with TFA being incorporated to chitosan followed by partial crosslinking and interpolymer complexation. The incorporation of TFA to the IPC reduced the degradation and fluid uptake capacity. The fluid uptake of the bioplatforms (PC CS-Alg and PC TFA-CS-Alg) were both fast. However, the amount of fluid that they could absorb was different between the two bioplatforms, with the PC CS-Alg having higher fluid uptake property compared to PC TFA-CS-Alg. The PC TFA-CS-Alg IPC displayed slow stepwise degradation overtime with a 53.5% degradation in 14 days (Figure 4.2b). This degradation percentage is lower relative to the degradation observed for PC CS-Alg which was 78.2% in 14 days (Mndlovu et al., 2019). Furthermore, the PC TFA-CS-Alg IPC displayed 3102% fluid uptake in 24 hours which was maintained for a total of 48 hours (Figure 4.2b). Given that PC CS-Alg IPC had higher degradation and water uptake capacity, it can be deduced that the crosslinked TFA-CS complexes induced resistance to degradation of the bioplatform.

The PC TFA-CS-Alg bioplatform followed the same hydrolytic degradation as observed for PC CS-Alg in chapter 3. However, a decrease in swelling behaviour was observed at day 3, whereas degradation still increased. This observation showed a slight change in the normal hydrolytic degradation mechanism of the bioplatforms. This could be due to the decomplexation of some parts of of PC TFA-CS-Alg IPC to their respective partial crosslinked forms after reaching maximum fluid absoption. The use of TFA could aslo have contributed to ease of discomplexation/disassociation of the bioplatform due to the reduced ionic moetis available for

formation of IPC from PC TFA-CS and PC Alg. These deductions are in line with the degreased bioplatform degradation observed after incorporation of TFA (PC CS-Alg 78%, PC TFA-CS-Alg 53.5% in day 14). Although the degradation and fluid uptake of PC TFA-CS-Alg IPC was not the highest amongst the tested bioplatforms, it was still higher than those observed in the comparative product when compared at the same time points (swelling of 1612.56% in 24 hours and degradation of 16.26% in 14 days) (Mndlovu et al., 2019). The fast fluid uptake by both bioplatforms was crucial for the *in situ* forming hydrogel and the gelling kinetics were subsequently assessed.

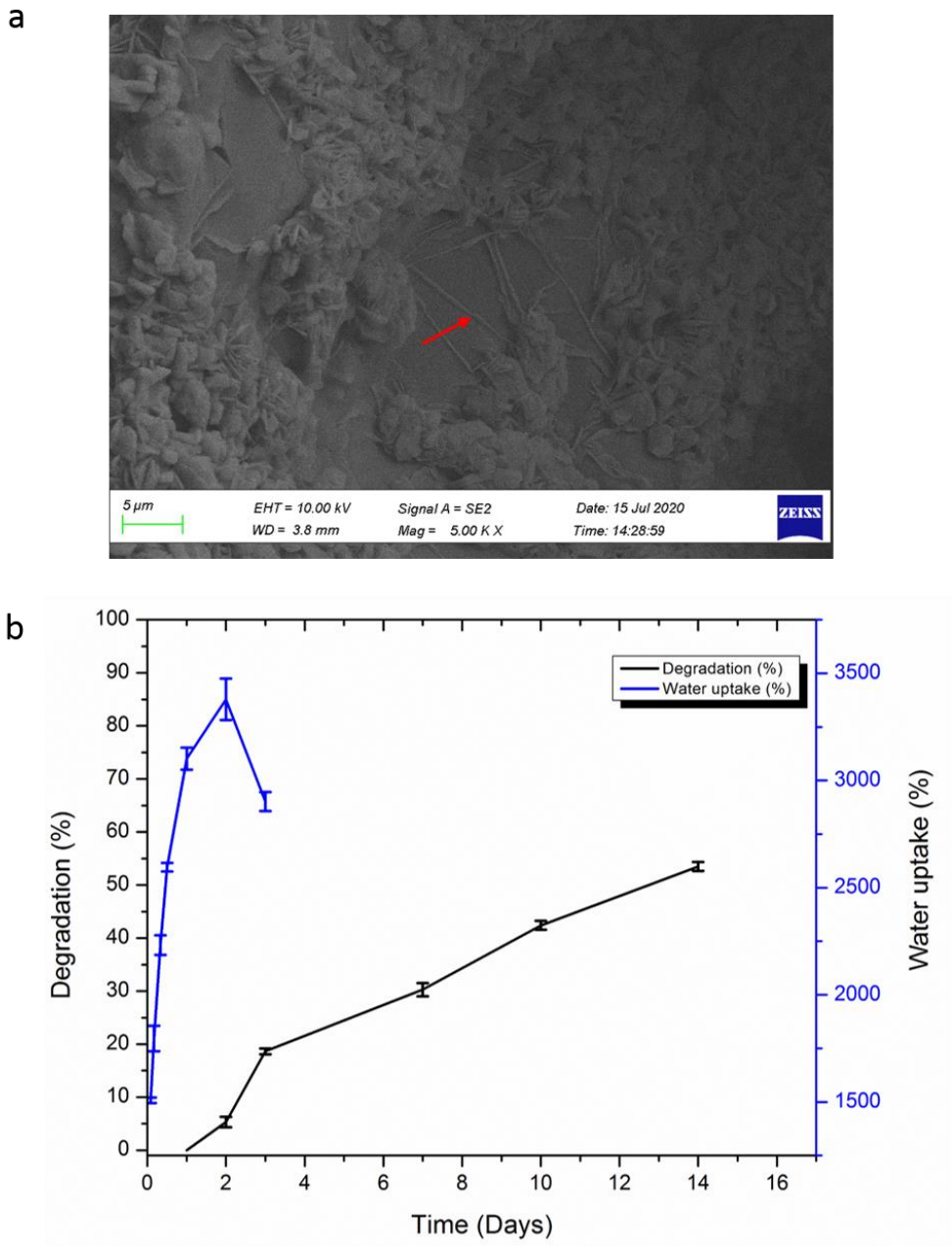


Figure 4.2. (a) Morphological evaluation via SEM and (b) fluid uptake capacity and degradation of PC TFA-CS-Alg IPC. Fluid uptake and degradation evaluation were performed in PBS (pH 7.4) solution at 37 °C at 50 rpm orbital shaker.

4.3.5. Gelling kinetics of PC TFA-CS-Alg interpolymer complex

The ElastoSense^{TM} Bio2 was used to measure gelling kinetics of PC TFA-CS-Alg interpolymer complex. It was evident from Figure 4.3 that *in situ* formation on interpolymer complex hydrogel between PC TFA-CS and PC Alg took place. This was evident from the initial increase of the shear storage modulus, loss modulus and complex modulus as the simulated wound fluid was mixed with the crosslinked, drug loaded, and pulverised bioplatforms. The sample height decreased as the storage modulus, loss modulus, and shear complex modulus was increasing. This was indicative of bioplatform's fluid absorption property over time. The point that there was no lagging phase on the mechanical parameters infer that the fluid absorption was fast. The lagging phase is normally represented by non-changing mechanical parameters (G', G", and G*) over temperature or time associated with no reactivity (sample interactions and environment induced mechanical changes) on tested bioplatforms. In the current study, the lagging phase was not observed owing to the fast fluid uptake and interaction of the bioplatforms *in situ* forming IPC hydrogel which was evaluated in real time.

The loss tangent which gives insights about the viscoelastic properties, displayed gradual increase as time proceeded, but the increase was not significant. This suggested that both viscoelastic properties were present in the hydrogel. However, the hydrogel tend to be more elastic as the interpolymer complex hydrogel formed (Moura et al., 2007). The storage modulus gives insights about the stretch of the hydrogel and it was observed that the storage modulus reached the heights of approximately 635 Pa. This was indicative of a soft hydrogel as it was below 1kPa. The hydrogel was formed instantly after fluid exposure, reached its highest gelling and interpolymer complexation storage modulus in 1h30 minutes, and maintained its interpolymer complexation and gelling rate with slight decrease in storage modulus (Figure 4.3a). The shear complex modulus remained constant at 640 Pa which implies that the gel was still stable and the rate of hydrogel formation was maintained. However, the storage modulus gradually decrease after 1h30 minutes as the loss modulus increases which implies that the hydrogel became more viscous while maintaining high elasticity properties. The increase on the viscosity properties would allow the hydrogel to remain in the wound cavity while absorbing more wound fluid. When comparing the *in situ* formed hydrogel with the one obtained from the previous chapter, the current hydrogel was softer than the one obtained before (Mndlovu et al., 2019). This suggests that the addition of the transferulic acid on the complex improved the hydrogel in terms of possessing skin mimicking mechanical properties.

The previous chapter which explored the partial-crosslinking and interpolymer complexation bioplatforms, indicated that the formed hydrogels were at KPa range except the one at pH 5 which was below 1 kPa. Furthermore, the reported hydrogel presented faster hydrogel formation kinetics (22 minutes) compared to the current hydrogel (1h30 minutes) (Mndlovu et al., 2019). These observations were based on the time taken to reach the highest storage modulus, complex modulus and loss modulus. The decrease on the hydrogel formation rate on the current bioplatform (PC TFA-CS-Alg) might be due to the incorporation of transferulic acid on chitosan thereby elongating the time taken for the NH_3^+ group of chitosan to interact with the COO^- groups of alginate. More assessment on the rigidity of the forming IPC were followed in different PC Alg to PCT TFA-CS ratios and it was observed that the increase on PC TFA-CS ratio resulted in an increase on the rigidity of the complex (Figure 4.3b). The 7:3 PC TFA-CS to PC Alg ratio resulted on the highest rigidity compared to the 9:1 PC TFA-CS: PC Alg ratio (Figure 4.3b). This may be due to the concept that in order for the interpolymer complex to form, the particles required fluid exposure to initiate the *in situ* interpolymer complexation. This was observed on the highly rigid

7:1 ratio whereas in the case of 9:1 the fluid may have been completely absorbed by the particles before exposing the rest of the particles to the fluid thereby limiting rigidity of the forming interpolymer complex. In order to have more controlled rigidity to mimic the mechanical properties of the skin and also take into account highly exudative conditions, the 1:1 ratio was used as the desired ratio. This ratio would be able to absorb high fluid volumes (such as when bleeding occurs) while maintaining its desirable mechanical properties

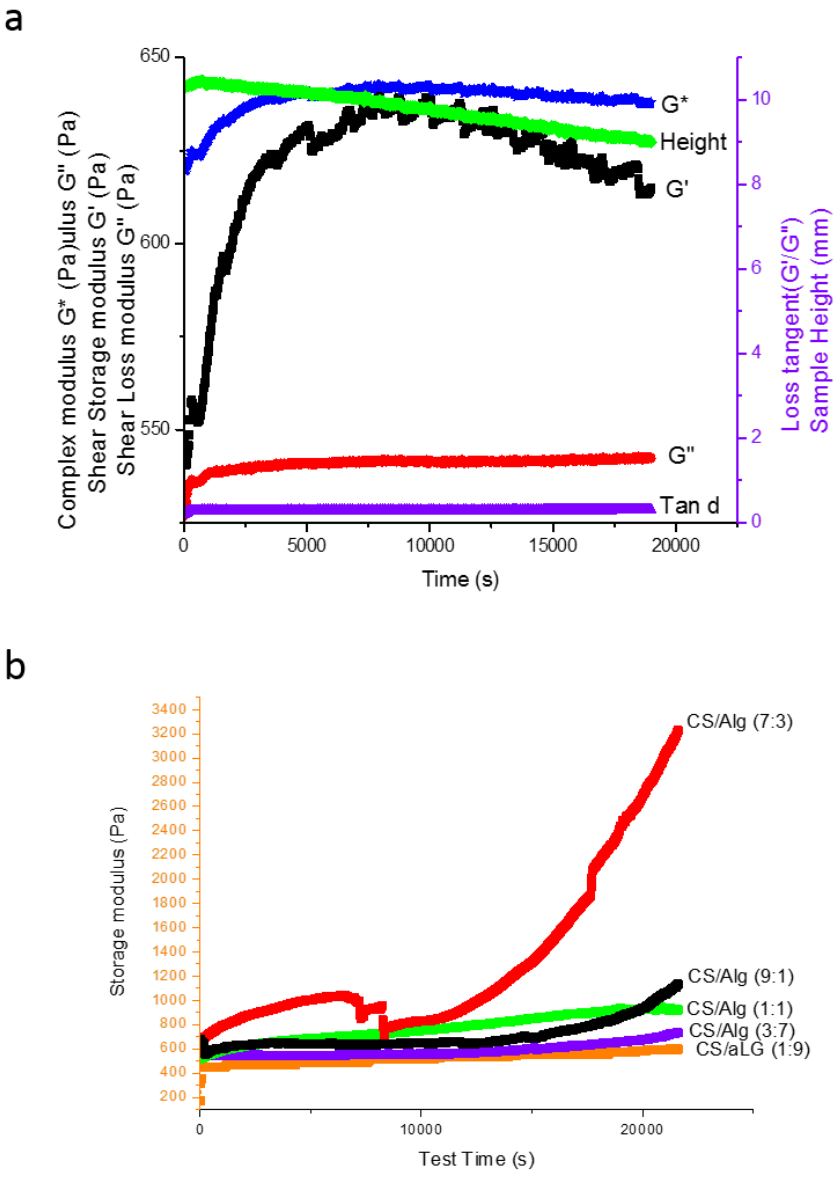


Figure 4.3. The hydrogel formation Kinetics of PC TFA-CS-Alg in simulated wound fluid (pH 7.4) at 25 °C. (a) The interpolymer complex hydrogel was formed *in situ* by mixing PC Alg (50 mg) and PC TFA-CS (50 mg) in 3 mL SWF. The shear storage modulus (gelling and elasticity measurements), shear loss modulus (viscosity), sample height (swelling and absorption functions), shear complex modulus and loss tangent (viscoelastic properties) were measured in real time. (b) Rate of interpolymer complexation in different bioplatform ratios.

4.3.6. *In vitro* drug incorporation, release and cytocompatibility evaluation of the bioplatforms

UV-Vis absorptive properties of bioactives allows for the assessment of bioactive incorporation and release from bioplatforms. The UV-Vis absorption spectra of the pristine polymers, bioplatforms and bioactives are reported in Figure 4.4a. The pristine polymers showed no UV-Vis absorptive properties in the scanned range (200 nm - 500 nm). However, partial crosslinking of alginate confirmed UV-Vis absorption properties such as having two peak maxima at 284 and 305 nm whereas PC CS displayed an increased absorbance without exhibiting definite peak maxima. PC CS-Alg also displayed UV absorption properties with two peak maxima at 283 and 305 which are from the PC Alg due to the same absorption wavelength (Figure 4.4a). TFA displayed absorption at ~230, 286 and 310 nm. The UV absorption of TFA followed in the current study was at 310 nm which correlated with the reported UV-Vis data of ferulic acid and related compounds on having an absorption wavelength (λ_{max}) at 310 nm for ferulic acid, 325 nm for ethyl ferulate (Pan et al., 2002). Studies have also reported bathochromic shift in ethyl ferulate to ferulic acid with ethyl ferulate still appearing under 400 nm (Pan et al., 2002). This suggests that the interaction of ferulic acid with other compounds may result in a change in the absorption wavelength (λ_{max}) of ferulic acid as seen in Figure 4.4a. Chitosan alone displayed no significant absorption bands whilst the incorporation of TFA in chitosan resulted on the bioplatforms (PC TFA-CS and PC TFA-CS-Alg) assuming the TFA absorption properties with (λ_{max}) at 310 nm. The SWF was used as a blank at pH 7.4 and the absorption spectra were observed (Figure 4.4a). The absorption properties of the bioplatforms gives insights on the use of the UV technique to study interactions of polymers and crosslinkers and also to follow degradation profile of the bioplatforms. The current study focused on the use of the UV-Vis technique to study the loading and release of TFA from the PC TFA-CS-Alg IPC bioplatform.

TFA was preferably incorporated into chitosan owing to the ionic interaction between the carboxylic parts of TFA with the amine group of chitosan. The encapsulation efficiency and drug loading studies were done on the TFA-CS-Alg bioplatform from the mixture of PC TFA-CS and PC Alg in SWF. The *in vitro* release studies were done on the PC TFA-CS-Alg interpolymer complex. The encapsulation efficiency was found to be 65.6% ± 2.3% and the drug loading was 9.4% ± 0.51%. The bioactive release studies were done under simulated wound environment (simulated wound fluid at pH 7.4). This study assessed the PC TFA-CS-Alg bioplatform's ability to present controlled TFA release in simulated wound environment conditions. The bioplatform showed a burst release of 58% in 8 hours followed by a sustained release of 1.91% per day up to 67.3% in 3 days (Figure 4.4b). The burst release infer that most parts of the bioactive was weakly bounded to the bioplatform, this led to the displacement of the drug by alginate to further form a stable interpolymer complex. The remaining tightly bound TFA (22.7%) may have been due to the hydrogen bonding between the two compounds and hydrophobic interaction between chitosan hydrophobic chain and TFA. In addition to the above interactions, the drug-to-polymer ratio, drug content, crosslinker type and crosslinking extent could also have contributed to the retained 22.7% TFA in the matrix. The previous chapter demonstrated controlled bioplatform degradation with reference to time (Mndlovu et al., 2019). The bioplatform withheld 22.7% of the drug which could be released as the bioplatform degrades. The encapsulation efficiency and release might seem low however, TFA has been associated with low encapsulation and release. The literature approaches employed in encapsulating TFA reported TFA encapsulation efficiency of 57.5%(Cota-Arriola et al., 2017), encapsulation efficiency of 88.83%, drug loading of 19.9%, coupled with burst release of 20% in 1 hour and total release of about 50% in 48 hours(Bairagi et

al., 2018), and in another independent study a total release of 61% in 1 hour (Trombino et al., 2014) was reported.

The reported studies have encapsulation efficiency that was below 90%, drug loading that was below 25%, and most of the studies reported drug release that was below 65%. The current study presented good encapsulation efficiency, a higher total release and a more controlled sustained release compared to the studies reported above. The TFA kinetic release demonstrated both the first and zero order release profile. The 58% release in 8 hours would contribute to have a physiological effect as an antioxidant, anti-inflammatory, and antimicrobial agent. The sustained release may assist in enhancing chitosan's prolonged antimicrobial properties. Previous studies on TPP crosslinked TFA-CS microparticles with different encapsulation efficiency has already reported that the incorporation of TFA (free and linked) into microparticles particles and nanoparticles significantly enhanced its fungistatic activity on growth, spore germination, and morphology of *A. parasiticus* (Cota-Arriola et al., 2017). The current study evaluated the cytocompatibility of the bioplatforms on NIH 3T3 cell line over a 72 hours period. Given that the burst release was after 8 hours, the effect of TFA would also take place from the given time frame. There was 68.6, 86.9, and 98.5% cell viability on cells treated with PC CS-Alg as previously reported whereas a cell viability of 60, 72, and 91% on cells treated with PC TFA-CS-Alg was observed over a 24, 48, and 72 hours period, respectively (Figure 4.4c).

The cytotoxicity of the bioplatform treated cells were ranked as previous reported by Dahl *et al.,* noncytotoxic >90% cell viability, slightly cytotoxic 60%–90% cell viability, moderately cytotoxic 30%–59% cell viability, and severely cytotoxic <30% cell viability (Dahl et al., 2006). Based on the rankings above, the two bioplatforms moved from slightly toxic (60%–90% cell viability) to nontoxic (>90% cell viability) over the three day period thus emphasizing the cytocompatibility property of the bioplatforms. The slightly lower cell viability of PC TFA-CS-Alg compared to PC CS-Alg may be attributed to the incorporation of TFA on the bioplatform. This was anticipated due to the lower cytocompatibility of TFA evaluated on the study which resulted in the cell viability of 25, 46 and 63% over the 24, 48, and 72 hours period, respectively (Figure 4.4c). The cytotoxicity ranking of TFA highlighted that TFA treated cells moved from severely cytotoxic to slightly toxic. However, the increase on the cell viability over the tested period infer that TFA was not highly toxic and cells were able to survive and proliferate daily. The comparative commercial product presented a similar cell viability trend as to that of TFA, with comparative product having a slightly better cell viability on the first 24 hours period. The Bioplatforms tested on the study presented more favourable environment for optimal cell growth as they all had higher cell viability compared to comparative product over the 72 hours period. The increase on the cell viability on cells treated with the bioplatform was indicative of their cytocompatible nature.

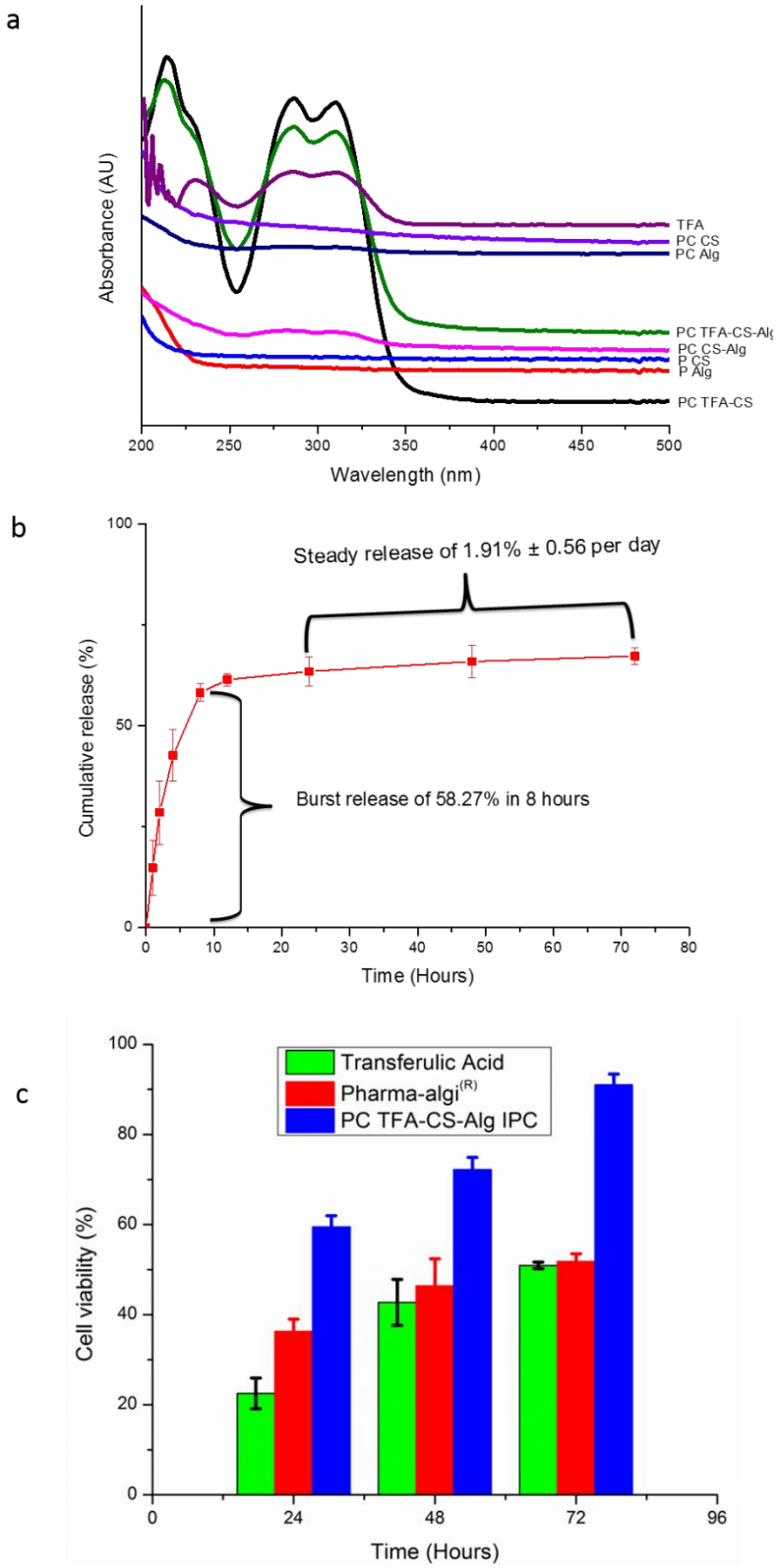


Figure 4.4**.** (a) UV-vis absorption spectra of bioplatforms, (b) Trans-Ferulic acid release from the PC FA-CS-Alg interpolymer complex in SWF (37 °C, pH 7.4) and (C) cell viability assessment of bioplatforms employing MTT assay.

4.3.7. Evaluation of *In vivo* wound healing performance of bioplatforms

Wound healing follows an extensive tissue remodelling and regenerative process necessitating wound closure. Wound closure would be used as the measure and physical sign of wound healing. Figure 4.5 shows the extent of wound closure on lesions in rat model treated with different bioplatforms. The wounds treated with the same bioplatforms displayed different wound closure percentages and appearance at the same wound healing time points. Thus, the mode appearance of lesions were used in the Figure to describe the overall wound appearance. An average wound closure percentage of each bioplatform at certain time point was used to get an average wound closure percentage of the wounds. PC TFA-CS-Alg exhibited accelerated early stage wound healing performance with more than 30% wound closure after the wounds were allowed for 3 days wound healing. The high wound closure percentage of PC TFA-CS-Alg at this early stage of wound healing may have resulted from the use of TFA which brought about the antioxidant, anti-inflammatory and contributed to enhanced tissue remodelling performances of the bioplatform. PC Alg-CS showed the second highest wound closure rate followed by the commercial product at the same 3 days wound healing period. The wound closure appearance of PC Alg-CS was similar to the wounds treated with PC TFA-CS-Alg. However, the wound closure percentage of PC CS-Alg was close to that of the comparative product treated lesions. The control group displayed the least wound closure percentage with less than 10% wound closure at day 3. Furthermore, the control lesions appeared fresh compared to the test groups. This attests to the superior wound healing attributes of the particulate bioplatforms.

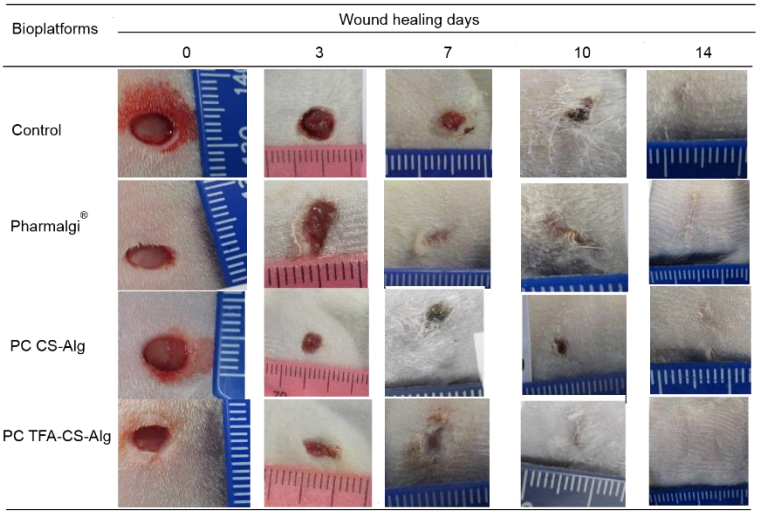
All treatment groups displayed more than 70% wound closure by day 7, with the PC TFA-CS-Alg bioplatform having the highest wound closure percentage of 90.45% followed by comparative product (86.62%), PC CS-Alg (85.65%) and lastly the control with 57.7%. PC CS-Alg bioplatform and comparative product displayed similar wound closure percentages over the healing course with comparative product displaying a slight edge over PC CS-Alg. All the treatment groups displayed 100% wound closure whilst the control displayed 98% wound closure after the wounds were allowed to heal for 14 days. Although the wound closure was 100% on the treatment groups, the quality of the healed wounds were different. After 14 days wound healing, there was no scar tissue or sign of lesion on the site where the wound was created on the animals treated with the PC TFA-CS-Alg bioplatform. A bruise like appearance was observed on the wounds treated with PC CS-Alg bioplatforms. This appearance was also present on the untreated group. Furthermore, the untreated group also showed scar tissues similar to those observed on the lesions treated with comparative product. The difference on the skin appearance and the absent of scar tissues infer that the wounds treated with PC TFA-CS-TA bioplatform were superior compared to other groups. The difference on the wound appearance was one of the signs of high-quality wound healing performance of the partially crosslinked bioplatforms. The wound remodelling at the epidermis and dermis were further investigated to evaluate the extent and quality of wound healing via histological assessment.

Automated Haematoxylin and Eosin (H&E) tissue staining was employed in skin tissues. This was followed by qualitatively grading lesions on the following five features; (1) Epithelisation which investigated the degree of epithelium covering the original defect in the skin/epidermis (Pastar et al., 2014). (2) Epidermal-dermal attachment which evaluates the epidermal layer advancing along the ulcer/defect surface that is/not adhered/tightly attached to the underlying fibroblastic reaction in the dermis, and this attachment was qualitatively scored (Nishiyama et al., 2000). (3) Angiogenesis assesses the variable capillaries associated with the dermal and/or subcutaneous fibroblastic reaction (Velnar and Gradisnik, 2018). The variability assessment of these capillaries

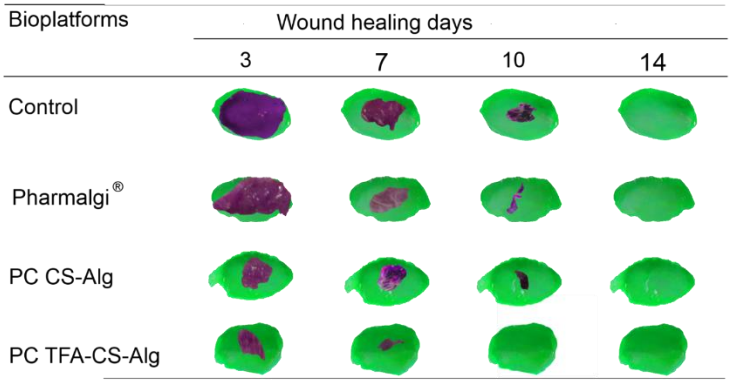
includes clearly arranged pattern typical for granulation tissue (vertical capillaries perpendicular to the skin surface and fibroblasts) mostly in the dermis. In the deeper subcutaneous reaction, they are more haphazardly arranged in the similarly haphazard fibroblastic reaction. They are more prominent in early lesions (Figure 4.6 and 4.7) and become less numerous in more advanced lesions (Figure 4.7-4.9). (4) Mononuclear leukocytes which is an infiltrate that is not associated with acute exudative inflammation. The inflammation could remain mild in some samples while becoming moderate in areas with endogenous or exogenous foreign material. In the current study, inflammation consisted of varying degrees of mononuclear cells that included lymphocytes, few plasma cells, macrophages, some of which were epithelioid, and multinucleate giant cells. (5) Fibroblasts reaction is very important in wound healing as it fills the defect and causes contraction, with the end result being complete apposition of the peripheral intact edges of the skin. Fibrosis may involve all layers of the affected skin and may be associated with inflammation or angiogenesis. It may appear as horizontal fibrosis between the edges of the defect in more mature lesions, or haphazard arrangement in less mature lesions. It may appear as granulation tissue when typical accompanying neovascularisation is evident, often beneath areas of ulceration in the dermis. Collagen fibres are associated with the fibroblasts in variable amounts.

The current study used the scoring of the fibroblastic reaction which was correlated with the percentage of fibroplasia within the lesion, regardless of the size of the lesion. Therefore, very small remaining lesions may show almost complete apposition of the peripheral edges, but still predominant presence of fibroblasts in the lesions. The macroscopical size/measurement of the lesion would thus differentiate it from larger lesions also with prominent/predominant fibroblastic cell presence. Detailed assessments of the above features were done on each of the test groups and compared to the comparative product and the control groups. A normal skin sample at day zero showed that the epidermis, dermis and adnexa, and subcutis appeared normal. The underlying muscle layer was intact with a single area showing presence of large blood vessels penetrating the muscle layer. The features mentioned above were evaluated after each of the wound healing days 3, 7, 10, and 14. Since the bioplatforms displayed different would healing performances on the lesions, the mode characteristics of the wound morphology was used to describe and assess the overall performance of each bioplatform on the lesions in terms of the five features mention above.

a



b



c

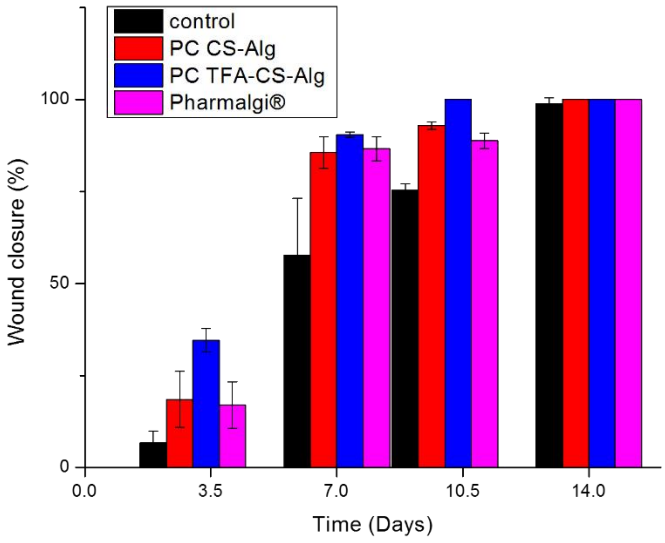


Figure 4.5. *In vivo* representation of the wound healing capabilities of the bioplatforms and commercial comparative product. (a) Wound closure images of SD rats treated with the bioplatforms and allowed to heal over a 14 day period. (b) A graphical representation of wound closure kinetics of rats treated with bioplatforms. The wound healing rate was calculated by employing the following equation: wound closure

(%) = $((A_0 - A_t)/A_0) \times 100$, where A_0 represents the area of the original wound and A_t represents the area of the wound at the testing time (days). The diameter and area of the lesions were calculated using the IMAGEJ software.

Effect of respective bioplatforms on the lesions after the wounds were allowed to heal for 3 days

The control lesion showed surface ulceration with adjacent moderate hyperplasia of the epidermis on the ulcer edge and early cell migration onto the ulcer although unattached to the underlying tissues. There was loss of the dermal tissues due to similar necrosis in the subcutis and focally in the underlying defect in the superficial muscle layer. Moderately cellular fibroblastic infiltrates were visible and they appeared haphazardly arranged and accompanied by small numbers of capillaries (Figure 4.6a). Deep dermal granulation tissue was present with prominent vertically arranged capillaries. Small amount of collagen was also observed in the deeper haphazard fibroblastic region. There was moderate haemorrhage on the ulcerated surface in areas accompanied by moderate numbers of epitheloid macrophages and multinucleate giant cells in the ulcer bed. Only a slit-like linear separation was visible in the middle of the underlying muscle tissue but not clearly a defect filled with fibrosis or inflammation. The features observed above were similar to those observed on the comparative product treated lesions. However, the commercial product treated lesions exhibited slightly better wound healing features compared to the control group. These lesions displayed focally-extensive full thickness epidermal ulceration with mild neutrophilic presence on the ulcerated surface (Figure 4.6b). The wound edges showed moderate epidermal hyperplasia. The remainder of the dermis and subcutis underlying the ulcer revealed moderately cellular haphazard fibrosis accompanied by mild capillary proliferation. Peripherally mild collagen presence was also visible. Inflammation was mild and interstitial, although more prominent on the edges of the fibroblastic reaction. It consisted of a mixture of macrophages lymphocytes and scattered mast cells. Fibrosis extended to the muscle edges and filled the defect within the muscle with few remaining muscle fibres embedded in the fibroblastic reaction and in those areas capillaries were more prominent. The mild collagen deposition on comparative product treated wound infer that the healing rate was comparable to PC CS-Alg but slightly lower compared to PC TFA-CS-Alg at this stage of wound healing.

The lesion treated with PC Alg-CS displayed severe presence of degenerate neutrophils few loose red blood cells and fibrinous material on the necrotic surface (Figure 4.6c). The globular eosinophilic material was much more prominent and multifocally numerous with surrounding marked inflammation mostly of neutrophilic and histiocytic appearance. Lightly eosinophilic to slightly basophilic serum like material was also present and occasionally form aggregates surrounded by neutrophils. Capillaries were quite prominent in the subcutis while the dermis showed extensive necrosis with accompanying acute neutrophilic inflammation rather than reactive fibrosis at this stage. Some of the eosinophilic globular structures also extended into the deep subcutis beyond the damaged muscle layer. The lesions treated with PC TFA-CS-Alg displayed a slightly advanced wound healing morphology at this stage compared to the one treated with PC CS-Alg. PC TFA-CS-Alg lesions displayed a surface ulceration with marked haemorrhage and fibrin deposition in the ulcer bed. On the periphery of the ulcer the epidermis was moderately hyperplastic and with early advancing of a thin layer of few thick keratinocytes that extended along the ulcer bed but it was unattached to it (Figure 4.6d). The dermis and subcutis consisted of a moderately cellular and fairly haphazardly arranged fibroblastic reaction accompanied by small numbers of vertically arranged capillaries perpendicular to the ulcerated surface (Figure 4.6d). Small to moderate numbers of lymphocytes and macrophages were visible especially on the edges of the fibroblastic reaction, accompanied by single neutrophils and small

amounts of collagen. The fibroblastic reaction also invaded the underlying muscle fibres superficially, but a defect was not clearly visible in the superficial muscle layer.

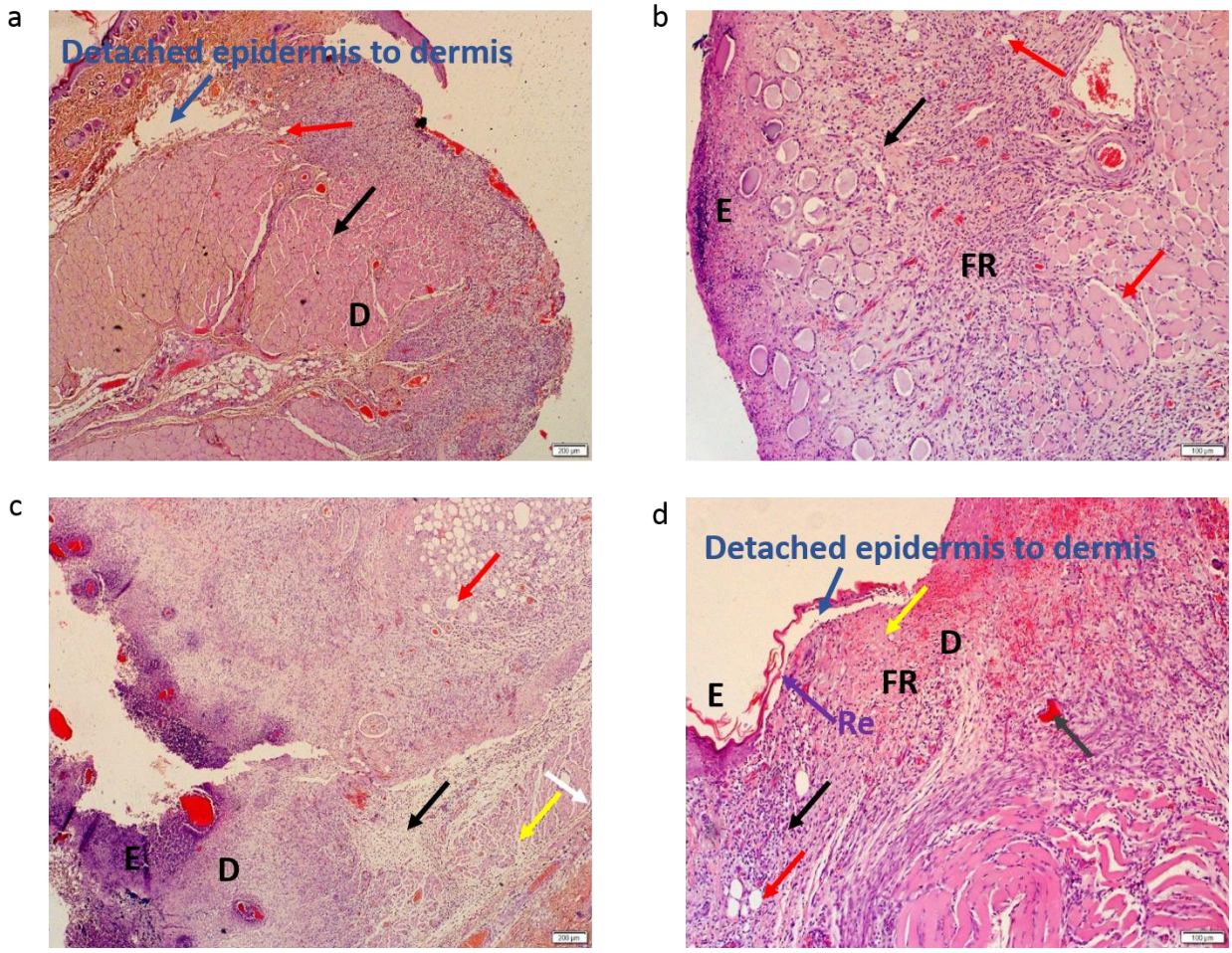


Figure 4.6. Early wound healing stage of tissues treated with different groups of bioplatforms. Histology of the wound tissues (a) Control group, (b) comparative product treated group, (c) is the PC Alg-CS treated group, and (d) is the PC TFA-CS-Alg treated group. The images of the control group and PC CS-Alg group were viewed at 200X magnification whereas the comparative product and PC TFA-CS-Alg groups were viewed at 100X magnification. E denotes epidermis development and D represent the dermis layer. FR denotes fibroblast reaction with collagen bundles labelled in yellow arrow, the grey arrow indicates the red blood cells materials and the purple arrow shows the regenerating edge. The plasma inflammatory cells are indicated by the black arrow, while the blood vessels are indicated by the red arrow.

Effect of respective bioplatforms on the lesions after the wounds were allowed to heal for 7 days.

The lesions at the early-to-mid phase of wound healing exhibited slightly advanced wound healing morphologies compared to the early phase of wound healing. The control lesions displayed re-epithelialisation of just less than 50% of the wound, and the epithelial layers appeared moderately hyperplastic (Figure 4.7a). The advancing edge of the epithelialisation was focally unattached to the underlying granulation tissue. The dermis contained a marked granulation tissue reaction with horizontally arranged fibroblasts parallel to the ulcerated surface in the dermis and they became more haphazard in the subcutis and slightly linear in the underlying muscle layer where they extended vertically between the damaged muscle edges that also had haphazardly arranged

fibroblasts associated with them (Figure 4.7a). Few loose hair shafts were also present in this reaction on the edges of the muscle. The granulation tissue had small amounts of collagen and it became more prominent in the subcutis in between the haphazardly arranged fibroblasts. There was also mild inflammation and mononuclear which consisted of lymphocytes and macrophages. The presence of granulation tissue and inflammation on the control infer that the lesions were still at early stage of wound healing. The wounds treated with the comparative product displayed a visible central ulceration but the surrounding re-epithelialisation from the edges was covered approximately 50% of the lesions (Figure 4.7b). Re-epithelialisation consisted of mildly hyperplastic epidermis and it was focally not attached to the underlying granulation tissue on the leading edge of the reepithelialisation. The dermis showed granulation tissue consisting of moderate numbers of capillaries and horizontally arranged fibroblasts accompanied by moderate amounts of collagen (Figure 4.6b). Scattered single lymphocytes and macrophages were visible in the granulation tissue. In the subcutis and in between the retracted muscle edges the fibroblasts were more haphazardly arranged and accompanied by small numbers of capillaries. They extended into the deeper subcutis and involved the muscle edges. Mild presence of perivascular lymphocytes macrophages and mast cells were visible in the subcutis. Areas showed moderate collagen presence in association with the fibroblasts which inferred that the lesions where at slightly better stage of healing compared to the control group.

The wound treated with PC Alg-CS showed complete covering epidermis which was moderately hyperplastic and attached (Figure 4.7c). The underlying dermis and subcutis contained a fibroblastic reaction which in the dermis had the appearance of granulation tissue and in the superficial, deep subcutis and in between the damaged muscle edges appeared more haphazardly arranged. The granulation tissue consisted of horizontally arranged fibroblasts parallel to the surface accompanied by moderate numbers of vertically arranged capillaries an interspersed by moderate amount of collagen. There was a mild to moderate inflammatory reaction visible in the fibroblastic reaction, consisting of lymphocytes histiocytic cells and multinucleate giant cells, and especially the latter multinucleate giant cells multifocally surround small aggregates of highly eosinophilic globular material (Figure 4.7c). The wounds treated with PC TFA-CS-Alg exhibited appearance similar morphology to that treated with PC CS-Alg, although the globular eosinophilic material was much less prominent and had small globules still surrounded by moderate amounts of granulomatous inflammation. The haphazardly arranged fibroblastic reaction in the subcutis was evident in both superficial and deep to the muscle layer and also infiltrated the muscle layer but a muscle defect was not clearly visible (Figure 4.7d). The hair follicle was starting to show in both PC TFA-CS-ALG and PC CS-Alg treated wound tissues whereas they were not clearly visible on comparative product treated tissues and the untreated group.

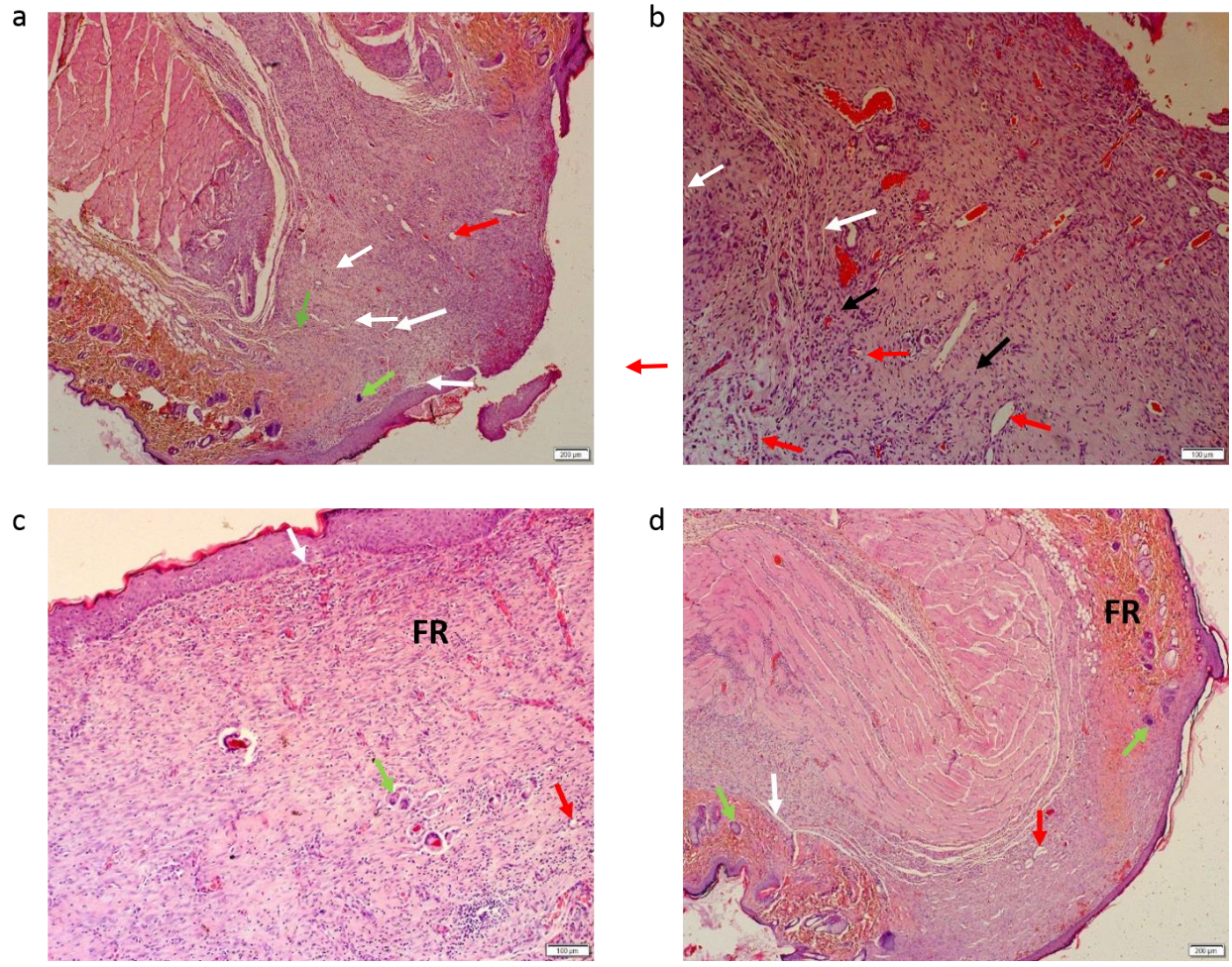


Figure 4.7. Mid wound healing stage of tissues treated with different groups of bioplatforms. Histology of the wound tissues (a) Control group, (b) comparative product treated group, (c) PC Alg-CS treated group, and (d) PC TFA-CS-Alg treated group. The images of the control group and PC TFA-CS-Alg treated group were viewed at 200X magnification whereas the comparative product and PC CS-Alg treated groups were viewed at 100X magnification. FR denotes fibroblast reaction. The plasma inflammatory cells are indicated by the black arrow, while the blood vessels are indicated by the red arrow. The green arrow show hair follicles, white arrow shows capillaries.

Effect of bioplatforms on the lesions after the wounds were allowed to heal for 10 days

The control lesions displayed a focal ulceration associated with serocellular crusting in the ulcer bed. Peripheral mild epithelialisation was taking place and the epidermis was mildly hyperplastic. A small central area of attached epithelialisation was also visible. In the underlying dermis horizontal to haphazard fibrosis was present accompanied by haphazard fibroplasia extending into the subcutis (Figure 4.8a). There was mild capillary presence especially underlying the area of ulceration. Minimal lymphocytes plasma cells and macrophages were present in the subcutaneous fibroblastic reaction. The epithelialization and slight epidermal-dermal attachment were superior on the control group compared to the commercial comparative product. However, fibroblast reaction was slightly higher on comparative product treated group. The comparative commercial product treated lesion showed presence of epithelialisation extending from the margins of the defect and covering less than 50% of the ulcerative surface. The hyperplastic

epidermis extending along the ulcer was mostly attached to the underlying fibrotic reaction in the dermis with only a small area of the advancing edge that was unattached. The dermal fibrosis was horizontal parallel to the ulcerated surface and associated with mild capillary proliferation (Figure 8b). In the deeper region of the reaction the fibrosis was haphazardly arranged and extends into the subcutis and up to the muscle layer. The haphazard fibroblastic reaction was accompanied by dilated citatory areas filled with fibrillar basophilic material and surrounded by flattened histiocytic cells. The stroma in this deep reaction contained a mild lymphoplasmacytic and histiocytic inflammatory reaction with few multinucleate giant cells present. Surrounding hair follicle structures multifocally appear mildly dilated with hyperplastic follicular infundibular walls.

The two test groups displayed superior wound healing capabilities compared to the control and the comparative product treated groups with PC CS-Alg being relatively better than the PC TFA-CS-Alg groups. PC CS-Alg displayed complete re-epithelialisation covering the surface and the mildly hyperplastic epidermis was attached to the underlying dermis throughout. Underlying horizontal fibrosis was present in the dermis and extended into the subcutis where it was slightly more haphazardly arranged (Figure 4.8c). Few inflammatory cells were present and consisted of lymphocytes plasma cells and macrophages as well as few multinucleate giant cells within the fibroblastic reaction and sometimes surrounding loose keratin and highly eosinophilic material (foreign body reaction). The fibroblastic reaction was accompanied by minimal capillary presence as seen in Figure 4.8c. Few adjacent hair follicles are enlarged and almost cystic. PC TFA-CS-Alg on the other hand displayed an ulcerative lesion that was partially covered by epithelium extending from the edges of the wound. The epidermal layers were mildly hyperplastic and partially attached to the underlying dermal reaction. The exposed ulcerative area consisted of mild serocellular crusting. In the underlying dermis horizontal fibrosis was present covering the lesion/defect and it was accompanied by moderate numbers of congested capillaries proliferating in the fibroblastic reaction beneath the ulcer (Figure 4.8d). The fibrosis also extended deeper into the subcutis with a more haphazard appearance. Lymphocytes plasma cells and macrophages were present in small numbers and in other areas become moderate in number but only in the subcutaneous stromal reaction. Several multinucleate giant cells and epitheloid macrophages surrounded areas with highly eosinophilic homogenous central material. The haphazard fibroblastic reaction also mildly extended into the underlying muscle bundles and adjacent subcutis

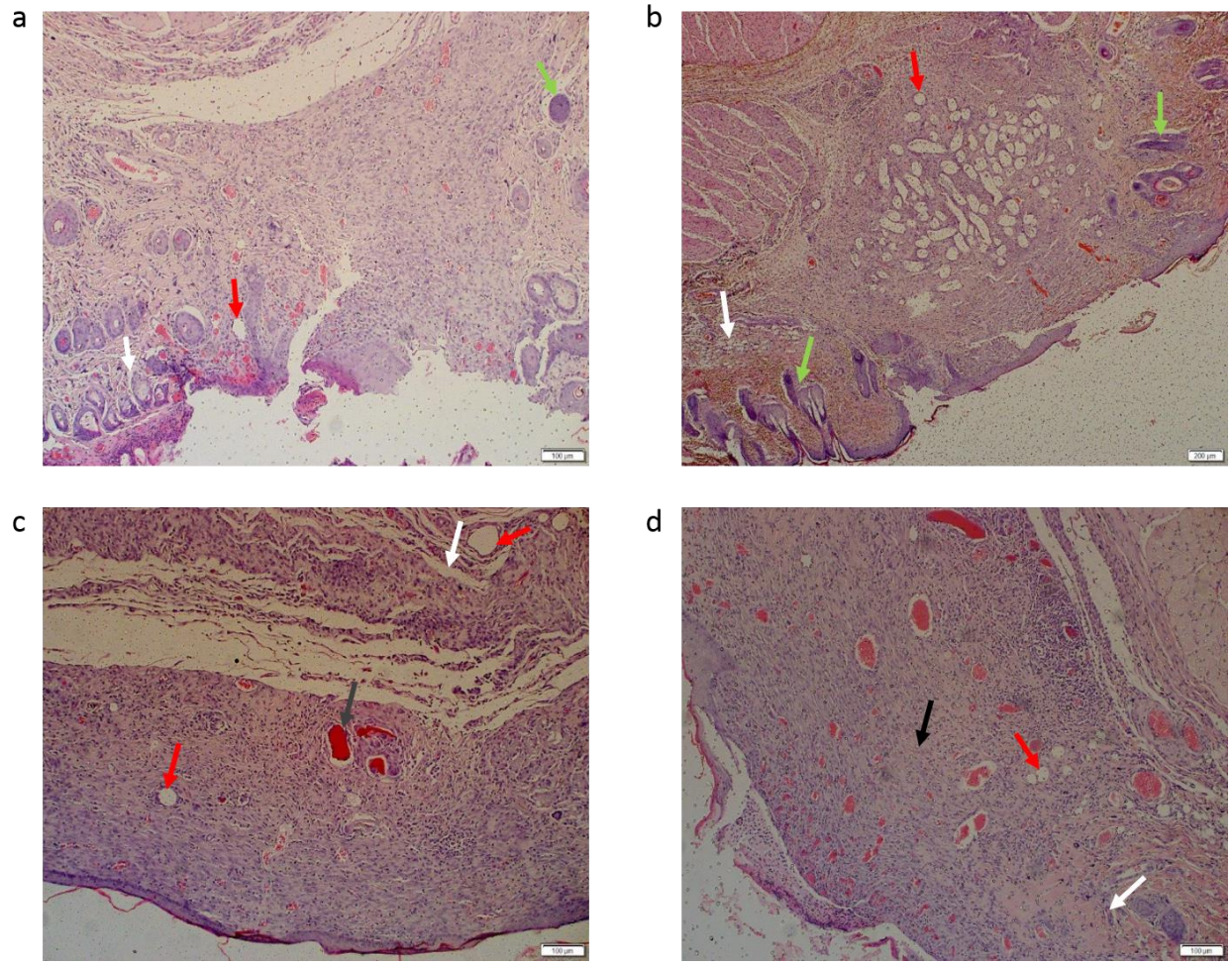


Figure 4.8. Mid-to-late wound healing stage of tissues treated with different groups of bioplatforms. Histology of the wound tissues (a) Control group, (b) comparative product treated group, (c) PC Alg-CS treated group, and (d) PC TFA-CS-Alg treated group viewed at 100X magnification except for comparative product treated tissues which were viewed at 200X magnification. The grey arrow indicates the red blood cells materials. The plasma inflammatory cells are indicated by the black arrow, while the blood vessels are indicated by the red arrow. The green arrow show hair follicles, white arrow shows capillaries.

Effect of respective bioplatforms on the lesions after the wounds were allowed to heal for 14 days

The control group exhibited horizontal fibroblastic reaction in the dermis causing mild thinning of the dermal layer and it extended up to the intact mildly hyperplastic epidermis overlying the wound. Inflammation was more haphazard in the subcutis (Figure 4.9a). The whole fibroblastic reaction consisted of moderate interstitial presence of lymphocytes and macrophages and several epitheloid macrophages along with multinucleate giant cells. The comparative product treated lesions exhibited intact epidermis indicative of complete re-epithelialisation and it appeared to be mildly to moderately hyperplastic (Figure 4.9b). In the underlying dermis haphazard fibrosis was still present and the dermis was resultantly thinner than normal. Few peripheral follicular structures were caught up in the fibroblastic reaction (Figure 4.9b). In the underlying subcutis the fibroblasts were admixed with macrophages and few multinucleate giant cells and they encircled central small cystic areas containing basophilic material, some of which was calcified. Only few capillaries were present in the dermal fibroblastic reaction.

PC CS-Alg bioplatform treated lesions displayed completely covered epidermis with minimal hyperplastic and the underlying dermis contains few haphazardly arranged fibroblasts, but normal pilosebaceous units in a regular pattern (Figure 4.9c). The subcutis appeared normal. PC CS-Alg-TFA also displayed completely covered epidermis with mild hyperplastic and in the underlying dermis a focal area of horizontal fibrosis becoming slightly haphazard in the deep dermis was observed (Figure 4.9d). There were few capillaries present in the horizontal dermal fibroblastic reaction. In the subcutis the fibroblastic cells were also haphazardly arranged and accompanied by moderate numbers of lymphoplasmacytic cells, epitheloid macrophages and few multinucleate giant cells. The reaction surrounded multifocal areas of mildly eosinophilic homogenous material that accumulated within the reaction. Moderate inflammation was also present in the dermis and subcutis.

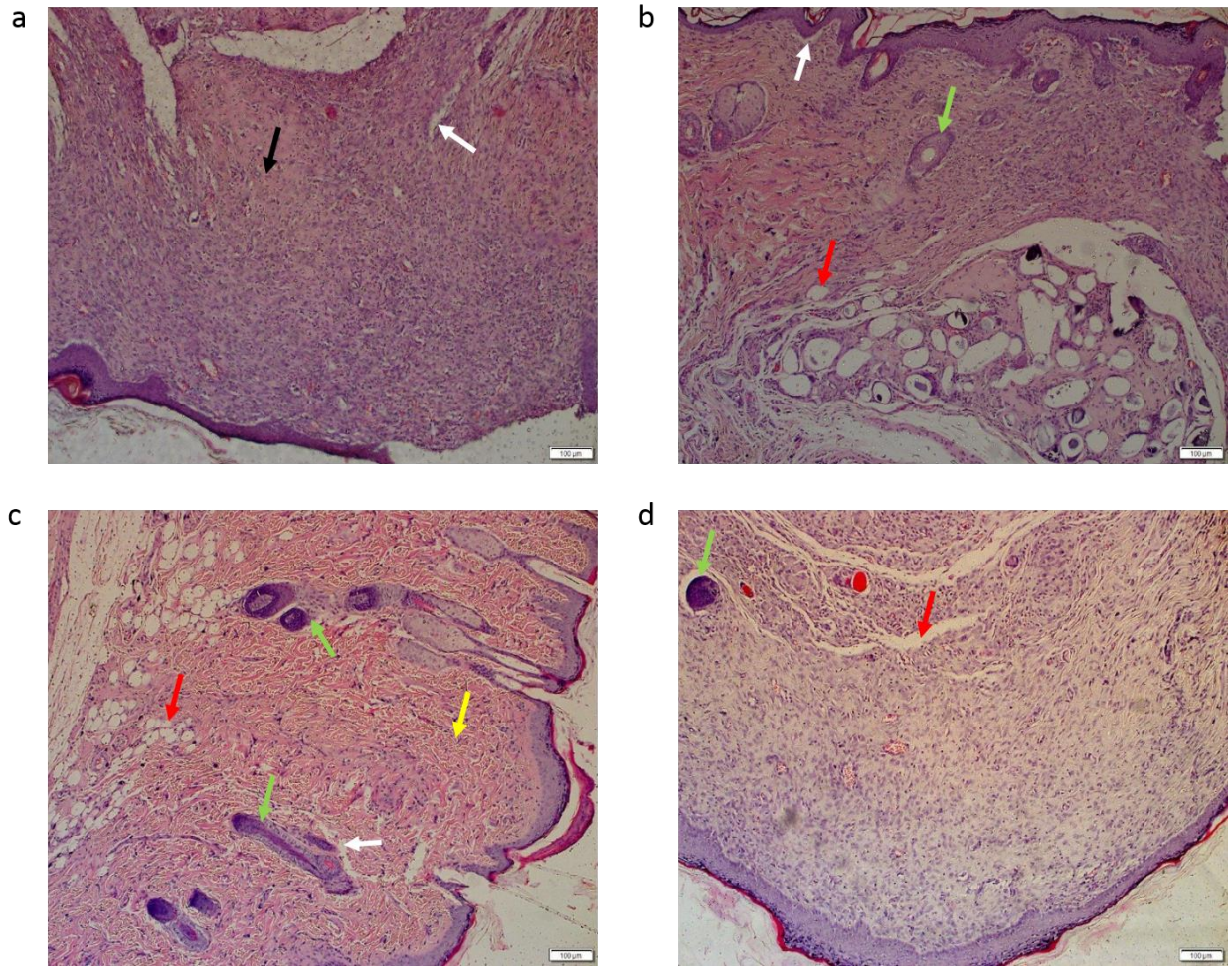


Figure 4.9. Late wound healing stage of tissues treated with different groups of bioplatforms. Histology of the wound tissues (a) Control group, (b) comparative product group, (c) PC Alg-CS treated group, and (d) PC TFA-CS-Alg treated group viewed at 100X magnification. Collagen bundles are labelled in yellow arrow. The plasma inflammatory cells are indicated by the black arrow, while the blood vessels are indicated by the red arrow.

The wounds assessed for tissue regeneration at each stage of wound healing provided insights on the wound healing capabilities of the bioplatforms. At the early stage of wound healing all groups lacked epidermal-dermal attachment. The differences amongst the groups was the

collagen deposition which was highest in both PC CS-Alg and PC TFA-CS-Alg followed by the comparative product and the lowest was observed in the control group. The presence of the fibroblastic reaction infer that there was tissue regeneration and the extent of tissue regeneration was highest in both partial crosslinked bioplatforms (McDougall et al., 2006). The control group displayed further damage at the dermal area whereas the test groups displayed fibroblast reaction taking place at the dermal subcutis. Inflammatory cells were observed on the test groups while it was not visible on the control groups which was a sigh that the lesions were exposed to foreign body (Coleman et al., 1974).

The early-to-mid stages of wound healing also displayed consistent would healing performances of the bioplatforms. The tests groups showed epidermal-dermal attachment whereas the comparative product and control groups displayed unattached epidermal-dermal morphology. The lack of epidermal-attachment on the control and the comparative product was indicative of inadequate wound healing performances compared to the test groups (Nishiyama et al., 2000). The control group was last on the wound healing capabilities at this stage of wound healing with less than 50% wound re-epithelialisation followed by the comparative product groups whereas re-epithelialisation was significant in both test groups PC CS-Alg and PC TFA-CS-Alg. The overall wound healing performance of both test groups was superior to the comparative product and control groups with PC TFA-CS-Alg exhibiting relatively better results than PC CS-Alg at this wound healing stage.

The mid-to-late phase of wound healing were also observed and assed as indicated above. The PC CS-Alg did not show any crusting and also displayed fewer inflammatory cells compared to the control. Serocellular crusting was observed in both PC TFA-CS-Alg and the control group with the control group showing more crusting than PC TFA-CS-Alg. The particulate bioplatforms displayed more covered ulcerated area compared to both the comparative product and the control. At this wound healing stage, the PC CS-Alg bioplatform displayed more favourable wound healing performance compared to PC TFA-CS-Alg, comparative product and the control. The slight wound healing edge of PC CS-Alg at this stage of wound healing may be due to the point that the bioactive (transferulic acid) had already played its part at the early stages of wound healing and the only contribution to wound healing at this stage was solely on the interaction of the regenerating tissues with polymeric bioplatforms.

The late stage of wound healing exhibited advanced wound healing. All groups displayed similar wound healing performances at this stage of wound healing. The only differences was the quality of healed tissues which exhibited normal skin morphology on both test groups whereas the comparative displayed caught up hair follicles and the control group still indicated horizontal fibroblastic reaction in the dermis causing mild thinning of the dermal layer. The presence of thinner dermis in both the control and the comparative group was evident of inadequate tissue remodelling performance highlighted by thinner collagen fibres characteristic of scar formation in both groups (Dale et al., 1996). Furthermore the control group still indicated Inflammation which was indicative of slower wound healing performance relative to the other groups. This is supportive of the superiority of the test groups in producing normal skin tissues compared to control and comparative groups.

4.4. Concluding remarks

The partial crosslinking approach allowed for transferulic acid incorporation into chitosan while maintaining high charge potential for further ionic interaction with partial-crosslinked alginate. This

approach gives insights on how polymer processing can be explored to fabricate bioactive loaded interpolymer complexes. The transferulic acid incorporation in chitosan and the interpolymer complex was confirmed by both FTIR, XRD, and Zeta potential. Cytocompatible, biocompatible and increased patient compliable wound dressings are promising directions in developing bioplatforms with enhanced wound healing capabilities. The encapsulation efficiency was found to be 65.6%, drug loading of 9.4%, burst release of 58.27% in 8 hours and a steady release of 1.91% per day. The encapsulation efficiency of TFA was higher than other encapsulation efficiency reported in literature noting the reported difficulties of optimizing encapsulation, *in vitro* release, and bioavailability of TFA. The *in situ* forming hydrogel presented both viscoelastic properties which allowed the bioplatforms to absorb wound fluid and remain in the wound cavity while maintaining optimal flexibility. The hydrogel increased viscosity (G") while presenting mechanical properties characteristic of a soft hydrogel (G' below 1 kPa). The porous character of the hydrogel as observed by SEM, allowed for fluid absorption of 3102% in 24 hours and stepwise degradation up to 53.5% in 14 days. The bioplatforms were also cytocompatible and cells proliferated in the presence of the bioplatform. Furthermore, it was observed that partial-crosslinking along with drug loading drastically improved the cytocompatibility of the bioplatform. The wound closure assessment indicated accelerated wound closure on lesions treated with PC TFA-CS-Alg and a comparable performance between PC CS-Alg and comparative product with the control (gauze) presenting the slowest wound closure capabilities. The histological evaluations of the lesions indicated better wound healing performances in lesions treated PC TFA-CS-Alg and PC CS-Alg compared to those treated with the commercial product comparative product and the control. The accelerated wound healing performance of the bioplatforms were more pronounced at the early stages (day 3) of wound healing with PC TFA-CS-Alg treated lesions exhibiting a slightly advanced wound healing morphology compared to those treated with PC CS-Alg. The lesions treated with the two bioplatforms presented normal skin tissue morphology compared to the comparative product and the contro at the later stages of wound healing. The application of the particulate bioplatform on the wound via sprinkles, the *in situ* hydrogel formation with exudate/fluid absorption properties and accelerated wound healing performance of the bioplatforms makes it a desirable candidate for use as a drug delivery system and in skin tissue regeneration.

4.5. References

Aderibigbe, B. & Buyana, B. 2018. Alginate in Wound Dressings. *Pharmaceutics,* 10**,** 42.

Bairagi, U., Mittal, P., Singh, J. & Mishra, B. 2018. Preparation, characterization, and in vivo evaluation of nano formulations of ferulic acid in diabetic wound healing. *Drug development and industrial pharmacy,* 44**,** 1783-1796.

Batista, R. 2014. Uses and potential applications of ferulic acid. *Ferulic acid: antioxidant properties, uses and potential health benefits. 1st ed. New York, NY.: Nova Science Publishers, Inc. p***,** 39-70.

Boonsongrit, Y., Mitrevej, A. & Mueller, B. W. 2006. Chitosan drug binding by ionic interaction. *European journal of pharmaceutics and biopharmaceutics,* 62**,** 267-274.

Borges, A., Ferreira, C., Saavedra, M. J. & Simoes, M. 2013. Antibacterial activity and mode of action of ferulic and gallic acids against pathogenic bacteria. *Microbial Drug Resistance,* 19**,** 256-265.

Chandrasekaran, A. R., Jia, C. Y., Theng, C. S., Muniandy, T., Muralidharan, S. & Dhanaraj, S. A. 2011. Invitro studies and evaluation of metformin marketed tablets-Malaysia. *Journal of applied pharmaceutical science,* 1**,** 214.

Coleman, D., King, R. & Andrade, J. 1974. The foreign body reaction: a chronic inflammatory response. *Journal of biomedical materials research,* 8**,** 199-211.

Cota-Arriola, O., Plascencia-Jatomea, M., Lizardi-Mendoza, J., Robles-Sánchez, R., Ezquerra-Brauer, J., Ruíz-García, J., Vega-Acosta, J. & Cortez-Rocha, M. O. 2017. Preparation of chitosan matrices with ferulic acid: physicochemical characterization and relationship on the growth of Aspergillus parasiticus. *CyTA-Journal of Food,* 15**,** 65-74.

Dahl, J. E., Frangou-Polyzois, M. J. & Polyzois, G. L. 2006. In vitro biocompatibility of denture relining materials. *Gerodontology,* 23**,** 17-22.

Dale, P. D., Sherratt, J. A. & Maini, P. K. 1996. A mathematical model for collagen fibre formation during foetal and adult dermal wound healing. *Proceedings of the Royal Society of London. Series B: Biological Sciences,* 263**,** 653-660.

Disa, J. J., Alizadeh, K., Smith, J. W., Hu, Q.-Y. & Cordeiro, P. G. 2001. Evaluation of a combined calcium sodium alginate and bio-occlusive membrane dressing in the management of split-thickness skin graft donor sites. *Annals of plastic surgery,* 46**,** 405-408.

Du, W.-L., Niu, S.-S., Xu, Y.-L., Xu, Z.-R. & Fan, C.L. 2009. Antibacterial activity of chitosan tripolyphosphate nanoparticles loaded with various metal ions. *Carbohydrate Polymers,* 75**,** 385-389.

Du, W.-L., Xu, Y.-L., Xu, Z.-R. & Fan, C.L. 2008. Preparation, characterization and antibacterial properties against E. coli K88 of chitosan nanoparticle loaded copper ions. *Nanotechnology,* 19**,** 085707.

Hosoda, A., Ozaki, Y., Kashiwada, A., Mutoh, M., Wakabayashi, K., Mizuno, K., Nomura, E. & Taniguchi, H. 2002. Syntheses of ferulic acid derivatives and their suppressive effects on cyclooxygenase-2 promoter activity. *Bioorganic & medicinal chemistry,* 10**,** 1189-1196.

Hussain, F., Khurshid, M., Masood, R. & Ibrahim, W. 2017. Developing antimicrobial calcium alginate fibres from neem and papaya leaves extract. *Journal of wound care,* 26**,** 778-783.

Il'ina, A., Varlamov, V., Ermakov, Y. A., Orlov, V. & Skryabin, K. 2008. Chitosan is a natural polymer for constructing nanoparticles. Doklady Chemistry. Springer, 165-167.

Kong, M., Chen, X. G., Xing, K. & Park, H. J. 2010. Antimicrobial properties of chitosan and mode of action: a state of the art review. *International journal of food microbiology,* 144**,** 51-63.

Lin, Y. H., Lin, J. H. & Hong, Y. S. 2017. Development of chitosan/poly-γ-glutamic acid/pluronic/curcumin nanoparticles in chitosan dressings for wound regeneration. *Journal of Biomedical Materials Research Part B: Applied Biomaterials,* 105**,** 81-90.

Lo, H.-H. & Chung, J. 1999. The effects of plant phenolics, caffeic acid, chlorogenic acid and ferulic acid on arylamine N-acetyltransferase activities in human gastrointestinal microflora. *Anticancer research,* 19**,** 133-139.

López-León, T., Carvalho, E., Seijo, B., Ortega-Vinuesa, J. & Bastos-González, D. 2005. Physicochemical characterization of chitosan nanoparticles: electrokinetic and stability behavior. *Journal of Colloid and Interface Science,* 283**,** 344-351.

Madgulkar, A., Bhalekar, M. & Swami, M. 2009. In vitro and in vivo studies on chitosan beads of losartan duolite AP143 complex, optimized by using statistical experimental design. *AAPS PharmSciTech,* 10**,** 743.

Mathew, S. & Abraham, T. E. 2007. Physico-chemical characterization of starch ferulates of different degrees of substitution. *Food chemistry,* 105**,** 579-589.

Mcdougall, S., Dallon, J., Sherratt, J. & Maini, P. 2006. Fibroblast migration and collagen deposition during dermal wound healing: mathematical modelling and clinical implications. *Philosophical Transactions of the Royal Society A: Mathematical, Physical and Engineering Sciences,* 364**,** 1385-1405.

Mndlovu, H., Du Toit, L. C., Kumar, P., Choonara, Y. E., Marimuthu, T., Kondiah, P. P. & Pillay, V. 2020. Bioplatform Fabrication Approaches Affecting Chitosan-Based Interpolymer Complex Properties and Performance as Wound Dressings. *Molecules,* 25**,** 222.

Mndlovu, H., Du Toit, L. C., Kumar, P., Marimuthu, T., Kondiah, P. P., Choonara, Y. E. & Pillay, V. 2019. Development of a Fluid-absorptive Alginate-Chitosan Bioplatform for Potential Application as a Wound Dressing. *Carbohydrate Polymers***,** 114988.

Moura, M. J., Figueiredo, M. M. & Gil, M. H. 2007. Rheological study of genipin cross-linked chitosan hydrogels. *Biomacromolecules,* 8**,** 3823-3829.

Müller, R., Jacobs, C. & Kayser, O. 2001. Nanosuspensions as particulate drug formulations in therapy: rationale for development and what we can expect for the future. *Advanced drug delivery reviews,* 47**,** 3-19.

Nagasaka, R., Chotimarkorn, C., Shafiqul, I. M., Hori, M., Ozaki, H. & Ushio, H. 2007. Anti-inflammatory effects of hydroxycinnamic acid derivatives. *Biochemical and Biophysical Research Communications,* 358**,** 615-619.

Nair, R., Reddy, B. H., Kumar, C. A. & Kumar, K. J. 2009. Application of chitosan microspheres as drug carriers: a review. *Journal of pharmaceutical sciences and research,* 1**,** 1.

Nishiyama, T., Amano, S., Tsunenaga, M., Kadoya, K., Takeda, A., Adachi, E. & Burgeson, R. E. 2000. The importance of laminin 5 in the dermal–epidermal basement membrane. *Journal of dermatological science,* 24**,** S51-S59.

Pan, G. X., Thomson, C. I. & Leary, G. J. 2002. UV–vis. spectroscopic characteristics of ferulic acid and related compounds. *Journal of wood chemistry and technology,* 22**,** 137-146.

Pastar, I., Stojadinovic, O., Yin, N. C., Ramirez, H., Nusbaum, A. G., Sawaya, A., Patel, S. B., Khalid, L., Isseroff, R. R. & Tomic-Canic, M. 2014. Epithelialization in wound healing: a comprehensive review. *Advances in wound care,* 3**,** 445-464.

Paul, W. & Sharma, C. P. 2004. Chitosan and alginate wound dressings: a short review. *Trends Biomater Artif Organs,* 18**,** 18-23.

Qandil, A. M., Obaidat, A. A., Ali, M. A. M., Al-Taani, B. M., Tashtoush, B. M., Al-Jbour, N. D., Al Remawi, M. M., Al-Sou'od, K. A. & Badwan, A. A. 2009. Investigation of the interactions in complexes of low molecular weight chitosan with ibuprofen. *Journal of solution chemistry,* 38**,** 695-712.

Rezaeiroshan, A., Saeedi, M., Morteza-Semnani, K., Akbari, J., Gahsemi, M. & Nokhodchi, A. 2020. Development of trans-Ferulic acid niosome: an optimization and an in-vivo study. *Journal of Drug Delivery Science and Technology***,** 101854.

Sakugawa, K., Ikeda, A., Takemura, A. & Ono, H. 2004. Simplified method for estimation of composition of alginates by FTIR. *Journal of Applied Polymer Science,* 93**,** 1372-1377.

Smith, M. M. & Hartley, R. D. 1983. Occurrence and nature of ferulic acid substitution of cell-wall polysaccharides in graminaceous plants. *Carbohydrate Research,* 118**,** 65-80.

Sudarsan, S., Franklin, D. & Guhanathan, S. 2015. Imbibed salts and pH-responsive behaviours of sodium alginate based eco-friendly biopolymeric hydrogels—a solventless approach. *Macromol Int J,* 11**,** 24-29.

Trombino, S., Ferrarelli, T. & Cassano, R. 2014. A New Pro-Prodrug Aminoacid-Based for Trans-Ferulic Acid and Silybin Intestinal Release. *Journal of functional biomaterials,* 5**,** 99-110.

Tsou, M., Hung, C., Lu, H., Wu, L., Chang, S., Chang, H., Chen, G. & Chung, J. 2000. Effects of caffeic acid, chlorogenic acid and ferulic acid on growth and arylamine N-acetyltransferase activity in Shigella sonnei (group D). *Microbios,* 101**,** 37-46.

Van Den Kerckhove, E., Stappaerts, K., Boeckx, W., Van Den Hof, B., Monstrey, S., Van Der Kelen, A. & De Cubber, J. 2001. Silicones in the rehabilitation of burns: a review and overview. *Burns,* 27**,** 205-214.

Velnar, T. & Gradisnik, L. 2018. Tissue augmentation in wound healing: the role of endothelial and epithelial cells. *Medical Archives,* 72**,** 444.

Wang, J., Cao, Y., Sun, B. & Wang, C. 2011. Characterisation of inclusion complex of trans-ferulic acid and hydroxypropyl-β-cyclodextrin. *Food Chemistry,* 124**,** 1069-1075.

Yadav, P., Yadav, H., Shah, V. G., Shah, G. & Dhaka, G. 2015. Biomedical biopolymers, their origin and evolution in biomedical sciences: A systematic review. *Journal of clinical and diagnostic research: JCDR,* 9**,** ZE21.

Yuvarani, I., Kumar, S. S., Venkatesan, J., Kim, S.-K. & Sudha, P. 2012. Preparation and characterization of curcumin coated chitosan-alginate blend for wound dressing application. *Journal of Biomaterials and Tissue Engineering,* 2**,** 54-60.

Zhang, Y., Li, Z., Zhang, K., Yang, G., Wang, Z., Zhao, J., Hu, R. & Feng, N. 2016. Ethyl oleate-containing nanostructured lipid carriers improve oral bioavailability of trans-ferulic acid ascompared with conventional solid lipid nanoparticles. *International Journal of Pharmaceutics,* 511**,** 57-64.

CHAPTER 5

Self-assembling Alg-RGD-CS-TA Hybrid Scaffold for Wound Healing and Skin Regeneration

5.1 Introduction

Skin is a thin layered tissue in a body that acts as a barrier against external factors such as pathogens. Infections, physical and chemical damages to the skin results in wound formation. The skin can heal itself naturally in a complex and continuous process. However, the healing process may results in scar formation, tissue loss and seldom wounds that do not heal into completion more specifically in chronic wounds. The above issues renders the treatment of skin lesions a matter of great importance in healthcare. The conventional approach in the treatment of skin loss is autografts and allografts, which both provide biocompatibility. However, these approaches have few draw backs such as the availability of matching tissues and damages another body site along with formation of scar tissues in allografts and autografts approach, respectively. This has led to the rise on tissue engineering as a promising approach in designing alternative treatment for excessive skin loss. Application of tissue engineering in the wound dressing field has shown enormous interest owing to its ability to combine different biopolymers with proteins, bioactives and nanoparticles for enhanced skin regenerative properties (Zhao et al., 2016, Ahmed and Ikram, 2016). The exploration of biopolymers played a vital role in facilitating notable advancement in biomedical technologies through designing, fabrication and application of these biomaterials. The desirable properties and the ability of biopolymers such as chitosan, chitin, alginate, gelatine and collagen to be processed into various forms has led to promising industrial applications (Singh, 2011).

Chitosan and alginate are amongst the widely used polymers in the wound dressing field owing to their biocompatibility, biodegradability and ability to facilitate wound healing. Chitosan is a natural cationic polymer with vast desirable biological properties such biocompatibility and antimicrobial capabilities necessitating enhanced wound healing process (Ueno et al., 2001, Hong et al., 2008, Dai et al., 2009). Alginate on the other hand is a natural anionic polymer with attractive biocompatible properties and most importantly it is also capable of maintaining a moist environment in wounds thereby facilitating tissue granulation and haemostasis (Dai et al., 2009, Ma et al., 2007). Chitosan-alginate based biomaterials have demonstrated efficient and effective *in vitro* properties and *in vivo (animal models)* wound healing (Caetano et al., 2015, Pires and Moraes, 2015, Ma et al., 2007, Dai et al., 2009). These two natural polymers form an interpolymer complex (IPC) with retained desirable polymeric biological properties and performances in accelerating wound healing (Caetano et al., 2015, Dai et al., 2009, Mndlovu et al., 2019). Having successfully designed a fabrication approach that improves bioplatform properties and performances. An alternative approach was employed to the chitosan-alginate formulation to improve performance such as wound remodelling and tissue regeneration. The observations made on the previous sections made use of the partial crosslinking approach. Herein, functionalization of the polymeric formulations with RGD peptide was undertaken followed by crosslinking the formulation to form a self-assembling hybrid scaffold hydrogel. The bioactives such as antibiotics and growth factors can be loaded in the chitosan-alginate systems to enhance their property and performance in the tissue engineering field (Dai et al., 2009, Caetano et al., 2015). Crosslinking of these chitosan-alginate IPCs can also improve the properties and

performance of these bioplatforms (Dai et al., 2009, Caetano et al., 2015, Mndlovu et al., 2019, Mndlovu et al., 2020). One of the natural based crosslinker is Tannic acid. Tannic acid was used as both a crosslinker and bioactive with anti-oxidation and anti-inflammatory properties.

Tannic acid is a cytocompatible polyphenol with antimicrobial, antioxidant, anti-inflammatory properties that are capable of facilitating wound healing environment (Kim et al., 2010, Ninan et al., 2016, Li et al., 2018). Furthermore, TA has crosslinking abilities which could be explored in facilitating interactions with polymers, peptides and proteins via intermolecular hydrogen bonding, and also ionic interactions(Li et al., 2018). The reactivity of TA with proteins makes it a desirable haemostatic agent by facilitating blood coagulation through these interactions (Kozlovskaya et al., 2012, Kozlovskaya et al., 2010, Li et al., 2018). The biocompatibility of TA has seen it being applied in different wounds (Beck and Powers, 1926, McClure and Allen, 1935). The above properties coupled with biodegradation, porosity, and tissue/cell attachment contribute greatly in an attempt to design an ideal wound dressing. Herein, TA was used as both a crosslinker and a bioactive that was incorporated into a scaffold for enhanced wound healing abilities.

The incorporation of polyphenols such as TA in biomaterials would act against pathogens. However, the growing prevalence of multidrug-resistant (MDR) pathogens such as methicillin-resistant *Staphylococcus aureus* (MRSA) in wound dressings is evident that polymers and antibiotics present limitations in dealing with drug resistant pathogens(Qu et al., 2019, Rai et al., 2017). Therefore, addition of antimicrobial peptides (AMPs) in wound dressing would greatly enhance wound healing while fighting against drug resistant pathogens(Rai et al., 2017, Dart et al., 2019). To this end, conjugation of peptides with polymers has garnered much attention in the skin tissue regeneration field owing to their biocompatibility, antimicrobial and the ability to facilitate collagen deposition(Mohamed et al., 2016, Otvos Jr and Ostorhazi, 2015). Collagen is one of the active ingredients that is stimulated in AMPs (Abdillahi et al., 2012, Dart et al., 2019), which means that the peptides could stimulate collagen deposition so as to counteract drug resistance. Arginine-glycine-aspartate (RGD) peptide is a ubiquitous sequence recognised by cells to facilitate cell attachment and adhesion proteins such as fibronectin and fibrinogen along with structural proteins such as collagen(Yamada, 1991, Hosoyama et al., 2019). RGD has adhesive properties with which the peptide binds to the receptors (integrin). Furthermore, the biocompatibility of RGD allows it to be conjugated with polymers and loading of bioactives for enhanced wound healing properties (Varshosaz et al., 2020, Patrulea et al., 2016). The self-assembly of peptides has been highly researched with the self-assembling mechanisms well documented in literature (Pandit et al., 2018, Mason and Buell, 2019, Fichman and Gazit, 2014). The self-assembling nature of RGD makes it an attractive biomolecule for conjugation with polymers for improved biocompatibility and as a drug delivery system(Patrulea et al., 2016, Gupta et al., 2020).

Polymers can also self-assemble into hydrogels via several interactions such as crosslinked or entangled networks of (a) linear homopolymers, (b) linear copolymers, and (c) block or graft copolymers(Hoffman, 2012, Baek et al., 2002). Furthermore, hydrogen bonding, hydrophobic interactions and ionic interactions between polymers and additives such as peptides, crosslinkers and bioactives contribute to assembling of macromolecules into hydrogels(Hoffman, 2012, Mndlovu et al., 2019). These interactions have been reported to the improve physical-chemical and mechanical properties of hydrogels (Hoffman, 2012, Mndlovu et al., 2019, Jing et al., 2019). Peptide-crosslinker conjugates also improves mechanical properties of hydrogel. One of those cases includes crosslinking of Silk Fibroin with Tannic Acid to produce a self-assembled hybrid

hydrogel with enhanced mechanical properties, antimicrobial properties and wound healing(Jing et al., 2019). Grafting of polymers is another approach used to facilitate assembly of polymers via controlled co-polymerisation of macromonomers with small molecules(Chang et al., 2017). These favourable interactions and their resulting desirable properties led to and warranted the design of the current study which focuses on the interaction between polymers, peptide and crosslinkers for preparation of bioplatforms with enhanced wound healing and tissue regeneration performances. The underlying principle of the study is that the combination of chitosan and TA would provide antimicrobial properties whilst the use of the natural polymers (chitosan and alginate) along with the use of RGD peptide would produce a self-assembling hybrid scaffold with enhanced cytocompatibility and accelerated skin tissue regenerative activity. In this regard, fabrication of the self-assembling Alg-RGD-CS hybrid scaffold with the use of TA as a bioactive and a crosslinker was investigated in terms of physical and mechanical properties necessitating translational performances such as cytocompatibility and tissue regeneration.

5.2. Methods and materials

5.2.1. Materials

Medium molecular weight chitosan (75-85% deacetylation) Sigma-Aldrich (St. Louis, MO, USA) was used in the study with the calculated degree of crosslinking of 84.36% (Mndlovu et al., 2019). Sodium alginate Sigma-Aldrich (St. Louis, MO, USA) with the calculated mannuronic acid and guluronic acid concentration ratio (A1025/A1078) of 1.51 was as also used in the study (Mndlovu et al., 2019). Tannic acid (TA), glacial acetic acid, 1-(3-Dimethylaminopropyl)-3-ethylcarbodiimide hydrochloride (EDC), and n-Hydroxysuccinimide (NHS) were purchased from Sigma-Aldrich (St. Louis, MO, USA). Arginine-glycine-aspartate (RGD) peptide was purchased from DLD Scientific (South Africa). A commercial alginate-based wound dressing (Pharma-Algi®, Pharmaplast) was acquired for comparative studies.

5.2.2. Fabrication of the self-assembling hybrid scaffold

The biomimetic hybrid scaffold was prepared following the ionic gelation approach. Briefly, the Alg-RGD-CS-TA assembled system was synthesized by activating RGD peptide (50mg) with 50 mg NHS and 100 mg EDC in 10 mL deionised water. A 0.5% $^{W}/_{V}$ chitosan solution was prepared in a 0.5% acetic acid solution. Alginate solution 0.5% was also prepared. The chitosan (0.5%) solution was mixed with COO^- group activated RGD solution (0.025%). The alginate (0.5%) solution was also separately mixed with activated RGD solution (0.025%). The reaction mixtures were allowed to proceed for 4 hours before the CS-RGD solution was poured drop wise into the Alg-RGD solution under high speed stirring and the reaction mixture was allowed to stir for 24 hours at room temperature (25 °C). The reaction mixture was purified using the snake skin dialysis membrane (MW 14.5 KDa) in distilled water for 24 hours to remove NHS and EDC. Tannic acid was poured drop wise into the Alg-RGD-CS formulation under high speed stirring to make a final TA concentration of 5 mg/mL (or 0.5%). The mixture was left to mix well for 24 hours under low speed stirring. The resulted mixture (Alg-RGD-CS-TA) was then freeze-dried and the resulted scaffolds were assessed via FTIR spectroscopy, UV-Vis, XRD, TGA, and DSC. The following scaffolds were fabricated; Alg, Alg-RGD, CS, CS-RGD, Alg-RGD-CS, Alg-RGD-CS-TA.

5.2.3. Assessing molecular vibrational transitions and diffraction pattern of the scaffolds

The FTIR spectra of the scaffolds were analysed to evaluate the structural transformation that resulted in bands appearances/disappearances from interactions amongst polymers, peptide and bioactive characterised by specific functional groups. FTIR parameters were set as follows; 64

scans at wavenumber range of 4000–650 cm^{-1} using a PerkinElmer Spectrum 2000 ATR-FTIR (PerkinElmer 100, Llantrisant, Wales, UK) spectrometer fitted with a single-reflection diamond MIRTGS detector. X-ray diffraction pattern of the scaffolds were recorded to further assess the incorporation of the peptide and bioactive on the polymeric scaffolds by following the phase changes in each of the scaffolds. X-ray diffraction spectra were recorded on the benchtop MiniFlex 600 (Rigaku, Japan) diffractometer using CuKα radiation at 40kV and 15mA. The 2θ scan range was selected between 3-90 degrees at a scan rate of 10 degrees/minute.

5.2.4. Evaluation of the thermo-stability properties of the scaffolds

The thermophysical properties of the scaffolds were evaluated using a differential scanning calorimeter (DSC) (Mettler Toledo, DSC, STARe System, Swchwerzenback, ZH, Switzerland). The scaffolds of 3 to 10 mg were sealed in aluminium crucibles and heated over a temperature range of 0°C to 400°C at a heating rate of 10°C/min under a N_2 atmosphere. DSC curves were plotted as heat flow against temperature. The thermo-stability decomposition temperature of the scaffolds were determined using thermo-gravimetric analyser (TGA) (PerkinElmer, TGA 4000, Llantrisant, Wales, UK). Samples were heated at a rate of 10°C/min from 30 to 900°C under continuous nitrogen purging. Thermograms were generated as percentage weight vs. temperature.

5.2.5. Evaluation of surface morphology of the scaffolds

Zeiss sigma scanning electron microscopy (FESEM, 300 VP, ZEISS Research Microscopy Solutions, Jena, Germany) with a 15kV voltage were employed for the evaluation of the surface morphology of the scaffolds. Before analysis, all formulations were mounted on aluminium stubs using a carbon adhesive tape and coated with carbon/gold in a 2:1 ratio.

5.2.6. Textural mechanical properties of the scaffolds

The mechanical properties of the scaffold such as the storage modulus and tensile strength (TS) were determined via the compression and tension analysis with the aid of the Texture Analyzer (TA) (TA.XT plus, Stable Microsystems, Surrey, UK). The scaffolds were cut into a rectangular shape and the surface area was calculated. The tests were acquired at 1% strain rate with 70% strain at room temperature. The strain, force and stress were obtained. The tensile strength was obtained from the highest stress point of stress vs. strain graph which was further confirmed with following equation: Tensile Strength (N/mm^2) = Maximum force at break (N)/Cross-section are of sample (mm^2).

5.2.7. Fluid uptake and degradation kinetics of the scaffolds

Fluid uptake and degradation (weight loss) of the scaffolds were performed using the orbital shaking incubator (LM-530-2, MRC Laboratory Instruments Ltd. Hahistadrut, Holon, Israel) maintained at 37 °C, and set at a speed of 25 rpm as previously reported. The scaffolds were cut and weighed into PBS 5mL (pH 7.4). Fluid uptake of the bioplatforms were measured at 1, 2, 4, 8, 12 and 24 hours. The fluid uptake was calculated using equation 4.1. The rate of degradation was measured after 1, 3, 7, 10, and 14 days. The degree degradation was obtained via the use of equation 4.2.

$$FU(\%) = \left(\frac{Mh-Md}{Md}\right) x\ 100 \qquad \text{Equation 5.1}$$

$$Degradation\ (\%) = \left(\frac{Mo-Md}{Md}\right) x\ 100 \qquad \text{Equation 5.2}$$

Where FU% is the percentage fluid uptake, Mo, in the initial dry mass of sample before immersed in fluid, Mh and Md is the mass of the bioplatforms in hydrated and dry state, respectively.

5.2.8. Encapsulation efficiency (EE), drug loading (DL) and *in vitro* release studies

Alg-RGD-CS-TA scaffold was exposed to 100 mL PBS (pH 7.4) and agitated the scaffold overnight for complete release. The drug loading was determined from the equation of the standard curve that was constructed from standards of 0, 5, 10, 15, 20, 25 µg/mL TA concentration in PBS standard solutions that were analysed at a wavelength of 280 nm using UV Visible nanophotometer ((IMPLEN, NP80 NPOS 4.2 built 14900 UV-Vis nanophotometer, Jena, Germany). Total drug to polymer ratio were calculated in order to determine the expected amount (mass in milligrams) of TA in a weighed scaffold amount (mass). The expected TA amount per scaffold mass would give insights on the encapsulation efficiency and drug loading of the scaffold which was obtained using the following equations;

$$\%\ EE\ = \left(\frac{actual\ amount\ of\ drug\ in\ the\ scaffold}{calculated\ amount\ of\ drug\ in\ the\ weighed\ scaffold\ for\ analysis}\right) x\ 100 \qquad \text{Equation 5.3}$$

$$\%\ DL\ = \left(\frac{actual\ amount\ of\ drug\ in\ the\ scaffold}{total\ weight\ of\ scaffold\ used\ for\ analysis}\right) x\ 100 \qquad \text{Equation 5.4}$$

The actual amount of drug in the scaffold used for the tests was determined from the standard curve using UV-Vis spec. whereas the calculated amount of drug per scaffold weight in the weighed scaffold for analysis was determined using the drug to total scaffold weight ratio. The release study was carried out in 100 mL PBS (pH 7.4) using the Snake Skin dialysis tube (3.5K MWCO, 22 mm, Separation Scientific SA (Pty) Ltd) diffusion technique maintained at 37 °C stirring at 30 rpm on the orbital shaking incubator (LM-530-2, MRC Laboratory Instruments Ltd. Hahistadrut, Holon, Israel) for 108 hours. Aliquots (0.5 mL) were withdrawn at predetermined time points (1, 2, 4, 8, 12, 24, 48, 72, 96, 108 and 120 hours) from the release medium and replaced with an equivalent volume of fresh PBS to maintain sink condition. The amount of the TA encapsulated in the scaffold and released at predetermined time points in the PBS medium was determined at 280 nm with UV-Vis nanophotometer. The cumulative drug release was determined using the following formula as previously documented by Chandrasekaran et al.,(Chandrasekaran et al., 2011);

$$Cumulative\ release\ =\ (sample\ volume\ with\ drown/bath\ volume)\ x\ p(t-1)+p \qquad \text{Equation 5.5}$$

Where pt is the percentage released at time t and p(t-1) is the percentage released previous to time t.

5.2.9. In vitro cytotoxicity assessment of the scaffolds

RGD, Alg, Alg-RGD, CS, CS-RGD, TA, Alg-RGD-CS, Alg-RGD-CS-TA, and the comperative product were used as treatment for the mouse embryonic fibroblast NIH-3T3 cell line to evaluate cell viability at 24, 48, and 72 hours. The NIH 3T3 cells were grown in RPMI medium supplemented with 10% FBS and 1% antibiotics. Cells were seeded overnight followed by treatment of a 5 mm diameter scaffolds in cell containing 100 µL DMEM medium (1 x 10^4 cell/ml) in a 96 well. The treated cells were incubated in a humidified chamber overnight at 37 °C with an atmosphere containing 5% CO_2 for predetermined time points; 24, 48, and 72 hours. For the positive control, NIH 3T3 cells where maintained with RPMI medium without any additions and for the negative control, the cells were killed and maintained with dimethyl sulfoxide (DMSO). Ten microliters of MTT (3-(4,5-Dimethyl-2-thiazolyl)-2,5-diphenyl tetrazolium bromide) was added to each well plate after each of the predetermined time points and incubated for 4 hours. Thereafter,

the medium and the scaffolds on the well plates were discarded followed by addition of 100 µL DMSO and incubated overnight on the orbital shaker (at 37 °C) to dissolve the formazan. The 96-well plates were measured at absorbance of 570 nm and 690 nm to subtract the 690nm absorbance from the 570 nm absorbance in order to calculate the percentage cell viability on each scaffold at the given time points.

5.2.10. *In vivo* Skin tissue regeneration and wound closure assessment of the scaffolds

In vivo assessment of the wound healing effects of the self-assembled scaffolds were carried out in a rat model. Female Sprague–Dawley rats (6-8 weeks old) were housed individually, in cages at room temperature (± 25 °C), maintained under a 12 hour light:dark cycle. The animals were fed water and *ad libitum* and allowed to acclimatize to the environment for a week prior to surgery. The animals were monitored according to prescribed central animal services (CAS) protocol. All procedures were done in accordance with the Animal Ethics Control Committee of the University of the Witwatersrand animal care regulations following approval by the Animal Ethics Screening Committee of the University of the Witwatersrand (ethics number: 2018/10/49c).

Rats were anesthetized with an Isofor and Oxygen gas at 1:3 % mixture and intraperitoneal injection of a 2.7 ml/kg mixture containing: midazolam (1.25 mg/ml), and 0.079 mg/ml fentanyl to maintain the rat. The skin over the dorsal area was shaved, application fields were outlined with a marking pen just before skin excisions. A full-thickness (2 mm thick) wound of 6 mm diameter was created on the dorsal area of the rat employing the skin punch biopsy apparatus (see image below). Using forceps the skin was lifted in the middle of the wound outline created by the punch biopsy and then an iris scissors (with curved tips) was used to excise the circular piece of tissue. The excised tissues (wound plugs) were fixed in 10% buffered-formalin for later processing as control/normal skin. A total of two wound areas were created on the dorsal area of each rat. In each group, the rats contained the following treatments on the wound area; control (gauze and bandage), the comparative product, Alg-RGD-CS, and Alg-RGD-CS-TA. The scaffolds (7mm diameter) were cut and sterilized with UV before applied on rats. The dressings were not changed but the bandages were changed weekly. The animals were allowed to heal for 3, 7, and 14 days whereas the wounds were examined, photographed, and excised to measure the reduction in wound size on day 4, 8, 11, and 15 respectively. Wound healing was followed by determining the degree of wound closure (%) given by the size of the wound calculated using the image J software and employed the following equation.

$$\% \text{ wound closure} = \frac{(Wound\ area\ day\ 0 - wound\ area\ day\ (n)}{(Wound\ area\ day\ 0)}\ x\ 100 \qquad \text{Equation 5.6}$$

Histological analysis

Skin tissue specimens were fixed in 10% formalin buffer, cut according to standard operating procedure (idexxSA-AP-SOP-26) and processed according to routine histological tissues processing in an automated tissues processor with a standard operating procedure IdexxSA-AP-SOP-27. Following processing, sections were cut to 5-6 um (IdexxSA-AP-SOP-205). The slides produced were stained with Haematoxilin and Eosion tissues stationer (IdexxSA-AP-SOP205) before histological evaluation. Epithelisation, epidermal-dermal attachment, angiogenesis, mononuclear infiltration and fibroblast reaction were evaluated on the specimens. The mode appearance of each wound plug was used to describe the overall morphology of each group.

5.3. Results and discussion

5.3.1 Development of the self-assembling scaffolds

A lower polymeric percentage (0.5% $^{W}/_{V}$) was used in the study due to the soft texture of the scaffolds that resulted from the percentage solution. Higher percentage solutions (1-2%) resulted in rough rigid texture on the scaffold, they were thus avoided. The ratio of the final Alg-RGD-CS-TA scaffold was 1:10:10:20 for RGD, alginate, chitosan, and tannic acid, respectively. The activation of RGD with EDC and NHS allowed for the carboxylic group of RGD to interact with the primary amine groups of chitosan thus forming CS-RGD. The activated RGD was also incubated with alginate and they also interacted to form Alg-RGD. These interactions between polymer and peptide resulted in the self-assembly of the formed conjugates. The self-assembled polymer-peptide mixtures (Alg-RGD and CS-RGD) were further mixed by addition of CS-RGD drop-wise into Alg-RGD while stirring at high speed to facilitate the co-assembly of the mixtures to form Alg-RGD-CS which was later on stabilized by TA crosslinking (Figure 5.1). The formed Alg-RGD-CS was a result of interactions between the polymers and also the interaction between polymers and the peptide thus named hybrid self-assembled polymer-peptide scaffold due to the interactions (Figure 5.1a). The hybrid part of the conjugates also took into account the interactions that took place between the individual polymers with the peptide, the interactions amongst the polymers, and the interactions between polymers, peptide and the crosslinker (Figure 5.1). To elucidate interactions above Figure 5.1a gives details on the type of interactions that took place in the reaction.

Peptide primary structures are made up of amino acids which also allows for chemical modification during scaffold fabrication. Different amino acids have different side chain polarity, hydrophilicity, charges, and sizes (Eskandari et al., 2017). These side chain properties enables amino acids to interact with different molecules such as polymers, crosslinkers and other protein/peptides. The amino acid sequence, number of repeats, and the type of amino acids drives the interacting molecules thus facilitating distinctive self-assembled peptide structures with specified secondary structures and chemical properties (Mandal et al., 2014, Eskandari et al., 2017). Self-assembly of carbohydrate polymers was reported to be facilitated through intermolecular and noncovalent interactions such as hydrogen bonding, π–π stacking, or electrostatic interactions (Guven et al., 2015). The combination of peptide and polymeric self-assembled structures gave rise to network structures which were mimicking extracellular matrix networks hence the term biomimetic. The network structures resulted from the interaction of chitosan and alginate. More stability of the structure was provided by the RGD peptide and tannic acid through R1A, R1B, R2A, R2B and R3 reactions (Figure 5.1a). Intermolecular hydrogen bonding also existed between the polymers-peptide with the TA as indicated by the reaction 4 (Figure 5.1).

Activation of the carboxylic groups of RGD peptide allowed for the increased percentage of functional groups available for interaction with chitosan, alginate and TA. The carboxylic groups of alginate interacted with amine groups of RGD and chitosan as shown in Figure 5.1a (R1B and R2A). The activated carboxylic groups RGD interacted with chitosan amine groups (R2B and R1A) whilst the other amine parts of the structure interacted with the hydroxyl groups of tannic acid (R3). Chitosan amine groups also interacted with hydroxyl groups of tannic acid (R3). The weak electrostatic interactions (R3) of tannic acid with polymers and RGD peptide inferred that it would be easily release from the scaffold. Furthermore, tannic acid served as both bioactive and crosslinker which was added last in the fabrication steps. Peptides self-assembly are governed

by their own unique mechanisms and polymers also self-assembles via their own interactions as previously described in literature (Pandit et al., 2018, Mason and Buell, 2019, Hoffman, 2012). The scaffold absorbs fluid and start getting hydrated from the surface towards the centre without destabilising the scaffold physical feature (Figure 5.1b). Morphological features of the self-assembled and co-assembled scaffolds were also evaluated via SEM.

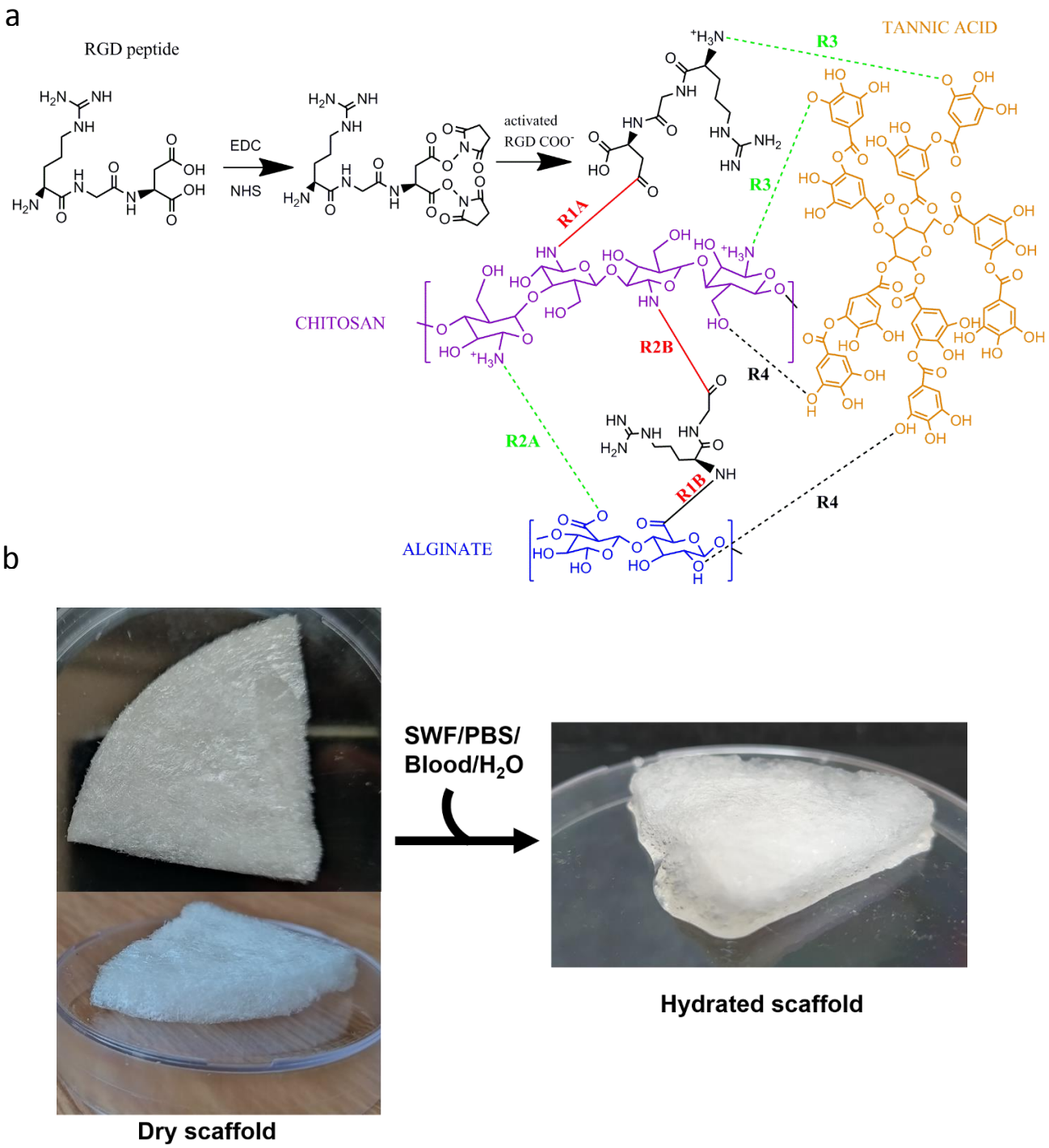


Figure 5.1. Schematic representation of the self-assembled hybrid scaffold (a) reaction schematic of the peptide activation and interactions between RGD, CS, Alg and TA. (b) dry and hydrated scaffold.

5.3.2. Morphological features of the self-assembled scaffolds.

The SEM was employed to evaluate the morphological features of the scaffolds which gave insights in the morphological features of the self-assembled and co-assembled polymers and peptide. The properties and stimulus required for tailoring self–assembly of biomolecules into different nanostructures has been well documented (Fichman and Gazit, 2014, Wang et al., 2019). Herein, activation of the RGD peptide followed by various interactions between the activated peptide and the polymers along with TA as a crosslinker and a bioactive was undertaken. The polymeric self-assembly can be depended on the ability of the polymer to assemble into nanostructures with the aid of pH changes, temperatures, and additives/stimulus. Herein, polymers formed different morphological features after freeze drying them into scaffolds. This was without the changes in pH, temperature or any additives. These features included the vertically arranged sheets with free standing micro-treads of 2.5 μm diameter in alginate scaffold and a large horizontally arranged sheet with pores (average pore size distribution of 168.4 μm^2) and two different types of micro-treads in chitosan scaffolds (Figure 5.2a and c). The rectangular shaped micro-treads of different sizes were connecting the large chitosan sheets with the end of the sheets containing the free-standing round treads of 3.47 μm diameter similar to those observed in alginate scaffolds (Figure 5.2c). Co-assembling of Alg-RGD resulted in changes on morphological features such as the transition of the vertically aligned sheets in alginate to horizontal arranged sheets connected by round micro-treads in Alg-RGD. The round micro-treads which were free standing in alginate scaffold were the ones connecting the sheets in Alg-RGD (Figure 5.2a and b). Furthermore the co-assembly of Alg-RGD resulted in the increase in pores on the sheets and created a 3-D architecture with the round micro-treads connecting one sheet to another and holding the sheets at different heights/levels (Figure 5.2b). Similarly to the co-assembled Alg-RGD scaffold, the co-assembled CS-RGD drastically changed the morphological features of CS from large horizontally arranged sheets to small 3-D arranged sheets interconnected by the rectangular thread-like sheets in CS-RGD (Figure 5.2c and d). The rectangular thread-like sheets were more uniform (average width of 5.6 μm) on the co-assembled CS-RGD scaffold than in the self-assembled CS scaffold. The decreased size of the sheets created more spaces between the sheets thus making it more porous for potential cell attachment and fluid absorption.

The incubation of the co-assembled solutions (Alg-RGD and CS-RGD) resulted in the interactions as described in the previous section to form a new morphological feature. The reactions allowed for the formation of large sheets arranged as 3-D structures in Alg-RGD-CS (Figure 5.2e). The large sheets were attached to each other and also connected by a form of tread which was assumed to be from the interactions of free carboxylic groups of alginate and the amine groups of chitosan thus forming network structures. These network thread-like structures were most likely due chitosan-alginate interactions given that the interaction of the two polymers formed network structures. This was also assumed so because the self-assembled polymers and the co-assembled polymer-peptide scaffolds did not display this type of thread-like network. The thread-like network went through each sheet connecting them to form a 3-D architecture. The round micro-thread and the rectangular thread-like structures disappeared when the Alg-RGD-CS scaffold formed. The 3-D architecture feature of Alg-RGD-CS was further enhanced by incorporation of TA as both a bioactive and a crosslinker. The addition of TA resulted in the Alg-RGD-CS-TA forming horizontal, vertical and other sheets arranged at different angles to form the 3-D structures. Furthermore, the micro-treads which disappeared in Alg-RGD-CS reappeared in Alg-RGD-CS-TA (Figure 2f). The thread-like network that connected the Alg-RGD-CS was still

present in Alg-RGD-CS-TA along with more nano-tread-like networks appearing on the surface of the sheets (Figure 5.2f). The presence of the thread-like network inferred that the interactions that had already taken place before adding TA were not affected after adding TA. The polymeric and peptide self-assembly along with the peptide-polymer co-assembly was congruent with the changing morphological features and formation of 3-D structures on the scaffolds. The functional groups on the polymers, peptide and the crosslinker allowed for the interactions which resulted in different morphological features. These changes in morphological features attest to the ability of the polymers to self-assembly and the capability of co-assembling with peptides and bioactives. The spaces between the sheets could allow for ease of cell attachment and movement throughout the scaffold's 3-D architecture.

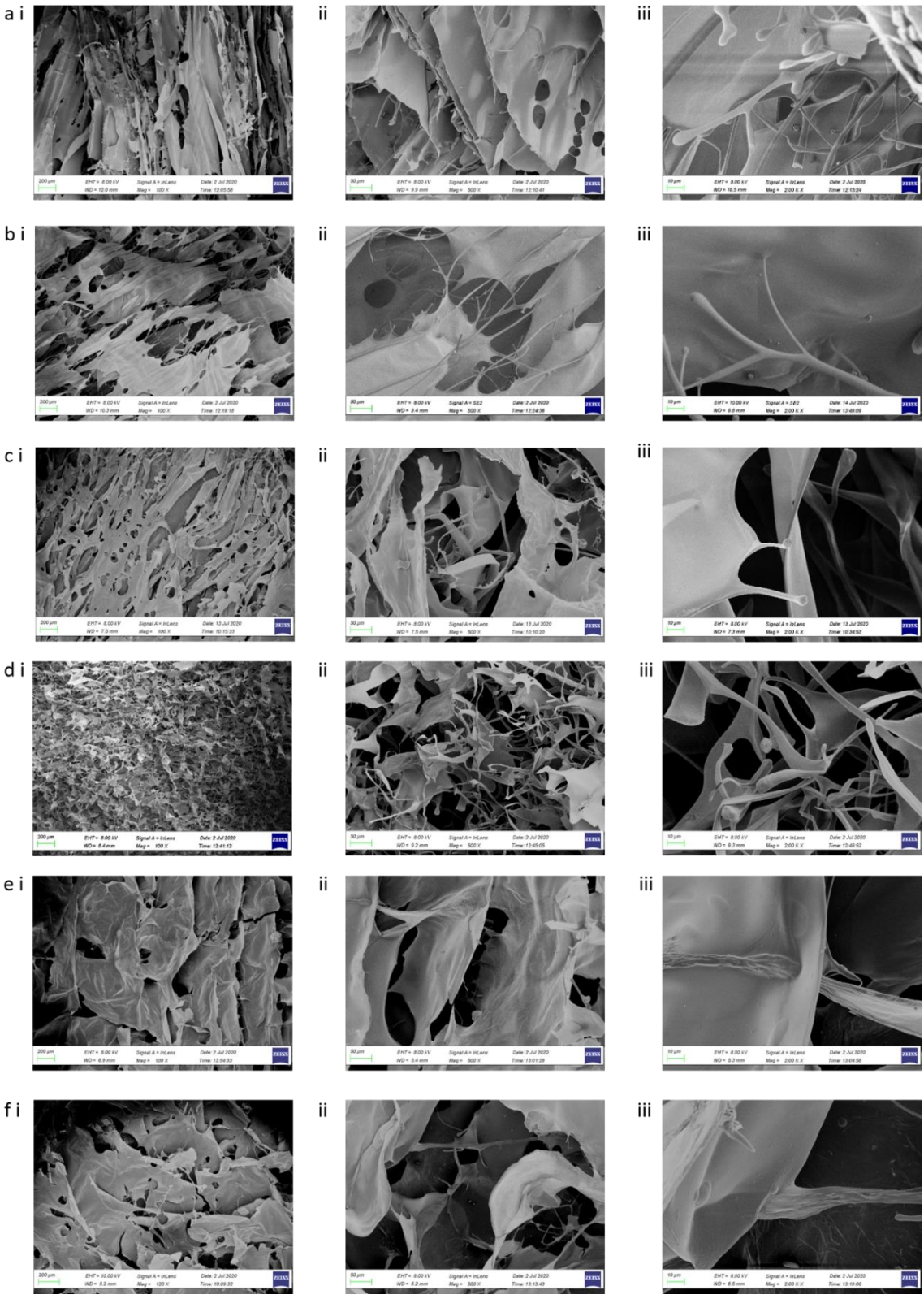


Figure 5.2. Morphological features of the self-assembled and co-assembled scaffolds (ai-iii) Alg , (bi-iii) Alg-RGD, (ci-iii) CS, (di-iii) CS-RGD, (ai-iii) Alg-RGD (ai-iii) Alg-RGD-CS-TA scaffolds at 100, 500, and 2000 X magnification respectively.

5.3.3. Chemical and physical properties of the scaffolds

The properties of polymeric systems coated or conjugated with RGD is well documented (Perlin et al., 2008, Hersel et al., 2003). Diffraction pattern, morphological features and thermostability properties of powdered or self-assembled RGD system has been hardly research. Herein some of these properties were recorded. Furthermore, the interactions that exist between the peptide, polymers and the crosslinker were evaluated. The change in morphological features between the self-assembled scaffolds and the co-assembled scaffolds inferred that there were interactions between the polymers, peptide and the bioactive. Therefore, FTIR was employed to elucidate the interactions that took place during the self-assembly and co-assembly of biomolecules. The FTIR spectrum of RGD exhibited the overall β-sheet and random coil secondary structure with the following bands; 3178 cm^{-1} (N-H stretch), 1657 cm^{-1} (-CO-NH) amide I signifying the random coils secondary structure, 1534 cm^{-1} (amide II) characteristic of β-sheet secondary structure, 1392 cm^{-1} (corresponding to guanidino N−H bends coupled to symmetric C−H bends), 1232 cm^{-1} amide III (coupled C-N stretching and NH bending motions), 1045 cm-1 further signifying the β-sheets secondary structure (Figure 5.3a). These RGD FTIR bands correspond to literature reports in terms of the band positions for specific RGD functional group arrangement and secondary structure properties (Bini et al., 2006, Di Foggia et al., 2011, Zhu et al., 2009, Li et al., 2006).

Alginate and chitosan displayed their saccharide characteristic bands at the following wavenumbers; 3222 cm^{-1} (O-H stretch), 2918 cm^{-1} (CH stretch), 1599 cm^{-1} (asymmetric stretching of carboxylate in the salt form ($COO^{-}Na^{+}$), 1408 cm^{-1} (symmetric carboxylate stretching (C=O)), and 1028 cm^{-1} (C-O-C stretching) for alginate scaffold while the chitosan scaffold displayed the following bands; 3089 cm^{-1} (O-H stretch), 2868 cm^{-1} (CH stretch), 1634 cm^{-1} (amide II stretch), 1535 cm^{-1} (C=O stretch), 1063 cm^{-1} (anti-symmetric stretching of the C-O-C bridge), 1016 cm^{-1} (skeletal vibrations around the C-O stretching) (Figure 5.3) (Lawrie et al., 2007). The Alg-RGD co-assembly resulted in the following bands; a more pronounced broad band at 3262 cm^{-1} representative of the contribution of O-H stretch from alginate and N-H stretch from the RGD, a weak band at 2928 cm^{-1} assigned to the C-H stretch from alginate, a strong band at 1596 cm^{-1} representative (asymmetric stretching of carboxylate salt group), a strong band at 1407 cm^{-1} ascribed to the symmetric carboxylate stretching (C=O) from alginate, a weak band at 1296 cm^{-1} representative of the amide III (coupled C-N stretching and NH bending motions) and contribution from alginate saccharide characteristics, and a strong band at 1027 cm^{-1} attributed to the C-O-C stretching from alginate. The IR-spectrum of Alg was more similar to that of Alg-RGD scaffolds than it was for RGD. The similarity in the spectrum of Alg and Alg-RGD scaffolds was due to the high alginate to RGD composition ratio which resulted on the overlapping of the RGD characteristic bands. However, the addition RGD had an effect in alginate properties such as the change in morphological features as mentioned in the previous section and also the chemical properties such as shifting and intensifying the 3222 band cm^{-1} in alginate to 3262 cm^{-1} in Alg-RGD. Similarly to Alg-RGD spectrum, the CS-RGD spectrum resembled the CS spectrum and showed the RGD characteristic bands. The CS-RGD scaffold displayed the following bands, 3072 cm^{-1} (O-H stretch), 2863 cm^{-1} (CH stretch), 1634 cm^{-1} (amide II stretch), 1537 cm^{-1} (C=O stretch), 1064 cm^{-1} (anti-symmetric stretching of the C-O-C bridge), 1018 cm^{-1} (skeletal vibrations around the C-O stretching) (Figure 5.3a).

Self-assembly of Alg-RGD-CS resulted in the following bands; a broad band at 3272 cm^{-1} representative of the O-H stretch contributed by both polymers and also the N-H stretch from RGD, two weak sharp bands at 2930 and 2886 cm^{-1} representative of the CH stretch from alginate

and chitosan, a strong slightly broad sharp band at 1598 cm^{-1} representative of the amide deformation, a sharp band at 1405 cm^{-1} which was a contribution from the symmetric carboxylate group and also the guanidino N−H bends coupled to symmetric C−H bends and a 1029 cm^{-1} band attributed to the C-O-C stretching. The FTIR-spectrum of Alg-RGD-CS was similar to that of Alg and Alg-RGD. The CS or CS-RGD 1634 cm^{-1} band disappeared while the their CH 2930 cm^{-1} stretch was still present along with the merging of the 1064 cm^{-1} and 1018 cm^{-1} to form the 1029 cm^{-1} band in Alg-RGD-CS. Although the Alg-RGD-CS spectrum highly resembled the Alg spectrum, the presence of the 2930 cm^{-1} CH stretch band was evident of the use of chitosan in the assembled scaffold.

Tannic acid was used to crosslink the self-assembled Alg-RGD-CS system. The FTIR spectrum of TA displayed the following phenolic characteristic bands, 3290 cm^{-1} (O-H stretch), 1697 cm^{-1} (C=O stretching), 1607-1445 cm^{-1} representing the $C_{aromatic}$-$C_{aromatic}$ stretch, 1308 cm^{-1} ($C_{aromatic}$-O-C stretch, $C_{aromatic}$–O–H in-plane bending, 1179 cm^{-1} (O-C-O and $C_{aromatic}$-C-O stretching, $C_{aromatic}$–OH in-plane bending) and 1079 cm^{-1} (C-O-C stretch) (Figure 5.3a). These distinguished bands were similar to the reported FTIR spectrum of TA (Ranoszek-Soliwoda et al., 2017, Cowen and Al-Abadleh, 2009, Falcão and Araújo, 2014). Crosslinking of self-assembled Alg-RGD-CS with TA resulted in the following FTIR bands, 3200 cm^{-1} (O-H stretch), two weak sharp bands at 2937 and 2879 cm^{-1} (C-H stretch), 1707 cm^{-1} (C=O stretching), ~1604-1445 cm^{-1} (contribution from amide deformation, symmetric carboxylate stretch and guanidino N−H bends coupled to symmetric C−H bends), 1318 cm^{-1} ($C_{aromatic}$-O-C stretch, $C_{aromatic}$–O–H in-plane bending, $C_{aromatic}$–$C_{aromatic}$ stretch), and 1198 cm^{-1} (O-C-O and $C_{aromatic}$-C-O stretching, $C_{aromatic}$–OH in-plane bending), and 1029 cm^{-1} (C-O-C stretch) (Figure 5.3a). The presence of bands at 1707 cm^{-1} and the 1604-1445 cm^{-1} in the FTIR spectrum of Alg-RGD-CS-TA suggest that TA was incorporated in Alg-RGD-CS. The complexation of Alg-RGD-CS with TA was further confirmed by the decreased intensity of the 1707 cm^{-1} band while increasing intensity at 1604-1445 cm^{-1} bands. The point that the 1697 cm^{-1} TA band was not split into two when the 1707 cm^{-1} Alg-RGD-CS-TA band formed suggests that TA was not oxidized to quinine, instead TA was protected from oxidation after the complexation process.

To further elucidate the interaction of these molecules, X-ray diffraction patterns of the scaffolds were assessed. The polymeric (chitosan and alginate) scaffolds displayed their semi-crystalline and amorphous characteristic diffraction pattern. These diffraction patterns included, the shoulder peak at 10° (amorphous phase) and at 21° (semi crystalline phase) for chitosan scaffold whilst alginate scaffolds exhibited the three diffraction peaks at 10, 22 and 40 degrees corresponding to amorphous phases (Figure 5.3b). These diffraction patterns were similar to those previously reported in previous chapter and published work (Mndlovu et al., 2019). The co-assembly of Alg-RGD resulted in the scaffold assuming the alginate amorphous properties due to the high alginate to RGD weight ratio. This amorphous regions in the scaffold was ascribed to 10, 21, and 40° peaks (Figure 5.3b). The assumed alginate amorphous character was also due to the semi-crystalline diffraction pattern of RGD with amorphous phases ascribed to peaks at 22 and shoulder peak at 36°. This amorphous character was accompanied by the weak peaks at 20, 27, 40 and 51° corresponding to crystalline phases. All the RGD peaks (denoting semi-crystallinity) were not visible in Alg-RGD scaffold due to the reasons mentioned above. Similar to the diffraction pattern of Alg-RGD, CS-RGD diffraction pattern highly resembled the CS characteristic diffraction pattern with the 10 and 21 degrees peaks as discussed above. The assembling of the Alg-RGD-CS system resulted in the formation of the following diffraction pattern, peaks at 21 and 40 degrees represented amorphous phases (Figure 5.3b). The shoulder peak at 10° from both

polymers diminished when the Alg-RGD-CS assembled. This suggests that there were interactions between the polymers and the peptide thus resulting in the deformation of the lattice structure leading to disappearance of peaks and slight peak shifts. However, the presents of the ~21° peak along with the 38° peak infer that both polymers were in the complex along with the peptide. This amorphous character was not affected by the addition of TA due to the amorphous character of tannic acid. The Alg-RGD-CS-TA displayed the consistent 22 and 42° peak (amorphous) whilst tannic acid displayed a peak at 25° (amorphous) (Figure 5.3b). The consistent ~21 and ~40° peaks (amorphous phases) were slightly shifted and decreased in intensity after incorporating TA. The decrease in peak intensity after crosslinking with TA correlate with what was previously observed for TA crosslinked nanofibers containing chitosan(Xu et al., 2015).

The scaffolds' interactions were further assessed via TGA and DSC with specific focus on their thermo-stability properties. The dehydration and degradation profiles for chitosan scaffold were at 149 and 286 °C whereas for alginate they were at 96 and 246 °C. The dehydration step was indicated by the endothermic (through) peak whereas the degradation was observed on the exothermic (crest) peak. The degradation profile of these polymers correlate with what was previously reported (Mndlovu et al., 2019). The RGD peptide displayed endothermic peaks at 90, 140, 200, 273 and 302 °C. The first two endothermic peaks (90 and 140 °C) of RGD were indicative of the dehydration and melting point of the peptide. The peptide degradation occurred at 250 °C which was represented by the exothermic peak. The co-assembly of Alg-RGD resulted in the scaffold assuming the DSC curve profile of alginate with the following peaks; endothermic dehydration peak at 96 °C and exothermic degradation peak at 246 °C. Similar to Alg-RGD, the CS-RGD scaffold assumed the thermal profile of chitosan. The self-assembly of the hybrid Alg-RGD-CS scaffold resulted in the following thermo profile; an endothermic dehydration peak at 100 °C and an exothermic degradation behaviour at 270 °C. TA displayed the following thermal profile; endothermic dehydration and melting point peaks at 104 °C and 189 °C and an exothermic degradation behaviour from 243 °C. Incorporation of TA in the hybrid scaffold resulted in the following thermal profile. An endothermic melting point at 119 °C and a poorly defined exothermic behaviour from 200 °C. The endothermic peak on the Alg-RGD-CS-TA was due to the melting of RGD peptide on the scaffold. The lack of a well-defined degradation peak in both Alg-RGD-CS and Alg-RGD-CS-TA was due to the complexation reactions that took place between the polymers, peptide, and tannic acid. The different degradation temperatures for each polymeric scaffold (alginate (246 °C) and chitosan (286 °C) contributed greatly to the loss of a well-defined degradation of the Alg-RGD-CS and Alg-RGD-CS-TA.

These thermo-stability properties were consistent with those observed in TGA of the scaffolds. The polymeric scaffolds displayed the characteristic degradation profile of 224-265 °C with 33% weight loss for alginate and 270-361 °C with 39% weight loss for chitosan. The RGD peptide displayed the following degradation profile 259-316 °C with 23 % weight loss. This degradation range correlates with the DSC thermogram observed. The Alg-RGD scaffold displayed the degradation at the following temperature range 224-270 °C with 30 % weight loss whereas for CS-RGD scaffold a 260-350 °C degradation temperature range was observed with 31 % weight loss (Figure 5.3d). These co-assembled scaffold degradation temperature ranges were very similar to their self-assembled polymeric scaffold degradation profile. The assembly of the Alg-RGD-CS scaffold exhibited a degradation temperature of 204-260 °C with 44% weight loss. This degradation temperature range was different from the self-assembled polymeric scaffolds and the co-assembled peptide-polymer scaffolds. The temperature with which the Alg-RGD-CS scaffold

started degrading was lower than those observed on polymeric and the peptide-polymer scaffolds. Furthermore, the temperature with which the Alg-RGD-CS scaffold finished degrading was also lower than the one presented by the polymeric and peptide-polymeric scaffolds. This suggests that the self-assembled Alg-RGD-CS scaffold was less thermally stable than the starting materials. However, the point that the degradation temperature range of Alg-RGD-CS scaffold was close to those of the starting materials confirms the use of the starting materials to produce the Alg-RGD-CS scaffold. The observed degradation temperature range of Alg-RGD-CS scaffold was not highly affected by incorporation of TA. This was concluded so due the similarity of the degradation profile of Alg-RGD-CS and Alg-RGD-CS-TA, where the Alg-RGD-CS-TA scaffold presented a 56% weight loss in a degradation temperature range of 205-252 °C. The self-assembly of Alg-RGD-CS resulted in an increased weight loss compared to starting material. This was due to the complexation reactions between peptide and the polymers thus rendering the complex less thermostable than the starting materials. Similarly to Alg-RGD-CS, incorporation of TA further increased the weight loss due to the interactions mentioned above and the contribution from the interactions of polymer and peptide with TA. TA itself displayed a high weight loss of 50% in a degradation temperature range of 252-362 °C, hence it contributed to the increased weight loss of Alg-RGD-CS-TA.

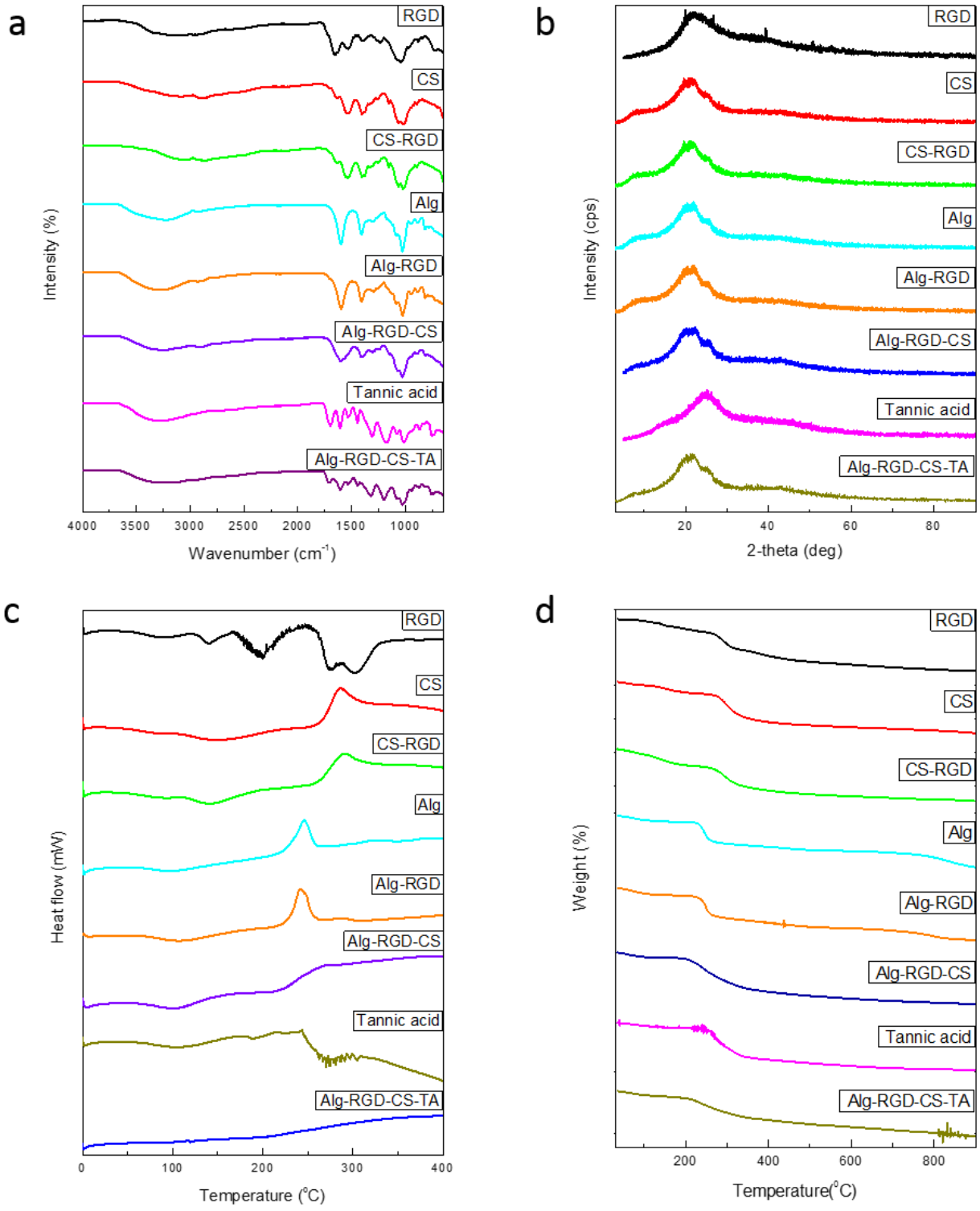


Figure 5.3. The scaffolds' functional groups, chemical composition, and phase changes induced by self-assembly via interactions described above were evaluated via the four analytical techniques (a) FTIR spectra, (b) X-Ray diffractograms, (c) DSC and (d) TGA thermogrames of the scaffolds.

5.3.4. Mechanical properties of the scaffolds

Flexibility, durability, malleability, elasticity, and resistance to deformation of dressings are among the few defining mechanical properties of an ideal wound dressing (Khan et al., 2000, Akiyode and Boateng, 2018). Wound dressings should have high durability so as to accommodate for stress applied to it during packaging. The high durability will aid in maintaining the scaffold mechanical properties during and after application to the wound area. The hardness/durability of the bioplatforms is obtained at the highest stress point of the stress against strain graph. This highest stress point is regarded as the tensile strength of the scaffolds. The dry Alg-RGD-CS scaffold tensile strength was 0.0038 ± 0.00081 MPa with no elongation at break owing to the scaffold's lack of plastic deformation (brittle failure) there by breaking very sharply without elongation. The high tensile strength (0.0038 ± 0.00081 MPa) showed that the scaffold's was strong and hard enough to withstand tension when it is prepared for packaging and also preparation for application in the wound area. The tension tensile strength of the dry Alg-RGD-CS-TA scaffold was 0.001725 ± 0.00035 MPa. Similar to the Alg-RGD-CS scaffold, the Alg-RGD-CS-TA scaffold did not display any elongation at break. This tensile strength value (0.001725 ± 0.00035 MPa) is lower than the one observed in dry Alg-RGD-CS scaffolds which further indicate that the addition of tannic acid decreased the tensile strength. The addition of TA decreased the scaffold's tensile strength while increasing the elasticity. This is in correlation with the observation made by Khan et al., which demonstrated that the increase in elasticity reduces the tensile strength of biomaterials thereby making the biomaterials less strong (Khan et al., 2000). The wet scaffolds were too soft to a point that the tension tensile strength could not be measured.

The compression mechanical properties of the scaffolds were evaluated and represented in the Table 5.1. Scaffolds should present adequate porosity and mechanical properties so as to prevent damage to regenerating tissue (Salerno et al., 2010). The ultimate compression strength of both scaffolds displayed a slight decrease from dry to wet state. The lack of tension tensile strength and the slight decrease in ultimate compression strength in wet scaffolds infer that the scaffold was soft enough to be applied to the wound without causing damage to skin tissues. The ultimate compression strength represents the maximum stress placed on a scaffold before it deforms completely and the compression strength of Alg-RGD-CS was found to be 0.0571 and 0.0565 MPa in dry to wet state, respectively. Unlike the tension tensile strength properties of the scaffolds, the compression strength of Alg-RGD-CS-TA was higher than that of Alg-RGD-CS with Alg-RGD-CS-TA having a compression ultimate strength of 0.07225 and 0.04698 MPa from dry wet state, respectively. The slight decrease in ultimate compression strength in Alg-RGD-CS scaffold infer that the durability of the scaffold was maintained. Alg-RGD-CS-TA scaffold exhibited a major decrease on the compressive ultimate strength from dry to wet state. The compression modulus (stiffness) and yield strength of the Alg-RGD-CS-TA scaffold decreased by more than 50% from dry to wet state. The decrease in these mechanical properties was evident of the soft nature of the scaffolds. The Young's modulus clearly exhibited the soft nature of the scaffolds which was displayed by the low stiffness (G' = 80.9 Pa for Alg-RGD-CS and 88.6 Pa for Alg-RGD-CS-TA) properties. The yield strength demonstrated the stress at which the scaffold started to deform and a decrease from 5200 Pa to 2200 Pa in Alg-RGD-CS scaffold's yield strength was observed from dry to wet state, respectively. Similarly to the yield strength of Alg-RGD-CS, the yield strength of Alg-RGD-CS-TA scaffolds also decreased from 5445 to 4200 Pa in dry and wet state, respectively. The compression distance of the scaffolds was a very useful test to gauge the extent with which the scaffold can be compressed. The Alg-RGD-CS scaffold allowed for more compression in the dry state compared to the wet state. The Alg-RGD-CS-TA scaffold on the

other hand increased compression distance from dry to wet state. This means a large quantity of the Alg-RGD-CS-TA scaffold could be compressed to fit a small wound size to act as a wound filler.

Table 5.1. Scaffold compression properties

Bioplatforms	Mechanical properties			
	Young's modulus (MPa)	Yield strength (MPa)	Ultimate Strength (MPa)	Compressive Distance (mm)
Alg-RGD-CS (Dry)	8.09E-05 ± 1.91E-05	0.0052 ± 0.0014 with 39.1 ± 0.71% strain	0.0571 ± 0.005	5.277 ± 0.2196
Alg-RGD-CS (Wet)	3.40E-05 ± 8.84E-06	0.0022 ± 0.0006 with 29.41 ± 1.45% strain	0.0565 ± 0.006	3.855 ± 0.4029
Alg-RGD-CS-TA (Dry)	8.859E-05 ± 1.0024E-05	0.00545 ± 0.00054 with 39.875 ± 0.629 strain	0.0723 ± 0.001	3.534 ± 0.1403
Alg-RGD-CS-TA (Wet)	4.457E-05 ± 9.213E-06	0.00421 ± 0.0006 with 41.75 ± 2.363 strain	0.047 ± 0.002	5.032 ± 0.1512

Properties were done in triplicates and obtained an average with ($P<0.007$).

5.3.5. Fluid absorption and degradation of the scaffolds

The scaffolds started absorbing fluid instantly from immersion in fluid and reached saturation in 8 hours for Alg-RGD-CS and 2 hours for Alg-RGD-CS-TA. Alg-RGD-CS scaffold displayed a fluid uptake of 5170% in 8 hours and reached a maximum fluid uptake of 5240% in 24 hours. Alg-RGD-CS scaffold on the other hand displayed an accelerated fluid uptake saturation with 3301% absorbed in 2 hours and a maximum of 3716% in 24hours. The Alg-RGD-CS exhibited a slightly better degradation profile compared to the Alg-RGD-CS-TA. Although the scaffolds exhibited different capabilities of fluid uptake, the amount absorbed by these scaffolds were regarded as high compared to the comparative product fluid uptake discussed in the previous chapter. This high fluid uptake property is a desirable attribute of the scaffolds as they would be able to absorb large volumes of exudate. The degradation profile of Alg-RGD-CS and Alg-RGD-CS-TA scaffolds were similar in the first three days. However, a major difference was observed from day 7 towards day 14 where the Alg-RGD-CS scaffold exhibited high degradation extent compared to the Alg-RGD-CS-TA scaffold.

The differences in degradation between the two scaffolds may been influenced by the fluid uptake capabilities. The non-crosslinked scaffold (Alg-RGD-CS) absorbed large volumes of fluid which allowed for higher hydrolytic activity during degradation. The crosslinking of the scaffold decreased the fluid uptake capabilities and introduced resistance to hydrolysis during degradation. Thus it can be assumed that the difference in the fluid uptake and degradation extent between the two scaffolds may be due to the use of tannic acid as both a crosslinker and a bioactive which decreases the degradation extent and fluid uptake in the Alg-RGD-CS-TA scaffold. These observations correlate with the reported effect of using crosslinkers in systems' capability of degrading and also fluid uptake (Demirgöz et al., 2000). The Alg-RGD-CS scaffold degraded twice as much as the Alg-RGD-CS-TA scaffold in day 14 with degradation percentages of 33.68% and 16.53%, respectively. Although the Alg-RGD-CS-TA scaffold displayed low degradation percentage, it was still comparable to the comparative product (16.26%) discussed in the previous chapters.

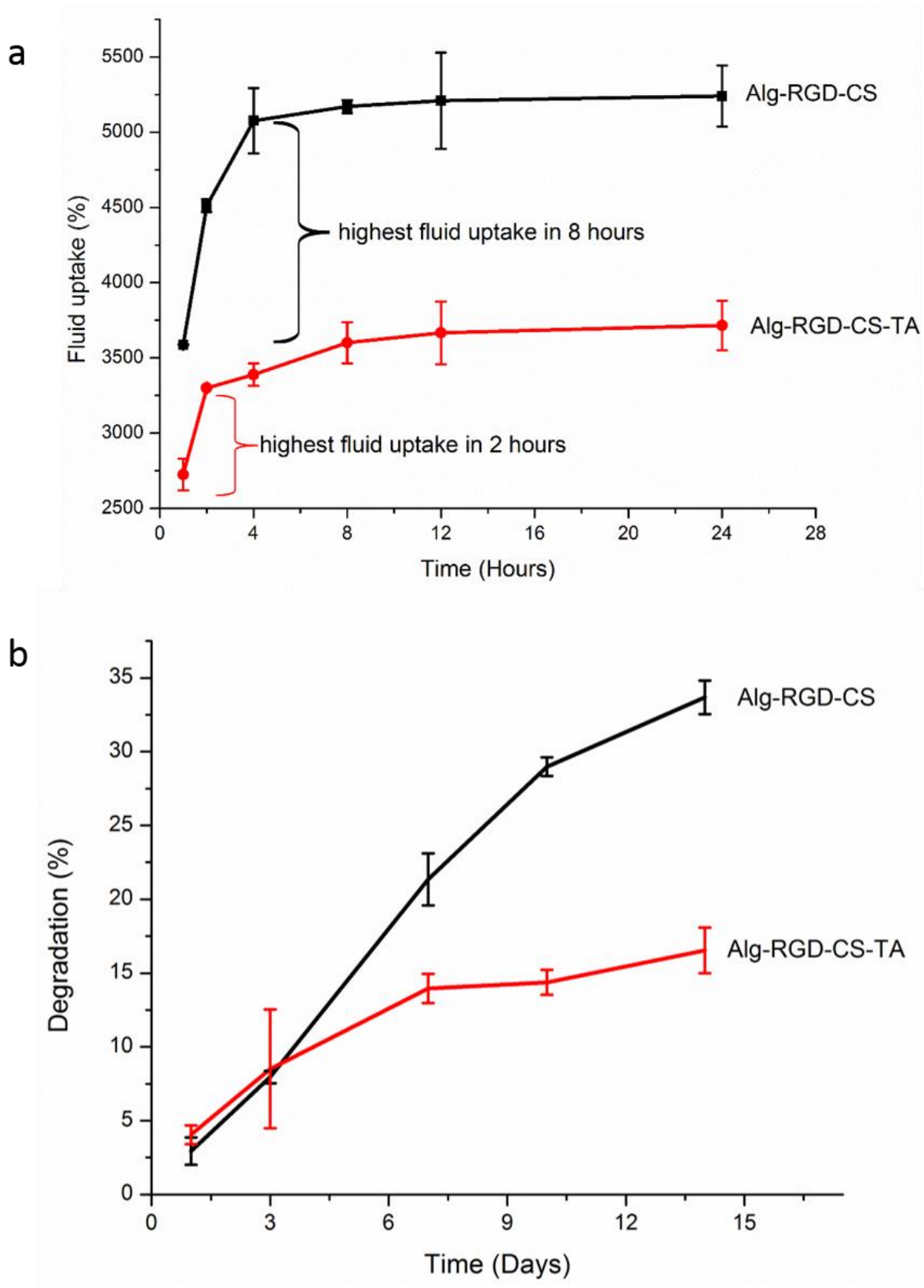


Figure 5.4. Fluid absorption and physical degradation of the scaffolds. Both assessments were done in PBS pH 7.4 at 37 °C in an orbital shaker shaking at 25 rpm.

5.3.6. UV-Vis absorption, bioactive release and *In vitro* cytocompatibility of scaffolds

UV-Vis absorption of biomolecules allows for biomolecules, complexes and formulations to be evaluated for different properties such as drug release, degradation and complexation. Herein, the UV-Vis technique was used to quantify the bioactive released from the self-assembled scaffolds. The natural polymers (chitosan and alginate) along with the RGD peptide did not exhibit any UV absorption bands. However, incubation of alginate with RGD resulted in the formation of a band at 257 nm whereas incubation of RGD with chitosan did not change the lack of absorption properties (Figure 5.5). This 257 nm Alg-RGD absorption band was also present in the Alg-RGD-CS complex. The incorporation of TA in the Alg-RGD-CS complex resulted in the complex assuming the absorption properties of TA with bands at 213 and 280 nm (Figure 5.5). Tannic acid was introduced at the final stage of the bioplatform fabrication. This allowed for TA to act as both the bioactive and a crosslinker as the OH groups of TA interacted with amine and amide groups of chitosan and the RDG peptides. Furthermore, there was intermolecular hydrogen bonding within and between TA, polymers and RGD. The carboxylic groups of alginate could also interact with the OH groups of TA thus forming more stable structures between polymers, peptide and tannic acid. The point that TA was added last to act as both a crosslinker and as a bioactive suggest that it would be released in an accelerated manner in order to respond and act immediately as an antioxidant, anti-inflammatory and a wound healing supplement.

The complexation of Alg-RGD-CS with TA allowed for an encapsulating efficiency of 86% and TA loading of 41%. The high TA loading was due to the point that TA has been reported as a non-toxic natural based polyphenol approved for human use by the FDA. Other studies have reported the use of TA at the following percentages and concentrations 0.5% $^{W}/_{V}$ (Ninan et al., 2016), 0.5, 2.5 and 5% (He et al., 2020), 0.1 g/mL (Wang et al., 2018), and 1.5 mg/mL (Natarajan et al., 2013). The varying reported TA concentrations along with their cytocompatibility and anti-microbial properties, shows that TA can induce its effect even at low concentrations such as 1.5 mg/mL and as high as concentrations 5%. Herein, 5 mg/mL (or 0.5%) was used in the study as both a crosslinker and a bioactive with an attempt to facilitate a high burst release. The TA release was carried out in PBS (pH 7.4) solution owing to the point that in deep cut wounds, blood oozes out which makes the wound milieu to be at pH 7.4 and decreases in pH to acidic conditions as the wound ages. The oozing of blood allows the scaffolds to absorb the blood along with wound exudate and wound fluid to use them for lubrication to facilitate the filling of the wound cavity with a glue like-property. In another study, it was reported that non-pH responsive hydrogels released TA in a similar profile independent of pH of the medium (Ninan et al., 2016). The addition of TA last in the fabrication steps as a both a crosslinker and a bioactive resulted in the interactions with polymers and peptide as described in the previous sections. The interactions of TA with polymers and peptide along with the fast fluid uptake property of the scaffolds contributed to the high burst release of TA. The burst release was 57.12% ± 3.214 in 24 hours, followed by gradual steady release of 8.45% ± 1.98 per day up to 90% in 5 days (Figure 5.5b). This release profile gives insight on how fast the scaffold would start to release TA to induce an effect on the lesions such as facilitating accelerated wound remodelling. The high burst release suggest that TA will have a major contribution to tissue remodelling at the early stages of wound healing. To further assess cytotoxicity of the scaffolds along with effect of TA release on cells, MTT was undertake to measure the cell viability of cells treated with scaffolds, peptide and TA over a three-day period.

The cytotoxicity of the scaffold treated cells were ranked as previously reported by Dahl *et al.,* as follows; noncytotoxic >90% cell viability, slightly cytotoxic 60%–90% cell viability, moderately

cytotoxic 30%–59% cell viability, and severely cytotoxic <30% cell viability (Dahl et al., 2006). Based on the ranking above, TA moved from moderately cytotoxic 49%) to nontoxic (113%) in 1 to 3 days, RGD moved from severely toxic (25%) to slightly toxic (64%), alginate moved from moderately cytotoxic (56%) to slightly toxic (88%) whereas chitosan remained slightly toxic (74%) over the given period (Figure 5.4c). The Alg-RGD scaffold moved from slightly toxic (63%) to nontoxic at all (117%) which attest to biocompatibility of the co-assembled scaffold. CS-RGD scaffold on the other was not as cytocompatible as Alg-RGD since it remained slightly toxic (65 to 82%) over the 3 days period. The Alg-RGD-CS scaffold moved from moderately cytotoxic (56%) to slightly toxic (84%) whereas Alg-RGD-CS-TA displayed a more favourable cellular environment with cell viability moving from slightly toxic (70%) to nontoxic at all with 100% cell viability over the three day period (Figure 5.4c). The non-toxic nature of the Alg-RGD-CS-TA scaffold was boosted by the high cytocompatibility property of TA. Notably although a high amount of TA was released in 24 hours, yet the scaffolds presented cytocompatible properties in 3T3 cells further support the non-toxic nature of TA. The increase on cell viability over the three day period attest to the cytocompatible environment provided by the scaffolds.

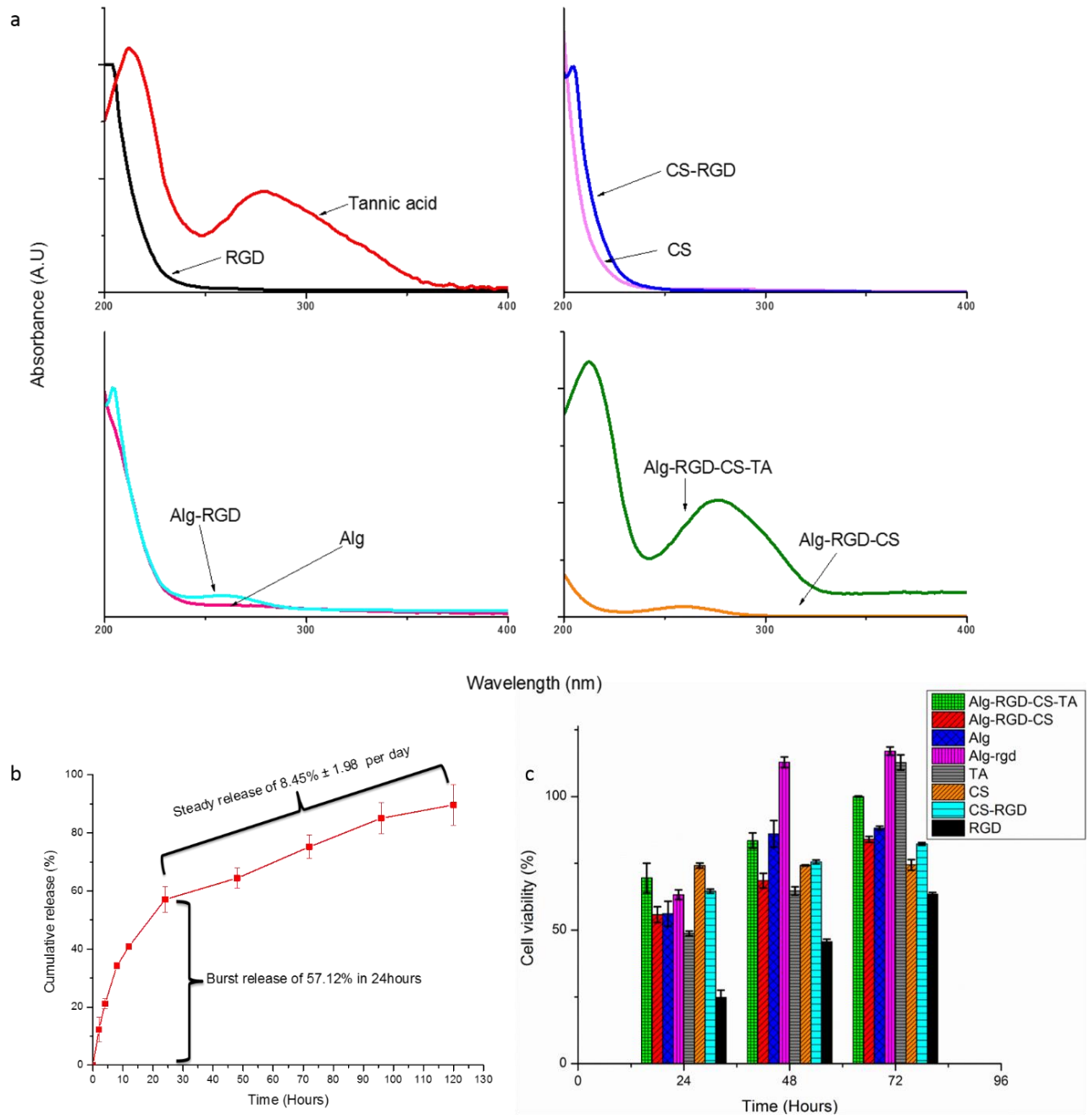


Figure 5.5. a) UV-Vis absorption of polymers, peptide and TA, b) *in vitro* cumulative TA release, and c) *in vitro* cytotoxicity evaluation of the peptide, TA and the scaffolds.

5.3.7. *In vivo* wound closure and tissue remodelling performance of the self-assembled scaffolds

Wound healing is an intricate tissue remodelling process taking place In the course of wound closure. Wound closure is one of the physical signs of wound healing. Figure 5.6 shows the extent of wound closure at each predetermined time points for each of the test and control groups. The wounds displayed several wound closure features even those which were treated with the same bioplatform. Thus the mode appearance of wounds was used to describe the overall

performance of each test or control group. The mode appearance was represented in a table format (Figure 5.6a&b) and the extent of wound closure was represented graphically (Figure 5.6b). Both scaffolds (Alg-RGD-CS and Alg-RGD-CS-TA) exhibited accelerated early stage wound healing as they both had more than 55% wound closure after the wounds were allowed for wound healing over three days (Figure 5.6). The comparative commercial product showed better wound healing signs than the control (untreated) group. However, they both displayed less than 20% wound closure after 3 days of wound healing. The superiority performance of scaffolds at the early stages of wound healing was due to the use of natural polymers known for their biocompatibility and excellent wound healing performances, RGD which is known to bind to integrins to facilitate collagen deposition and also a contribution from TA known for its excellent anti-inflammatory, anti-oxidant and tissue remodelling properties.

All wounds displayed more than 50% wound closure after 7 days, with the scaffolds having the highest wound closure percentages followed by the commercial product and the control group. The same observations were also made after 10 days wound healing. All the treatment groups displayed 100% wound closure whilst the control displayed 98% wound closure after 14 days of wound healing. Although the wound closure was 100% on the treatment groups, the quality of the healed wounds was different. There was no scar tissue or sign of a lesion on the site where the wound was created on the animals treated with the Alg-RGD-CS scaffold whereas Alg-RGD-CS scaffold displayed bruise like appearance after 14 days wound healing. A bruise like appearance and in other cases a scar was observed on the animals treated with commercial product and the control groups (Figure 5.6a). This further attest to the high quality of wound closure attributes unique to the scaffolds. The difference on the wound appearance was one of the signs of accelerated wound healing on the surface. The wound remodelling at the epidermis and dermis was further investigated to evaluate the extent and quality of wound healing performances of the test and control groups. Automated Haematoxylin and Eosin (H&E) tissue staining was employed in skin tissues. This was followed by qualitatively grading lesions on the following five features; (1) Epithelisation, Epidermal-dermal attachment, Angiogenesis, Mononuclear leukocytes, and Fibroblasts reaction as discussed in the previous chapter.

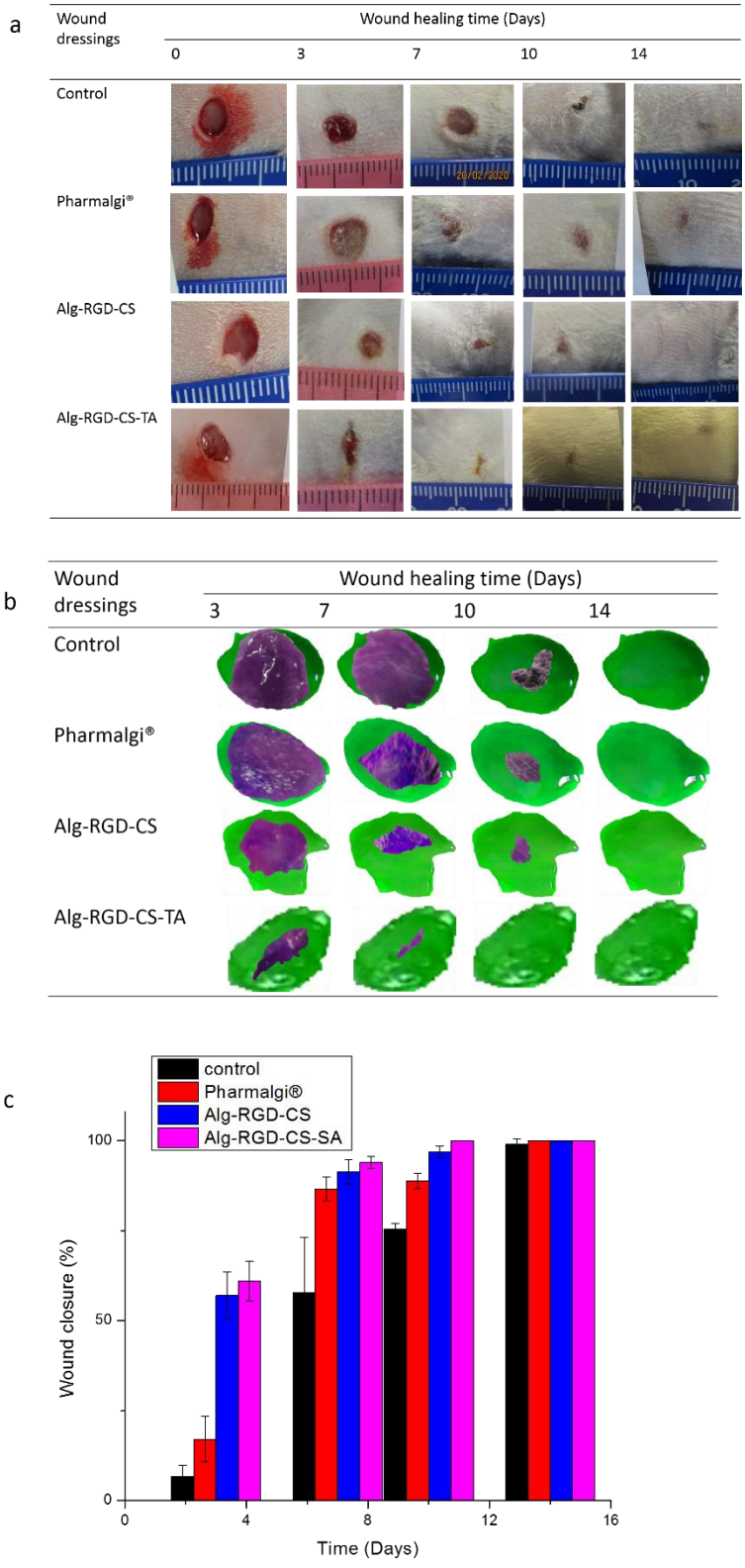


Figure 5.6. *In vivo* performance of the bioplatforms and commercial product. (a) Wound closure images of SD rats treated with the scaffold and allowed to heal over a 14 day period. (b) and (c) are a graphical representation of wound closure kinetics of rats treat with test and control groups. The wound healing rate

was calculated by employing the following equation: wound closure (%) = $((A_0 - A_t)/A_0)X\ 100$, where A_0 represents the area of the original wound and A_t represents the area of the wound at the testing time (days). The diameter and area of the lesions were calculated using the IMAGEJ software.

Early wound healing effect of scaffolds on lesions

The lesions displayed varying morphological features even in cases where the same test scaffold was used. Therefore, the mode appearance of the lesions treated with each group was used to describe the overall test group performance at each of the predetermined wound healing time points. The early wound healing effect of the scaffolds was evaluated after 3 days of healing. At this stage of wound healing, the covering epidermis over the wound treated with Alg-RGD-CS scaffold was complete and mildly hyperplastic and the underlying dermis showed normal appearances although had a slightly more haphazard arrangement of dermal collagen with regularly interspersed and arranged pilosebaceous units. The superficial subcutis exhibited a mild perivascular reaction in which small numbers of fibroblasts and moderate numbers of lymphocytes were present accompanied by few macrophages. There was a moderate to fairly linear fibroblastic reaction visible between the edges of the damaged muscle layers filling the defect and associated with few hypertrophic skeletal muscle fibres (Figure 5.7c). In the deep subcutis beneath the muscle, a severe granulation tissue reaction was present and it consisted of moderately cellular haphazardly arranged fibroblasts accompanied by moderate numbers of dilated and congested capillaries. Mild collagen presence was visible also present. Small numbers of lymphocytes and macrophages had infiltrated in the granulation tissue reaction and in other areas they formed small aggregates accompanied by epitheloid macrophages. Similarly to Alg-RGD-CS treated lesions, Alg-RGD-CS-TA treated lesions also displayed complete epidermal attachment. Furthermore, the surface of the lesions exhibited minimal serocellular crusts. However, the skin surface was completely covered by intact, attached and mildly hyperplastic epidermis. The lesion showed slightly haphazard dermal collagen with an otherwise fairly normal appearance with few fibroblasts remaining just beneath the epidermis (Figure 5.7d). In the underlying subcutaneous, muscle layers (involving the damaged edges) infiltration by haphazard fibroblasts were observed. Small numbers of lymphocytes and macrophages were also visible, especially around mildly proliferative and congested deep subcutaneous blood vessels beneath the damaged muscle layer.

Contrary to the Alg-RGD-CS and Alg-RGD-CS-TA treated lesions, the wounds treated with the comparative commercial product displayed an ulcerated surface associated with underlying severe necrosis in the dermis accompanied by presence of multiple aggregates of serum-like lightly eosinophilic to slightly basophilic material surrounded by a single layer of macrophages. There was moderate presence of neutrophils in the necrotic tissue and in the underlying deep dermis and subcutis fibroplasia was also of a moderate degree accompanied by numerous capillary structures. The fibroblastic reaction and inflammation extended through a defect in the underlying superficial muscle layer which was also damaged, into the deep subcutis (Figure 5.7b). Moderate presence of lymphocytes plasma cells and macrophages was visible in the deep areas as well. Few small areas of calcified material were visible in the deep subcutis surrounded by granulomatous inflammation. Similarly to the commercial product treated lesions, the control group did not show any epidermal to dermal attachment due to the complete loss of both epidermis and dermis tissues. The edge of the ulcer was sharply demarcated from the surrounding tissues and the adjacent epidermis was moderately hyperplastic. The ulcer bed had fibrinous material in small amounts multifocally as well as few loose red blood cells. The wound extended to the subcutis and there was complete loss of the epidermal and dermal tissues. There

was a complete full thickness defect involving the whole muscle layer and muscle edges being far apart. The fibroblastic reactions were present in the above and below subcutis and also infiltrated the damaged muscle edges (Figure 5.7a). The reaction shows minimal central deep subcutaneous arrangement in the appearance of early granulation tissue formation. Collagen was scant. The inflammation was mild, but more prominent close to the ulcerated surface and lymphohistiocytic infiltrates were accompanied by single multinucleate giant cells and neutrophils.

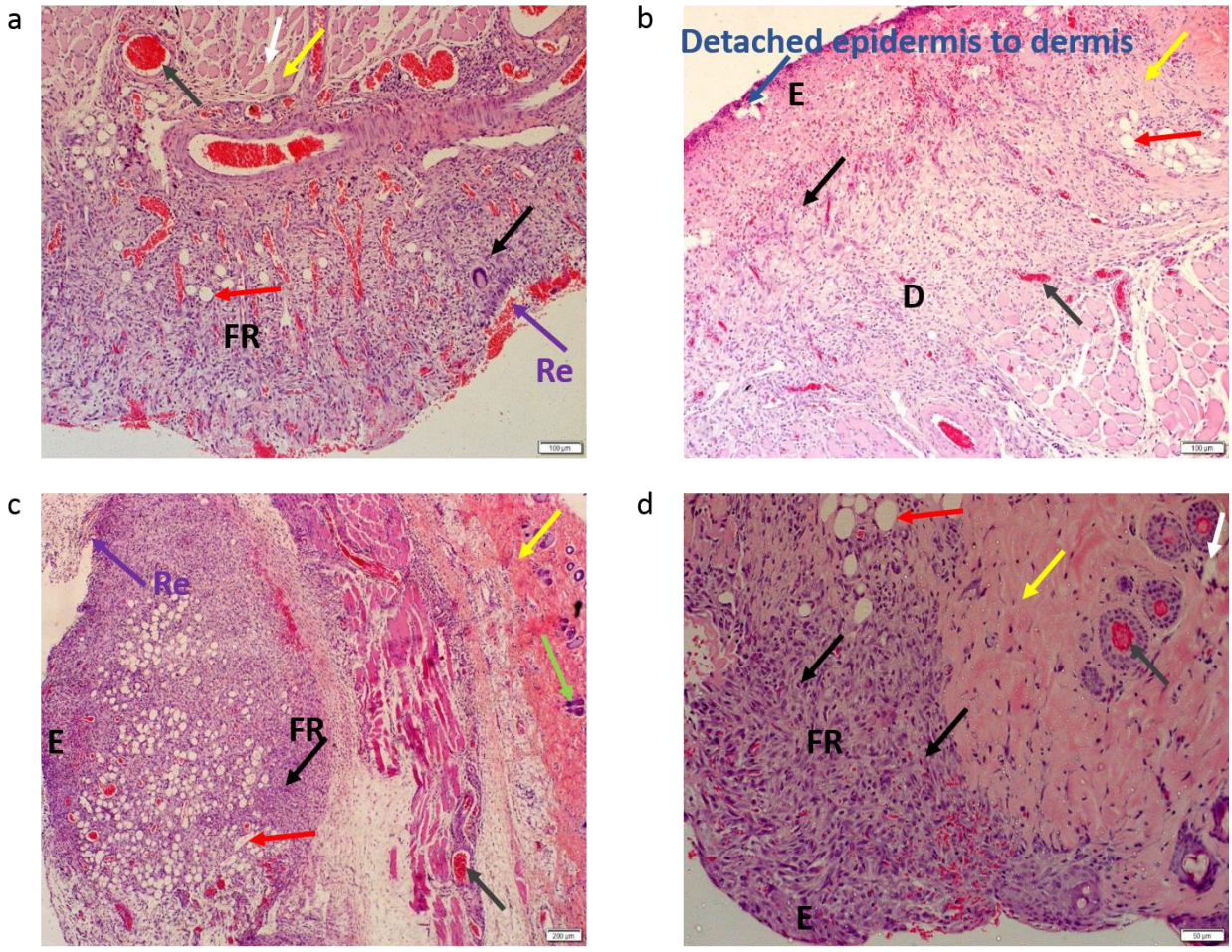


Figure 5.7. Early wound healing stage of tissues treated with different groups of bioplatforms. Histology of the wound tissues (a) Control group, (b) the comparative product treated group, (c) is the PC Alg-CS treated group, and (d) is the PC FAC-CS-Alg treated group. The images of the control group and PC CS-Alg group were viewed at 200X magnification whereas the comparative product and PC FA-CS-Alg groups were viewed at 100X magnification. E denotes epidermis development and D represent the dermis layer. FR denotes fibroblast reaction with collagen bundles labelled in yellow arrow, the grey arrow indicates the red blood cells materials and the purple arrow shows the regenerating edge. The plasma inflammatory cells are indicated by the black arrow, while the blood vessels are indicated by the red arrow and the green arrow indicates hair follicles while the white arrow shows capillaries.

Early-to-mid phase wound healing effect of the scaffolds on lesions

The early-to-mid phase of wound healing was observed after 7 days of wound healing. At this stage of wound healing, the margins of the control wound showed epidermal hyperplasia of a mild

to moderate degree with early partially attached sliding of the peripheral covering epidermis along the surface ulceration (Figure 5.8a). The epithelialisation was scant and only evident on the edges of the ulcerated region, which infers that the tissue remodelling started at the edges of the lesions. There was loss of dermal structures in the deep dermis and subcutis along with the muscle layer showing moderately cellular, haphazard arranged fibroblastic infiltrates. These were accompanied by few capillaries and mild interstitial to perivascular infiltration by lymphocytes and macrophages as well as scattered single neutrophils and plasma cells (Figure 5.8a). In the deep subcutis inflammatory cells especially lymphoplasmacytic cells became more prominent. Superficially, few multinucleate giant cells were present. Similarly to the control group, the wound treated with the comparative product displayed an early advancing of the hyperplastic epidermis from the wound edges onto the ulcerated surface. Unlike the control group, the comparative product treated lessions exhibited a fully attached epidermis to the underlying dermal granulation tissue reaction (Figure 5.8b). This reaction displayed moderate amounts of collagen in between the horizontally arranged fibroblasts and moderate amounts of vertical perpendicular capillaries (Figure 5.8b). In the subcutis, the reaction appeared uniform but more haphazard, and few to moderate numbers of inflammatory cells were visible, mostly lymphocytes and macrophages as well as scattered mast cells and neutrophils. Few small areas of calcification were present in the dermal granulation tissue. There was no defect in the superficial muscle layer and no signs of fibroblastic infiltration into this layer.

The wound treated with Alg-RGD-CS displayed re-epithelialisation from the edges covering a large proportion of the ulcer, but one small area remained completely ulcerated. The one advancing edge of re-epithelialisation was unattached to the underlying granulation tissue. This epithelial reaction was mildly hyperplastic. The underlying dermal granulation tissue consisted of horizontally arranged fibroblasts accompanied by small capillaries that become more prominent in the subcutis (Figure 5.8c). Moderate amounts of collagen were visible and became more prominent in the subcutis. Inflammation was minimal in the dermal granulation tissue reaction but became mild in the subcutaneous more haphazard fibroblastic reaction. The fibroblast reaction consisted of a mixture of lymphocytes plasma cells macrophages and mast cells. The reaction extended in between the retracted muscle edges and into the deeper subcutis. Haphazard fibrosis was also seen in the damaged muscle edges. At this stage of wound healing, the Alg-RGD-CS-TA treated group displayed a better performance compared to the Alg-RGD-CS treated group. The wounds treated with Alg-RGD-CS-TA displayed a completely covered epidermis, there was no ulcer/defect remaining and the covering epidermis was mildly hyperplastic. Horizontally collapsed embedded hair follicles were visible forming a linear reaction embedded in the fibroblastic reaction in the dermis and subcutis and some follicles even extended in between the retracted muscle edges from the damaged muscle layer (Figure 5.8d). Some of those follicles were dilated and had hair shafts. The fibroblastic reaction in which they were embedded was mostly haphazard although in the dermis it had a horizontal arrangement pattern. Capillaries were minimal and mostly present in between the muscle edges in the deep subcutis (Figure 5.8d). Small numbers of lymphocytes macrophages and multinucleate giant cells were visible in the deep subcutis and in the dermis few mast cells were also present.

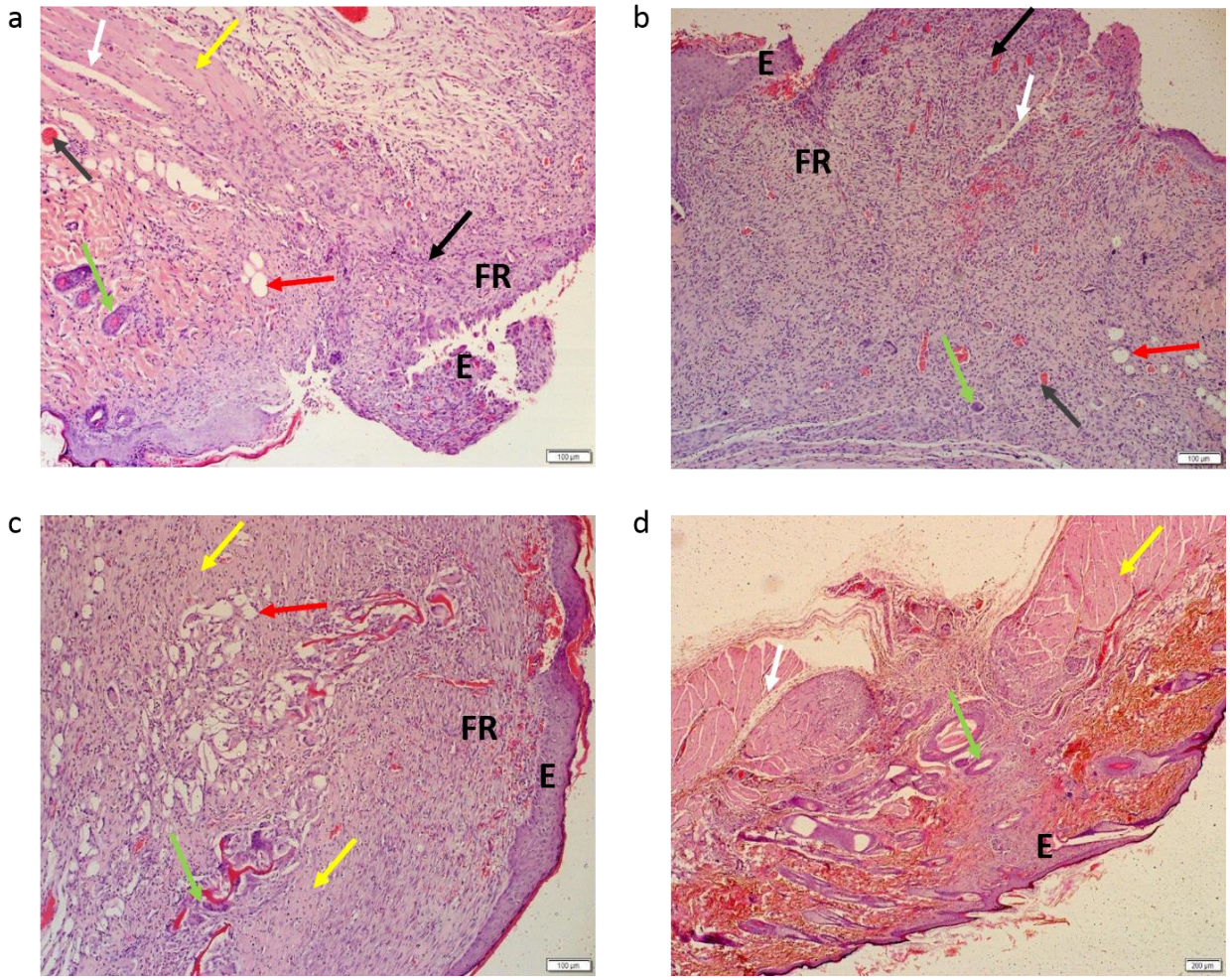


Figure 5.8. Mid wound healing stage of tissues treated with different groups of bioplatforms. Histology of the wound tissues (a) Control group, (b) the comparative product treated group, (c) PC Alg-CS treated group, and (d) PC FAC-CS-Alg treated group. The images of the control group and PC FA-CS-Alg treated group were viewed at 200X magnification whereas the Pharmalgi® and PC CS-Alg treated groups were viewed at 100X magnification. FR denotes fibroblast reaction. The plasma inflammatory cells are indicated by the black arrow, while the blood vessels are indicated by the red arrow. The green arrow show hair follicles, white arrow shows capillaries.

Mid to late wound healing effect of the scaffolds on lesions

The mid-to-late phase of wound healing was observed after 10 days wound healing. At this stage of wound healing, Alg-RGD-CS treated tissues exhibited an intact and moderately to completely covered hyperplastic epidermis and also attached to the underlying dermal fibroblastic reaction which was haphazardly arranged and accompanied by moderate numbers of collagen fibres and prominent capillaries (Figure 5.9c). The fibroblastic reaction extended into the subcutis where it was more horizontally arranged, with few areas still slightly disorganised. Single multinucleate giant cells, lymphocytes and macrophages were also observed mostly surrounding refractory material suggestive of small hair shaft fragments. The dermal fibroblastic reaction was discreetly nodular and replaced several pilosebaceous units at this stage. Similarly to observations made at the early-to-mid phase of wound healing, the Alg-RGD-CS-TA displayed better wound healing performance than Alg-RGD-CS. The wound treated with Alg-RGD-CS-TA displayed the covering

epidermis overlying the wound being hyperplastic and completely covering the region and was completely attached to the underlying granulation tissue reaction in the dermis (Figure 5.9d). This dermal reaction consisted of horizontally arranged fibroblasts with interspersed collagen and vertical perpendicular capillaries which were less prominent. In the subcutis and in between the damage muscle edges the fibroblastic reaction was haphazardly arranged and moderately cellular with very few single lymphocytes and macrophages present.

The wounds treated with the scaffolds (Alg-RGD-CS or Alg-RGD-CS-TA) displayed superior performance compared to the control and the compartive product treated tissues. The control samples displayed focal ulceration associated with serocellular crusting in the ulcer bed. Peripheral mild epithelialisation was also observed and the epidermis was mildly hyperplastic. In the underlying dermis horizontal to haphazard fibrosis, fibrosis was accompanied by haphazard fibroplasia extending into the subcutis. Mild capillary was also observed especially underlying the area of ulceration (Figure 5.9a). Minimal lymphocytes plasma cells and macrophages were also present in the subcutaneous fibroblastic reaction. The comparative commercial product had lesion that was partially covered by mildly hyperplastic epidermis and it also exhibited partial attachment of the epidermis to the underlying fibrosing dermis (Figure 5.9b). There was mild serocellular crusting within peripheral parts of the ulcer bed. The horizontal fibrosis in the dermis was accompanied by mild capillary formation and in the subcutis the fibroblastic reaction was haphazardly arranged and accompanied by small numbers of lymphocytes plasma cells epitheloid macrophages and few multinucleate giant cells (Figure 5.9b). Dilated cavities lined by flattened histiocytic cells were present in the subcutaneous fibroblastic reaction, and those spaces contained basophilic fibrillar material. The underlying muscle layer was still damaged and the 2 edges were associated with a fibroblastic reaction that was continuous with the subcutaneous reaction and also associated with small numbers of epitheloid macrophages and multinucleate giant cells. These findings further attest to the scaffolds being the superior wound dressing with accelerated wound healing performances compared to the control and the comparative commercial product.

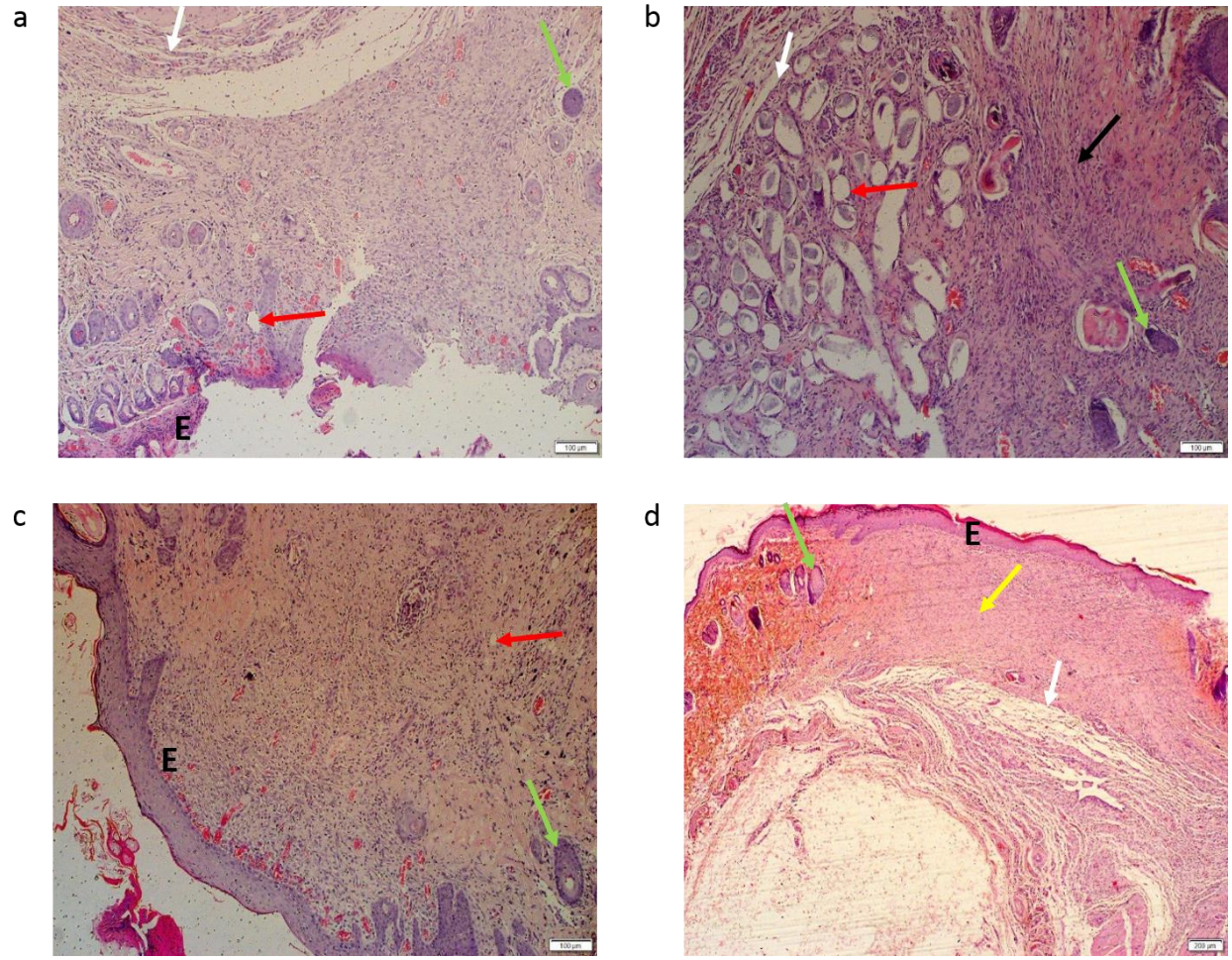


Figure 5.9. Mid-to-late wound healing stage of tissues treated with different groups of bioplatforms. Histology of the wound tissues (a) Control group, (b) comparative product treated group, (c) PC Alg-CS treated group, and (d) PC FAC-CS-Alg treated group viewed at 100X magnification except for the comparative product treated tissues which were viewed at 200X magnification. The grey arrow indicates the red blood cells materials. The plasma inflammatory cells are indicated by the black arrow, while the blood vessels are indicated by the red arrow. The green arrow show hair follicles, white arrow shows capillaries.

Late wound healing effect of the scaffolds on lesions

The late phase of wound healing was observed after 14 days of wound healing. At this stage of wound healing, the wounds were older and the features of the wounds were moving towards full regeneration. Similarly to the observations made at day 10 (mid-late phase wound healing), the Alg-RGD-CS scaffolds displayed complete re-epithelialisation of the lesion and the covering epidermis was mildly hyperplastic (Figure 5.10c). The haphazard fibrosis in the dermis was visible between the adnexal structures with no clear loss of pilosebaceous units (they appeared regularly arranged). Single macrophages and multinucleate giant cells were visible in the subcutaneous haphazard fibroblastic reaction that also extended into the small defect in the underlying superficial muscle layer. Minimally hyperplastic was observed on the epidermis with no loss of surface epithelium at this stage. It also appeared completely attached to the underlying

immediately adjacent dermis where few odd interstitial lymphoplasmacytic cells were visible. The lesions treated with the Alg-RGD-CS-TA appeared predominantly normal with a focal area of mild epidermal hyperplasia and a small underlying localised area where the dermal collagen was increased without regularly positioned pilosebaceous units in this small region. Although the wound closure displayed complete closure and neither scar nor sign of wound was seen in Alg-RGD-CS treated group and Alg-RGD-CS-TA which was indicative of enhanced wound healing performances in wound's depth.

The performance of the scaffold was far superior to the control and comparative groups. The control group displayed horizontal fibroblastic reaction in the dermis causing mild thinning of the dermal layer and it extended up to the intact mildly hyperplastic epidermis overlying the wound. Inflammation was more haphazard in the subcutis. The whole fibroblastic reaction consisted of moderate interstitial presence of lymphocytes and macrophages with several epitheloid macrophages and multinucleate giant cells. In other areas re-epithelialisation was present on the margins of the lesion (Figure 5.10a). However, it was multifocally unattached to the underlying dermis and it also showed a central remaining ulcerative defect not covered by the surrounding mildly hyperplastic epidermis. The defect in the dermis was filled with haphazard fibroblasts and no pilosebaceous units were present in that region. Similar to the scaffold test groups, the comparative commercial product also displayed complete re-epithelialisation of the lesion and the covering epidermis was mildly hyperplastic (Figure 5.10b). There was a focal area in the dermis, consisting of what appeared to be loss of a single pilosebaceous unit in the dermis where a thin vertical strip of fibrosis was present extending from the hyperplastic epidermis into the subcutis. It contained single mast cells and lymphocytes. In the subcutis fibrosis was more extensive and haphazard, and covered the small defect remaining in the deeper muscle layer. Few lymphocytes were visible deep to that area of fibrosis.

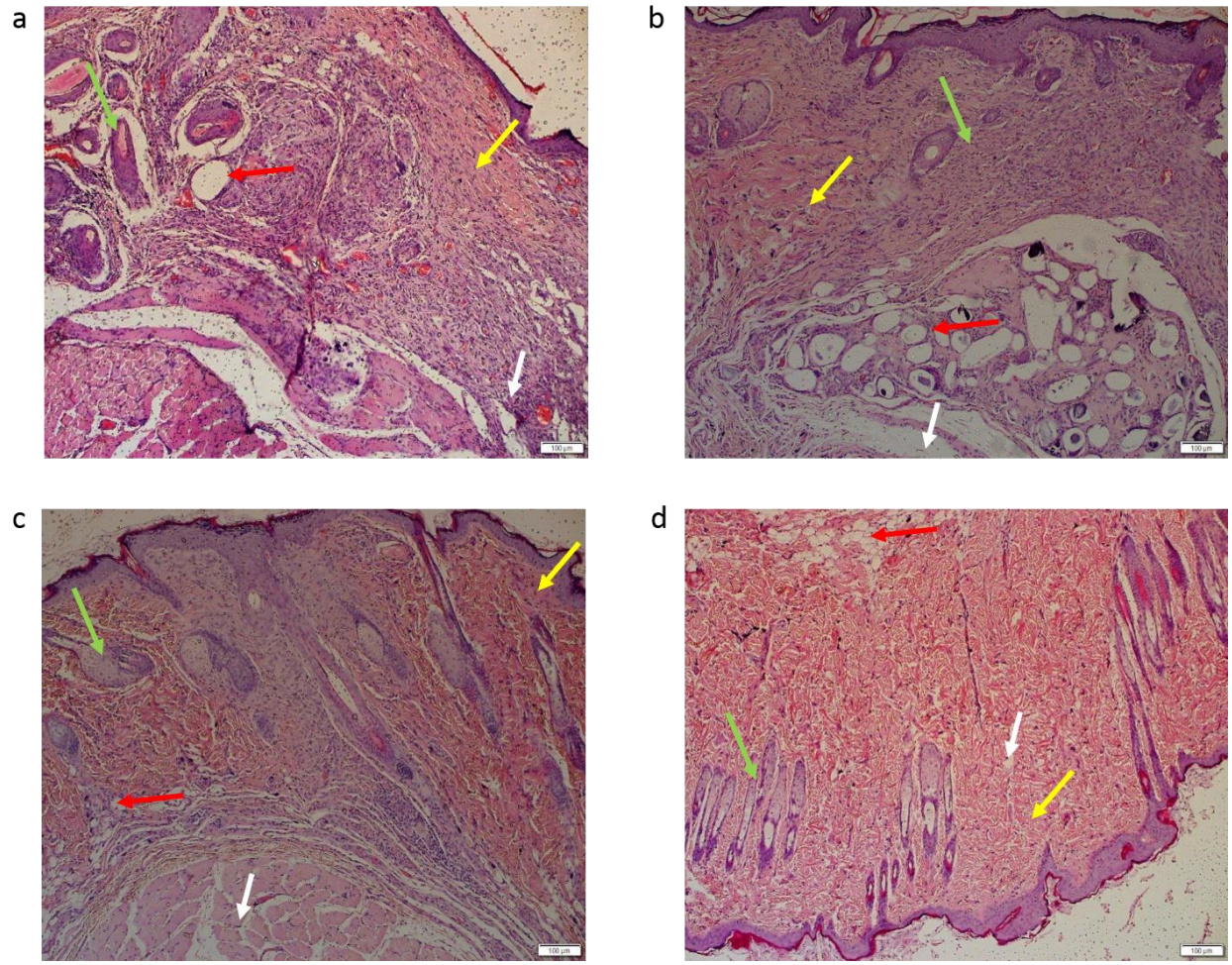


Figure 5.10. Late wound healing stage of tissues treated with different groups of bioplatforms. Histology of the wound tissues (a) Control group, (b) the comparative product group, (c) PC Alg-CS treated group, and (d) PC FAC-CS-Alg treated group viewed at 100X magnification. Collagen bundles are labelled in yellow arrow. The plasma inflammatory cells are indicated by the black arrow, while the blood vessels are indicated by the red arrow.

Based on the morphological features of the lesions discussed above, it is apparent that both scaffold treated groups had superior early wound healing performance relative to the comparative product and the control group. These accelerated wound healing performances includes fibroblast reactions, angiogenesis, and epidermal-dermal attachment on the test groups which are the signs of regenerating tissues (Pastar et al., 2014, Nishiyama et al., 2000, Velnar and Gradisnik, 2018). These observations correlate with the accelerated early wound closure performance of scaffold treated groups described in Figure 5.6 above. It is evident that the biocompatibility of the scaffolds played a role in accelerating tissue remodelling and early wound healing performances. The high prevalence of inflammatory cells and large blood vessels in Alg-RGD-CS-TA treated lesions suggest that there was enhanced tissue remodelling on the wound (Figure 5.7d). The development of hair follicle was also indicative of the accelerated wound repair property of Alg-RGD-CS (Figure 5.7c). All treatment groups, Alg-RGD-CS, Alg-RGD-CS-TA, and the comparative product treated lessions displayed better early tissue remodeling performances compared to the control group.

The overall performance of the test groups at the early-to-mid stage of wound healing was more pronounced compared to the early stages of wound healing discussed above. These performances includes the comparable performance between the comparative product and Alg-RGD-CS which were far better than the control group but not as excellent as the performance of Alg-RGD-CS-TA which displayed advanced tissue regenerative capabilities. These tissue regenerating capabilities had the Alg-RGD-CS-TA treated lesions showing no defect at all. The scaffolds and comparative product displayed high level of tissue regeneration compared to the control group at the mid and late stages of wound healing. The Alg-RGD-CS-TA scaffold had healed completely and resembled normal skin. The control and comparative product treated lesions displayed epidermal thinning which were indicative of scarring (Dale et al., 1996). Given the histological evaluation above, it is evident that the scaffolds displayed more favourable wound remodelling and tissue regenerative performance compared to the control and the comparative commercial product.

5.4. Concluding remarks

The study has demonstrated the design of self-assembled hybrid scaffolds for wound healing and tissue regeneration. Polymeric self-assembly, peptide self-assembly and the co-assembly of peptide-polymer scaffolds was investigated. Morphological features of the self-assembled scaffolds and co-assembled scaffolds were evaluated. The co-assembly resulted in the change on the 3-D architecture of the scaffolds from vertically aligned sheets to horizontal aligned sheets in Alg-RGD and the opposite arrangement was observed in CS-RGD scaffolds. Chemical and thermo-stability properties of the scaffolds were not highly affected by the co-assembly due to low RGD to polymer ratios. Mechanical properties of the scaffolds were improved by crosslinking the scaffolds. These mechanical properties included the tension tensile strength and compressive storage modulus, yield strength, ultimate strength and the compressive distance. The use of TA as both a crosslinker and a bioactive allowed for high encapsulation efficiency and high burst release in less than 24 hours necessitating the anti-inflammatory and antioxidant properties of TA to be induced at early stages of wound healing. The release of TA allowed for enhanced cytocompatibility of the scaffolds. The accelerated tissue remodelling property of the scaffolds at the early stages of wound healing were complemented by the released TA. The scaffolds displayed superior wound healing and skin tissue regeneration performance at all stages of wound healing compared to the comparative and the control groups. The quality of the regenerated tissues was important because the goal was to regenerate skin tissue to normal appearance and this was observed on the scaffolds tested in the current study which displayed normal appearance and no scar tissue was observed after 14 days of wound healing. The use of natural polymers, peptide, and tannic acid produced desirable properties and performances for application in both wound healing and drug delivery.

5.5. References

Abdillahi, S. M., Balvanović, S., Baumgarten, M. & Mörgelin, M. 2012. Collagen VI encodes antimicrobial activity: novel innate host defense properties of the extracellular matrix. *Journal of innate immunity,* 4**,** 371-376.

Ahmed, S. & Ikram, S. 2016. Chitosan based scaffolds and their applications in wound healing. *Achievements in the life sciences,* 10**,** 27-37.

Akiyode, O. & Boateng, J. 2018. Composite biopolymer-based wafer dressings loaded with microbial biosurfactants for potential application in chronic Wounds. *Polymers,* 10**,** 918.

Baek, K. Y., Kamigaito, M. & Sawamoto, M. 2002. Synthesis of star-shaped copolymers with methyl methacrylate and n-butyl methacrylate by metal-catalyzed living radical polymerization: Block and random copolymer arms and microgel cores. *Journal of Polymer Science Part A: Polymer Chemistry,* 40**,** 633-641.

Beck, C. S. & Powers, J. H. 1926. Burns treated by tannic acid. *Annals of surgery,* 84**,** 19.

Bini, E., Foo, C. W. P., Huang, J., Karageorgiou, V., Kitchel, B. & Kaplan, D. L. 2006. RGD-functionalized bioengineered spider dragline silk biomaterial. *Biomacromolecules,* 7**,** 3139-3145.

Caetano, G. F., Frade, M. A. C., Andrade, T. A. M., Leite, M. N., Bueno, C. Z., Moraes, Â. M. & Ribeiro-Paes, J. T. 2015. Chitosan-alginate membranes accelerate wound healing. *Journal of Biomedical Materials Research Part B: Applied Biomaterials,* 103**,** 1013-1022.

Chandrasekaran, A. R., Jia, C. Y., Theng, C. S., Muniandy, T., Muralidharan, S. & Dhanaraj, S. A. 2011. Invitro studies and evaluation of metformin marketed tablets-Malaysia. *Journal of applied pharmaceutical science,* 1**,** 214.

Chang, A. B., Lin, T.-P., Thompson, N. B., Luo, S.-X., Liberman-Martin, A. L., Chen, H.-Y., Lee, B. & Grubbs, R. H. 2017. Design, synthesis, and self-assembly of polymers with tailored graft distributions. *Journal of the American Chemical Society,* 139**,** 17683-17693.

Cowen, S. & Al-Abadleh, H. A. 2009. DRIFTS studies on the photodegradation of tannic acid as a model for HULIS in atmospheric aerosols. *Physical Chemistry Chemical Physics,* 11**,** 7838-7847.

Dahl, J. E., Frangou-Polyzois, M. J. & Polyzois, G. L. 2006. In vitro biocompatibility of denture relining materials. *Gerodontology,* 23**,** 17-22.

Dai, M., Zheng, X., Xu, X., Kong, X., Li, X., Guo, G., Luo, F., Zhao, X., Wei, Y. Q. & Qian, Z. 2009. Chitosan-alginate sponge: preparation and application in curcumin delivery for dermal wound healing in rat. *BioMed Research International,* 2009.

Dale, P. D., Sherratt, J. A. & Maini, P. K. 1996. A mathematical model for collagen fibre formation during foetal and adult dermal wound healing. *Proceedings of the Royal Society of London. Series B: Biological Sciences,* 263**,** 653-660.

Dart, A., Bhave, M. & Kingshott, P. 2019. Antimicrobial Peptide-Based Electrospun Fibers for Wound Healing Applications. *Macromolecular bioscience,* 19**,** 1800488.

Demirgöz, D., Elvira, C., Mano, J. F., Cunha, A. M., Piskin, E. & Reis, R. L. 2000. Chemical modification of starch based biodegradable polymeric blends: effects on water uptake, degradation behaviour and mechanical properties. *Polymer Degradation and Stability,* 70**,** 161-170.

Di Foggia, M., Taddei, P., Torreggiani, A., Dettin, M. & Tinti, A. 2011. Self-Assembling Peptides for Biomedical Applications: IR and Raman Spectroscopies for the Study of Secondary Structure. *Proteomics Research Journal,* 2**,** 231.

Eskandari, S., Guerin, T., Toth, I. & Stephenson, R. J. 2017. Recent advances in self-assembled peptides: Implications for targeted drug delivery and vaccine engineering. *Advanced drug delivery reviews,* 110**,** 169-187.

Falcão, L. & Araújo, M. E. M. 2014. Application of ATR–FTIR spectroscopy to the analysis of tannins in historic leathers: the case study of the upholstery from the 19th century Portuguese Royal Train. *Vibrational Spectroscopy,* 74**,** 98-103.

Fichman, G. & Gazit, E. 2014. Self-assembly of short peptides to form hydrogels: Design of building blocks, physical properties and technological applications. *Acta biomaterialia,* 10**,** 1671-1682.

Gupta, S., Singh, I., Sharma, A. K. & Kumar, P. 2020. Ultrashort peptide self-assembly: Front-runners to transport drug and gene cargos. *Frontiers in bioengineering and biotechnology,* 8.

Guven, S., Chen, P., Inci, F., Tasoglu, S., Erkmen, B. & Demirci, U. 2015. Multiscale assembly for tissue engineering and regenerative medicine. *Trends in biotechnology,* 33**,** 269-279.

He, X., Liu, X., Yang, J., Du, H., Chai, N., Sha, Z., Geng, M., Zhou, X. & He, C. 2020. Tannic acid-reinforced methacrylated chitosan/methacrylated silk fibroin hydrogels with multifunctionality for accelerating wound healing. *Carbohydrate Polymers***,** 116689.

Hersel, U., Dahmen, C. & Kessler, H. 2003. RGD modified polymers: biomaterials for stimulated cell adhesion and beyond. *Biomaterials,* 24**,** 4385-4415.

Hoffman, A. S. 2012. Hydrogels for biomedical applications. *Advanced drug delivery reviews,* 64**,** 18-23.

Hong, H.-J., Jin, S.-E., Park, J.S., Ahn, W. S. & Kim, C.K. 2008. Accelerated wound healing by smad3 antisense oligonucleotides-impregnated chitosan/alginate polyelectrolyte complex. *Biomaterials,* 29**,** 4831-4837.

Hosoyama, K., Lazurko, C., Muñoz, M., Mctiernan, C. D. & Alarcon, E. I. 2019. Peptide-based functional biomaterials for soft-tissue repair. *Frontiers in Bioengineering and Biotechnology,* 7**,** 205.

Jing, J., Liang, S., Yan, Y., Tian, X. & Li, X. 2019. Fabrication of Hybrid Hydrogels from Silk Fibroin and Tannic Acid with Enhanced Gelation and Antibacterial Activities. *ACS Biomaterials Science & Engineering,* 5**,** 4601-4611.

Khan, T. A., Peh, K. K. & Ch'ng, H. S. 2000. Mechanical, bioadhesive strength and biological evaluations of chitosan films for wound dressing. *J Pharm Pharm Sci,* 3**,** 303-311.

Kim, T., Silva, J., Kim, M. & Jung, Y. 2010. Enhanced antioxidant capacity and antimicrobial activity of tannic acid by thermal processing. *Food Chemistry,* 118**,** 740-746.

Kozlovskaya, V., Kharlampieva, E., Drachuk, I., Cheng, D. & Tsukruk, V. V. 2010. Responsive microcapsule reactors based on hydrogen-bonded tannic acid layer-by-layer assemblies. *Soft Matter,* 6**,** 3596-3608.

Kozlovskaya, V., Zavgorodnya, O., Chen, Y., Ellis, K., Tse, H. M., Cui, W., Thompson, J. A. & Kharlampieva, E. 2012. Ultrathin polymeric coatings based on hydrogen-bonded polyphenol for protection of pancreatic islet cells. *Advanced functional materials,* 22**,** 3389-3398.

Lawrie, G., Keen, I., Drew, B., Chandler-Temple, A., Rintoul, L., Fredericks, P. & Grøndahl, L. 2007. Interactions between alginate and chitosan biopolymers characterized using FTIR and XPS. *Biomacromolecules,* 8**,** 2533-2541.

Li, B., Chen, J. & Wang, J. H. C. 2006. RGD peptide-conjugated poly (dimethylsiloxane) promotes adhesion, proliferation, and collagen secretion of human fibroblasts. *Journal of Biomedical Materials Research Part A,* 79**,** 989-998.

Li, N., Yang, X., Liu, W., Xi, G., Wang, M., Liang, B., Ma, Z., Feng, Y., Chen, H. & Shi, C. 2018. Tannic acid cross-linked polysaccharide-based multifunctional hemostatic microparticles for the regulation of rapid wound healing. *Macromolecular Bioscience,* 18**,** 1800209.

Ma, L., Yu, W. & Ma, X. 2007. Preparation and characterization of novel sodium alginate/chitosan two ply composite membranes. *Journal of Applied Polymer Science,* 106**,** 394-399.

Mandal, D., Shirazi, A. N. & Parang, K. 2014. Self-assembly of peptides to nanostructures. *Organic & biomolecular chemistry,* 12**,** 3544-3561.

Mason, T. O. & Buell, A. K. 2019. The Kinetics, Thermodynamics and Mechanisms of Short Aromatic Peptide Self-Assembly. *Biological and Bio-inspired Nanomaterials.* Springer.

Mcclure, R. D. & Allen, C. I. 1935. Davidson tannic acid treatment of burns: ten year results. *The American Journal of Surgery,* 28**,** 370-388.

Mndlovu, H., Du Toit, L. C., Kumar, P., Choonara, Y. E., Marimuthu, T., Kondiah, P. P. & Pillay, V. 2020. Bioplatform Fabrication Approaches Affecting Chitosan-Based Interpolymer Complex Properties and Performance as Wound Dressings. *Molecules,* 25**,** 222.

Mndlovu, H., Du Toit, L. C., Kumar, P., Marimuthu, T., Kondiah, P. P., Choonara, Y. E. & Pillay, V. 2019. Development of a Fluid-absorptive Alginate-Chitosan Bioplatform for Potential Application as a Wound Dressing. *Carbohydrate Polymers***,** 114988.

Mohamed, M. F., Abdelkhalek, A. & Seleem, M. N. 2016. Evaluation of short synthetic antimicrobial peptides for treatment of drug-resistant and intracellular Staphylococcus aureus. *Scientific reports,* 6**,** 29707.

Natarajan, V., Krithica, N., Madhan, B. & Sehgal, P. K. 2013. Preparation and properties of tannic acid cross-linked collagen scaffold and its application in wound healing. *Journal of Biomedical Materials Research Part B: Applied Biomaterials,* 101**,** 560-567.

Ninan, N., Forget, A., Shastri, V. P., Voelcker, N. H. & Blencowe, A. 2016. Antibacterial and anti-inflammatory pH-responsive tannic acid-carboxylated agarose composite hydrogels for wound healing. *ACS applied materials & interfaces,* 8**,** 28511-28521.

Nishiyama, T., Amano, S., Tsunenaga, M., Kadoya, K., Takeda, A., Adachi, E. & Burgeson, R. E. 2000. The importance of laminin 5 in the dermal–epidermal basement membrane. *Journal of dermatological science,* 24**,** S51-S59.

Otvos Jr, L. & Ostorhazi, E. 2015. Therapeutic utility of antibacterial peptides in wound healing. *Expert review of anti-infective therapy,* 13**,** 871-881.

Pandit, G., Roy, K., Agarwal, U. & Chatterjee, S. 2018. Self-Assembly Mechanism of a Peptide-Based Drug Delivery Vehicle. *ACS omega,* 3**,** 3143-3155.

Pastar, I., Stojadinovic, O., Yin, N. C., Ramirez, H., Nusbaum, A. G., Sawaya, A., Patel, S. B., Khalid, L., Isseroff, R. R. & Tomic-Canic, M. 2014. Epithelialization in wound healing: a comprehensive review. *Advances in wound care,* 3**,** 445-464.

Patrulea, V., Hirt-Burri, N., Jeannerat, A., Applegate, L., Ostafe, V., Jordan, O. & Borchard, G. 2016. Peptide-decorated chitosan derivatives enhance fibroblast adhesion and proliferation in wound healing. *Carbohydrate polymers,* 142**,** 114-123.

Perlin, L., Macneil, S. & Rimmer, S. 2008. Production and performance of biomaterials containing RGD peptides. *Soft matter,* 4**,** 2331-2349.

Pires, A. L. R. & Moraes, Â. M. 2015. Improvement of the mechanical properties of chitosan-alginate wound dressings containing silver through the addition of a biocompatible silicone rubber. *Journal of Applied Polymer Science,* 132.

Qu, J., Zhao, X., Liang, Y., Xu, Y., Ma, P. X. & Guo, B. 2019. Degradable conductive injectable hydrogels as novel antibacterial, anti-oxidant wound dressings for wound healing. *Chemical Engineering Journal,* 362**,** 548-560.

Rai, M., Ingle, A. P., Pandit, R., Paralikar, P., Gupta, I., Chaud, M. V. & Dos Santos, C. A. 2017. Broadening the spectrum of small-molecule antibacterials by metallic nanoparticles to overcome microbial resistance. *International journal of pharmaceutics,* 532**,** 139-148.

Ranoszek-Soliwoda, K., Tomaszewska, E., Socha, E., Krzyczmonik, P., Ignaczak, A., Orlowski, P., Krzyzowska, M., Celichowski, G. & Grobelny, J. 2017. The role of tannic acid and sodium citrate in the synthesis of silver nanoparticles. *Journal of Nanoparticle Research,* 19**,** 273.

Salerno, A., Zeppetelli, S., Di Maio, E., Iannace, S. & Netti, P. A. 2010. Novel 3D porous multi-phase composite scaffolds based on PCL, thermoplastic zein and ha prepared via supercritical CO2 foaming for bone regeneration. *Composites Science and Technology,* 70**,** 1838-1846.

Singh, A. V. 2011. Biopolymers in drug delivery: a review. *Pharmacologyonline,* 1**,** 666-674.

Ueno, H., Mori, T. & Fujinaga, T. 2001. Topical formulations and wound healing applications of chitosan. *Advanced drug delivery reviews,* 52**,** 105-115.

Varshosaz, J., Arabloo, K., Sarrami, N., Ghassami, E., Yazdani Kachouei, E., Kouhi, M. & Jahanian-Najafabadi, A. 2020. RGD peptide grafted polybutylene adipate-co-terephthalate/gelatin electrospun nanofibers loaded with a matrix metalloproteinase inhibitor drug for alleviating of wounds: An in vitro/in vivo study. *Drug Development and Industrial Pharmacy,* 46**,** 484-497.

Velnar, T. & Gradisnik, L. 2018. Tissue augmentation in wound healing: the role of endothelial and epithelial cells. *Medical Archives,* 72**,** 444.

Wang, C., Zhou, H., Niu, H., Ma, X., Yuan, Y., Hong, H. & Liu, C. 2018. Tannic acid-loaded mesoporous silica for rapid hemostasis and antibacterial activity. *Biomaterials science,* 6**,** 3318-3331.

Wang, L., Gong, C., Yuan, X. & Wei, G. 2019. Controlling the self-assembly of biomolecules into functional nanomaterials through internal interactions and external stimulations: a review. *Nanomaterials,* 9**,** 285.

Xu, F., Weng, B., Gilkerson, R., Materon, L. A. & Lozano, K. 2015. Development of tannic acid/chitosan/pullulan composite nanofibers from aqueous solution for potential applications as wound dressing. *Carbohydrate polymers,* 115**,** 16-24.

Yamada, K. M. 1991. Adhesive recognition sequences. *Journal of Biological Chemistry,* 266**,** 12809-12812.

Zhao, W., Li, J., Jin, K., Liu, W., Qiu, X. & Li, C. 2016. Fabrication of functional PLGA-based electrospun scaffolds and their applications in biomedical engineering. *Materials Science and Engineering: C,* 59**,** 1181-1194.

Zhu, J., Tang, C., Kottke-Marchant, K. & Marchant, R. E. 2009. Design and synthesis of biomimetic hydrogel scaffolds with controlled organization of cyclic RGD peptides. *Bioconjugate chemistry,* 20**,** 333-339.

CHAPTER 6

Conclusions and Recommendations

6.1. Conclusions

There are several approaches employed in developing bioplatforms in the wound dressing field, these include but not limited to solution/ionic gelation, electrospinning, 3-D printing, Polymer coating, grafting, phase separation, solvent evaporation, and solvent casting approaches (Morgado et al., 2017, Siafaka et al., 2016, Lu et al., 2016, Yang et al., 2017, Reneker et al., 2000, Ahn et al., 2006, Guvendiren et al., 2016, El-Feky et al., 2017). Herein the solution/ionic gelation approach was used to develop two different bioplatforms for wound dressing applications. The partial crosslinking approach was used to develop the particulate bioplatforms. The controlled degree of crosslinking allowed for incorporation of transferulic acid into chitosan and left room for further *in situ* interpolymer complexation between partial crosslinked TFA-CS and alginate. The solution gelation approach also allowed for the co-assembly of RGD-polymer bioplatforms. The co-assembly of polymer-peptide influenced the architecture of the scaffolds which were stabilized by tannic acid crosslinking. The use of inexpensive natural polymers and phenolic agents lowers the cost of developing wound dressing bioplatforms. The simplicity of the bioplatform fabrication approach further attest to the lower cost of producing these bioplatforms which is a crucial factor in up scaling production.

Chemical composition of polymers was not drastically changed due to the controlled degree of crosslinking on particulate bioplatform. The interactions were strategically planned to take place on the carboxylic groups of alginate and amine groups of chitosan. The effect of crosslinking, drug loading and interpolymer complexation was observed on the polymeric groups mentioned above. Crosslinking of polymers resulted in a rough surface with deposition of particles on the surface. Transferulic acid loading and interpolymer complexation introduced a different morphological feature compared to native polymers. This morphological features consisted of smooth surface, bundle structure morphology, and threads like structures. These effects changed the physical morphological characteristics of bioplatforms which in turn influenced the fluid uptake and degradation. The PC CS-Alg IPC displayed the highest fluid uptake compared to PC TFA-CS-Alg IPC. This could have been influenced by the changed in morphological feature of the bioplatforms. Furthermore, incorporation of TFA in the bioplatform introduced some resistance to degradation as the PC CS-Alg IPC displayed accelerated degradation compared to PC TFA-CS-Alg IPC. The particulate bioplatform absorbed fluid fast to allow for *in situ* interpolymer complexation.

Similarly to particulate bioplatforms, the scaffolds absorbed higher amounts of fluids with the scaffolds exhibiting high fluid uptake compared to the particulate bioplatforms. The non-crosslinked scaffolds absorbed more fluid compared to the crosslinked scaffolds. Furthermore, the non-crosslinked scaffolds exhibited higher degradation extent compared to the crosslinked scaffold. However, the particulate bioplatform exhibited higher degradation extent compared to the scaffolds. This decrease in fluid absorption capability and degradation extent from non-crosslinked to crosslinked bioplatform was consistent in both particulate and scaffold bioplatforms.

The fluid absorption properties of the bioplatforms allowed for evaluation of their mechanical properties. The particulate bioplatform displayed pH dependent mechanical properties with PC CS-Alg (2090 Pa) having a higher storage modulus compared to PC TFA-CS-Alg (640 Pa). This

further attest to the interaction of TFA and the polymers to lower the rigidity of the bioplatform. The self-assembled scaffolds displayed a much softer nature with the Alg-RGD-CS scaffold displaying the lowest rigidity (80.9 Pa) compared to Alg-RGD-CS-TA (88.6 Pa). The incorporation of tannic acid on the scaffolds increased the compressive strength while decreasing the tension tensile strength. Although the particulate bioplatform and the scaffolds' mechanical properties were evaluated using different techniques, they still displayed a soft nature given that the young's modulus (rigidity), tensile and compressive strength were not at MPa range instead they were all below 2.5 kPa.

The approach applied in incorporating bioactives affected the drug release property of the bioplatforms. The crosslinking of TFA loaded chitosan before in situ interpolymer complexation resulted in limited release of TFA. There was 65.6% encapsulation efficiency and a burst release of 57.5% in 8 hours to a total release of 67.3%. This was low encapsulation efficiency and release. However, TFA is associated with poor encapsulation efficiency and release. Unlike the particulate bioplatforms, the scaffolds displayed high tannic acid encapsulation efficiency of 86%, a burst release of 57.12% in 24 hours, followed by gradual steady release of 8.45% per day up to 90% in 5 days. The two bioplatforms displayed a high burst release in 24 hours which is crucial in acting as anti-inflammatory and anti-oxidant agents at the early stages of wound healing. The burst release had appositive effect on the NIH3T3 cell viability as the cells grew in the presence of the bioplatforms.

The burst release was more effective at the inflammatory phase of wound healing as the wounds treated with the drug loaded bioplatforms displayed accelerated tissue regeneration and wound closure. The bioplatforms displayed better wound healing performances compared to the control and comparative commercial product. The PC FA-CS-Alg bioplatform and the Alg-RGD-CS-TA bioplatforms displayed slightly better but comparable tissue remodelling performances compared to the PC CS-Alg and the Alg-RGD-CS scaffold. The overall performances of these bioplatforms was the regeneration of scar less skin. The closing of the wound and regeneration of scar-less skin suggest that the properties of the bioplatforms translated to optimal performances required for high quality tissue regeneration.

6.2. Recommendation

A novel fabrication approach was explored in designing drug loading bioplatforms with optimal properties translating to effective wound tissue regeneration and wound healing performances. The partial crosslinking, lyophilization and pulverisation technique was employed in designing the *in situ* interpolymer complex forming hydrogel. Properties such as thermo-physical properties, fluid uptake, rheological properties (yield stress, thixotropy, and visco-elastic properties), and degradation were improved to suit performances such as drug loading, cytocompatibility and tissue regeneration. TFA was used incorporated to the bioplatform prior crosslinking of partial crosslinked bioplatform. The design of the particulate bioplatform was to allow it to be stable for long storage and can only form the interpolymer complex *in situ* under fluid exposure. To look at the tenability of the polymeric formulations, the self-assembly approach was undertaken to developed biocompatible scaffolds. Instead of partial crosslinking the polymers, the RGD peptide was introduced to enhance the wound healing capability of the polymers. The self-assembled formulations were crosslinked with tannic acid. The idea behind the use of tannic acid was twofold; to function as a crosslinker and as a bioactive. The properties of bioplatforms such as the malleability of the scaffold and the in situ hydrogel formation of the particulate bioplatforms allows the bioplatforms to be applied in wounds of different sizes and shapes. The selection of both

phenolic agents was strategically planned to have an effect at the early stages of wound healing. The developed particulate and scaffolds bioplatforms displayed accelerated wound healing and high quality tissue regeneration which confirmed the tailoring of bioplatforms properties necessitating optimal performances. This study demonstrated an approach with which bioplatform's performances can be improved by targeting their properties (physical, chemical, and mechanical properties). The improved properties along with the biological properties of stating materials have proved to enhance the performances mentioned above. Thus, the thought process could be employed in developing bioplatforms for different applications. The concept highlighted in the study can be employed in developing bioplatforms of different textural properties along with chemical and mechanical properties that can be tailored for specific performances in tissue engineering.

6.3. References

Ahn, Y., Park, S., Kim, G., Hwang, Y., Lee, C., Shin, H. & Lee, J. 2006. Development of high efficiency nanofilters made of nanofibers. *Current Applied Physics,* 6**,** 1030-1035.

El-Feky, G. S., Sharaf, S. S., El Shafei, A. & Hegazy, A. A. 2017. Using chitosan nanoparticles as drug carriers for the development of a silver sulfadiazine wound dressing. *Carbohydrate polymers,* 158**,** 11-19.

Guvendiren, M., Molde, J., Soares, R. M. & Kohn, J. 2016. Designing biomaterials for 3D printing. *ACS biomaterials science & engineering,* 2**,** 1679-1693.

Lu, B., Wang, T., Li, Z., Dai, F., Lv, L., Tang, F., Yu, K., Liu, J. & Lan, G. 2016. Healing of skin wounds with a chitosan–gelatin sponge loaded with tannins and platelet-rich plasma. *International journal of biological macromolecules,* 82**,** 884-891.

Morgado, P. I., Miguel, S. P., Correia, I. J. & Aguiar-Ricardo, A. 2017. Ibuprofen loaded PVA/chitosan membranes: A highly efficient strategy towards an improved skin wound healing. *Carbohydrate polymers,* 159**,** 136-145.

Reneker, D. H., Yarin, A. L., Fong, H. & Koombhongse, S. 2000. Bending instability of electrically charged liquid jets of polymer solutions in electrospinning. *Journal of Applied physics,* 87**,** 4531-4547.

Siafaka, P. I., Zisi, A. P., Exindari, M. K., Karantas, I. D. & Bikiaris, D. N. 2016. Porous dressings of modified chitosan with poly (2-hydroxyethyl acrylate) for topical wound delivery of levofloxacin. *Carbohydrate polymers,* 143**,** 90-99.

Yang, D. H., Seo, D. I., Lee, D.-W., Bhang, S. H., Park, K., Jang, G., Kim, C. H. & Chun, H. J. 2017. Preparation and evaluation of visible-light cured glycol chitosan hydrogel dressing containing dual growth factors for accelerated wound healing. *Journal of industrial and engineering chemistry,* 53**,** 360-370.

Appendix A: Animal Ethics Clearance Certificate

STRICTLY CONFIDENTIAL

ANIMAL ETHICS SCREENING COMMITTEE (AESC)

CLEARANCE CERTIFICATE NO. 2018/10/48/C

APPLICANT: Mr H Mndlovu

SCHOOL: Pharmacy
DEPARTMENT:
LOCATION:

PROJECT TITLE: In vivo assessment of the wound healing effects of a composite platform in a rat model

Number and Species

45X 6-8 weeks old, 250g - 300g in body mass male Sprague-Dawley rats

Approval was given for the use of animals for the project described above at an AESC meeting held on 2018/10/30. This approval remains valid until 2021/02/12.
Unreported changes to the application may invalidate the clearance given by the AESC
An annual progress report must be provided

The use of these animals is subject to AESC guidelines for the use and care of animals, is limited to the procedures described in the application form and is subject to any additional conditions listed below:

Signed: _____ Date: 2019-02-18
(Chairperson, AESC)

I am satisfied that the persons listed in this application are competent to perform the procedures therein, in terms of Section 23 (1) (c) of the Veterinary and Para-Veterinary Professions Act (19 of 1982)

Signed: _____ Date: 14/02/2019
(Registered Veterinarian)

cc: Supervisor: Prof V Pillay, Prof Y Choonara and Dr P Kumar
Director: CAS

Works 2000\win001\AESCCert.wps

Appendix B: Review Paper

molecules

MDPI

Review

Bioplatform Fabrication Approaches Affecting Chitosan-Based Interpolymer Complex Properties and Performance as Wound Dressings

Hillary Mudlovu, Lisa C. du Toit, Pradeep Kumar, Yahya E. Choonara, Thashree Marimuthu, Pierre P. D. Kondiah and Viness Pillay*

Wits Advanced Drug Delivery Platform Research Unit, Department of Pharmacy and Pharmacology, Faculty of Health Sciences, School of Therapeutics Sciences, University of the Witwatersrand, Johannesburg, 7 York Road, Parktown 2193, South Africa; 674238@students.wits.ac.za (H.M.); lisa.dutoit@wits.ac.za (L.C.d.T.); pradeep.kumar@wits.ac.za (P.K.); yahya.choonara@wits.ac.za (Y.E.C.); thashree.marimuthu@wits.ac.za (T.M.); pierre.kondiah@wits.ac.za (P.P.D.K.)

* Correspondence: viness.pillay@wits.ac.za; Tel.: +27-11-717-2274

Academic Editors: Jens Smiatek and Derek J. McPhee

Received: 21 November 2019; Accepted: 26 December 2019; Published: 6 January 2020

check for updates

Abstract: Chitosan can form interpolymer complexes (IPCs) with anionic polymers to form biomedical platforms (BMPs) for wound dressing/healing applications. This has resulted in its application in various BMPs such as gauze, nano/microparticles, hydrogels, scaffolds, and films. Notably, wound healing has been highlighted as a noteworthy application due to the remarkable physical, chemical, and mechanical properties enabled though the interaction of these polyelectrolytes. The interaction of chitosan and anionic polymers can improve the properties and performance of BMPs. To this end, the approaches employed in fabricating wound dressings was evaluated for their effect on the property–performance factors contributing to BMP suitability in wound dressing. The use of chitosan in wound dressing applications has had much attention due to its compatible biological properties. Recent advancement includes the control of the degree of crosslinking and incorporation of bioactives in an attempt to enhance the physicochemical and physicomechanical properties of wound dressing BMPs. A critical issue with polyelectrolyte-based BMPs is that their effective translation to wound dressing platforms has yet to be realised due to the unmet challenges faced when mimicking the complex and dynamic wound environment. Novel BMPs stemming from the IPCs of chitosan are discussed in this review to offer new insight into the tailoring of physical, chemical, and mechanical properties via fabrication approaches to develop effective wound dressing candidates. These BMPs may pave the way to new therapeutic developments for improved patient outcomes.

Keywords: chitosan; polyelectrolytes; biomedical platforms; interpolymer complex; wound dressing; wound healing; IPC fabrication approaches

1. Introduction

Wound healing is an intricate physical systematic series of skin restoration reactions necessitating translational therapeutic approaches capable of aiding the overlapping of inflammatory, migratory, proliferative, and remodelling phases for accelerating tissue filling and restoration. The wound dressing biomedical platforms (BMPs) fabricated from the wound-based translational therapeutic approaches should present an ideal tissue restoration environment by (a) providing and maintaining balanced hydration levels through the absorption and control of the wound exudates; (b) facilitating gaseous exchange across the wound site; (c) preventing secondary infections; (d) controlling and localizing the release of incorporated bioactives; and (e) demonstrating extracellular matrix (ECM)-equivalent

Appendix C: Research Paper 1

Carbohydrate Polymers 222 (2019) 114988

Contents lists available at ScienceDirect

Carbohydrate Polymers

journal homepage: www.elsevier.com/locate/carbpol

Development of a fluid-absorptive alginate-chitosan bioplatform for potential application as a wound dressing

Hillary Mndlovu, Lisa C. du Toit, Pradeep Kumar, Thashree Marimuthu, Pierre P.D. Kondiah, Yahya E. Choonara[1], Viness Pillay*,[1]

Wits Advanced Drug Delivery Platform Research Unit, Department of Pharmacy and Pharmacology, School of Therapeutic Sciences, Faculty of Health Sciences, University of the Witwatersrand, Johannesburg, 7 York Road, Parktown 2193, South Africa

ARTICLE INFO

Keywords:
Carbohydrate polymers
Ionic polysaccharides
Biopolymers
Partially-crosslinked
Co-complexed
Bioplatforms
Wound dressing
Biocompatible

ABSTRACT

This study introduces a novel approach in fabricating bioplatforms with favourable physical, chemical, and mechanical properties for wound dressing applications. The approach employs a three-step method; partial-crosslinking of polymers into soft macromatrices, lyophilization, and pulverization of those macromatrices to obtain polymer particles with improved properties. For investigation of this approach, the ionic polysaccharides, sodium alginate and chitosan were partially crosslinked with calcium chloride and sodium tripolyphosphate, respectively, followed by interpolymer complexation (IPC) for formation of the bioplatform. The formulations displayed good thermal stability with enhanced water uptake. The IPC exhibited water uptake of 4343.4% over 24 h and displayed 78% biodegradation over 14 days, which was superior to that of a commercial alginate-based wound dressing (1612.56% swelling and 16.26% biodegradation). The bioplatform thus possessed promising fluid-absorptivity and biodegradability, for potential application as a wound therapeutic system.

1. Introduction

Wound dressings contribute greatly towards acceleration of wound healing and can act as both physical and mechanical barrier to prevent blood loss and against foreign bodies such as bacteria. Natural polymers such as chitosan (CS) and alginate (Alg) have drawn much attention in the wound dressing field due to their ionic character and biological properties. Their ionic character allows them to form interpolymer complexes (IPCs) which can be tuned into various bioplatforms (BPs) such as gauze (Ge et al., 2018), beads (Fathi et al., 2018), nanoparticles (Venkatesan et al., 2017), films/membranes (Bueno, Moraes, de Sousa, & Binga, 2016; Silva, García, Reis, García, & Mano, 2017), and hydrogel sponges/scaffolds (Chen et al., 2017). To date, there is still no promising gauze, film, or scaffold capable of treating wounds, such as deep cuts. This leaves foams, injectable hydrogels, nanoparticles and beads/microparticles as potentially desirable bioplatforms to treat deep cut wounds were conventional dressings cannot be applied. Recent studies on CS-Alg IPC beads/microparticles have indicated great advancement in potential properties such as improving bioplatform swelling capacity, erythrocyte adhesion, cytocompatibility, antimicrobial, and drug/growth factor release (Chen et al., 2017; Fathi et al., 2018; Venkatesan et al., 2017). Incorporation of toxic agents such as silver and zeolite, and UV-radiation crosslinking of CS-Alg IPC bioplatforms may improve physical properties such as swelling ratio and pore size while introducing cytotoxicity (Dowling et al., 2011; Fathi et al., 2018; Venkatesan et al., 2017). The use appropriate crosslinkers and selection of suitable fabrication approaches can produce cytocompatible CS-Alg IPCs with optimal physicochemical and physicomechanical properties. The current study was undertaken for the attainment of enhanced physicochemical and physicomechanical properties of the CS-Alg IPC microparticles by the use of $CaCl_2$ and sodium tripolyphosphate for partial crosslinking of chitosan and alginate.

Further, in this investigation, surfactants, drugs, and potentially toxic compounds have been excluded. Thus the fabricated bioplatform performance would depend on the biological properties of the polymers and the improved properties attained via the partial-crosslinking approach. The biological properties of chitosan include tissue repair, antimicrobial, immune-enhancing, antioxidant, metal chelating, hypocholesterolemic, lipid binding, anti-inflammatory, anticancer, and antitumor effects (Rabea, Badawy, Stevens, Smagghe, & Steurbaut, 2003; Xia, Liu, Zhang, & Chen, 2011). Additional chitosan properties, such as the ability to be tuned into an amphiphilic biopolymer with the

* Corresponding author.
E-mail address: viness.pillay@wits.ac.za (V. Pillay).
[1] Prof. Yahya E. Choonara and Prof. Viness Pillay are joint Senior Authors.

https://doi.org/10.1016/j.carbpol.2019.114988
Received 31 January 2019; Received in revised form 30 May 2019; Accepted 9 June 2019
Available online 10 June 2019
0144-8617/ © 2019 Elsevier Ltd. All rights reserved.

Appendix D: Research Paper 2

In Situ Forming FA-Loaded Partially-Crosslinked Chitosan-Alginate Interpolymer Complex Hydrogel for Wound Dressing Skin Tissue Regeneration

Hillary Mndlovu, Pradeep Kumar, Lisa C. du Toit, Thashree Marimuthu, Pierre P.D. Kondiah, Yahya E. Choonara, Viness Pillay*

Wits Advanced Drug Delivery Platform Research Unit, Department of Pharmacy and Pharmacology, Faculty of Health Sciences, School of Therapeutics Sciences, University of the Witwatersrand, Johannesburg, 7 York Road, Parktown 2193, South Africa

Abstract

Cytocompatible, biocompatible and increased patient compliable wound dressings are promising options in developing bioplatforms with enhanced wound healing capabilities. A previous study introduced a novel approach in fabricating bioplatforms with favourable physical, chemical, and mechanical properties for wound dressing applications. Herein, the same three step approach was employed in fabricating particulate partially-crosslinked transferulic acid-chitosan-alginate IPC for enhanced wound healing capabilities. The PC TFA-CS-Alg displayed fluid uptake of 3102% in 24 hours and stepwise degradation upto 53.5% in 14 days. The PC TFA-CS-Alg bioplatform was used as a drug delivery system with an encapsulation efficiency of 65.6%, drug loading of 9.4%, burst release of 58.27% and a steady release of 1.91% per day. The wound closure assessment indicated accelerated wound closure on lesions treated with PC TFA-CS-Alg and a comparable performance between PC CS-Alg and Pharmalgi® with the control (gauze) presenting the slowest wound closure capabilities. The histopathological evaluations of the lesions indicated better wound healing performance in lesions treated PC TFA-CS-Alg and PC CS-Alg compared to those treated with the commercial product (Pharmalgi®) and the control. The accelerated wound healing performance of the bioplatforms were more pronounced at the early stages (day 3) of wound healing with PC TFA-CS-Alg treated lesions exhibiting a slightly advanced wound healing morphology compared to those treated with PC CS-Alg. The application of the particulate bioplatform on the wound via sprinkles, the *in situ* hydrogel formation with exudate/fluid and accelerated wound healing performance of the bioplatforms makes it a good candidate for drug delivery system and skin tissue regeneration.

Keywords: partial crosslinking, interpolymer complex, transferulic acid, drug delivery, bioplatform, carbohydrate polymers, NIH 3T3, and wound healing

Appendix E: Research Paper 3

Tunable Biomimetic self-assembling Alg-RGD-CS-TA Hybrid Scaffold for Wound Healing and Skin Regeneration

Hillary Mndlovu, Pradeep Kumar, Lisa C. du Toit, Thashree Marimuthu, Pierre P.D. Kondiah, Yahya E. Choonara, Viness Pillay*

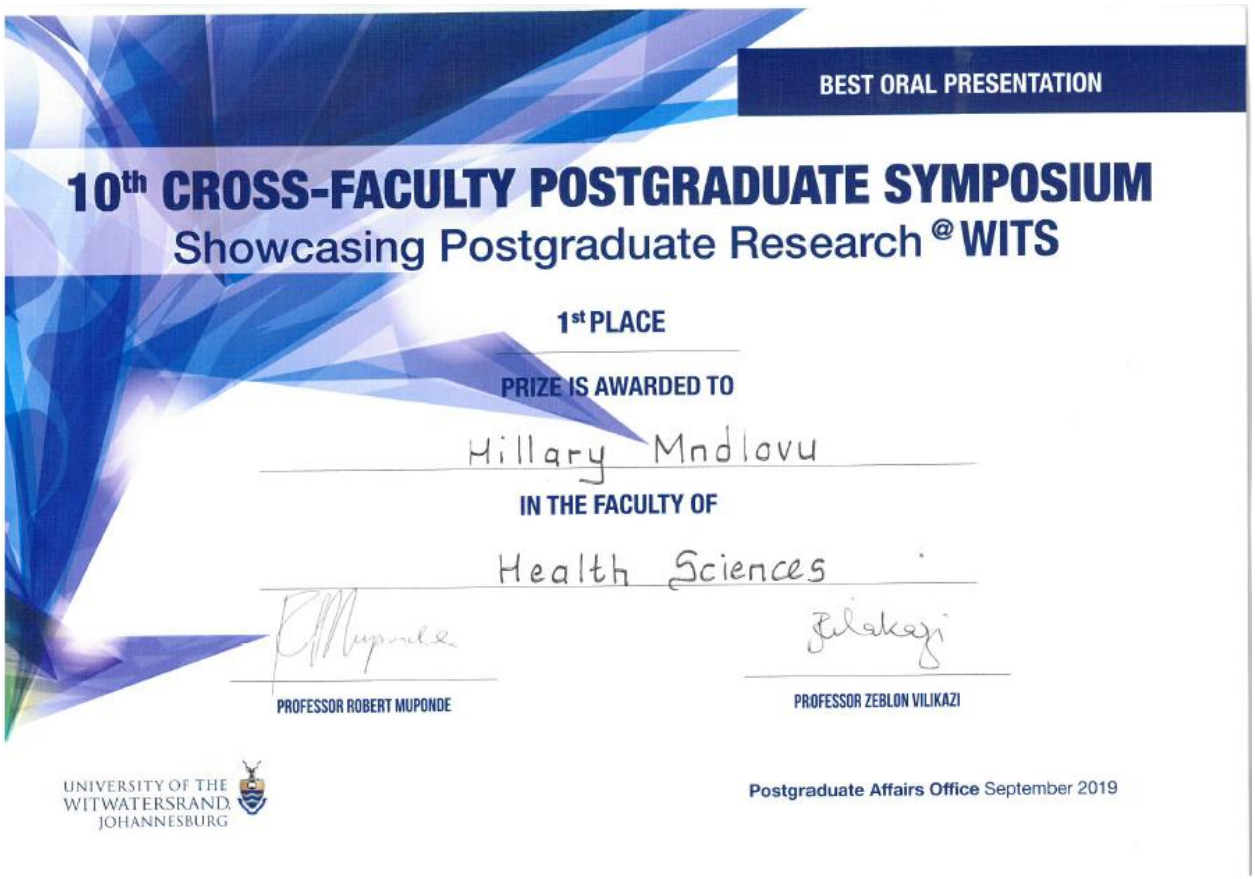
Wits Advanced Drug Delivery Platform Research Unit, Department of Pharmacy and Pharmacology, Faculty of Health Sciences, School of Therapeutics Sciences, University of the Witwatersrand, Johannesburg, 7 York Road, Parktown 2193, South Africa

Abstract

Self-assembled hydrogels have drown much attention in the tissue regeneration and wound healing field due to the use biocompatible peptides to tailor tunable structural features necessitating optimal tissue remodeling performances. The polymeric and peptide self-assembly was explored in the current study to develop biomimetic scaffolds for wound healing and skin tissue regeneration. Alginate, chitosan and RGD were used to fabricate the self-assembled hybrid scaffolds crosslinked with tannic acid. The use of RGD changed the physical features of the 3-D architectural scaffolds and TA crosslinking of the scaffolds increased the mechanical properties such tension tensile strength and compressive Young's modulus, yield strength, ultimate strength and compressive distance. The incorporation of TA as both a crosslinker and a bioactive allowed for 86% encapsulation efficiency and burst release of 57% in 24 hours accompanied by a 8.5% steady release per day up to 90% in 5 days. The scaffolds increased cell viability over the 3 day period, moving from slightly cytotoxic to non-cytotoxic. Detailed wound closure and tissue regeneration evaluations at predetermined wound healing time points highlighted the superiority of the Alg-RGD-CS and Alg-RGD-CS-TA scaffolds over the commercial comparative product Pharmalgi® and control groups. The superiority performance of the scaffolds includes accelerated tissue remodeling performance from the early stages of wound healing to late stages of wound healing indicated by lack of defect and scar on scaffold treated tissues. These performances gives insights on the design of wound dressings that can act as delivery systems for treatment of acute wounds.

Keywords: self-assembly, co-assembly, RGD peptide, chitosan, alginate, tannic acid, scaffold, drug delivery, cytocompatible and wound healing.

Appendix F: Conference Presentation Certificates



BEST ORAL PRESENTATION

10th CROSS-FACULTY POSTGRADUATE SYMPOSIUM

Showcasing Postgraduate Research @ WITS

1st PLACE

PRIZE IS AWARDED TO

Hillary Mndlovu

IN THE FACULTY OF

Health Sciences

PROFESSOR ROBERT MUPONDE

PROFESSOR ZEBLON VILIKAZI

UNIVERSITY OF THE WITWATERSRAND JOHANNESBURG

Postgraduate Affairs Office September 2019

9th CROSS-FACULTY POSTGRADUATE SYMPOSIUM

Showcasing Postgraduate Research @ WITS

WE ARE PROUD TO CONFIRM THAT

Hillary Mndlovu

PRESENTED A FLASH/POSTER PRESENTATION AT THE 9th CROSS FACULTY POSTGRADUATE SYMPOSIUM

PROFESSOR NEIL COVILLE

PROFESSOR ZEBLON VILIKAZI

UNIVERSITY OF THE WITWATERSRAND JOHANNESBURG

Postgraduate Affairs Office October 2018

CERTIFICATE

OF PARTICIPATION IN THE

4th International Conference on
Biomedical Polymers & Polymeric Biomaterials

ISBPPB 2018

15–18 July 2018 KRAKÓW POLAND

FOR

Hillary Mndlovu

Prof. Jan Chłopek
Chair of the Organizing Committee

Prof. Elżbieta Pamuła
Vice-Chair of the Organizing Committee